The Effect of Fiber Diameter on the Degradation Profile, Elastic Modulus, Yield Strength and Hydrophilicity of Electrospun PCL/gelatin Tissue Engineering Scaffolds

by

Beste Avci

A thesis submitted in partial fulfillment of the requirements for the degree of

Master of Science

Department of Mechanical Engineering
University of Alberta

Abstract

Tissue loss is a health problem that affects millions of people globally. The conventional methods such as the transplantation of autografts and allografts do not always result in full recovery of damaged tissues. Tissue engineering emerged as a field with the ultimate goal of obviating the need for transplantation of tissues. In tissue engineering, a construct created by combining a scaffold, cells, and growth factors is implanted to the damaged site to induce and facilitate tissue regeneration.

Nanofibrous membranes are ideal to be used as a scaffold and to promote cellar activity because their structure resembles the structure of the native extracellular matrix (ECM). Electrospinning is the most preferred method to fabricate nanofibrous membranes.

The selection of material determines the performance of a tissue engineering scaffold. Natural polymers such as collagen and gelatin have the binding sites, which promote the adhesion, growth, and proliferation of cells, in their structure. Therefore, their selection as a scaffolding material is favored. Electrospun collagen and gelatin membranes are soluble in water and require being crosslinked. However, crosslinking induces cytotoxicity. Alternative to natural polymers, synthetic polymers were electrospun to fabricate scaffolds. Synthetic polymers lack of binding sites but they are biocompatible and have good mechanical properties. Polycaprolactone (PCL) is a synthetic polymer, which is hydrophobic and insoluble in water. A scaffold, which is insoluble in water without being crosslinked, with improved mechanical properties and binding sites promoting cellular activity can be fabricated by electrospinning the blends of PCL and gelatin.

The degradation profile, mechanical properties and hydrophilicity of a scaffold determine its performance. In the literature, the dependence of degradation profile on surface area of

electrospun PCL/gelatin membranes has not been investigated yet. In this study, the surface area of electrospun PCL/gelatin membranes was tuned by varying the fiber diameter. PCL/gelatin solutions at three different concentrations were electrospun to fabricate PCL/gelatin membranes at three different fiber diameters. Then, each membrane was degraded in order to study the effect of fiber diameter on degradation profile and the effect of degradation profile on mechanical properties and hydrophilicity.

PCL/gelatin solutions with 1:1 PCL to gelatin ratio at the total polymer concentrations of 6%, 10% and 14% (w/v) were electrospun and membranes at the average fiber diameters of 184 ± 51 nm, 803 ± 349 nm and 2131 ± 701 nm were obtained, respectively. It has been found that the fibrous structure of the membrane electrospun at the concentration of 6% (w/v) could not be maintained during degradation, whereas the integrity of the fibers was preserved and the average fiber diameter did not change during degradation for the membranes electrospun at the concentrations of 10% and 14% (w/v). After 1, 3, 6 and 10 days of degradation, the remaining mass% was found as approximately 76%, 61%, 55% and 55% of the initial membrane mass, respectively for all the fiber diameters. After 10 days of degradation, a significant decrease in the elastic modulus of the membranes electrospun at the total polymer concentrations of 6%, 10% and 14% (w/v) was seen from 522 ± 63 MPa, 546 ± 56 MPa and 426 ± 77 MPa to 287 ± 128 MPa, 194 ± 27 MPa and 104 ± 20 MPa, respectively. The yield strength dropped significantly from 15.4 ± 0.4 MPa and 13.8 ± 2.3 MPa to 5.6 ± 0.2 MPa and 4.7 ± 1 MPa for the membranes electrospun at total polymer concentrations of 10% and 14% (w/v), respectively, after 10 days of degradation. It was seen that the contact angle increased after 10 days of degradation for the membranes electrospun at the total polymer concentration of 10% and 14% (w/v) indicating that the membranes became more hydrophobic as they are being degraded.

Preface

This thesis is an original work by Beste Avci. No part of this thesis has been previously published.

This thesis will be used to write a journal article in the future.

Acknowledgments

I would like to take this opportunity to thank my supervisor, Dr. Cagri Ayranci, for his kindness, encouragement and guidance. I was so lucky for being his student. I am also thankful to my co supervisor, Dr. Hasan Uludag, for his valuable inputs and support.

I would like to thank to Dr. Mohtada Sadrzadeh for letting me do the contact angle measurements in his lab.

Special thanks to my colleagues Eyüp, Samir, and Irina for their support and help.

I am deeply grateful to my friend, Daniel, who supported, encouraged and helped me to do my best not only in research but also in every aspect of my life.

Finally, I owe my deepest gratitude to my father, my mother, my grandmother and my uncle. I wouldn't be able to achieve this much without your love and support. Thank you so much for always being there for me. I would like to especially thank to my mother for encouraging me to push my limits.

Table of Contents

List of Tables

List of Figures

List of Abbreviations

Symbol	Description
c^*	Critical chain overlap concentration
c_e	Critical entanglement concentration
$[\eta]$	Intrinsic viscoisty
K	Mark-Houwink-Sakurada equation constant
a	Mark-Houwink-Sakurada equation constant
M	Molecular weight in Mark-Houwink-Sakurada equation
ε	Strain
Δl	Change in sample length
L	Initial sample length
σ	Stress
σ_{sp}	Specific stress
ρ_{fiber}	Density of one fiber
F	Applied force
W	Sample width
ρ_{areal}	Sample Areal density
PBS	Phosphate buffer saline
ECM	Extra cellular matrix

1. Introduction

1.1. The Clinical Need for Tissue Engineering

Tissue loss resulting from diseases, trauma, and defects from birth is a health problem that millions of people suffer globally. The traditional treatment methods involve reconstruction of the damaged site surgically, administration of drugs, implantation of prosthesis and transplantation of healthy tissues [1][2]. However, these treatments do not always lead to satisfactory results where the damaged tissues are fully recovered both functionally and esthetically [2]. Transplantation of an autograft, which is the tissue transplanted from the donor site to the damaged site in the same individual, and transplantation of an allograft, which is the healthy tissue transplanted from one individual to another, are both hampered by the shortage of donor tissues [3]. Autograft harvesting is an expensive and painful process associated with the complication of morbidity at the donor-site. There are also some risks for the transplantation of allografts such as the rejection of the transplant by the immune system and transmission of diseases to the patient from the donated tissue [3].

Tissue engineering emerged as a field providing an alternative approach to overcome the issues with the conventional treatment methods [4]. In tissue engineering, biological constructs are developed by combining cells, a scaffold, and signals to regenerate patient's own tissues with the ultimate goal of obviating the need for organ and tissue transplantation [2] [5].

1.2. Fundamentals of Tissue Engineering

Tissue engineering has three important components, which are the scaffold, growth factors, and cells. The scaffold guides and facilitates cell adhesion, proliferation, migration and differentiation by providing a temporary substrate that mimics the extracellular matrix of the

native tissue [6]. The cells form the new tissue by synthesizing the extracellular matrix that replaces the scaffold as it degrades [7]. Growth factors guide cell growth and differentiation towards the expression of the target tissue phenotype [8][9].

If sufficient numbers of local cells are present at the site of damaged tissue, these native cells can be recruited for the regeneration of the damaged tissue [7]. In this case, the scaffold is simply used as a vehicle for the local delivery of growth factors, which modulate the differentiation and migration of the endogenous progenitor cells [7] [8]. For the cases where the local cell concentration of the native tissue at the damaged site is low, a construct in which cells are seeded onto a scaffold can be implanted [7] [8]. The seeded cells can be from cell lines, primary cells or stem cells [8]. Before the implantation of a potential scaffold, its performance is tested *in vitro* to confirm that the scaffold satisfies the basic requirements such as biocompatibility, appropriate porosity, and bioactivity [8]. Cells from established cell lines are commonly preferred by researchers for the *in vitro* assessment of the scaffolds because they can proliferate rapidly, be expanded indefinitely and easily cultured. However, these cells are genetically and phenotypically different then the tissue that they have been originated from. Therefore, they may not reflect a scaffold's *in vivo* performance [10] [11]. Primary cells are derived directly from tissues and their expansion capacity is limited [8] [10] [11]. However, primary cells have many of the endogenous cell markers and they function similar to the endogenous cells [8] [10] [11]. Therefore, they reflect a scaffold's *in vivo* performance more accurately compared to the cells from cell lines [8] [10] [11]. Stem cells, which possess a high self-renewal and differentiation capacity, can be classified as embryonic and adult stem cells [9]. Embryonic cells can differentiate into all cells that originated from any of the three germ layers but their usage is limited because of the ethical concerns related to the destruction of the embryo

in the process of obtaining the cells [6]. On the other hand, the differentiation capacity of adult stem cells is more limited compared to embryonic stem cells [9]. Mesenchymal stem cells, which are one type of adult stem cells that can be isolated from bone marrow and adipose tissue, are able to differentiate into various types of cells of a single germ layer [6]. Induced pluripotent stem cells (iPSCs), which are obtained by reprogramming adult somatic cells, have a great potential to be used in tissue engineering because of their capacity to differentiate into various cell types of any of the three germ layers [6]. However, the underlying mechanisms for the differentiation of iPSCs into specific cell types should be further elucidated [6].

Growth factors can be incorporated to scaffolds in various ways and delivered to the cells as they are being released from the scaffold [6]. Covalent binding of the growth factor to the scaffold, encapsulation of the growth factor within in the scaffold and adsorbing the growth factors on the scaffold physically are methods for the immobilization of growth factors to the scaffold [6]. Growth factors can also be attached to the scaffold through the ionic attraction between the positively charged growth factor and the negatively charged scaffold [6]. In such a system, the release of the growth factor can be induced upon a significant change in the environment [6]. Growth factors are soluble polypeptides that function as signaling molecules [12]. Signals created by the binding of growth factors to specific transmembrane proteins on target cells are transduced through complex signaling networks within the cell and result in specific cellular responses [12]. These responses can provide control over proliferation, differentiation, and migration of cells [12]. Bone morphogenetic proteins, basic fibroblast growth factor, vascular epithelial growth factor and transforming growth factor-β are among the commonly used growth factors in tissue engineering [6]. Alternative to the delivery growth factors, the growth factors can be synthesized by the cells, which were transfected with specific

genes [13]. The genes combined with viral and non-viral vectors can be incorporated into the scaffolds and delivered to the cells as they are being released [8].

1.1.1. Requirements for Scaffolds

In order to promote and guide tissue regeneration at the implantation site, scaffolds should satisfy several requirements such as biocompatibility, porosity, degradability, mechanical strength and hydrophilicity [6].

An ideal scaffold should be biocompatible to promote cell adhesion [6]. The material which the scaffold is made of shouldn't be toxic to the cells [7]. The regeneration of the tissue shouldn't be hampered because of the immune reaction and inflammation elicited by the scaffold [14].

Hydrophilicity is also an important criterion determining the performance of the scaffold. Initial attachment and migration of cells can be affected significantly by the hydrophilicity of the scaffold [15]. In the literature, it has been reported that the attachment of the cells at the initial stage of culture is lower for hydrophobic surfaces [15].

Scaffolds should have interconnected porous structures for cells to penetrate and migrate into the scaffold, for the formation of blood vessels into the regenerated tissue and for nutrients, wastes, O_2 and CO_2 to diffuse [14]. The pore size should be optimal to both allow cell migration into the scaffold and ensure cells to have enough contact with the binding sides on the scaffold [14].

The scaffold should not fail under the physiological forces occurring at the site of implantation [7] [14]. Moreover, morphology, proliferation, and differentiation of the cells can change depending on the mechanical properties of the scaffold [7]. Therefore, an ideal scaffold should have the same mechanical properties as the native extracellular matrix of the tissue at the

anatomical site that the scaffold is going to be implanted [6]. However, the mechanical strength of the scaffold should diminish as the regeneration of the tissue proceeds [14]. In addition, the scaffold should be able to maintain its integrity while the surgeon is implanting it [6].

An ideal scaffold should provide physical and biochemical support for cell attachment, proliferation, migration, and differentiation. However, it should degrade to allow the synthesis of the new extracellular matrix by the cells, leading to the complete replacement of the scaffold with the regenerated tissue's own extracellular matrix [6]. Therefore, the degradation rate of the scaffold should be synchronized with the formation rate of the new tissue [7]. In addition, the by-products formed during degradation should not be toxic and they should leave the body without inducing any adverse reaction in other organs [14].

1.1.2. Degradation Mechanisms for Polymeric Scaffolds

Degradation of polymers involves the formation of low molecular species such as monomers or oligomers due to the cleavage of the polymer chains [16]. There are two mechanisms for the biodegradation of polymeric scaffolds, which are enzymatic and hydrolytic degradation [17]. Scaffolds of natural polymers with the cleavage sites for the enzymes degrade enzymatically, which is the main degradation mechanism that occurs initially *in vivo* [17].

In hydrolysis, the chemical bonds in polymer chains are broken down due to reacting with water molecules [16]. The scaffold starts losing mass due to erosion. Erosion specifically refers to the reduction of the polymer mass due to dissolution of low molecular weight species formed during degradation [16]. The rate of degradation depends on various factors such as the easy access of the water molecules to the cleavable bonds, the crystallinity, hydrophilicity and the molecular weight of the polymer [16]. There are two types of polymer erosion, which are bulk and surface erosion.

In bulk erosion, polymer chains are cleaved throughout the entire scaffold. As a result, molecular weight and consequently, the mechanical properties decrease over time [16]. When the cleavage of the polymer chains proceeds to a certain extent, soluble degradation products with low molecular weight start to form. As these products diffuse through the bulk of the material and dissolve in water, the scaffold loses mass. Therefore, molecular weight and the mechanical properties start decreasing before the scaffold starts losing mass [16]. The external scaffold dimensions are preserved during bulk erosion up to a point where the scaffold comes apart [16].

When the rate for the hydrolysis reaction is higher than the rate for the diffusion of water into the bulk of the material, degradation occurs only at the surface of the scaffold leading to surface erosion [16]. In surface erosion, external dimensions and the mass of the scaffold decreases over time while the molecular weight and the mechanical properties do not change significantly [16]. The rates for mass loss and for reduction in external dimensions are proportional to the surface area of the scaffold [16].

1.3. Techniques for the Fabrication of Scaffolds

There are mainly three techniques to form artificial porous scaffolds, which are salt leaching, rapid prototyping and the creation of nanofibrous structures [18]. In salt leaching, salts are dispersed in a polymer solution. A continuous polymer matrix containing the salts is formed by casting this polymer solution into a mold and the subsequent evaporation of the solvent. Then, The crystals of salts are leached out by using water, allowing the formation of pores inside the mold [19] [20]. In order to control the architecture of the pores in three dimensions precisely, three-dimensional (3D) printing was adopted as a scaffold fabrication technique [20]. In 3D printing of scaffolds, the layers of polymer powder are sequentially laid and a binder is ink jet printed onto these layers based on a computer-assisted design (CAD) of the scaffold [20].

Nanofibrous membranes are utilized as scaffolds in tissue engineering due to their interconnected micro porous structure, high porosity, high surface area to volume ratio and the morphological similarity between the nanofibers and the collagen fibrils, which are one of the major constitutes of the native extracellular matrix (ECM) with diameters ranging between 50–500 nm [14][21][22][23]. The interconnected porous structure of nanofibrous scaffolds facilitates the transport of nutrients [23]. The nanofibrous structure, which mimics ECM closely, provides an environment that cells can grow and function [21]. The adhesion, migration, proliferation, and differentiation of the cells are promoted by the interconnected microscale pores and the high surface area to volume ratio of the nanofibers [21].

There are several methods utilized in the literature for the production of nanofibers, which are drawing, template synthesis, phase separation, and electrospinning [24] [25] [26] [27]. Among these methods, electrospinning is vastly employed by the researchers and the industry because it is a continuous, cost effective, and simple process, which yields long continuous fibers and can be scaled up [27] [28]. In addition, diameter of electrospun fibres, the porosity and the size of the pores, which affect the cellular infiltration of the scaffold, and can be tailored for a specific tissue engineering application by varying the parameters of electrospinning [7] [29] [30].

1.4. Electrospinning

Fibers with diameters at nanoscale have an extremely high length to diameter and surface area to volume ratios [31]. Therefore, structures of nanofibers possess some unique properties such as high specific surface area and interconnected porous structure with a very high porosity [32]. These unique properties of nanofibrous structures make them ideal for various applications such as protective clothing, air filtration, biocatalysts, lithium-ion batteries, drug delivery, wound dressing, and tissue engineering [33] [34] [35] [36] [37] [38] [39].

1.4.1. History of Electrospinning

The first apparatus producing artificial filaments by passing solutions through an electrical field was patented in 1934 by Anton Formhals. In his design, a spinning wheel has been employed as one of the electrodes supplying the solution to the electrical field and an electrically conductive mobile device like a real has been employed as the other electrode collecting the filaments in parallel arrays, which can be unwound continuously [40]. In the apparatus patented by Simons in 1966, the polymer solution was discharged from a capillary point and the electrically spun filaments were collected on a revolving metal drum with holes on its surface. The fiber density was lower on the holes, which allowed the fabrication of non-woven fabrics with a certain pattern [41]. In 1971, Baumgarten studied the effect of solution viscosity, flow rate, applied voltage, and spinneret to collector spacing on the diameter of polyacrylonitrile fibers produced by a conventional electrospinner [42]. A list of common polymers that have been electrospun is given in Table 1-1.

Table 1-1 Polymers solutions that have been electrospun commonly

Polymer	**Polymer Concentration**	**Solvent**	**Source**
Nylon 6,6 (262.35 g/mol)	18 wt%	Formic Acid	[43]
Poly (Ɛ-caprolactone) PCL (M_n:80 000)	7-9 wt%	Methylene chloride/N,N-dimethylformamide (85/15, v/v)	[44]
Polydioxanone (PDS)	42-167mg/ml	1,1,1,3,3,3 hexafluoro-2-propanol (HFIP)	[45]
Polyglycolide (PGA) (M_w: 108,000)	8 wt %	1,1,1,3,3,3- hexafluoro-2-propanol (HFIP)	[46]
Poly(L-lactide)(PLA) (M_w: 14,000–20,000)	5 wt %	1,1,1,3,3,3- hexafluoro-2-propanol (HFIP)	
Poly(lactide-co-glycolide) (PLGA) (M_w: 450,000)	15 wt %	Chloroform	
Polyacrylic acid (PAA) (M_w 250 000)	6 wt.%	H_2O/Ethanol (Mass Ratios: 100/0, 50/50, and 0/100)	[47]

Poly(vinyl chloride) (PVC)	10-15 wt %	Tetrahydrofuran (THF)/ N,N-dimethylformamide (DMF) (100/0, 80/20, 60/40, 50/50, 40/60, 20/80, and 0/100 v/v)	[48]
Polystyrene (PS) (M_w: 140,000)	13 wt%	Tetrahydrofuran (THF)/N,N-dimethyl formamide (DMF) 100/0, 75/25, 50/50, 25/75 and 0/100 (v/v)	[49]
Poly (Ɛ-caprolactone) (PCL) (M_w: 80,000)	10 wt%	Chloroform	[50]
Polyurethane (M_w: 110,000)	25 wt%	Tetrahydrofuran (THF)/N,N-dimethylformamide (DMF) (70/30 v/v)	[38]
Poly(ethy1eneoxide) (PEO) (M_w, 2,000,000 g/mol)	0.5-3 wt%	Water	[51]
Poly(vinylalcoho1) (PVA) (M, 186,000 g/mol)	8 wt.% 16 wt.%	Water	
Cellulose acetate (CA) (M_w: 30,000 Da)	15 wt%	N,N-dimethylacetamide/acetone (1:2 mass ratio)	[52]
Type B gelatin from bovine skin	8.3 wt%	1,1,1,3,3,3 Hexafluoro-2-Propanol (HFP)	[53]
Type I collagen from calf skin	8.3 wt%		
Alpha-elastin	20 wt%		
Tropoelastin	20 wt%		
Type A Gelatin	5-12.5 % (w/v)	2,2,2-trifluoroethanol (TFE)	[54]

1.4.2. Description of Electrospinning Process

In conventional electrospinning, a syringe fitted with a blunted needle is filled with a polymer solution. Then, the syringe is installed in a syringe pump. A collector, which is a metal plate, is positioned at a certain distance from the needle tip. An electrical field is created between the collector and the needle tip by connecting the grounding and the positive electrodes of a

power supply to the collector and the needle, respectively [7]. A schematic of the electrospinning set-up and the formation of fibers is shown in Figure 1-1. A droplet of polymer solution at the tip of the needle adopts a semispherical shape due to surface tension [28].When the electrical field is created, charges are induced within the droplet. The repulsion between the induced charges creates shear stresses acting opposite to the surface tension. As a result, the droplet deforms into a cone, which is referred as Taylor cone. When the voltage creating the electrical field exceeds a critical value, the repulsion forces overcomes surface tension and a charged jet of polymer solution emanates from the conical droplet [55].The solution in the syringe is discharged to the electrical field at a certain feed rate by the syringe pump. There is a minimum feed rate to maintain the balance between the rate at which the solution is delivered and the rate at which the solution is drawn from the needle tip [56] [57]. The jet ejected from the conical droplet follows a straight line up to a certain distance from the needle, which is referred as the stable region. At the end of the stable region, the jet starts to bend and follows a path of spiraling loops increasing in diameter until the fibers are deposited on the collector, which is referred as unstable region [58] [59]. The columbic repulsion between the charges on the surface of the jet and the electrostatic force arising from the electric field stretches the jet as it travels towards the collector [60][61]. Especially, the bending of the jet in the unstable region causes the jet to be elongated extensively, which results in rapid reduction in the diameter of the jet [62]. The drop in jet diameter increases the area of the surface, which is in contact with the air surrounding the jet, and reduces the path for solvent molecules to diffuse outward from the jet [62]. As a result, the solvent evaporates rapidly and solidified nanofibers are deposited randomly on the collector [61] [62].

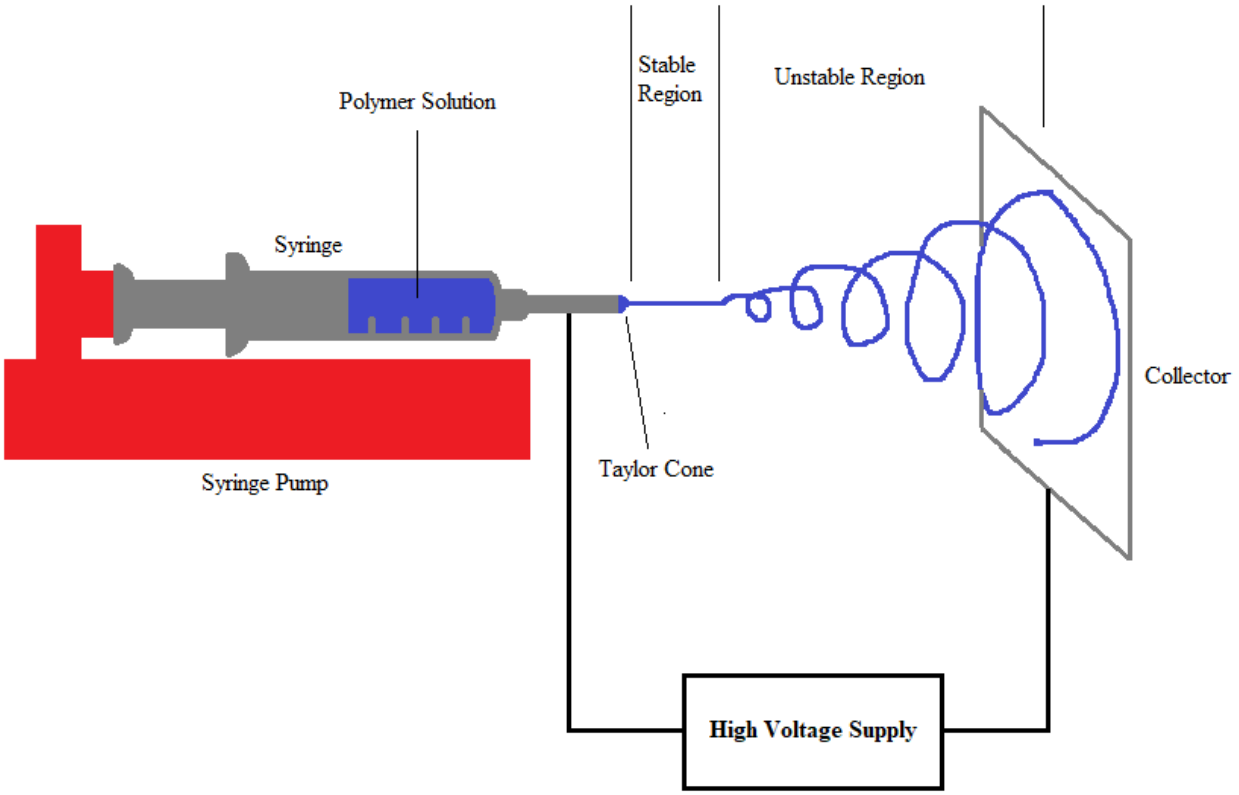

Figure 1-1: Schematic illustrating the formation of nanofibers with a conventional electrospinning set-up

1.4.3. The Effect of Electrospinning Parameters on Fiber Morphology

Morphology of the nanofibers can be altered by varying the parameters of electrospinning such as viscosity, applied voltage, flow rate and distance [7].

There is a range for the viscosity of an electrospinning solution at which continuous and bead-free fibers are formed [57]. J. Doshi reported that PEO fibers were successfully electrospun when the viscosity of the electrospinning solution is between 800 cP and 4000 cP [31]. For the viscosities lower than 800 cP, the electrospinning jet broke because the solution was too dilute to form a continuous jet. The electrospinning process was hampered at viscosities higher than 4000 cP because the solution dried at the needle tip [31]. Viscosity of the electrospinning solution has also a significant effect on the morphology of the fibers [63]. H. Fong et al. showed that beads on

electrospun PEO fibers disappeared when the viscosity of the solution is increased from 289 cP to 527 cP [64]. P. Baumgarten reported that the diameter of polyacrylonitrile fibers electrospun out of dimethyl formamide (DMF) increases as the viscosity of the electrospinning solution is increased [42]. The viscosity of a polymer solution increases with an increase in the molecular weight of the dissolved polymer or the concentration of the polymer solution, which both govern the entanglement of the polymer chains in a solution [27].

For the formation of continuous, bead-free, smooth fibers, there should be a sufficient level of polymer chain entanglement in the electrospinning solution [65] [57].Four concentration regimes have been introduced to refer to the degree of polymer chain entanglement in a solution, which are dilute, semidilute unentangled, semidilute entangled and concentrated concentration regimes in the order of increasing concentration [66]. In the dilute concentration regime, there is no overlap of polymer chains. The polymer chains start to overlap at a minimum concentration, which is referred as the critical chain overlap concentration and denoted as c* [67]. The critical overlap concentration is the concentration in which the transition from the dilute regime to semidilute unentangled regime occurs and it is inversely proportional to the intrinsic viscosity, [η] as it is shown in Eqn. 1 [67].

$$c^* \sim \frac{1}{[\eta]} \qquad \text{Equation 1}$$

Intrinsic viscosity of the polymer solution is related to the molecular weight of a linear polymer as it is shown by the Mark-Houwink-Sakurada equation (Eqn. 2), where the constants *K* and *a* depend on solvent, polymer, and temperature [68].

$$[\eta] = KM^a \qquad \text{Equation 2}$$

The crossover concentration between the semidilute unentangled and semidilute entangled regimes is referred as the critical entanglement concentration and denoted as c_e [66].

At the critical entanglement concentration, the polymer chains are entangled to a significant extent [67].

M. McKee et al. studied the effect of polymer chain entanglements on the morphology of the electrospun poly(ethylene terephthalate-*co*-ethylene isophthalate) (PET-co-PEI) fibers [69]. The electrospinning of the solutions, which are in the semidilute entangled regime, yielded beaded fibers whereas the electrospinning of the solutions, which are in the concentrated regime, yielded bead-free fibers [69]. This indicates that there is a minimum concentration for PET-co-PEI solutions at which the polymer chains entangle to the extent that continuous bead-free fibers are electrospun [69]. Gupta et al. reported that the electrospinning of poly(methylmethacrylate) PMMA/ dimethylformamide (DMF) solutions in semidilute entangled regime formed beads at a molecular weight of 12 470 g/mol [67]. When the molecular weight of PMMA is increased to 125 900 g/mol, uniform fibers were electrospun from the solutions in the semidilute entangled regime [67]. This demonstrates that the minimum concentration that is necessary to yield bead-free uniform fibers decreases as the molecular weight of the PMMA solution increases [67]. C. Ki et al. reported that the diameter of gelatin fibers increases as the electrospinning solution concentration increases [70]. Similarly, Z. Jun reported that the diameter of Poly-L-lactide (PLA) fibers decreases as the concentration of PLA in the electrospinning solution is reduced [71].

J. Lee et. al. reported that the diameter of the nanofibers electrospun from the aqueous solutions of poly(vinyl alcohol) (PVA) decreases as the applied voltage is increased [72]. The reason could be that an increase in voltage gives rise to a stronger electric field and greater columbic repulsion between the charges, which stretches the jet to a greater extent. As a result, the diameter of the fibers decreases [27] [63]. Conversely, S. Zhao et. al. reported increasing diameters for increasing applied voltages for ethyl-cyanoethyl cellulose fibers electrospun out of

tetrahydrofuran [73]. This has been attributed to the decrease in the speed of the jet due to the weaker electric field at lower voltages. As the jet speed decreases, the flight time increases, which allows the jet to be stretched for a longer period of time. Consequently, thinner fibers are obtained as the applied voltage is decreased down to the critical voltage required for jet initiation [73]. In another study, it has been reported that the Taylor cone receded into the syringe needle and beads are formed on the fibers electrospun from the solution of poly(ethylene oxide) (PEO)/water when the voltage is increased from 5.5 kV to 7 kV [74].

C. Wang et al. reported that the diameter of the nanofibers electrospun from the solution of poly(D,L-lactic acid) in dimethyl formamide (DMF) increases as the flow rate is increased [75]. Similarly, H. Hall et al. reported that the diameter of poly(D,L-lactic acid) fibers almost doubled when the flow rate is increased from 4 ml/h to 12 ml/h [76]. The reason for fibers to become thicker could be due to lower stretching of the jet at higher flow rates [77]. W. Zuo et al. reported that increasing flow rate did not change the diameter of poly(hydroxybutyrate-co-valerate) fibers [78]. However, it had a significant effect on the formation of beads such that the beads appeared on the fibers, when the flow rate is increased from 2 ml/h to 3.5 ml/h, and the further increase in flow rate caused the beads to become larger [78]. It has been also reported that beads are formed on polysulfone nanofibers electrospun out of N,N-dimethylacetamide/acetone solvent system, when the flow rate is increased from 0.40 ml/h to 0.66 ml/h [79]. The reason could be that the time for solvent evaporation was not enough to prevent the formation of beads at the higher flow rate [79]. Incomplete evaporation of the solvent at high flow rates may also result in formation of flat (ribbon-like) fibers [80].

C.S. Ki et al found that under constant electric field, diameter of the gelatin fibers electrospun out of formic acid did not change significantly, when the distance between the

needle tip and the collector is varied between 7.5 mm – 20 mm [70]. S. Zhao et al. reported that diameter of ethyl–cyanoethyl cellulose fibers electrospun out of tetrahydrofuran decreased as the distance is increased [73]. The reason could be that the decrease in the electric field strength due to the increase in distance results in a lower speed of jet flight, which allows the jet to be elongated for a longer period of time and the formation of thinner fibers [73]. On the other hand, T. Wang et al. reported that the diameter of the fibers electrospun from Polyacrylonitrile (PAN)/ N,N-dimethylformamide solutions decreased as the distance from the needle to the collector is reduced keeping all the other parameters constant [81]. This may be due to the greater stretching of the jet under a stronger electric field at a shorter distance [56] [63]. J. Lee et al. found that beads are formed on poly(vinyl alcohol) fibers electrospun out of water when the distance is reduced [72]. In another study, merged fibers of Naylon 6,6 with junctions are observed when the distance is reduced from 2 cm to 0.5 cm [27]. This may be due to the incomplete evaporation of the solvent at the shorter distance [27].

1.5. Natural and Synthetic Polymers as Tissue Engineering Scaffolding Materials

The material, which the scaffold is going to be made of, is an important choice, which determines the performance of the tissue engineering construct.

In native tissues, interactions between the ligands present on ECM components and integrins on the surface of the cells regulate cellular events such adhesion, proliferation and differentiation [8]. Therefore, natural polymers derived from native extracellular matrices are capable of promoting attachment, proliferation and differentiation of cells through the binding sites and ligands present in their structures [7] [14]. As a result, natural polymers such as

collagen and gelatin can be used to fabricate biocompatible and bioactive scaffolds, which resemble the native environment of the cells [8].

Type 1 collagen has a triple helix structure formed by the intertwining of three polypeptide chains, two α1 chains and one α2 chain [82]. The formation of the triple helix structure is possible due to the specific amino acid sequence of the chains, which consists of (Glycine)-X-Y repeats, where X and Y are often proline and hydroxyproline, respectively [3] of [82]. The alpha chains are synthesized separately by the expression of type I collagen alpha 1 and type I collagen alpha 2 genes [83]. Then, the chains are assembled into a triple helix and the resulting collagen molecule is secreted to the extracellular space, where the carboxy and amino terminal propeptides of the molecule are cleaved [84]. Next, the collagen molecules are assembled and crosslinked to form collagen fibrils [83]. Type I collagen, constitute around 20–40% of the bone matrix, which has a nanocomposite structure in which hydroxyapatite crystals are embedded in the space between collagen fibrils [85][86]. In addition to bone, Type 1 collagen is also present in other connective tissues such as skin, tendon and ligament [82].

Collagen is hydrolyzed in a controlled manner and gelatin is obtained from collagen [54]. Therefore, gelatin can be defined as a mixture of denatured collagen molecules at various molecular weights ranging between 15,000 and 400,000 [87]. There are two types of gelatin, which are Type A and Type B. The extraction and processing of Type A gelatin is done by acid pretreatment whereas Type B gelatin extracted and processed by alkaline pretreatment [54]. Type B gelatin has a higher content of carboxylic acid compare to Type A gelatin because glutamine and asparagine residues are converted into glutamic and aspartic acid during alkaline pretreatment [54]. Gelatin can absorb water 5 to 10 times its own weight. Therefore gelatin swells in water [87]. Gelatin dissolves in water at temperatures above 40°C and it forms a gel at

temperatures between 35 and 40°C. Bloom number is an indicative used to express the gel strength. As the molecular weight increases, gel strength and consequently the bloom number increases [87]. Gelatin has been electrospun into fibrous membranes for tissue engineering applications [88] [89].

The similarity between the electrospun nanofibers and the natural extracellular matrix can be further improved by electrospinning solutions of natural polymers such as collagen and gelatin. Binding sites on the collagen molecules, which the electrospun fibres are made of, can promote the formation of new tissue by regulating the cellular events such as adhesion, proliferation, migration and differentiation. Collagen has been electrospun into fibrous membranes for tissue engineering applications [90] [91] [92]. Gelatin has been electrospun into fibrous membranes for tissue engineering applications [88] [89]. However, the poor mechanical properties of natural polymers limit their use as a scaffolding material [14].

Alternative to natural polymers, biocompatible and degradable synthetic polymers with good mechanical properties can be used for the manufacturing of scaffolds. However, binding sites are absent in synthetic polymers [14]. Polycaprolactone is one of the biocompatible synthetic polymers, which has been electrospun into fibrous membranes for bone tissue engineering [50]. It is a semi-crystalline and hydrophobic polyester synthesized by the ring opening polymerization of ε-caprolactone. Its melting point and glass-transition temperature are 63°C and -60°C, respectively [17]. It is a slowly degrading polymer, whose degradation can take about two years [17].

Natural and synthetic polymers can be combined in one scaffold in order to overcome the limitations of each other [54]. The resulting hybrid scaffold would both have the binding sites,

which contributes to mimic the native extracellular matrix, and improved mechanical properties [54] [93].

1.5.1. Electrospun PCL/gelatin Scaffolds

In the literature, it has been reported that collagen denatures to gelatin during electrospinning due to the harsh solvents used to prepare the electrospinning solution and the resulting fibrous mat is soluble in water [94]. Therefore, gelatin, which has almost the same chemical composition as collagen and is commercially available with a lower cost, can be preferred as the polymer to be electrospun instead of collagen [95]. However, same as electrospun collagen, gelatin fibers also dissolve rapidly under normal cell culture conditions [93]. In order to impart stability, agents such as glutaraldehyde, genepin and glyceradehyde have been used to crosslink the electrospun gelatin fibers [93]. However, it has been found that there is a cytotoxicity associated with crosslinking agents [93]. On the other hand, the absence of binding sites and hydrophilicity of PCL lower cell affinity [15]. Therefore, electrospun composite fibers of gelatin and PCL have been studied by many researchers. In these composite fibers, PCL imparts stability in cell culture medium and gelatin promotes the attachment and growth of the cells through the binding sites in its structure [15].

Y. Zhang et al reported the contact angle of the PCL/Gelatin membrane electrospun from a solution with 1:1 PCL to gelatin weight ratio as 0°, which is much more hydrophilic than Gelatin only and PCL only electrospun membranes having contact angles of 76.5° and 109°, respectively. The diameter of the fibers ranged between tens of nanometers to approximately 1 um. In the same study, elastic modulus of PCL/Gelatin membrane was reported as 30.8 MPa, which is in between the Gelatin only and PCL only membranes having elastic moduli of 105 and 30.8 MPa, respectively [54].

In another study, the porosity of a PCL/Gelatin membrane, which has an average fiber diameter of 663 ± 107 nm, was calculated as 68% by using apparent and bulk densities. This mat lost 20% of its initial mass upon 5 days of in vitro degradation, then the rate of degradation reduced significantly resulting in around 25% overall mass loss after 14 days of degradation while PCL only nanofibrous mat did not demonstrate any mass loss during 14 days of degradation. ATR-FT-IR analysis for the degradation of the PCL/gelatin mat revealed that gelatin was broken down into its amino acids as a result of hydrolysis whereas ATR-FT-IR analysis for the PCL mat revealed that it did not degrade during 14 days of degradation [96].

Ghasemi-Mobarakeh et. al. electrospun a PCL membrane with an average fiber diameter of 431 ± 118 nm. The average fiber diameters for PCL/Gelatin membranes with 70:30 and 50:50 PCL to Gelatin ratio were reported as 189 ± 56 nm and 113 ± 33 nm, respectively. In the same paper, the pore diameter for the PCL fibers and PCL/Gelatin fibers was found to be around 1.70 and 1.00 um, respectively, which has been attributed to the reduction of pore size possibly due to the greater overlap of fibers as the fiber diameter decreases. It was also reported that the contact angle for the PCL/Gelatin fibers increased from 0° to around 32° as the PCL to Gelatin ratio of the fibers increases from 50:50 to 70:30. In the same study, the neuron cells found to grow and elongate parallel to the fiber orientation on aligned PCL/Gelatin (70:30) fibers. The proliferation of neuron cells after 6 days of cell seeding on aligned PCL/Gelatin (70:30) fibers were found to be at least around 30% higher than the random PCL/Gelatin (70:30), aligned and random PCL fibers. This suggests that the elongation of the cells parallel to the aligned fibers and the presence of gelatin on the fiber surface, which is confirmed by ATR-FTIR analysis, improve the proliferation of neural cells significantly [15].

Heydarkhan-Hagvall et. al. reported that electropsun pure gelatin membranes with fiber

diameters of 0.66 ± 0.25 um and 0.59 ± 0.09 um have a Young's modulus of 3.72 ± 1.40 MPa and 24.54 ± 3.41 MPa, respectively indicating that Young's modulus is increasing with decreasing fiber diameter. In the same paper, PCL/Gelatin fibers with 1:1 PCL to gelatin ratio, which are 0.88 ±0.09 um in diameters, has been reported to have a Young's modulus of 138.34 ± 11.42 MPa [97].

Guarino et. al. has been reported that gelatin content in electrospun PCL/Gelatin fibers, which are 0.536 ± 0.230 um in diameter, are preserved more during 6 days of degradation compared to porous PCL/Gelatin films containing porous PCL domains with an average pore size of 5.19 ± 1.67 um and non-porous gelatin domains. In IR Spectra of the fibers, the characteristic peaks of the protein were present with reduced intensity during 6 days of degradation whereas the peaks almost disappeared after 1 day of degradation in PCL/Gelatin films. Human mesenchymal cells were found to attach better on PCL/Gelatin fibers compared to PCL fibers in the first 24 hours indicating the promotion of cell attachment in the presence of gelatin. In the same study, it has also been shown that the hMSCs attached more on PCL/Gelatin and PCL fibers than the PCL/Gelatin and PCL films in the first 24 hours, demonstrating the contribution of the fibrous texture of the material to cell adhesion. It has also been reported that cell viability increased in the order of PCL films, PCL/Gelatin films, PCL fibers and PCL/Gelatin fibers validating the contribution of the presence of gelatin and fibrous structure on cellular growth [93].

D. Kai et al reported that an electrospun PCL membrane, which has an average fiber diameter of 430 ± 108 nm, with randomly distributed fibers, was hydrophobic with a contact angle of 146.5 ± 2.6° whereas randomly distributed PCL/Gelatin fibers with 239 ± 37 nm fiber diameter were hydrophilic with the complete adsorption of the droplet. No significant difference

between the diameters of the random and aligned fibers of PCL or PCL/Gelatin has been reported. In aligned PCL/Gelatin fibers, the contact angle measured perpendicular and parallel to fiber orientation was found to be 71.2 ± 9.1° and 43.5 ± 5.6°, respectively indicating that the contact angle changes depending on the fiber orientation. It has been reported that the elastic modulus of the randomly distributed PCL/Gelatin fibers was found to be 21.96 ± 1.09 MPa, which is around two times higher than the elastic modulus of PCL fibers, in dry state and reduced to 1.45 ± 0.20 MPA after it is soaked in PBS. Aligned PCL/Gelatin fibers was found to have an elastic modulus of 48.91 ± 14.23 MPa perpendicular to the fiber orientation, which is around 5 times higher than the elastic modulus measured parallel to fiber orientation as 10.30 ± 1.50 MPa. After soaked in PBS, aligned PCL/Gelatin fibers were found to have an elastic modulus of 5.41 ± 0.61 MPa perpendicular to fiber orientation, which is much less than the elastic modulus of aligned PCL fibers in wet state having a value of 24.8 ± 3.02 MPa perpendicular to fiber orientation. The FTIR spectra of PCL and PCL/Gelatin fibers confirmed the decrease of PCL content in PCL/Gelatin fibers compared to PCL fibers through the reduction in strength of the peaks for PCL. In addition, the characteristic peaks of gelatin in FTIR spectra of PCL/Gelatin fibers confirmed the presence of gelatin on the fiber surface [98].

Crystallinity of gelatin, PCL and PCL/Gelatin fibers were examined by Gautam et. al. Gelatin fibers did not show any peaks in their XRD pattern indicating the amorphous nature of gelatin whereas XRD pattern of PCL fibers displayed peaks indicating the crystalline nature of PCL. XRD pattern for PCL/Gelatin fibers showed all the characteristic peaks of PCL fibers with a lower intensity indicating the reduced crystallinity of the PCL/Gelatin fibers compared to PCL fibers. Assessment of mouse fibroblast proliferation on PCL and PCL/Gelatin fibers revealed that proliferation on PCL/Gelatin fibers is around 9 times higher than it is on PCL fibers [99].

Fu et al. fabricated PCL/Gelatin fibers with 1:1 PCL to gelatin ratio at a fiber diameter of 386.9 ± 102.5 nm. The PCL/Gelatin fibers were found to be hydrophilic with 0 contact angle and complete absorption of the droplet. Elastic modulus for the PCL/Gelatin fibers in wet state dropped from 1.49 ± 0.06 MPa to 0.75 ± 0.15 MPa after six weeks of *in vivo* degradation [100].

A PCL/Gelatin electrospun membrane with 1:1 PCL to gelatin ratio was fabricated at an average fiber diameter and pore size of of 409 ± 88 nm and 7.2 ± 1.5 μm, respectively by Duan et al. The elastic modulus of the membrane during two weeks of incubation and the elastic modulus of the membrane seeded with human keratinocytes after 1 week of incubation in culture medium were similar and found to be around 1.5 MPa. In the same study, around 95% recovery for mouse skin wounds obtained for the PCL/Gelatin membrane and the human keratinocyte seeded PCL/Gelatin membranes [101].

PCL/Gelatin fibers were elecetrospun from solutions of the same total concentration but with varying PCL to gelatin ratio. It has been reported that the viscosity and the conductivity of the solution decreases and increases, respectively as the gelatin content increases. It has been reported that the fiber diameter is around 200 nm and did not change significantly with the variations in gelatin content of the fibers. The contact angles for the PCL/Gelatin fibers were found to be around 140°, 70°, 60° and 0° for the fibers with 100:0, 70:30, 60:40 and 50: 50 PCL to gelatin ratio, respectively, indicating that the fibers become more hydrophilic as the gelatin content of the fibers increases. Remaining mass for the fibers after 12 weeks of degradation were found to be around 100%, 60%, 40% and 30%, for the fibers with 100:0, 70:30, 60:40 and 50: 50 PCL to gelatin ratio, respectively, indicating that mass loss upon degradation increases with increasing gelatin content of the fibers. In the same study, hMSCS were found to proliferate the most on fibers with 70:30 PCL to Gelatin ratio compared to fibers with PCL to gelatin ratio of

50:50 and PCL fibers [4].

Zheng et. al. measured the Young's modulus of Gelatin/PCL fibers with 70:30, 50:50 and 30:70 Gelatin to PCL ratio in wet state as around 0.5, 1.5 and 3.5 MPa, respectively, indicating that the elastic modulus increases as the PCL content of the fibers increases. It has been reported that hydrophilicity decreases as the PCL content of the Gelatin/PCL fibers increases, which is demonstrated by the contact angles of 0°, 10.8° and 32.7° measured for Gelatin/PCL fibers with 70:30, 50:50 and 30:70 Gelatin to PCL ratios [102].

It has been reported that the ECM deposition and Young's modulus after three weeks *in vivo* implantation for the construct, which is prepared by culturing chondrocytes and Gelatin/PCL fiber layers with 30:70 gelatin to PCL ratio, were found to be less than it is for the constructs with 70:30 and 50:50 gelatin to PCL ratio. This indicates that higher PCL content discourages early cartilage formation. However, when the constructs were implanted for 12 weeks, it has been seen that there wasn't any significant difference in terms of ECM deposition and Young's modulus indicating that higher PCL content does not hinder long term cartilage formation [102].

Kuppan et. al. reported the elastic modulus of the aligned Gelatin/PCL fibers (7:3 PCL to gelatin ratio), which are 155 ± 55 nm in fiber diameter, in axial direction as 36 ± 5.0 MPa, which is less than the aligned PCL fiber modulus of 81 ± 2.0 MPa in axial direction. The elastic modulus of the Gelatin/PCL fibers was found to be significantly less in circumferential direction compared to its axial modulus and measured as 1.84 ± 0.56 MPa. The contact angle for the aligned Gelatin/PCL and PCL fibers were reported as and 0° and 128.2 ± 0.1°, respectively, indicating increased hydrophilicity resulting from the presence of gelatin in the fibers. It has been reported that aligned PCL and PCL/Gelatin fibers losses 15% and 36% of their initial

masses over 5 weeks of *in vitro* degradation, respectively. Young's modulus of aligned PCL/Gelatin fibers was found to be 36 ± 5.1 MPa, increased to 53 ± 13 MPa after 1 week of *in vitro* degradation and did not change after the 2nd week of degradation. On the other hand, the Young's modulus of aligned PCL fibers after 2 weeks of degradation was found to be higher than it is for aligned PCL/Gelatin fibers and reported as 70 ± 19 MPa [103].

Z. Guo et. al. reported that the electrospinning of aligned and randomly distributed PCL/Gelatin fibers from solutions with 1:2, 1:1 and 2:1 PCL to gelatin weight ratio yielded fibers with similar fiber diameters ranging between 334.96 ± 41.43 nm and 363.78 ± 50.49 nm. It was found that elastic modulus of aligned and randomly distributed PCL/Gelatin fibers with 1:2, 1:1 and 2:1 PCL to gelatin ratios found to be statistically not different and ranging between 30.45 ± 9.15 MPa and 45.34 ± 9.34 MPa. It has been reported that the proliferation and ALP activity of MC3T3-E1 cells were higher on aligned PCL/Gelatin fibers compared to randomly distributed PCL/Gelatin fibers [104].

L. Chong electrospun solutions having the same PCL concentration of 10% (w/v) but varying gelatin concentrations of 2%, 4% and 8% (w/v). The resulting mats had average fiber diameters of 15.9 nm, 87.7 nm and 547.6 nm and pore sizes of around 25 nm, 175 nm and 50 nm for 12%, 14% and 18% (w/v) total concentrations, respectively. ATR-FTIR analysis of PCL/Gelatin fibers (10:4 PCL to Gelatin ratio) confirmed the presence of gelatin through the peaks of amide groups and demonstrated the decrease in PCL content of the PCL/Gelatin fibers compared to PCL fibers through the peaks for PCL with reduced intensity. The contact angles for the fibers with the same PCL concentration of 10% (w/v) but varying gelatin concentrations of 2%, 4% and 8% (w/v) were found as 98 ± 2.0°, 49.5 ± 3.2° and 0°, respectively indicating that the hydrophilicity increases as the gelatin content of the fibers increases. The weight loss for the

PCL/Gelatin fibers (10:4 PCL to Gelatin ratio) was reported as 3.3 ± 1.1% and 15.5 ± 2.0% for 7 and 14 days of in vitro degradation, respectively whereas PCL fibers did not lose weight over 14 days degradation [105].

R. Yao fabricated PCL/Gelatin fibers with the 4:1, 2:1, 1:1, 1:2 and 1:4 PCL to gelatin weight ratios and found that mesenchymal stem cell viability on these fibers increased throughout 6 days of culture for all the weight ratios, indicating fibers with all the different weight ratios are biocompatible. It has been reported that there wasn't a significant difference in optical densities between the fibers with different PCL to gelatin weight ratio at the end of 6 days of culture, indicating that PCL to gelatin ratio of the fibers did not affect the viability of mesenchymal stem cells significantly [106].

The viability of epithelial cells on aligned and randomly distributed PCL/Gelatin fibers, which have the average fiber diameters of 155 ± 55 and 242 ± 30 nm, respectively, was found to be significantly higher compared to the epithelial cell viability on aligned and randomly distributed PCL fibers, which may be attributed to the exposure of the RGD motif on gelatin in fibers to the cells. No significant difference for the epithelial cell viability has been reported between the aligned and randomly distributed PCL/Gelatin fibers [107].

It has been reported that PCL fibers and PCL/Gelatin fibers with 9:1, 8:2 and 7:3 PCL to Gelatin weight ratio remain 100%, 95%, 85% and 75% of their initial masses after 90 days of *in vitro* degradation, which indicates that the mass loss is resulting from the leaching of gelatin considering that the pure PCL fibers did not lose any weight during degradation. The contact angles for of PCL/Gelatin fibers with 9:1, 8:2 and 7:3 PCL to Gelatin weight ratios found to be increasing after 90 days of *in vitro* degradation to around 130°, which is the contact angle for pure PCL fibers. This indicates that PCL/Gelatin fibers become as hydrophobic as pure PCL

fibers at the end of 90 days of *in vitro* degradation regardless of the initial Gelatin content in the fibers. It has been reported that the Young's modulus of the PCL/Gelatin and PCL/Collagen fibers with 9:1 PCL to natural polymer ratio increases steeply during roughly the first 5 days of *in vitro* degradation from around 45 MPa and 40 MPa, respectively to approximately 60 MPa and decreases back to their initial values at the end of 90 days of degradation [108].

Gelatin and Gelatin/PCL fibers with 50:50 and 25:75 weight ratios were found to be more hydrophilic with contact angles around 50° than the PCL fibers at a contact angle of around 85° [109]. In the FTIR spectra of Gelatin/PCL fibers, the area under the amide 1 and ester peaks, which are the characteristic peaks of gelatin and PCL, respectively, was integrated and the ratio of these areas were used to determine the gelatin to PCL ratio of the fibers. By applying this method, it has been found that gelatin to PCL ratio of the fibers, which were electropsun from the solutions with 50:50 and 25:75 Gelatin to PCL ratios, are 0.46:0.54 and 0.32:0.68, respectively. This confirms that the Gelatin to PCL ratio of the fibers can be adjusted by adjusting the PCL to gelatin ratio of the electrospinning solution [109].

FTIR quantitative analysis of PCL/Gelatin fibers electrospun from acetic acid doped solution of PCL and Gelatin at 50:50 weight ratio revealed that the gelatin content in fibers stayed constant at 50% during 5 hours of electrospinning. On the other hand, the gelatin content in fibers electrospun from the solution that does not contain acetic acid stays constant at 50% during the first hour, dips down to 30% between 2-3 hours and rises up to around 60% between 4-5 hours, which indicates that acetic acid mediated PCL-Gelatin miscibility is essential to prevent phase separation in the electrospinning solution and to keep the Gelatin to PCL ratio of the fibers constant throughout electrospinning. For the PCL/Gelatin fibers electrospun from the acetic acid doped solutions and collected at different 1 hour time intervals of 5 hours

electrospinning, mouse fibroblast cell attachment and proliferation did not change significantly. On the other hand, it has been reported that the attachment and proliferation of mouse fibroblast cells on PCL/Gelatin fibers collected in the last hour of 5 hour electrospinning is significantly higher than the fibers collected during the first one and two hours of electrospinning. This might be attributed to the higher gelatin to content of the fibers collected in the last hour of electrospinning, which results from phase separation at the absence of acetic acid. It has been found that mouse fibroblast and HaCaT cell proliferation on Gelatin/PCL fibers increases in the order of 30:70, 50:50 and 70:30 gelatin to PCL ratio of the fibers indicating that cell proliferation is promoted to a greater extent by higher gelatin content in fibers [110].

In the literature, the phase separation behavior of gelatin and PCL was explained by two interrelated mechanisms. The first mechanism is based on the fact that protein solubility decreases as the isoelectric point of the protein and the pH of the solution become closer to each other. For a PCL/Gelatin (50:50 PCL to gelatin weight ratio) solution in TFE, the isoelectric point of the gelatin and the pH of the solution were found as 6.14 and 5.64, respectively, and close enough to render gelatin and PCL immiscible in each other. After the solution is doped with 0.2% (v/v) acetic acid with respect to TFE, the pH of the solution decreases to 4.4, which is a pH value far away from the isoelectric point, rendering gelatin soluble. The second mechanism is based on the fact that a homogenous solution of gelatin forms when the gelatin chains are stretched out rather than being contracted. The presence of hydrophobic PCL molecules in the solution causes gelatin molecules to be in contracted form where hydrophobic groups on the gelatin molecules are present on the surface and the polar protic groups are present at the interior of the molecule. Gelatin molecules that are hydrophobic at the surface adhere to each other over time and form aggregates that are heavy enough to settle down. The addition of acetic acid at

0.2% (v/v) with respect to TFE causes the pH to drop and amino groups on gelatin molecules to be protonated. The positively charged gelatin chains stretch out and penetrate into PCL chains, which cause gelatin and PCL molecules to be homogenously distributed throughout the solution [111]. Dynamic Light Scattering (DLS) analysis of the PCL/Gelatin solution (50:50 PCL to gelatin weight ratio) revealed that the particle size increases significantly from 0 to around 40000 nm by the end of 40 minutes of time period which confirms that phase separation occurs [111]. Only the characteristic bands of gelatin were found to be present in the FTIR spectra of the sediment, which indicates that only gelatin settles out as phase separation occurs [111]. It has been demonstrated that the miscibility of the Gelatin and PCL phases can be improved and a homogenous solution of PCL and Gelatin in TFE can be obtained by introducing a tiny amount of acetic acid to the solution by analyzing the transmittance of PCL/Gelatin solutions (50:50 PCL to gelatin weight ratio) before and after the introduction of acetic acid. Transmittance of the Gelatin/PCL solutions in TFE without acetic acid found to be 0, whereas it increases significantly to around 70% by doping the solution with 0.1% (v/v) acetic acid with respect to TFE and it goes up to around 90% upon the introduction of acetic acid at 0.2% and 0.3% (v/v) with respect to TFE [111]. ATR-FTIR spectroscopy of the Gelatin/PCL fibers electrospun without acetic acid revealed that the gelatin content of the fibers shows variations due to phase separation. The gelatin content decreases to around 30% after 2.5 hours of electrospinning and rises up to 65% at the end of 5 hours [111]. Young's modulus of the Gelatin and PCL only fibers were found to be around 45 MPa and 2 MPa, respectively. The Young's modulus of the Gelatin/PCL fibers at 50:50 PCL to gelatin ratio was found to be around 30 MPa regardless of whether the electrospinning solution is acetic acid doped with various amount of acetic acid (0.1%, 0.2% and 0.3% (v/v) with respect to TFE) or not [111].

It has been reported that the conductivity, viscosity and pH of an electrospinning solution composed of PCL and Gelatin (50:50 PCL to Gelatin weight ratio) at a total concentration of 10% (w/v) in TFE changed significantly after the introduction of 0.3 % (v/v) 10M NaOH solution with respect to TFE. The conductivity increased from 23.8 to 100 uS/cm, the viscosity dropped from 298.7 to 186.0 cP and the pH increased from 5.5 to 8.3. No significant difference between the diameters of the fibers electrospun with and without alkali doping reported despite the changes in solution conductivity and viscosity [112]. Prevention of phase separation in PCL-Gelatin solutions by alkali and acid doping was demonstrated by optical transmittance, dynamic light scattering (DLS), differential scanning calorimetry (DSC) and X-ray diffraction (XRD) analyses. Optical transmittance analysis revealed that the solution formed by dissolving PCL and gelatin in TFE has zero transparency, which indicates that PCL and gelatin are immiscible in the absence of NaOH. Doping the solution with 0.3 % (v/v) 10 M NaOH with respect to TFE rendered PCL and gelatin miscible, which is indicated by around 90% transparency. DLS analysis revealed that the particle size range dropped from 550.3 - 7579.0 nm to 49.0 - 396.9 nm upon the addition of 10 M NaOH. XRD analysis revealed that the intensity of the characteristic peaks of PCL in PCL/Gelatin fibers electrospun with alkali doping is lower than the peaks of the fibers electrospun without alkali doping. This demonstrates that the crystallinity of PCL reduced more for the PCL/Gelatin fibers electrospun with alkali doping as a result of improved miscibility of PCL and gelatin and homogenous integration of gelatin chains into PCL chains in the electrospun fibers. DSC analysis confirms the miscibility of PCL and gelatin through the 2.1 °C difference between the melting points of PCL fibers and PCL/Gelatin fibers electropsun from the alkali doped solution and the absence of transition signals arising from pure PCL and Gelatin phases [112]. PCL/Gelatin fibers electrospun from the alkali doped solution found to be more

hydrophilic with a contact angle of 0° compared to PCL and PCL/Gelatin fibers electropsun without NaOH, which have contact angles of 98.2° and 11.0°, respectively. This demonstrates that the wettability of Gelatin/PCL fibers can be further improved by ensuring the homogenous distribution of PCL and gelatin in the fibers [112]. It has been reported that Young's modulus can be increased by ensuring PCL and Gelatin miscibility, which is indicated by the increase in Young's modulus upon alkali doping from 59.0 ± 11.5 MPa to 154.7 ± 12.9 MPa and from 3.3 ± 1.3 MPa to 14.1 ± 4.2 MPa in dry and wet states, respectively [112]. It has been found that the proliferation of iPSC-MSCs can be improved by ensuring the homogenous distribution of PCL and gelatin in the fibers, which is indicated by higher cell proliferation on the fibers electrospun from the alkali doped Gelatin/PCL solution compared to the proliferation on PCL/Gelatin fibers electrospun at the absence of NaOH [112].

In summary, the disadvantages of the conventional methods used to regenerate tissues were discussed briefly. Next, how tissue engineering can obviate the need for tissue transplantation was mentioned. The individual components of tissue engineering, which are the scaffold, cells and the growth factors, were discussed. Next, how the unique properties of nanofibers can be utilized in tissue engineering and the superiority of electrospinning over other scaffold fabrication techniques were explained. Then, the history of electrospinning was mentioned briefly. Next, the principles governing of the electrospinning process, as well as the effects of various parameters on the morphology of electrospun fibers were discussed. Then, both advantages and disadvantages of natural and synthetic polymers as scaffolding materials were mentioned. Finally, the studies regarding the electrospun PCL/Gelatin membranes, which possess the advantages of both natural and synthetic polymers, were reviewed.

1.6. Objective of This Thesis

As it is mentioned before, the degradation profile, mechanical properties, and hydrophilicity are important characteristics of a tissue engineering scaffold, which influence the performance of the scaffold significantly. Therefore, elucidating how the surface area of electrospun PCL/Gelatin membranes affects the degradation profile and the effect of degradation on mechanical properties and hydrophilicity is crucial to understand the structure-property relationships in electrospun PCL/Gelatin scaffolds.

Q. Zhang et al. found that the reduction in molecular weight, mass and compressive modulus of degraded PCL scaffolds was severer for those with higher porosity [113]. This indicates that the degradation is accelerated for scaffolds with high porosity. J. Širc et al demonstrated that porosity and surface area of electrospun membranes increases as the fiber diameter decreases [114]. However, there has been no study conducted to investigate the effect of surface area of electrospun PCL/Gelatin membranes on degradation profile.

In this study, the surface area of PCL/gelatin membranes was tuned by changing the fiber diameter. PCL/Gelatin membranes at three different fiber diameters were fabricated by electrospinning PCL/Gelatin solutions at three different concentrations. Then, each membrane was degraded in order to see the effect of fiber diameter on degradation profile. Next, the effect of degradation on mechanical properties and hydrophilicity of the electrospun PCL/Gelatin membranes was investigated.

2. Materials and Methods

2.1. Materials

Polycaprolactone (PCL) in pellet form with average M_n of 80,000 g/mol (CAS Number: 24980-41-4, Product Number: 440744) and type A gelatin in powder form that was obtained from porcine skin at a gel strength of 300 g bloom (CAS Number: 9000-70-8, EC number: 232-554-6) were purchased from Sigma-Aldrich. 2,2,2-Trifluoroethanol (catalogue no: AAA1078818, purity ≥ 99%) and Glacial Acetic Acid (catalogue no: A38-500, purity >95% weight) were purchased from Fisher Scientific and used without any further modification.

Phosphate buffered saline (PBS), which was used for the hydrolytic degradation of electrospun membranes, was prepared by dissolving KCl (J.T. Baker, Lot No: 35051), NaCl (PCode: 1002427394, Sigma Aldrich), Na_2HPO_4 (Fisher Scientific, Lot No: 140471), and KH_2PO_4 (Fisher Scientific, Lot No: 141121) at the concentrations of 2.7 mM, 137 mM, 10 mM, and 1.8 mM in distilled water.

2.2. Methods

2.2.1. Preparation of the Electrospinning Solutions

PCL/Gelatin solutions with 1:1 PCL to gelatin weight ratio were prepared at the total polymer concentrations of 6%, 10% and 14% (w/v). First, PCL and gelatin were dissolved separately in 2,2,2-Trifluoroethanol (TFE) at the concentrations of 6%, 10% and 14% (w/v). The PCL pellets and the gelatin powder were incubated in TFE for at least 12 hours and completely dissolved. Then, each solution was vortexed at the maximum speed for 2 minutes. The resulting transparent PCL and gelatin solutions having the same concentration were blended at a ratio of 1:1. For example, 6% (w/v) gelatin solution was blended with 6% (w/v) PCL solution. After 2

minutes of vortexing at the maximum speed, the blended PCL and gelatin solutions were appeared to be cloudy and non-transparent and separated into two phases over time. The dissolved gelatin and PCL the bottom and upper layers, respectively. In order to prevent phase separation, acetic acid at a concentration of 2.4 % (v/v) with respect to TFE was introduced in each blended PCL/Gelatin solution. After 2 minutes of vortexing at the maximum speed, all the solutions cleared up, became transparent, and remained transparent and homogenous permanently. The appearances for the individual PCL and gelatin solutions the cloudy PCL/gelatin solution at the absence of acetic acid, the phase separation of PCL/gelatin solution at the absence of acetic acid and the homogenous PCL/gelatin solution with 2.4 % (v/v) acetic acid doping are shown in Figure 2-1.

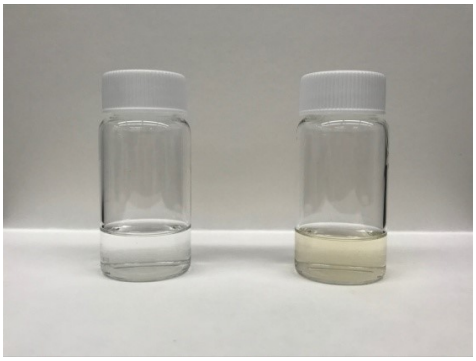

a) 10% (w/v) PCL (left) and 10% (w/v) gelatin (right) solutions

b) The cloudy 10% (w/v) PCL/gelatin solution with 1:1 PCL to gelatin ratio without acetic acid doping

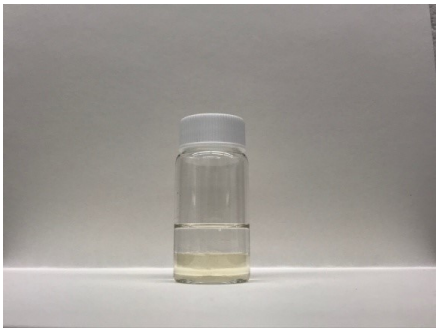

c) The phase separation of 10% (w/v) PCL/gelatin solution with 1:1 PCL to gelatin ratio without acetic acid doping

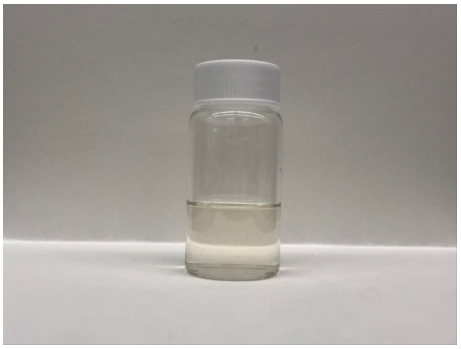

d) The homogeneous 10% (w/v) PCL/gelatin solution with 1:1 PCL to gelatin ratio after 2.4 % (v/v) acetic acid doping

Figure 2-1 The appearance of individual PCL and gelatin solutions (a), the cloudy PCL/gelatin solution at the absence of acetic acid (b), the phase separation of PCL/gelatin solution at the absence of acetic acid (c), and homogenous PCL/gelatin solution with 2.4 % (v/v) acetic acid doping (d)

2.2.2. Electrospinning of the PCL/gelatin Membranes

Three types of PCL/Gelatin membranes were prepared by electrospinning PCL/Gelatin solutions (1:1 PCL to Gelatin ratio) at three different total polymer concentrations of 6%, 10% and 14% (w/v). The electrospinning equipment used in study is shown in Figure 2-2 2.For the electrospinning of the membranes, the electrospinning solution was loaded into a 1 ml BD plastic syringe fitted with a 19 Gauge blunted needle. Then, the syringe was installed into a syringe

pump (Legato 101, by GENEQ Inc., Montreal, Quebec), which was placed across a metal plate horizontally at a distance of 12 cm. The metal plate served as the collector for the fiber deposition and it was wrapped with aluminum foil, which was covered with PTFE to create a non-sticky surface for the easy removal of the deposited fibers. The positive and negative electrodes of a voltage supply (model ES30P-5W/DDPM, by Gamma High Voltage Research, Inc., Ormond Beach, Florida, USA) were clipped to the needle and the collector, respectively. A voltage of 15 kV was applied and the solution was discharged to the electrical field at a constant rate of 0.5 ml/h. The electrospinning process was conducted inside a fume hood at 20°C and 4% humidity. The electrospinning equipment described above is shown in Figure 2-2.

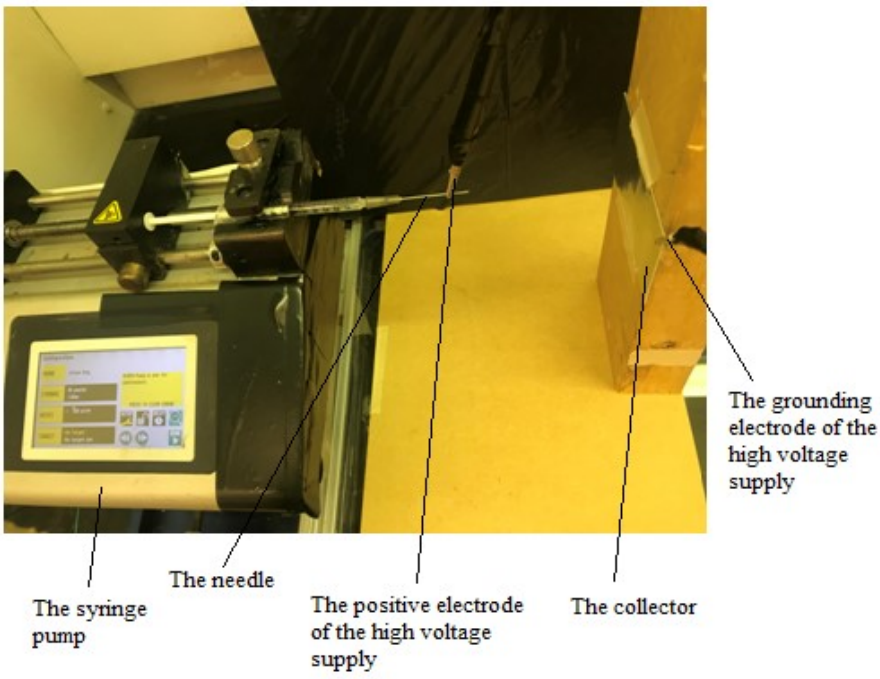

Figure 2-2 The electrospinning set-up

2.2.3. Determination of Average Diameters for the Electrospun PCL/gelatin Membranes

Samples cut from five different regions on the electrospun PCL/Gelatin membranes were carbon coated and imaged by Scanning Electron Microscopy (SEM) with the instrument Zeiss Sigma 300 VP-FESEM. The SEM micrographs were processed by Image J. software and the fiber diameter for each electrospun membrane was calculated as the average of at least 100 fibers.

2.2.4. In Vitro Degradation of the Electrospun PCL/gelatin Membranes

Rectangular samples with the dimensions of 1 x 7.5 cm were cut from the electrospun PCL/Gelatin membranes for gravimetric analysis and tensile test. The samples were incubated in PBS at 37°C for 1, 3, 6 and 10 days. At the end of each incubation period, the samples were dried in a vacuum oven at 40°C for 21 hours. The degradation of the rectangular electrospun PCL/gelatin sample is shown in Figure 2-3-a. For the gravimetric analysis of the in vitro degradation, the samples were weighted before degradation and after drying. The remaining mass after degradation was calculated as it is shown in Equation 1 by averaging the remaining mass values of 5 samples prepared for each of the 15 groups with the degradation periods of 0, 1, 3, 6 and 10 days and the total polymer concentrations of 6%, 10% and 14% (w/v).

$$\textbf{Remaining Mass}\% = \frac{\textbf{Wbefore degradation (mg)} - \textbf{Wafter degradation (mg)}}{\textbf{Wbefore degradation (mg)}} \textbf{x100} \qquad \textbf{Equation 1}$$

In order to study the effect of degradation on fiber diameter, electrospun PCL/Gelatin membranes were removed as a whole from the aluminum foil and incubated in PBS at 37°C for 1, 3, 6 and 10 days. The degradation of the electrospun PCL/gelatin membrane is shown in Figure 2-3-b. At the end of each incubation period, the membranes were dried in a vacuum oven at 40°C for 21 hours. Then, the average fiber diameter for each of the 15 types of electrospun

PCL/Gelatin membranes with the degradation periods of 0, 1, 3, 6 and 10 days and the total polymer concentrations of 6%, 10% and 14% (w/v) was calculated by following the procedure described in Section 2.2.3.

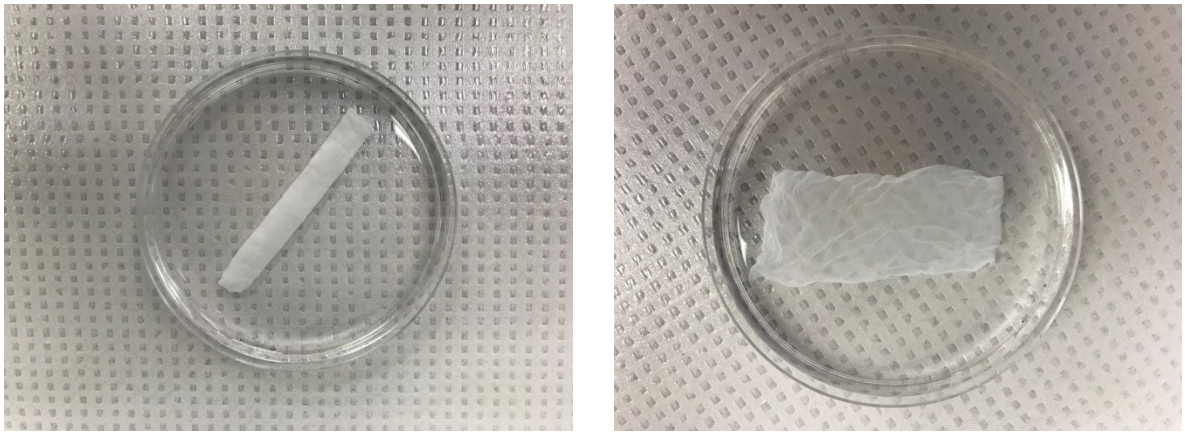

a) The degradation of the electrospun PCL/gelatin sample for gravimetric analysis and tensile test

b) The degradation of the electrospun PCL/gelatin membrane for fiber diameter measurement

Figure 2-3: The degradation of the electrospun membranes for tensile test and fiber diameter measurment

2.2.5. Mechanical Properties of the Electrospun PCL/gelatin Membranes

Tesile test applied to the rectangular specimens with the dimensions of 1 x 7.5 cm cut from the electrospun PCL/Gelatin membranes before and after the specimens were degraded for 1, 3, 6 and 10 days and dried in a vacuum oven at 40°C for 21 hours. The tests were conducted with ES Series III ElectroForce tensile testing machine (BOSE, Framingham, Massachusetts, USA) equipped with a 10 N load cell at a cross-head speed of 10 mm/min. A rectangular sample of electropsun PCL/Gelatin installed in the tensile test machine is as it is shown in Figure 2-3. The strain was calculated as it is shown in Equation 2. The stress was calculated as it is shown in Equation 3 and Equation 4, where ε, Δl, L, σ, σ_{sp}, ρ_{fiber}, F, W, and ρ_{areal} are the strain, change in

the length of the sample, initial length of the sample, stress, specific stress, the density of one fiber, applied force, width of the sample and areal density of the sample, respectively.

$$\varepsilon = \frac{\Delta l}{L} \qquad \textbf{Equation 2}$$

$$\sigma = \sigma_{sp} \, x \, \rho_{fiber} \qquad \textbf{Equation 3}$$

$$\sigma_{sp} = \frac{F}{W} x \frac{1}{\rho_{Areal}} \qquad \textbf{Equation 4}$$

The elastic modulus and the yield strength were calculated for each of the 15 groups with the degradation periods of 0, 1, 3, 6 and 10 days and the total polymer concentrations of 6%, 10% and 14% (w/v). The elastic modulus was calculated as the slope of the linear portion of the strain-stress curve. The yield strength was calculated with the 0.2% offset rule.

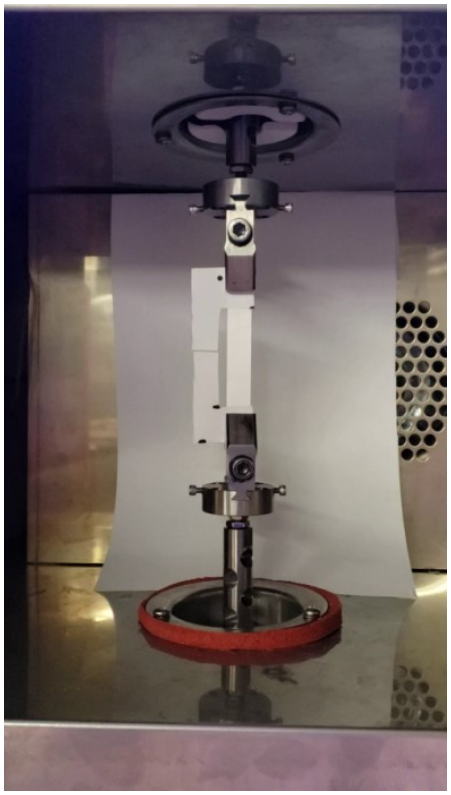

Figure 2-3 Rectangular sample of electropsun PCL/gelatin prepared for tensile test

2.2.6. Water Contact Angle Measurements

Hydrophilicity for each of the 15 types of electrospun PCL/Gelatin membranes with the degradation periods of 0, 1, 3, 6 and 10 days and the total polymer concentrations of 6%, 10% and 14% (w/v) was determined through contact angle measurements. The images of water droplets (~4 μL) on the electropsun membrane surfaces were collected by a drop shape analyzer (Krüss DSA 100E, Hamburg, Germany) shown in Figure 2-4. For each membrane type, the average value of the contact angles measured at three different locations on the membrane surface was reported. The collected images of the droplets on the membrane surfaces were analyzed and the contact angles were measured by ImageJ software with the plug-in ContactAngle.

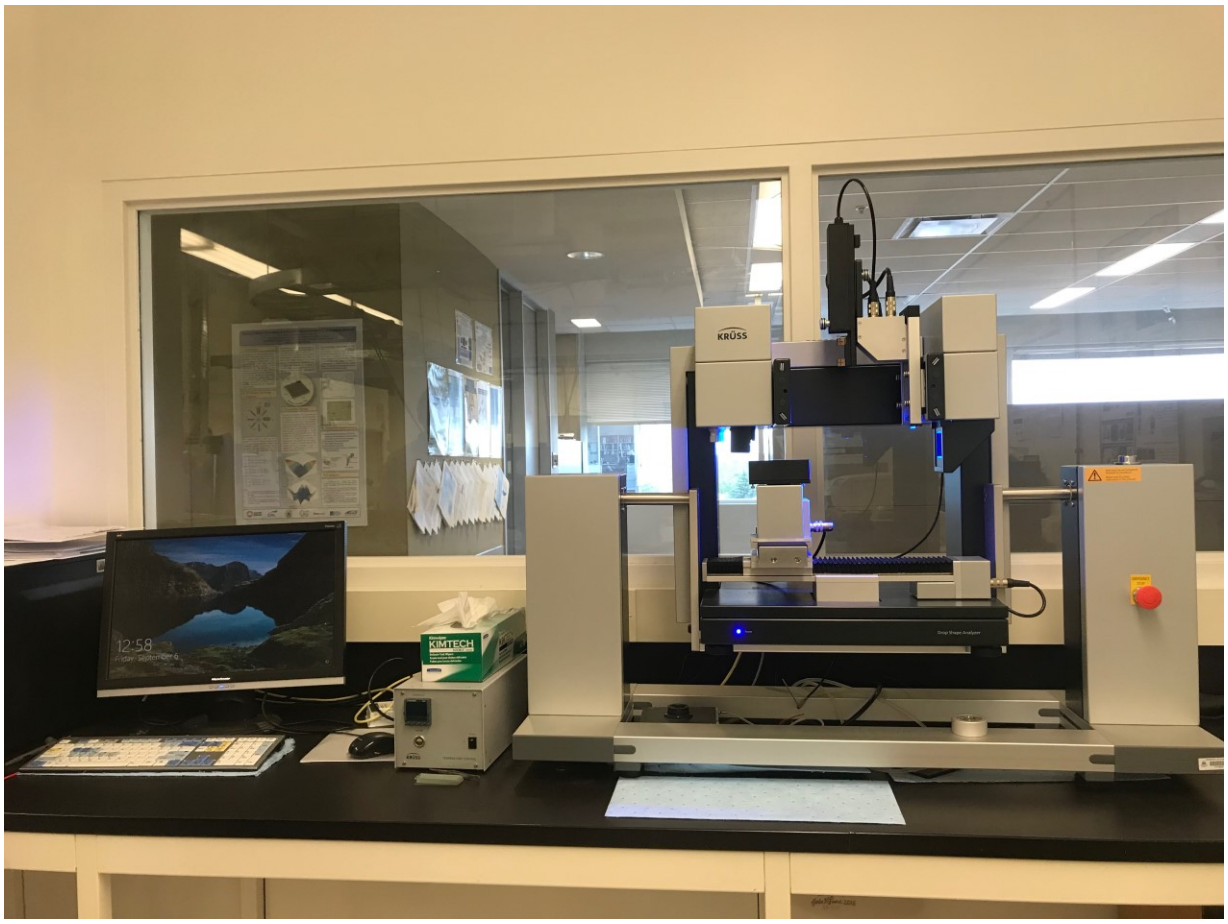

Figure 2-4 Drop shape analyzer used for contact angle measurements

3. Results and Discussion

3.1. Fiber Diameter Measurements

Solutions of PCL and gelatin with 1:1 PCL to gelatin weight ratio at three different total polymers concentrations, which are 6%, 10%, and 14% (w/v), were prepared and electrospun keeping all the other parameters constant to understand the effect of solution concentration on fiber morphology and diameter. In order to explore the effect of fiber morphology and diameter on degradation rate, electrospun PCL/gelatin membranes with three distinct average fiber diameters were incubated in PBS for 1, 3, 6 and 10 days and were imaged under SEM at the end of each degradation period.

The fiber morphology for the membrane electrospun from the solution at the total polymer concentration of 6% (w/v) before degradation and after 1, 3, 6, and 10 days of degradation were shown in Figure 3-1 and Figure 3-2. As it is seen from the figures, the membrane electrospun from the solution at the total polymer concentration of 6% (w/v) lost its fibrous structure after 1 day of degradation.

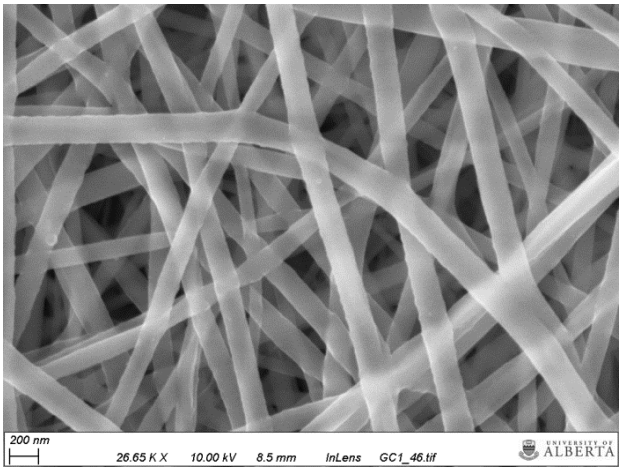

a) Before Degradation

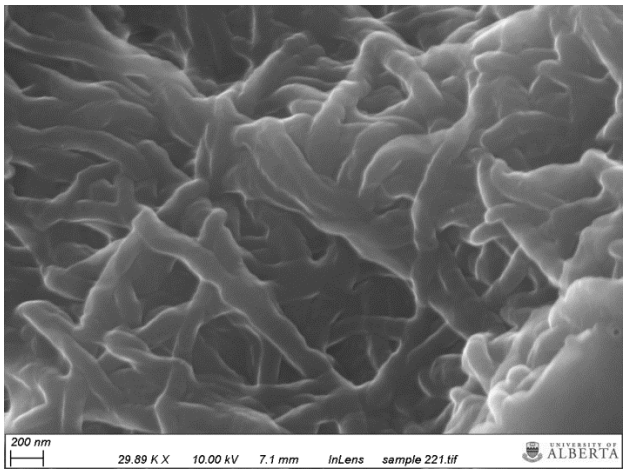

b) Day 1

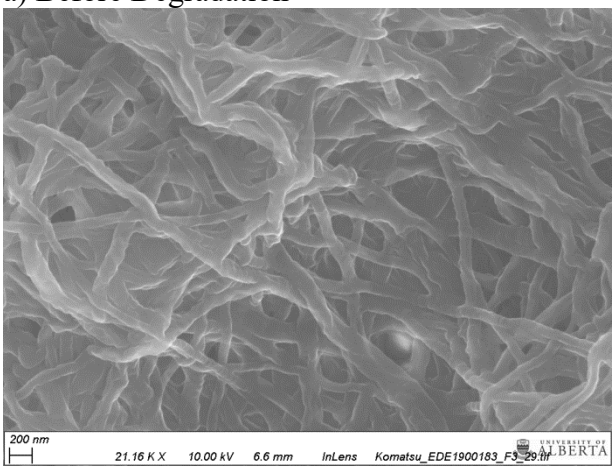

c) Day 3

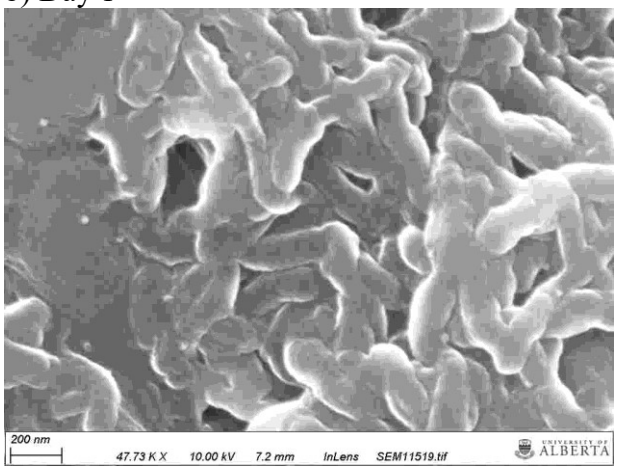

d) Day 6

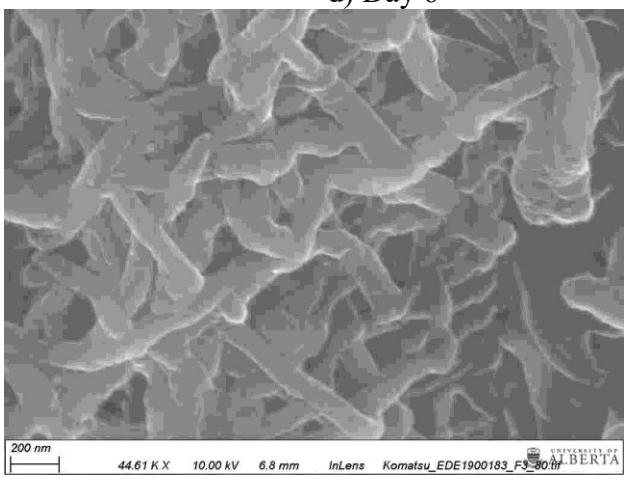

e) Day 10

Figure 3-1 The SEM micrographs for the membrane electrospun from the solution at the total polymer concentration of 6% (w/v) before degradation and after 1, 3, 6 and 10 days of degradation (close view)

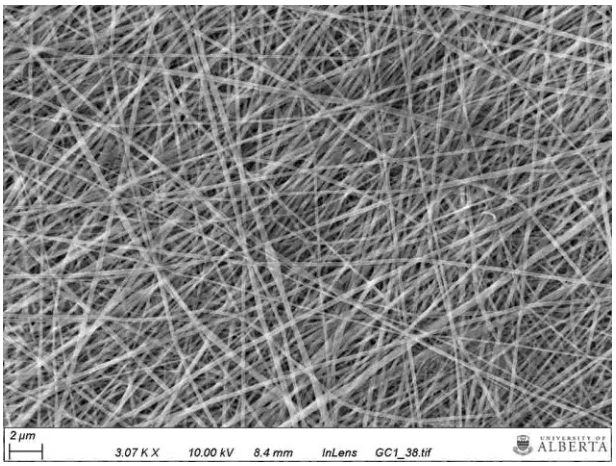

a) Before Degradation (6.2-1 D0)

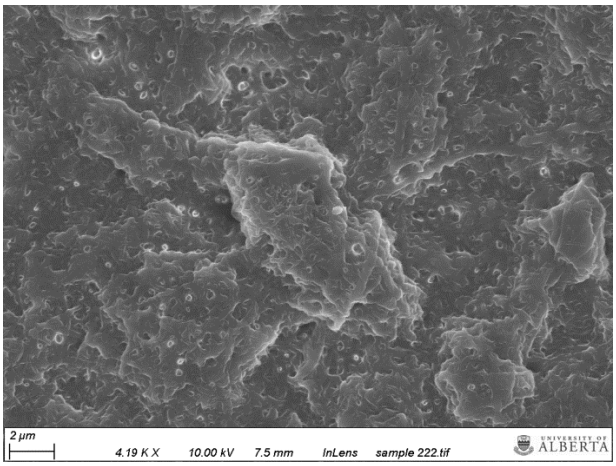

b) Day 1

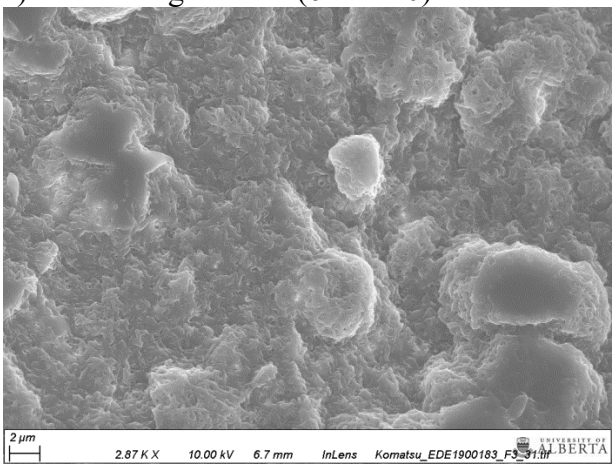

c) Day 3

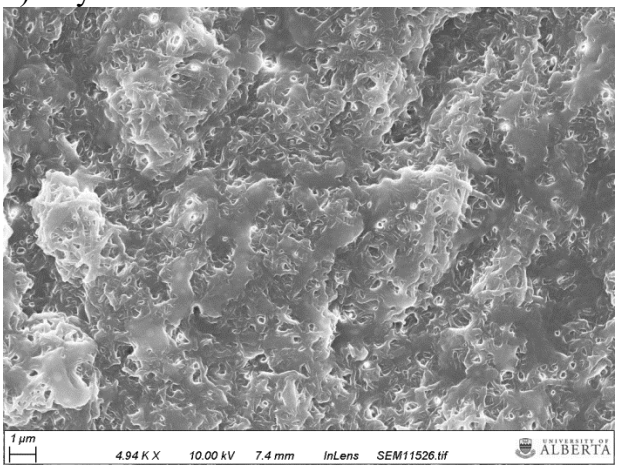

d) Day 6

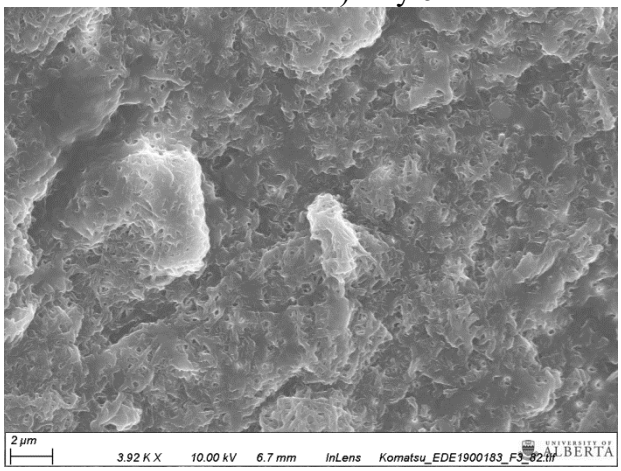

e) Day 10

Figure 3-2 The SEM micrographs for the membrane electrospun from the solution at the total polymer concentration of 6% (w/v) before degradation and after 1, 3, 6 and 10 days of degradation (overview)

As it is seen from the histogram shown in Figure 3-3, the fiber diameter distribution of the non-degraded membrane electrospun from the solution at the total polymer concentration of 6% (w/v) is roughly symmetric, unimodal and centered at 184 nm. There is an outlier to the right, which is around 380 nm. The diameters of the fibers range over an interval of approximately 290 nm from around 80 nm to around 370 nm.

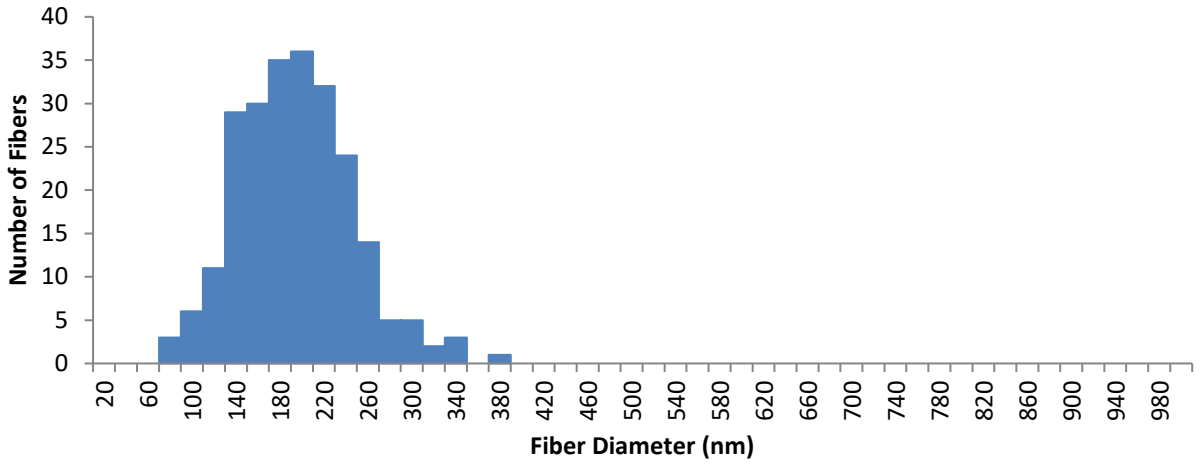

Figure 3-3 Fiber diameter distribution for the membrane electrospun from the solution at the total polymer concentration of 6% (w/v) before degradation

The morphology of the fibers for the membrane electrospun from the solution at the total polymer concentration of 10% (w/v) before degradation and after 1, 3, 6, and 10 days of degradation are shown in Figure 3-4. As it is seen from Figure 3-4, the fibrous structure was preserved over 10 days of degradation for the membrane electrospun from the solution at the total polymer concentration of 10% (w/v).

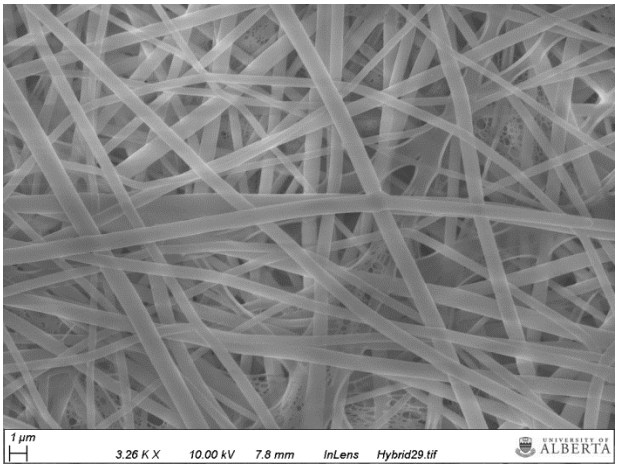

a) Before Degradation (10.2-1 D0)

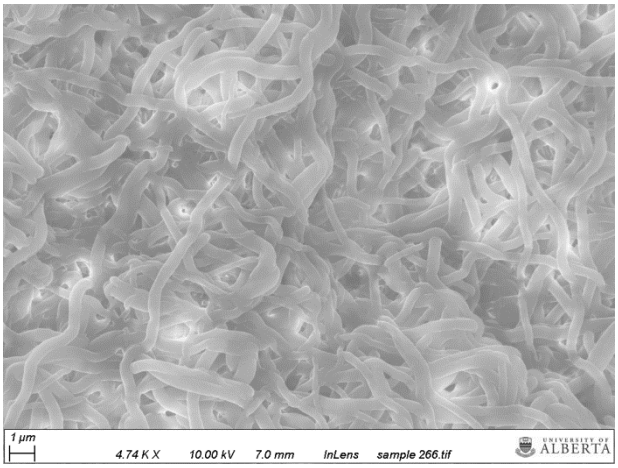

b) Day 1 (10.5-3 D1)

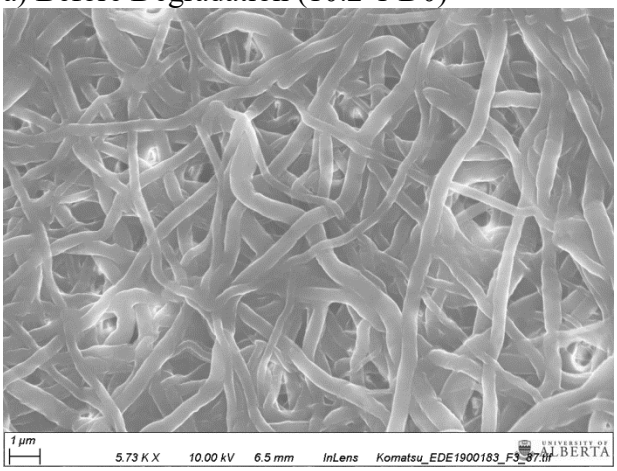

c) Day 3 (10.2-1 D3)

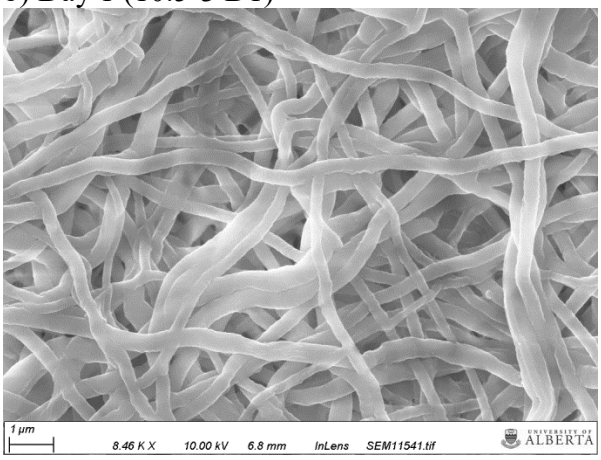

d) Day 6 (10.3-4 D6)

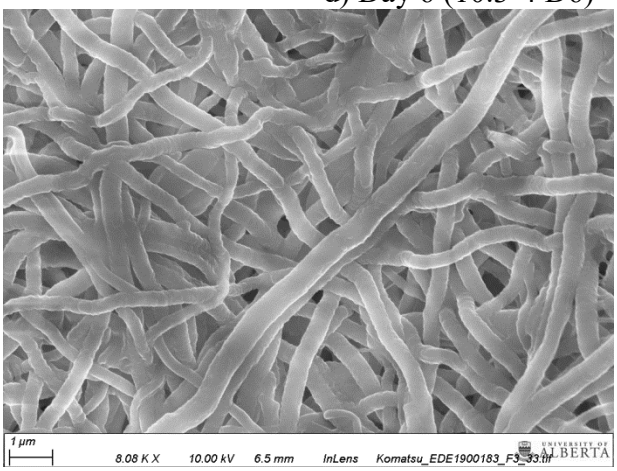

e) Day 10 (10.1-3 D10)

Figure 3-4 The SEM micrographs for the membrane electrospun from the solution at the total polymer concentration of 10% (w/v) before degradation and after 1, 3, 6 and 10 days of degradation

The distribution for the fiber diameter of the membranes electrospun from the solution at the total polymer concentration of 10% (w/v) before degradation and after 1, 3, 6 and 10 days of degradation was shown in Figure 3-5. As it is seen from the histogram shown in Figure 3-5-a, the fiber diameter distribution of the non-degraded membrane electrospun from the solution at the total polymer concentration of 10% (w/v) is skewed to the right and multimodal. It has a center at 803 nm. The highest two modes are around 760 nm and 800 nm. There are two other clear modes around 520 nm and 880 nm, which the fiber diameter measurements are concentrated considerably. There are also two other clear modes around 620 nm and 940 nm, which the fiber diameter measurements are concentrated moderately. The distribution of the fiber diameter spreads across a range of approximately 2360 nm from about 260 nm to about 2620 nm with seven outliers between about 1940 nm and about 2620 nm.

The fiber diameter distribution of the membrane electrospun from the solution at the total polymer concentration of 10% (w/v) after 1 day of degradation is shown by the histogram in Figure 3-5-b. The distribution is skewed right, multimodal, and centered at 443 nm. There are three clear modes around 360 nm, 420 nm and 520 nm, which the fiber diameter measurements are concentrated considerably. There are five outliers between 620 nm and 700 nm. The range for the distribution is approximately 400 nm from about 300 nm to about 700 nm.

As it can be seen from the histogram shown in Figure 3-5-c, the fiber diameter distribution of the membrane electrospun from the solution at the total polymer concentration of 10% (w/v) after 3 days of degradation is skewed right and unimodal. The mode is around 360 nm, which the measurements for the fiber diameter are concentrated moderately. The distribution is centered at 438 nm and spread across a range of approximately 660 nm from about 260 nm to about 920 nm. There are to outliers around 740 nm and 920 nm.

The fiber diameter distribution of the membrane electrospun from the solution at the total polymer concentration of 10% (w/v) after 6 days of degradation is shown by the histogram in Figure 3-5-d. The distribution is skewed to the right and bimodal. One of the modes is around 360 nm, which the fiber diameter measurements are concentrated significantly. The other mode is around 520 nm, which the measurements for the fiber diameter are concentrated moderately. The distribution has a center at 404 nm. There is an outlier around 820 nm. The range for the distribution is approximately 540 nm from about 280 nm to 820 nm.

As it is seen from the histogram shown in Figure 3-5-e, the fiber diameter distribution of the membrane electrospun from the solution at the total polymer concentration of 10% (w/v) after 10 days of degradation is skewed to the right and bimodal. The center is at 472 nm. The distribution has a range of approximately 480 nm from 340 nm to 820 nm. One of the modes is around 460 nm, which the fiber diameter measurements are concentrated significantly. The other mode is around 520 nm, which the measurements for the fiber diameter are concentrated moderately. There are two outliers between 780 nm and 820 nm.

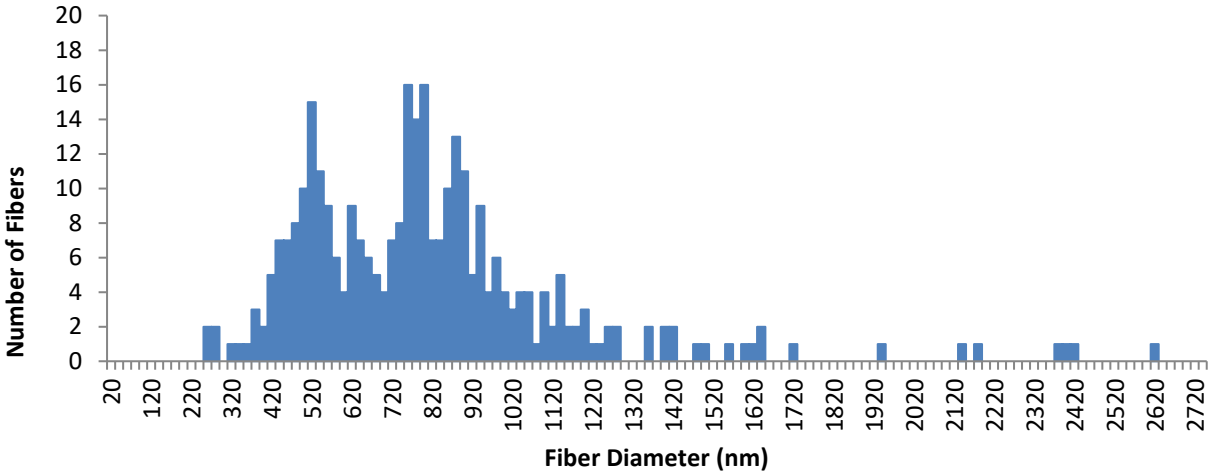

a) Day 0

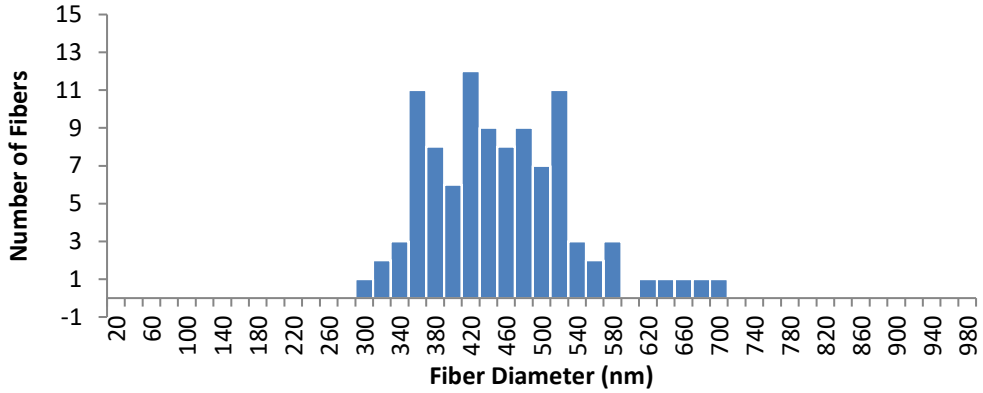

b) Day 1

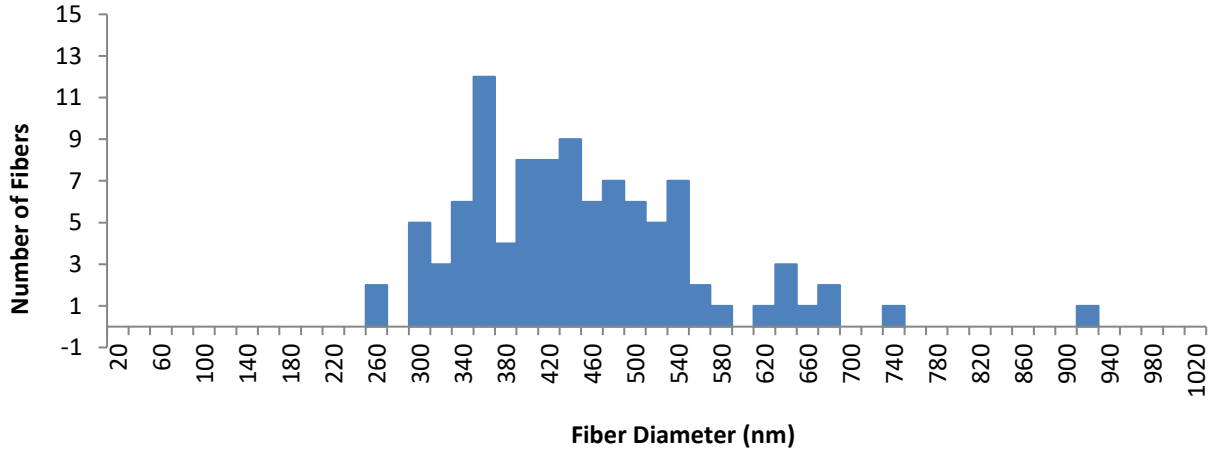

c) Day 3

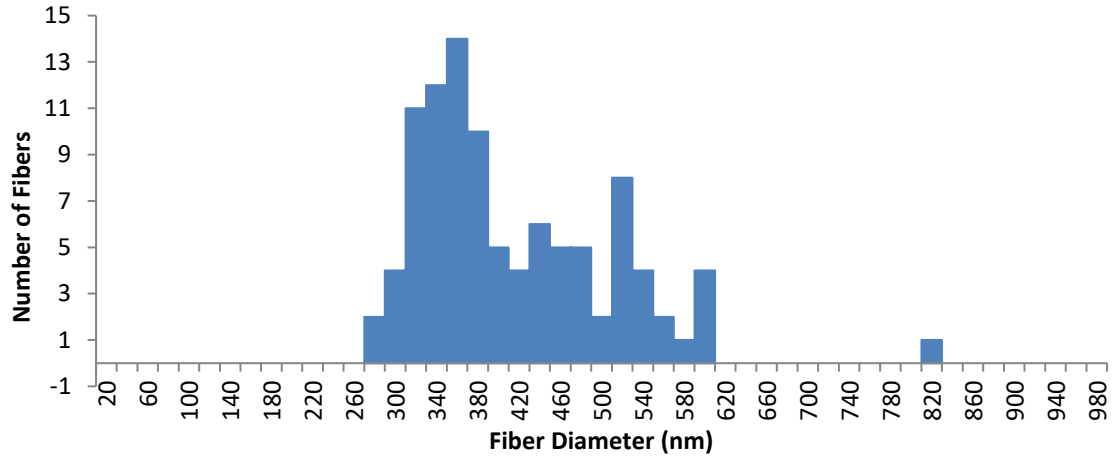

d) Day 6

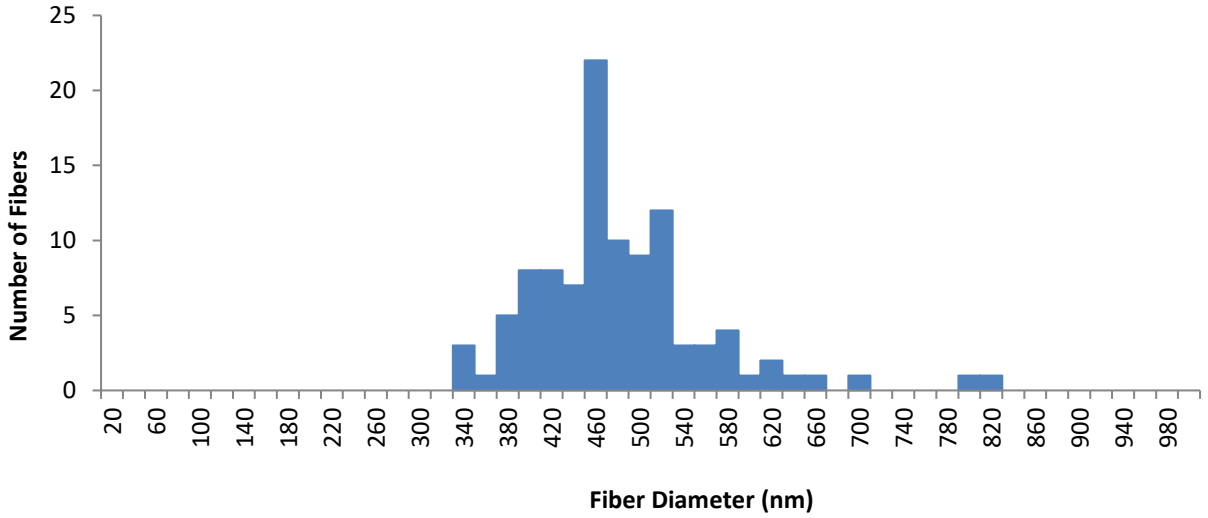

e) Day 10

Figure 3-5 Fiber diameter distribution for the membrane electrospun from the solution at the total polymer concentration of 10% (w/v) before degradation and after 1, 3, 6 and 10 days of degradation

The morphology of the fibers for the membrane electrospun from the solution at the total polymer concentration of 14% (w/v) before degradation and after 1, 3, 6, and 10 days of degradation were shown in Figure 3-6. As it is seen from Figure 3-6, the fibrous structure was preserved over 10 days of degradation for the membrane electrospun from the solution at the total polymer concentration of 14% (w/v).

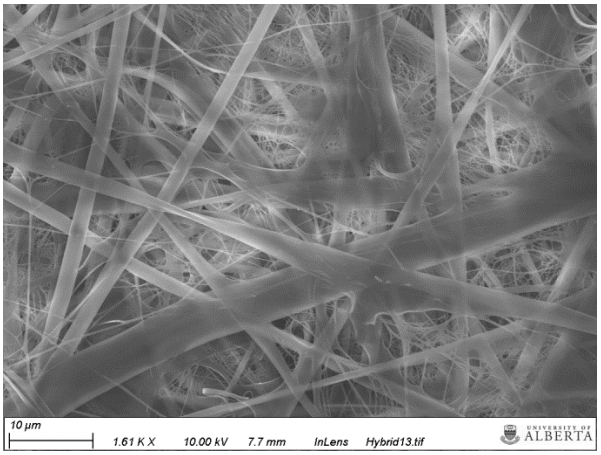

a) Before Degradation (14.2-1 D0)

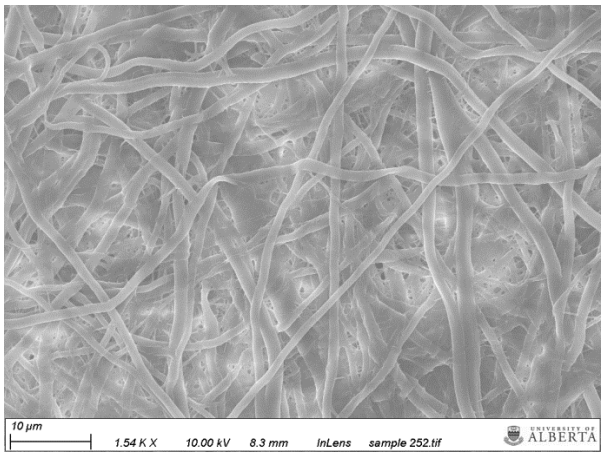

b) Day 1 (14.5-3 D1)

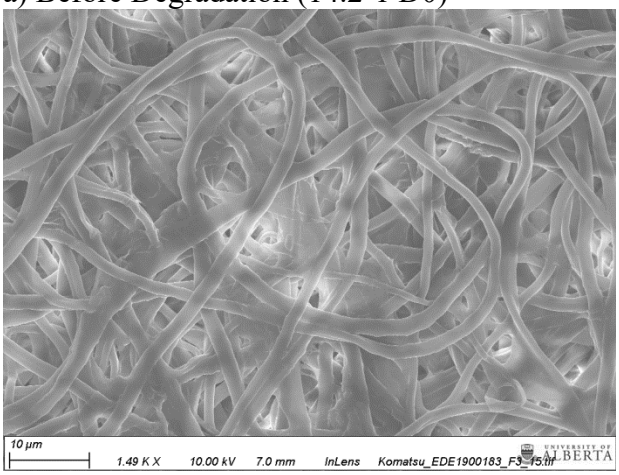

c) Day 3 (14.3-4 D3)

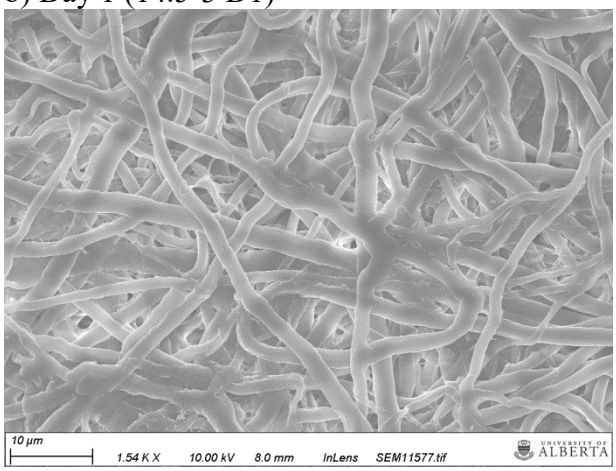

d) Day 6 (14.5-2 D6)

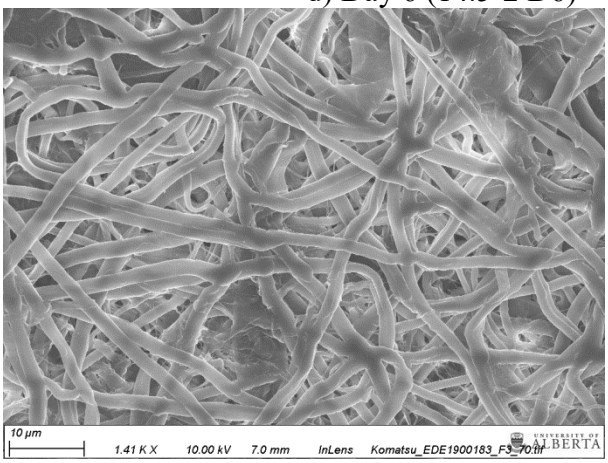

e) Day 10 (14.4-3 D10)

Figure 3-6 The SEM micrographs for the membrane electrospun from the solution at the total polymer concentration of 14% (w/v) before degradation and after 1, 3, 6 and 10 days of degradation

The distribution for the fiber diameter of the membranes electrospun from the solution at the total polymer concentration of 14% (w/v) before degradation and after 1, 3, 6 and 10 days of degradation was shown in Figure 3-7. As it is seen from the histogram shown in Figure 3-7-a, the fiber diameter distribution of the non-degraded membrane electrospun from the solution at the total polymer concentration of 14% (w/v) is roughly symmetric and multimodal. It has a center at 2131 nm. The highest mode is around 1980 nm. The second highest mode is around 2500 nm. There are also modes around 1540 nm, 1620 nm, 2200 nm and 2740 nm, which the measurements for the fiber diameter were concentrated considerably. The range of the distribution is approximately 3340 nm from 1060 nm to 4400 nm. There are eleven outliers between about 3120 nm and about 4400 nm.

The fiber diameter distribution of the membrane electrospun from the solution at the total polymer concentration of 14% (w/v) after 1 day of degradation is shown by the histogram in Figure 3-7-b. The distribution is slightly skewed to the left and multimodal. It is centered at 1579 nm. There are two modes around 1680 nm and 1780 nm, which the fiber diameter measurements are concentrated considerably. There is a smaller third mode around 1300 nm. The distribution is spread across a range of approximately 2480 nm from about 800 nm to about 3280 nm with two outliers around 2440 nm and 3280 nm.

As it can be seen from the histogram shown in Figure 3-7-c, the fiber diameter distribution of the membrane electrospun from the solution at the total polymer concentration of 14% (w/v) after 3 days of degradation is skewed to the left and unimodal. The mode is around 2140 nm, which the measurements for the fiber diameter are concentrated significantly. The distribution has a center at 1846 nm. The rage for the distribution is approximately 2020 nm from about 1000 nm to about 3020 nm. There are two outliers around 2720 nm and 3020 nm.

The fiber diameter distribution of the membrane electrospun from the solution at the total polymer concentration of 14% (w/v) after 6 days of degradation is shown by the histogram in Figure 3-7-d. The distribution is roughly uniform and unimodal. There is a small mode around 1020 nm. The distribution has a center at 1630 nm and spread across a range of approximately 2100 nm from about 820 nm to about 2920 nm. There are two outliers around 2820 nm and 2920 nm.

As it is seen from the histogram shown in Figure 3-7-e, the fiber diameter distribution of the membrane electrospun from the solution at the total polymer concentration of 14% (w/v) after 10 days of degradation is slightly skewed to the right and multimodal with no outliers. The center is at 1414 nm. The range of the distribution is approximately 1980 nm from 680 nm to 2660 nm. There are three modes around 780 nm, 920 nm and 1220 nm, which the fiber diameter measurements are concentrated significantly.

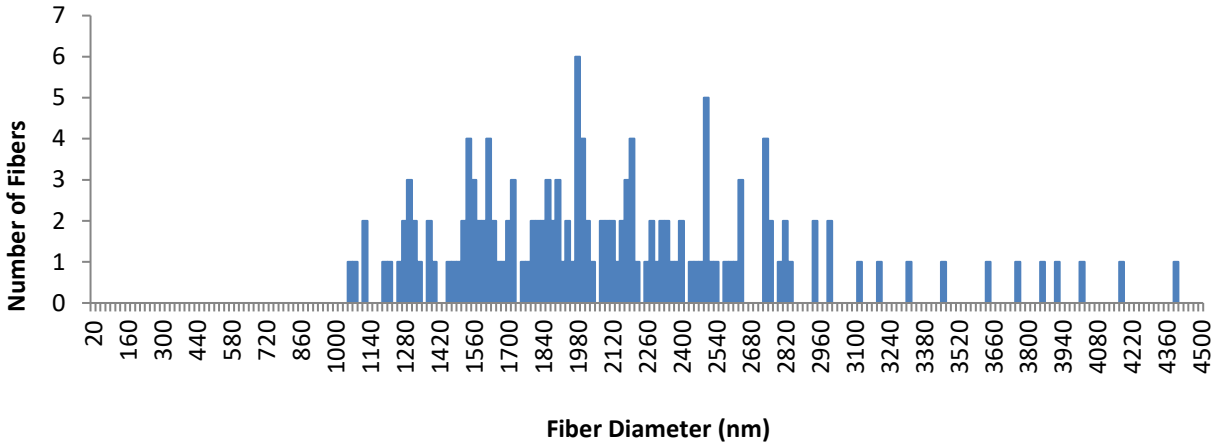

a) Day 0

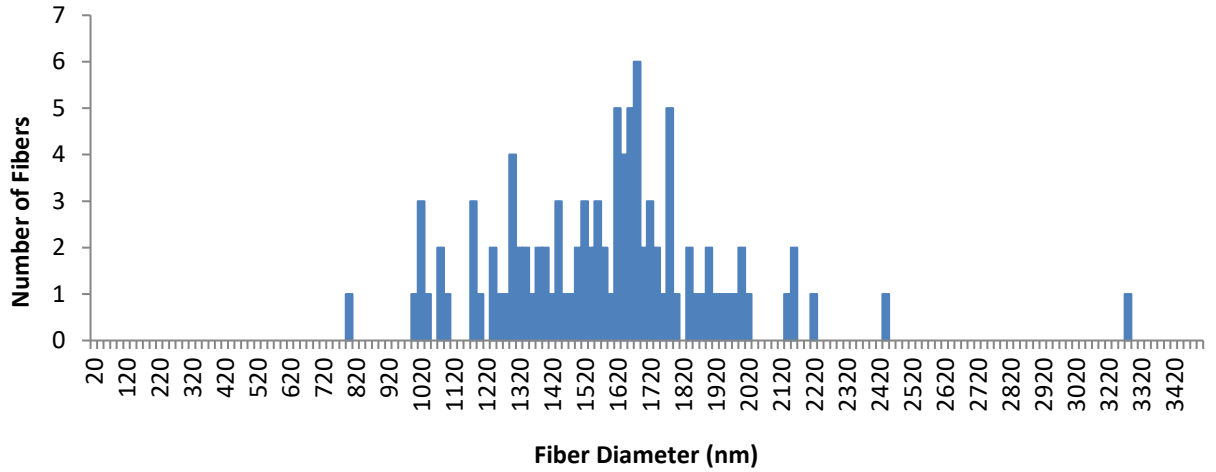

b) Day 1

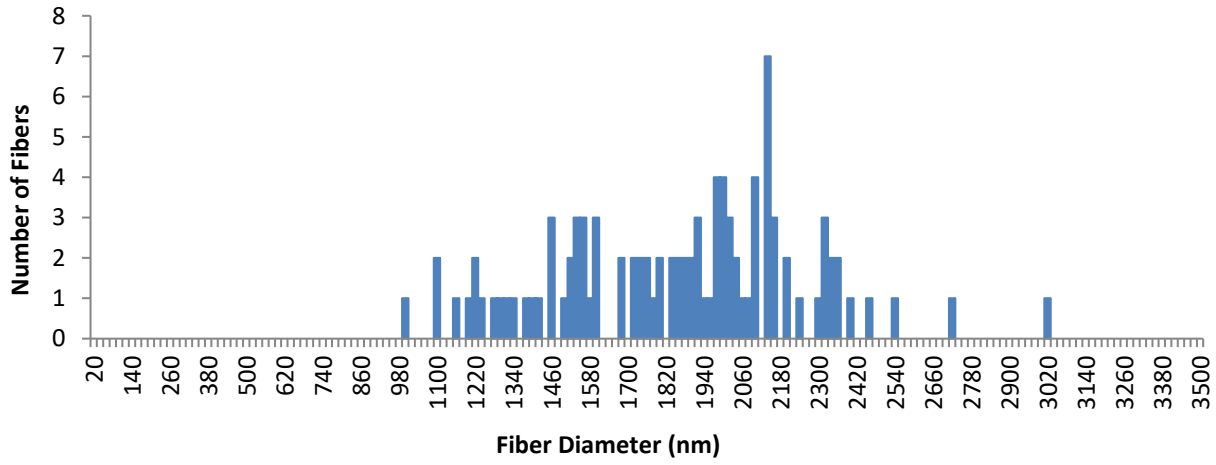

c) Day 3

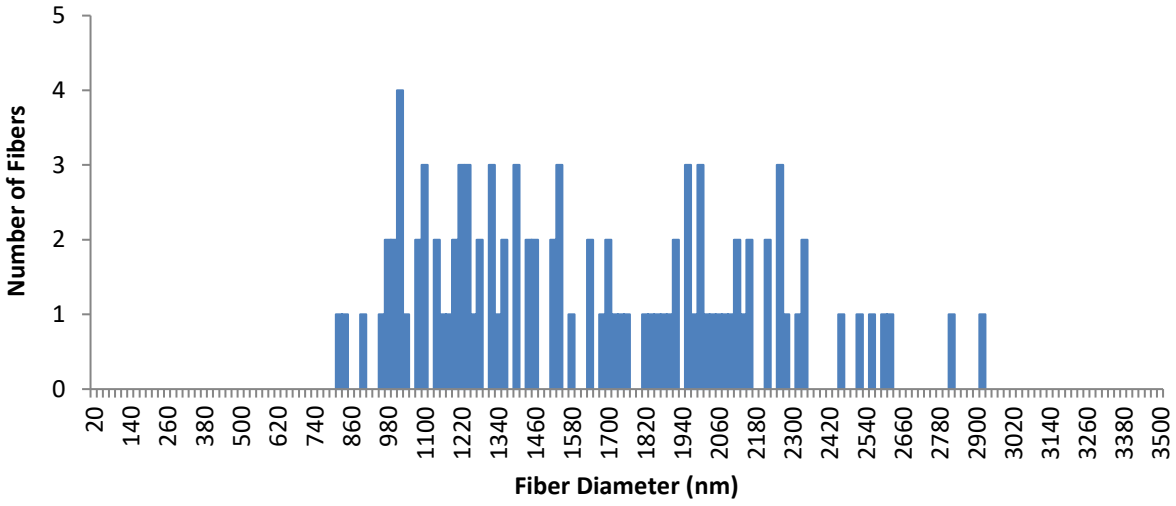

d) Day 6

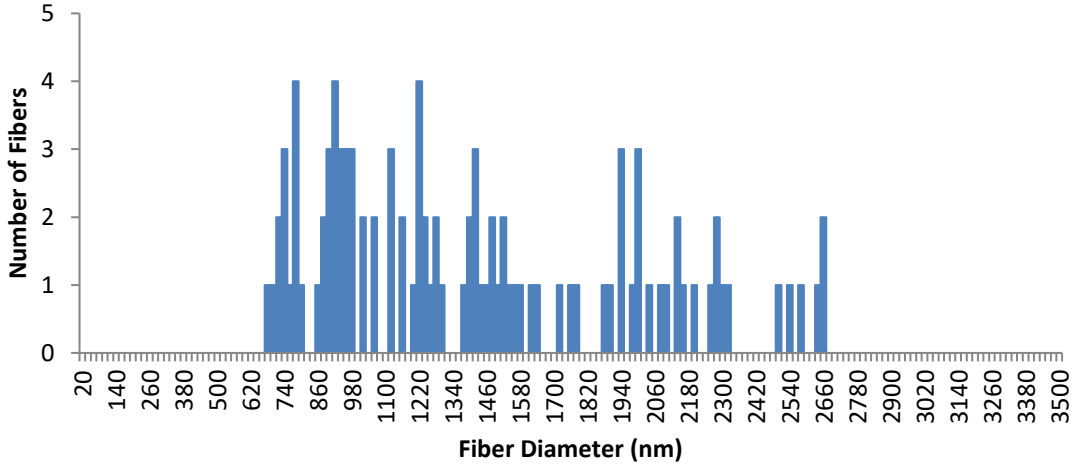

e) Day 10

Figure 3-7 Fiber diameter distribution for the membrane electrospun from the solution at the total polymer concentration of 14% (w/v) before degradation and after 1, 3, 6 and 10 days of degradation

From the fiber diameter measurements on SEM micrographs, the average fiber diameter for the mats electrospun from the solutions at the total polymer concentrations of 6%, 10% and 14% (w/v) before degradation and after 1, 3, 6 and 10 days of degradation were calculated, tabulated in Table 3-1 and plotted as it is shown in Figure 3-8.

Table 3-1 Fiber diameters for the membranes electrospun from the solutions at the total polymer concentrations of 6%, 10% and 14% (w/v) before degradation and after 1, 3, 6 and 10 days of degradation

Days	6% (w/v)		10% (w/v)		14% (w/v)	
	Average Fiber Diameter (nm)	Standart Deviation (nm)	Average Fiber Diameter (nm)	Standart Deviation (nm)	Average Fiber Diameter (nm)	Standart Deviation (nm)
0	184	51	803	349	2131	701
1	-	-	443	81	1579	339
3	-	-	438	109	1846	383
6	-	-	404	95	1630	506
10	-	-	472	82	1414	555

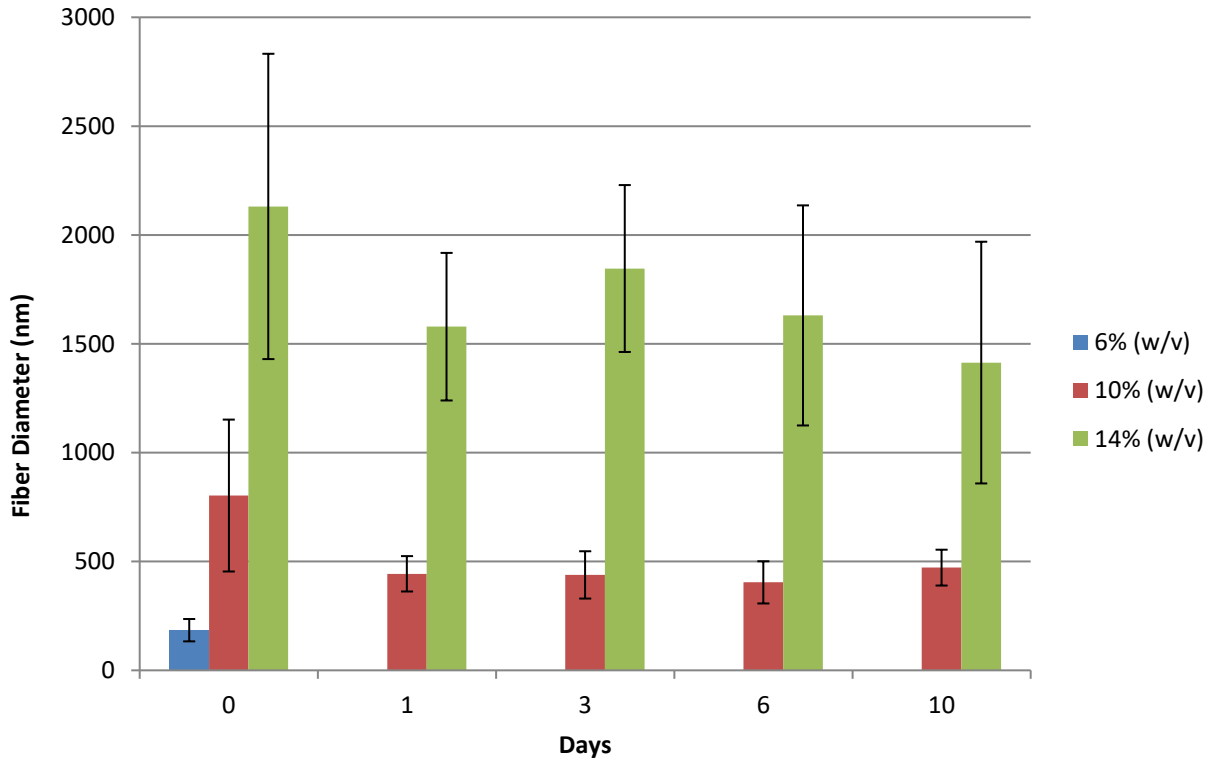

Figure 3-8 Fiber diameters for the mats electrospun from the solutions at the total polymer concentrations of 6%, 10% and 14% (w/v) before degradation and after 1, 3, 6 and 10 days of degradation

As it is seen in Figure 3-8, the average fiber diameters for the PCL/gelatin membranes electrospun from solutions with 6%, 10% and 14% (w/v) before degradation were found to be significantly different then each other and increasing with increasing total polymer concentration of the electrospinning solution. When the total polymer concentration was increased from 6 % (w/v) to 10% (w/v), the average fiber diameter went up by a factor of almost 4.4 from 184 nm with a standard deviation of 51 nm to 803 nm with a standard deviation of 349 nm. The average fiber diameter for the membrane electrospun from the solution at 14% (w/v) total polymer concentration was found as 2131 nm with a standard deviation of 701 nm, which is considerably larger than the average fiber diameter of the membrane electropsun from the solution with 10% (w/v) total polymer concentration by a factor of almost 2.7. These results confirmed that the fiber diameter of the PCL/gelatin membranes depends heavily on the concentration of the electrospinning solution. The reason is that the increase in total polymer concentration results in higher viscosity due to greater polymer chain entanglements [27]. As the concentration of the solution increases, the viscoelastic forces acting against the columbic forces increases, which results in reduced stretching of the electrospinning jet and causes the deposited fibers to become larger in diameter [115]. Another important point is that the fiber diameter is more uniform throughout the mat electrospun from the solution with a lower total polymer concentration. This is indicated by the increasing standard deviations of 51 nm, 349 nm and 701 nm for the average fiber diameters of the membranes electrospun from the solutions with increasing total polymer concentrations of 6%, 10%, and 14% (w/v), respectively.

The average fiber diameter of the membrane electrospun from the solution at the total polymer concentration of 10% (w/v) reduced by almost half after 1 day of degradation and measured as 443 nm with a standard deviation of 81 nm. The average fiber diameter after 3, 6

and 10 days of degradation were found as 438 nm, 404 nm and 472 nm with the standard deviations of 109 nm, 95 nm and 82 nm, respectively. However, these variations in fiber diameter were not found to be statistically significant because of the overlap of standard deviations. Therefore, it has been concluded that the average fiber diameter of the membrane electrospun from the solution at the total polymer concentration of 10% (w/v) did not change significantly over the course of 10 days of degradation.

For the electrospinning of the solution at the total polymer concentration of 14% (w/v), the average fiber diameter of the degraded membranes was found to be less than the average fiber diameter of the non-degraded membrane. After 1, 3, 6 and 10 days of degradation, the average fiber diameter was measured as 1579 nm, 1846 nm, 1630 nm and 1414 nm with the standard deviations of 339 nm, 383 nm, 506 nm and 555 nm, respectively. Nonetheless, it has been concluded that the average fiber diameter of the membrane electrospun from the solution at the total polymer concentration of 14% (w/v) did not change significantly before and after any period of degradation due to the overlap of standard deviations.

Finally, it should be noted that after any period of degradation, the average fiber diameter of the membrane electrospun from the solution at the total polymer concentration of 14% (w/v) was significantly higher than the average fiber diameter of the membrane electrospun from the solution at the total polymer concentration of 10%. This indicates that the difference between the concentrations of the electrospinning solutions caused fibers electrospun from the solution with the higher concentration to remain significantly larger than fibers electrospun from the solution with the lower concentration at any point of degradation.

SEM micrographs and the fiber diameter measurements for each sample for each degradation period were shown in Appendix A.

3.2. Gravimetric Analysis of Degradation

In this study, it has been hypothesized that electrospun Gelatin/PCL membranes will degrade faster as the diameter of the fibers become smaller due to the increase in surface area. In order to asses this hypothesis, membranes of three distinct average fiber diameters, which were fabricated by electrospinning the solutions at the total polymer concentrations of 6% (w/v), 10% (w/v) and 14% (w/v), were degraded for the time periods of 1, 3, 6 and 10 days. Then, the degradation profile of each membrane, which is shown in Figure 3-9, was established by weighing the membranes before and after each period of degradation. Remaining mass% values for the degradation profiles of each membrane were tabulated in Table 3-2. The weight measurement for each sample before and after each degradation period was shown in Appendix B.

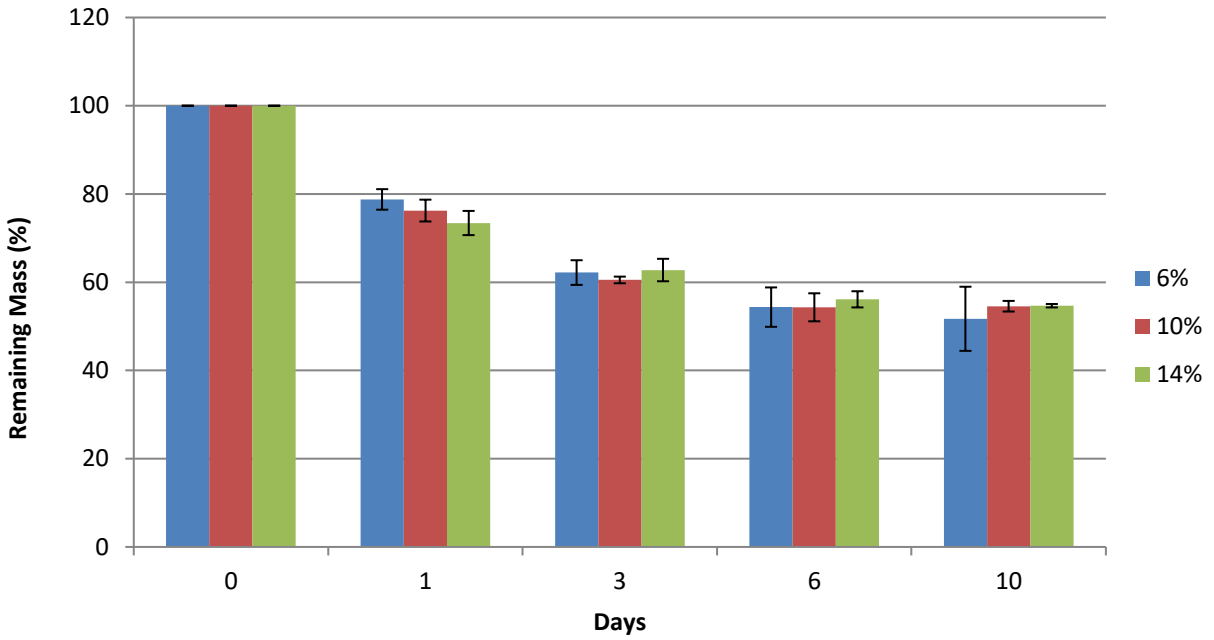

Figure 3-9 Remaining mass % of the membranes electrospun from the solutions at the total polymer concentrations of 6%, 10% and 14% (w/v) solutions for 1, 3, 6 and 10 days of degradation

Table 3-2 Remaining mass % for the membranes electrospun from the solutions at the total polymer concentrations of 6%, 10% and 14% (w/v) before degradation and after 1, 3, 6 and 10 days of degradation

	6% (w/v)		10% (w/v)		14% (w/v)	
Days	Remaining Mass %	Standart Deviation	Remaining Mass %	Standart Deviation	Remaining Mass %	Standart Deviation
1	78.8	2.3	76.2	2.5	73.4	2.7
3	62.2	2.8	60.5	0.8	62.8	2.5
6	54.4	4.5	54.3	3.2	56.1	1.8
10	51.7	7.3	54.6	1.2	54.7	0.4

For all the membranes, the rate of mass loss was highest for the 1st day of degradation. The average remaining masses for the membranes electrospun from the solutions at the total polymer concentrations of 6% (w/v), 10% (w/v) and 14% (w/v) were found as 78.8%, 76.2% and 73.4% with standard deviations of 2.3, 2.5 and 2.7, respectively after 1 day of degradation. The masses of the membranes declined considerably for all the membranes between the 1st and 3rd days of degradation. At the end of three days of degradation, the average remaining masses for the membranes electrospun from the solutions at the total polymer concentrations of 6% (w/v), 10% (w/v) and 14% (w/v) were found as 62.2%, 60.5% and 62.8% with standard deviations of 2.8, 0.8 and 2.5, respectively. Between the 3rd and the 6th days of degradation, there was a slight decrease in the masses of all membranes. The average remaining masses for the membranes electrospun from the solutions at the total polymer concentrations of 6% (w/v), 10% (w/v) and 14% (w/v) were found as 54.4%, 54.3% and 56.1% with standard deviations of 4.5, 3.2 and 1.8, respectively after 6 days of degradation. However, none of the membranes lost any significant mass between the 6th and 10th days of degradation. The average remaining masses for the

membranes electrospun from the solutions at the total polymer concentrations of 6% (w/v), 10% (w/v) and 14% (w/v) were found as 51.7%, 54.6% and 54.7% with standard deviations of 7.3, 1.2 and 0.4, respectively after 10 days of degradation.

In the previous studies, a decrease in the intensity of the characteristic peaks of gelatin in the FTIR spectra of the degraded gelatin/PCL fibers was reported, which indicates that mass loss of electrospun PCL/Gelatin membranes occurs through the dissolution of gelatin content of the fibers [93]. In addition, in another study, it has been found that electrospun PCL membranes did not lose any weight when they were subjected to in vitro degradation for 14 days [105]. Hydrophobic polyesters such as PCL degrade through bulk erosion [16]. PCL scaffolds do not lose mass until the hydrolytic break down of the bonds residing at the backbone of the polymer chains proceeds to the extent where low molecular species, which are soluble in water, are formed [16]. In our case, 10 days of hydrolytic degradation was not enough for the formation of such low molecular and water soluble oligomers or monomers to form. As a result, PCL content of the fibers were preserved completely throughout the degradation. Considering that gelatin is a hydrophilic polymer that dissolves in water at 37 °C, which is the temperature of hydrolytic degradation for this study, it has been concluded that the mass loss of the electrospun PCL/Gelatin membranes occurred only due to the rapid dissolution gelatin during the first 6 days of *in vitro* degradation. After the 6^{th} day of degradation, remaining mass% of the scaffolds did not change because almost all the gelatin has been already dissolved and PCL content of the fibers were fully preserved. This conclusion is also supported by the fact that the remaining mass % of all the membranes after 10 days of degradation was approximately 55%, which is pretty close to gelatin% of all the electrospinning solutions.

The remaining mass % for the membranes electrospun from the solutions at different total polymer concentrations of 6%, 10% and 14% (w/v) was found as approximately 76%, 61%, 55% and 55% after 1, 3, 6 and 10 days of degradation, respectively. In other words, the remaining mass % of all membranes was statistically the same after a specific period of degradation. The reason can be that surface area to volume ratios of the fibers were small enough for the diffusion of water molecules into and dissolved gelatin chains to diffuse out of the core of the fibers for the electrospun PCL/Gelatin membranes at all fiber diameters. In other words, none of the membranes had a large enough fiber diameter to inhibit the rapid dissolution of gelatin out of the fiber cores. As a result, gelatin content of membranes at all fiber diameters diminished at the same rate.

It has been previously mentioned in Section 3.1 that the membrane electrospun from the solution at the total polymer concentration of 6% (w/v) lost its fibrous structure after 1 day of degradation whereas the fibrous structure was preserved in the membranes electrospun from the solutions at the total polymer concentrations of 10% (w/v) and 14% (w/v). The reason could be related to the amount of PCL chains in each individual fiber. Fibers, which are larger in diameter, consist of a larger number of PCL chains. In the literature, it has been reported that external dimensions of the hydrolytically degrading specimens made of polyesters do not change until the bulk degradation proceeds to a critical level which the specimens disintegrate [16]. In the membranes electrospun from the solutions at the total polymer concentrations of 10% (w/v) and 14% (w/v), fibers were large enough that the amount of PCL chains in each individual fiber was high enough to maintain the integrity of the fibers during the course of hydrolytic bulk degradation. However, in the membranes electrospun from the solution at the total polymer concentration of 6% (w/v), the amount of PCL chains making up each individual fiber was not

high enough to support fibrous structure after the gelatin chains dissolve away as well as over the course of hydrolytic bulk degradation. As a result, the fibrous structure could not be maintained in the membrane electrospun from the solution at the total polymer concentration of 6% (w/v).

3.3. Measurement of the Mechanical Properties

In this study, the effect of fiber diameter on the degradation dependent change of mechanical properties of Gelatin/PCL membranes was investigated. In order to measure the mechanical properties of non-degraded and degraded Gelatin/PCL membranes, tensile test was utilized. Specimens cut from the Gelatin/PCL membranes were tested before degradation and after 1, 3, 6 and 10 days of degradation for each of the three different fiber diameters. The stress-strain curves obtained from the tensile tests of the membranes electrospun from the solutions at the total polymer concentration of 6%, 10% and 14% (w/v) are as it is shown in Figure 3-10, Figure 3-11 and Figure 3-12, respectively.

.

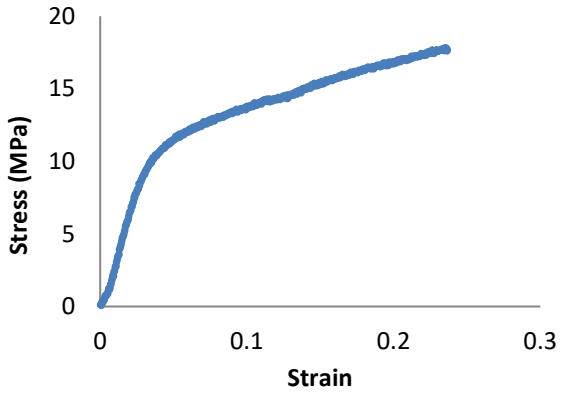

a) Before degradation

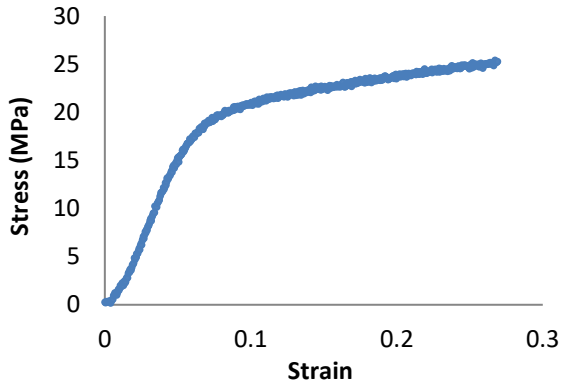

b) After 1 day of degradation

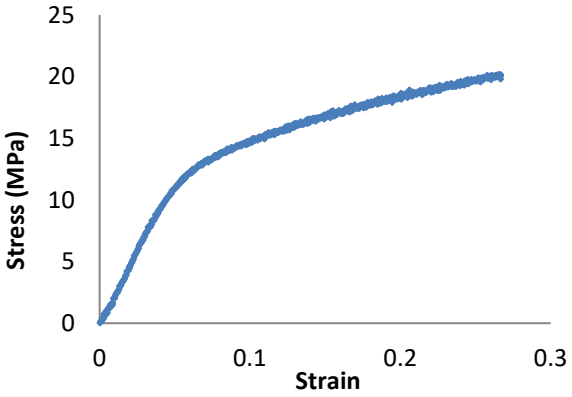

c) After 3 days of degradation

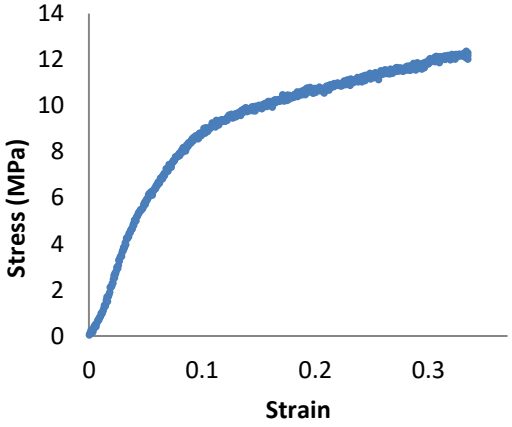

d) After 6 days of degradation

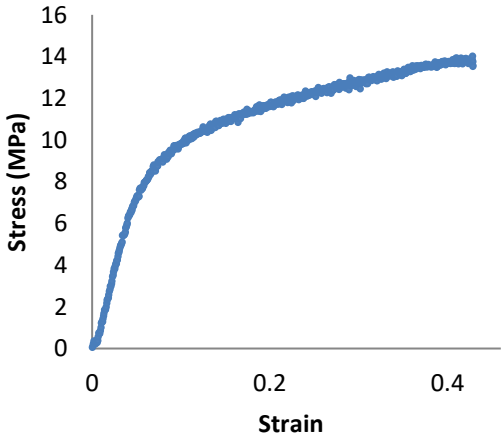

d) After 10 days of degradation

Figure 3-10 Strain-stress curves for the membrane electrospun from the solution at the total polymer concentration of 6% (w/v) before degradation and after 1, 3, 6 and 10 days of degradation

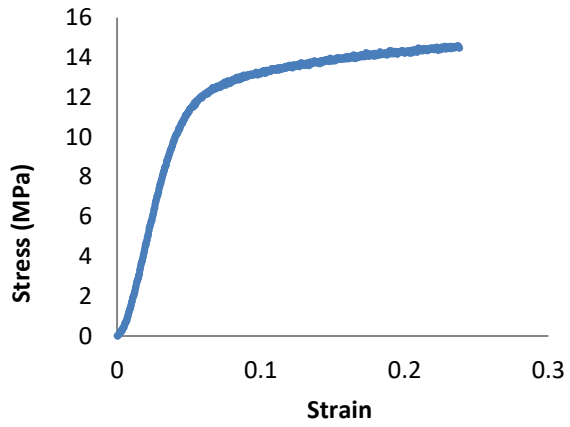

a) Before degradation

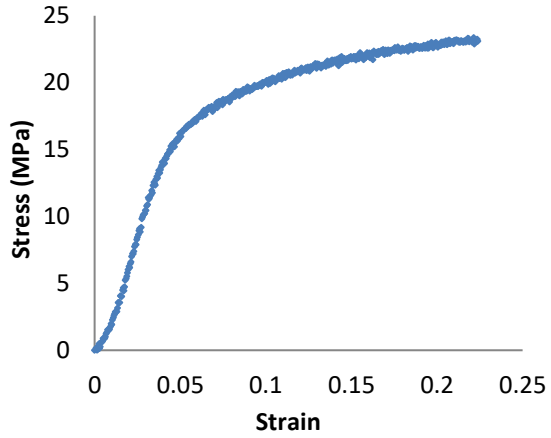

b) After 1 day of degradation

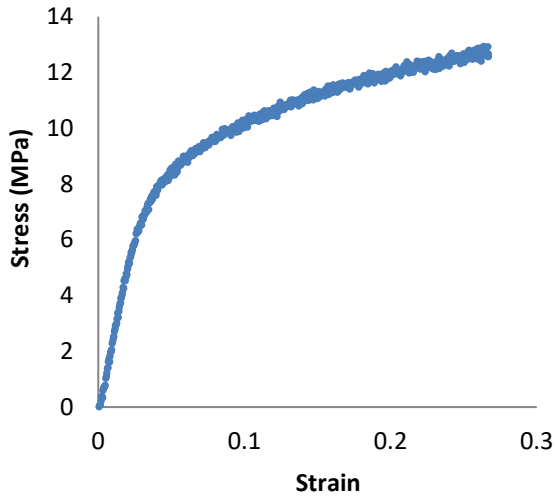

c) After 3 days of degradation

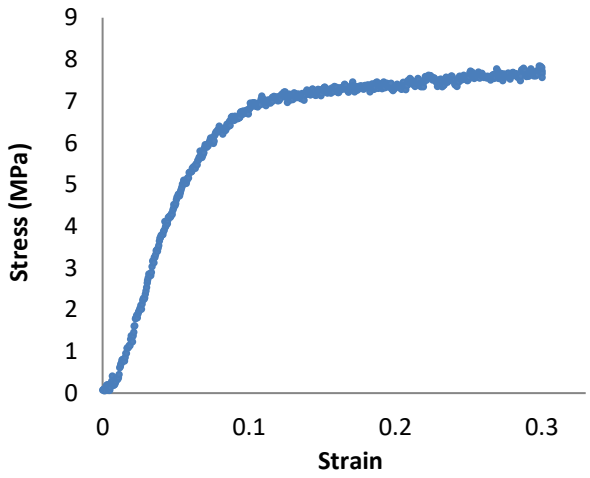

d) After 6 days of degradation

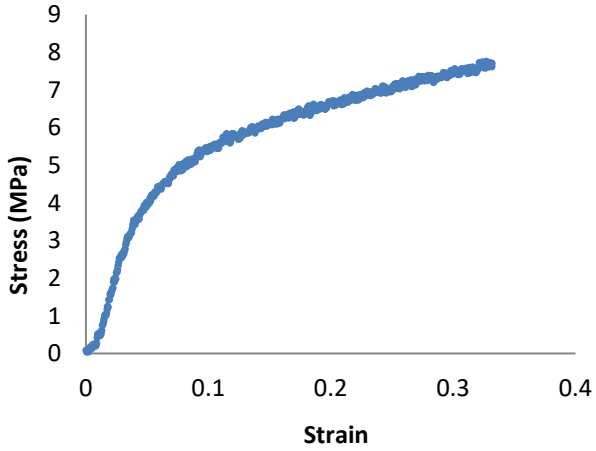

d) After 10 days of degradation

Figure 3-11 Strain-stress curves for the membrane electrospun from the solution at the total polymer concentration of 10% (w/v) before degradation and after 1, 3, 6 and 10 days of degradation

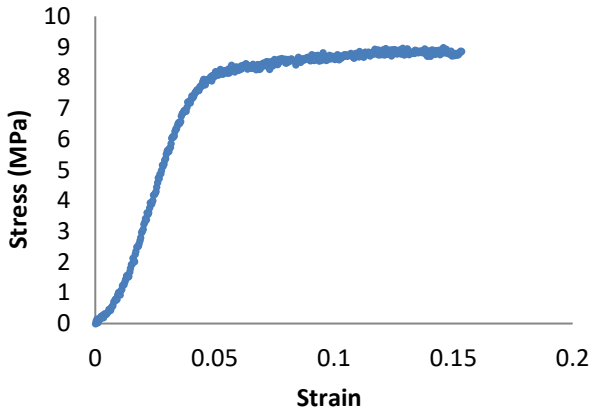

a) Before degradation

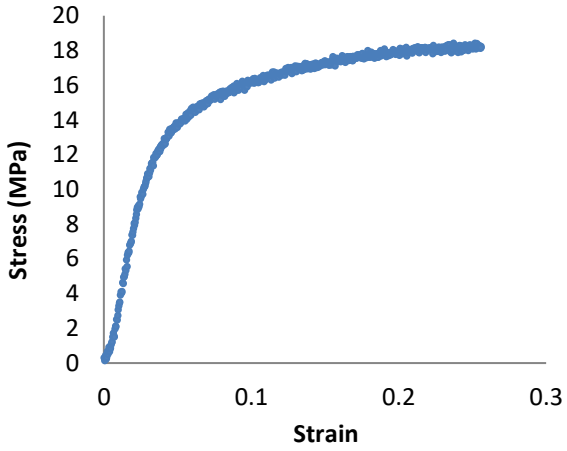

b) After 1 day of degradation

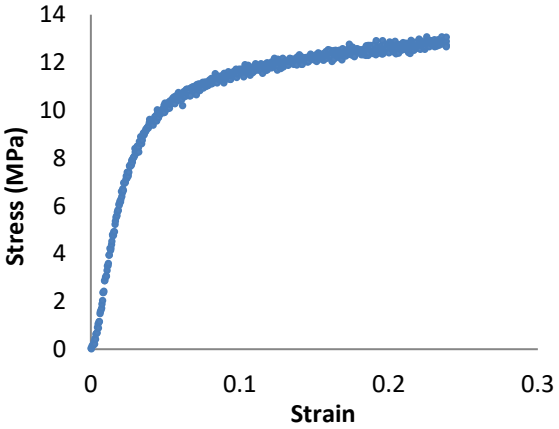

c) After 3 days of degradation

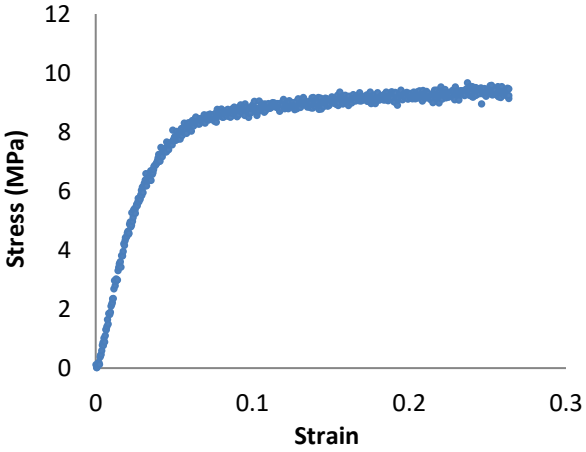

d) After 6 days of degradation

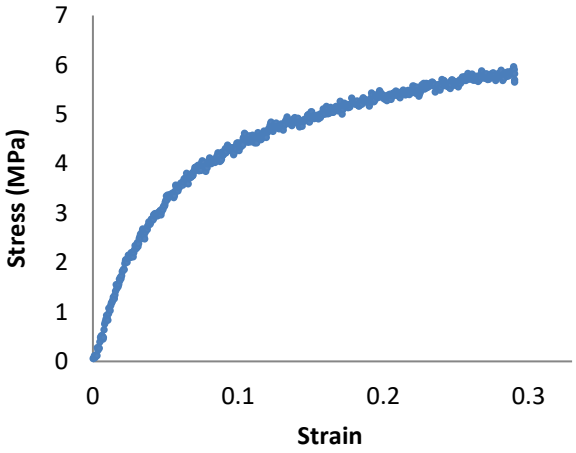

d) After 10 days of degradation

Figure 3-12 Strain-stress curves for the membrane electrospun from the solution at the total polymer concentration of 14% (w/v) before degradation and after 1, 3, 6 and 10 days of degradation

Since all the specimens failed at the grip due to stress concentration and a maximum displacement of 12 mm was utilized due to machine availability, stress-strain curves were able to provide only the elastic modulus and the yield strength as the mechanical properties for the electrospun membranes. The elastic modulus of the membranes at all fiber diameters for each degradation period was plotted as it is shown in Figure 3-13. The measurements for the elastic modulus of the membranes at all fiber diameters for each degradation period were tabulated in Table 3-3.

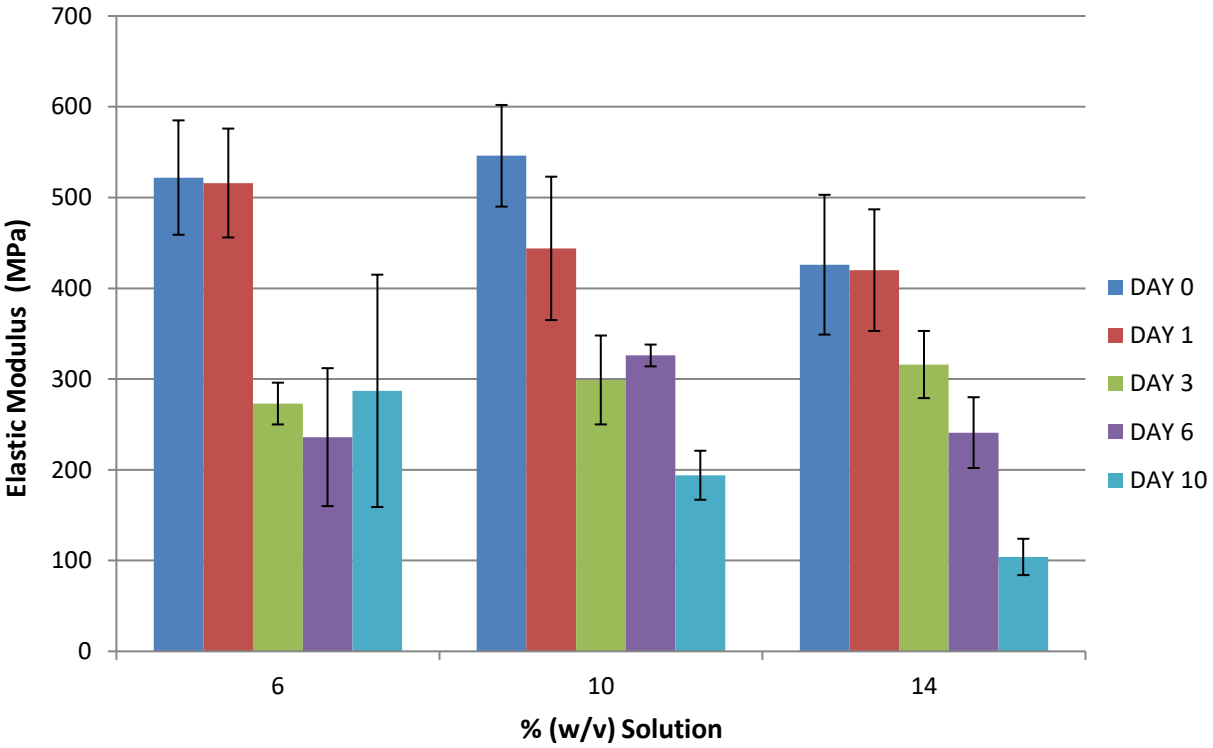

Figure 3-13 The elastic modulus for the membranes electrospun from the solutions at the total polymer concentrations of 6%, 10% and 14% (w/v) before degradation and after 1, 3, 6 and 10 days of degradation

Table 3-3 Elastic modulus for the membranes electrospun from the solutions at the total polymer concentrations of 6%, 10% and 14% (w/v) before degradation and after 1, 3, 6 and 10 days of degradation

Days	6% (w/v)		10% (w/v)		14% (w/v)	
	Average Elastic Modulus (MPa)	Standard Deviation (MPa)	Average Elastic Modulus (MPa)	Standard Deviation (MPa)	Average Elastic Modulus (MPa)	Standard Deviation (MPa)
0	522	±63	546	±56	426	±77
1	516	±60	444	±79	420	±67
3	273	±23	299	±49	316	±37
6	236	±76	326*	±12*	241	±39
10	287	±128	194	±27	104	±20

*4 measurements were averaged due to an outlier.

Before degradation, the elastic modulus of the membranes electrospun form the solutions at the total polymer concentration of 6%, 10%, and 14% (w/v) were found as 522 MPa, 546 MPa and 426 MPa with the standard deviations of 63 MPa, 56 MPa and 77 MPa, respectively. However, these values were not found be statistically significantly different then each other due to the overlap of standard deviations. Therefore, it has been concluded that elastic modulus was the same for all the fiber diameters before degradation. This indicates that fiber diameter does not have a significant influence on the elastic modulus of electrospun Gelatin/PCL membranes.

The elastic modulus for the membrane electrospun form the solution at the total polymer concentration of 6% (w/v) decreased slightly to 516 MPa with a standard deviation of 60 MPa after 1 day of degradation. However, this slight drop in elastic modulus was not found significant due to the overlap of standard deviations. There was a significant decrease in elastic modulus from the 1st to 3rd day of degradation and the elastic modulus was measured as 273 MPa with a standard deviation of 23 MPa at the end of 3 days of degradation. Elastic modulus continued to decrease and measured as 236 MPa with the standard deviation of 76 MPa at the end of 6 days of degradation. Then, there was a statistically insignificant increase to 287 MPa with a standard

deviation of 128 MPa, on the 10th day of degradation. The change in elastic modulus between the 3rd and the 10th day of degradation was not found to be significant due to the overlap of standard deviations.

The elastic modulus for the membrane electrospun from the solution at the total polymer concentration of 10% (w/v) decreased to 444 MPa with a standard deviation of 79 MPa after 1 day of degradation. However, this decrease in elastic modulus was not found to be statistically significant due to the overlap of standard deviations. After 3 days of degradation, the elastic modulus decreased significantly and measured as 299 MPa with a standard deviation of 49 MPa. A slight increase in elastic modulus, which was found statistically insignificant due to the overlap of standard deviations, was seen from the 3rd to the 6th day of degradation and it was measured as 326 MPa with a standard deviation of 12 MPa after 6 days of degradation. The elastic modulus decreased significantly between the 6th and 10th day of degradation and measured as 194 MPa with a standard deviation of 27 MPa after 10 days of degradation.

The elastic modulus for the membrane electrospun form the solution at the total polymer concentration of 14% (w/v) decreased slightly to 420 MPa with a standard deviation of 67 MPa after 1 day of degradation. However, this slight drop was found statistically insignificant due to the overlap of standard deviations. A significant decrease in elastic modulus was seen between the 1st and the 3rd day of degradation and it was measured as 316 MPa with a standard deviation of 37 MPa after 3 days of degradation. There was a moderate decrease in elastic modulus between the 3rd and the 6th of day of degradation and it was measured as 241 MPa with a standard deviation of 39 MPa after 6 days of degradation. From the 6th to the 10th day of degradation, the elastic modulus dropped sharply and was measured as 104 MPa with a standard deviation of 20 MPa after 10 days of degradation.

The elastic modulus of the PCL/Gelatin membranes electrospun from the solutions at all concentrations dropped significantly after 10 days of degradation as it is seen in Figure 3-13. One possible explanation for this decrease might be that the elastic modulus dropped due to the decrease in gelatin content of the fibers. However, there is no statistically significant decrease in elastic modulus for any of the fibers after the first one day of degradation, which is the degradation period that the gelatin content of the fibers found to be diminished sharpest as it is shown in Figure 3-9. In addition, the most prominent decrease in elastic modulus found to be between the 6^{th} and 10^{th} days of degradation, which is the period with no change in gelatin content of the fibers as it is shown in Figure 3-9, for the membranes electrospun from the solutions at the total concentrations of 10% and 14% (w/v). Considering all these factors, it was concluded that there must be another reason for the decrease in elastic modulus.

In the literature, it was found that after 2 and 4 months of incubation in PBS, the elastic modulus of PCL membranes fabricated by phase inversion decreased to approximately 60% and 20% of the elastic modulus before degradation, respectively [116]. In the same study, the molecular weight of the PCL chains found to be decreasing during hydrolytic degradation. The decrease in molecular weight was suggested as the reason for the decrease in elastic modulus of the degraded PCL membranes [116]. Similarly, the decrease in the molecular weight of the PCL chains in the electrospun fibers during hydrolytic bulk degradation might have been caused the elastic modulus of the electrospun membranes to decrease. At this point, it should be noted that the decrease in molecular weight and consequently, the elastic modulus of PCL membranes fabricated by phase inversion occurred in a much longer period of time (2-4 months), whereas the decrease in elastic modulus of our electrospun PCL/Gelatin membranes occurred in a much shorter period of time (10 days). The reason could be that the larger surface area of electrospun

membranes allowed water molecules to diffuse into the polymer chains much more easily compared to the membrane fabricated by phase inversion. This higher level of water diffusion into polymer chains might have accelerated the hydrolytic bulk degradation of the fibers. As a result, the molecular weight of PCL chains and consequently, the elastic modulus of the electrospun membranes might have decreased much faster compared to the PCL membranes fabricated by phase inversion.

The yield strength of the membranes at all fiber diameters for each degradation period was plotted as it is shown in Figure 3-14**.** The measurements for the elastic modulus of the membranes at all fiber diameters for each degradation period were tabulated in Table 3-4.

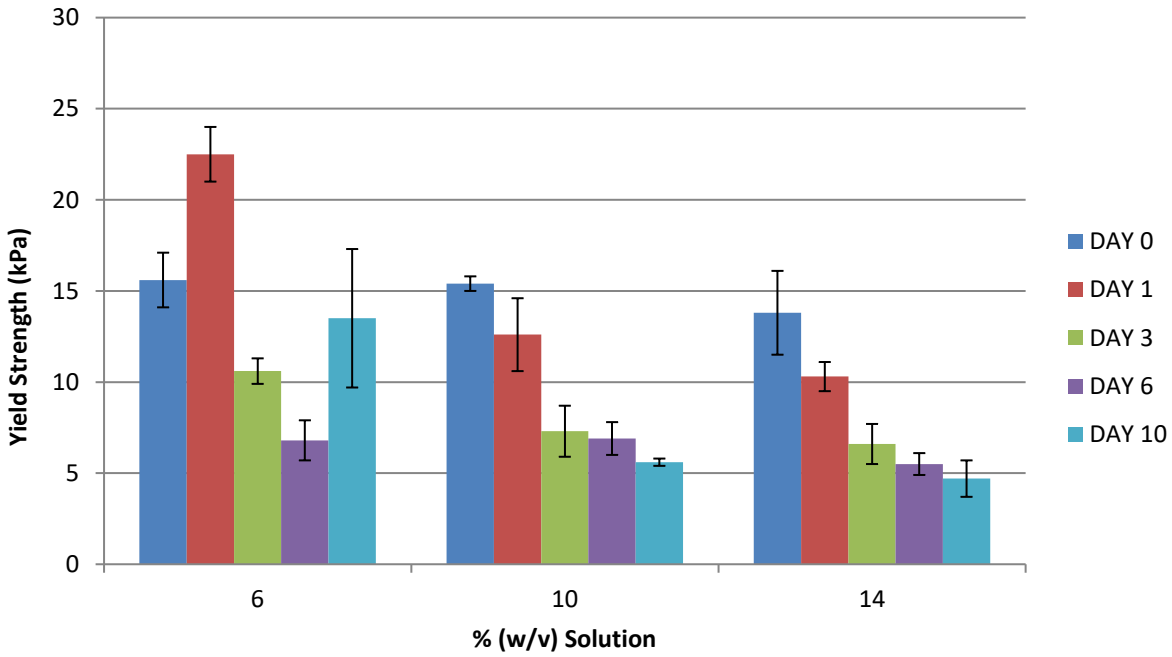

Figure 3-14 Yield strength for the membranes electrospun from the solutions at the total polymer concentrations of 6%, 10% and 14% (w/v) before degradation and after 1, 3, 6 and 10 days of degradation

Table 3-4 Yield strength for the membranes electrospun from the solutions at the total polymer concentrations of 6%, 10% and 14% (w/v) before degradation and after 1, 3, 6 and 10 days of degradation

Days	6% (w/v)		10% (w/v)		14% (w/v)	
	Average Yield Strength (MPa)	Standard Deviation (MPa)	Average Yield Strength (MPa)	Standard Deviation (MPa)	Average Yield Strength (MPa)	Standard Deviation (MPa)
0	15.6	±1.5	15.4	±0.4	13.8	±2.3
1	22.5	±1.5	12.6	±2	10.3	±0.8
3	10.6	±0.7	7.3	±1.4	6.6	±1.1
6	6.8	±1.1	6.9	±0.9	5.5	±0.6
10	13.5	±3.8	5.6	±0.2	4.7	±1

The yield strengths of the membranes electrospun from the solutions at the total polymer concentrations of 6%, 10% and 14 % (w/v) were found as 15.6 MPa, 15.4 MPa and 13.8 MPa with the standard deviations of 1.5 MPa, 0.4 MPa and 2.3 MPa, respectively, before degradation. However, these variations were not found significant due to the overlap of standard deviations. Therefore, it has been concluded that yield strength was the same and around 14 MPa for all the fiber diameters before degradation. This indicates that fiber diameter does not affect the yield strength of electrospun Gelatin/PCL membranes.

The yield strength of the membrane electrospun from the solution at the total polymer concentration of 6% (w/v) increased sharply to 22.5 MPa with a standard deviation of 1.5 MPa after the 1st day of degradation and dropped back to 10.6 MPa with a standard deviation of 0.7 MPa after 3 days of degradation. A significant decline in yield strength was seen between the 3rd and 6th days of degradation and the yield strength was found as 6.8 MPa with a standard deviation of 1.1 MPa after 6 days of degradation. From the 6th to 10th day of degradation, the yield strength increased moderately and found as 13.5 MPa with a standard deviation of 3.8 MPa at the end of 10 days of degradation.

The yield strength of the membrane electrospun from the solution at the total polymer concentration of 10% (w/v) decreased to 12.6 MPa with a standard deviation of 2 MPa after the 1st day of degradation. There was a considerable decrease between the 1st and 3th days of degradation and the yield strength was measured as 7.3 MPa with a standard deviation of 1.4 MPa after 3 days of degradation. The yield strength declined slightly between 3rd and 6th days of degradation and measured as 6.9 MPa with a standard deviation of 0.9 MPa after 6 days of degradation. A significant decrease was seen from the 6th to 10th day of degradation and the yield strength was measured as 5.6 MPa with a standard deviation of 0.2 MPa at the end of 10 days of degradation.

The yield strength of the membrane electrospun from the solution at the total polymer concentration of 14% (w/v) decreased statistically significantly to 10.3 MPa with a standard deviation of 0.8 MPa after the 1st day of degradation. There was a substantial decrease between the 1st and 3rd days of degradation and the yield strength was measured as 6.6 MPa with a standard deviation of 1.1 MPa at the end of 3 days of degradation. A slight decrease, which was not found statistically significant due to the overlap of standard deviations, was seen from the 3rd to 6th day of degradation and the yield strength was measured as 5.5 MPa with a standard deviation of 0.6 MPa at the end of 6 days of degradation. There was a statistically insignificant decrease between the 6th and 10th days of degradation and the yield strength found as 4.7 MPa with a standard deviation of 1 MPa at the end of 10 days of degradation.

It was seen that the yield strength decreased significantly over 10 days of degradation for the membranes electrospun from the solutions at the total polymer concentrations of 10% and 14% (w/v). The reason could be related to the loss of gelatin content over time because a consistent statistically significant decreasing trend was observed over the course of the first three

days of degradation, which is the period that the decrease in gelatin content is the most prominent as it is shown in Figure 3-9. Moreover, for the membranes electrospun from the solutions at the total polymer concentrations of 10% and 14% (w/v), the yield strength did not change significantly between the 3rd and 10th days of degradation, which is the degradation period that corresponds to almost no change in gelatin content as it is shown in Figure 3-9. Therefore, it was deduced that the decrease in yield strength is due to the decrease in gelatin content of the fibers.

It was seen that the yield strength remained unchanged over 10 days of degradation for the membranes electrospun form the solution at the total polymer concentrations of 6%. The reason might be related to the loss of fibrous structure upon degradation.

The stress-strain curves, elastic modulus and yield strength for each sample before and after each degradation period were shown in Appendix C.

3.4. Contact Angle Measurements

The degradation dependent change of contact angles for the membranes electrospun from the solutions at the total polymer concentrations of 6%, 10%, and 14% (w/v) was shown in Figure 3-15. For each degradation period, the contact angle measurements for the membranes electrospun from the solutions at all concentrations are tabulated in Table 3-5.

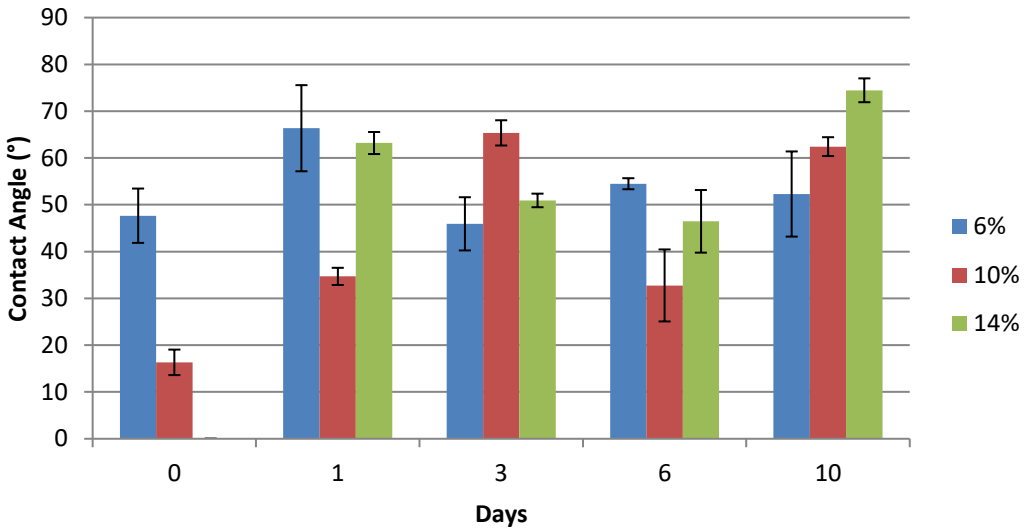

Figure 3-15 The contact angles for the membranes electrospun from the solutions at the total polymer concentrations of 6%, 10% and 14% (w/v) before degradation and after 1, 3, 6 and 10 days of degradation

Table 3-5 The contact angles for the membranes electrospun from the solutions at the total polymer concentrations of 6%, 10% and 14% (w/v) before degradation and after 1, 3, 6 and 10 days of degradation

Days	6% (w/v)		10% (w/v)		14% (w/v)	
	Average Contact Angle (°)	Standard Deviation (°)	Average Contact Angle (°)	Standard Deviation (°)	Average Contact Angle (°)	Standard Deviation (°)
0	48	±6	16	±3	0	±0
1	66	±9	35	±2	63	±2
3	46	±6	65	±3	51	±1
6	55	±1	33	±8	46	±7
10	52	±9	62	±2	74	±3

For the membrane electrospun from the solution at the total polymer concentration of 14% (w/v), the contact angle was measured as 0° due to the complete absorption of the droplets by the membrane. After the 1st day of degradation, the contact angle rose up sharply to 63° with a standard deviation of 2°, which indicates a significant decrease in hydrophilicity due to the loss of gelatin content as it is shown in Figure 3-9. The contact angle decreased slightly from the 1st to 3rd day of degradation and found as 51° with a standard deviation of 1°. A slight decline in

contact angle was seen between the 3th and 6th day of degradation and the contact angle was measured as 46° with a standard deviation of 7° after 6 days of degradation. However, this slight decline was not found to be significant due to the overlap of standard deviations. The contact angle rose sharply from the 6th to 10th day of degradation and found as 74° with a standard deviation of 3°.

For the membrane electrospun from the solution at the total polymer concentration of 10% (w/v), the contact angle was measured as 16° with a standard deviation of 3°. A significant increase was seen after the 1st day of degradation due to the loss of gelatin content, and the contact angle was measured as 35° with a standard deviation of 2°. At the 3rd day of degradation, the contact angle rose considerably to 65° with a standard deviation of 3°, which indicates that the membrane became consistently more hydrophilic over the first 3 days of degradation. However, the contact angle declined back to 33° with a standard deviation of 8° after 6 days of degradation and went up again to 62° with a standard deviation of 2° after 10 days of degradation.

For the membrane electrospun from the solution at the total polymer concentration of 6% (w/v), the contact angle was measured as 48° with a standard deviation of 6°. The contact angle increased significantly to 66° with a standard deviation of 9° after 1 day of degradation and went down again to 46° with a standard deviation of 6° after the 3rd day of degradation. A significant increase was seen between the 3rd and 6th days of degradation and the contact angle was measured as 55° with a standard deviation of 1° after 6 days of degradation. The contact angle decreased slightly from the 6th to 10th day of degradation and measured as 52° with a standard deviation of 9°. However, this slight decrease was not found to be statistically significant due to the overlap of standard deviations.

The contact angle for the non-degraded Gelatin/PCL membranes found to be increasing as the concentration of the electrospinning solution is decreasing as it is seen in Figure 3-15, which indicates that contact angle increases as the fiber diameter decreases. In the literature, the contact angle for the electrospun Gelatin/PCL membranes with 1:1 gelatin to PCL weight ratio was measured as 0° due to the complete absorption of the droplet [54]. The contact angle of the membrane with the largest fiber diameter, which was electrospun from the solution with 14% (w/v) concentration, was also found 0. This indicates that Gelatin/PCL membranes with 1:1 Gelatin to PCL weight ratio are capable of absorbing the droplet completely when the fiber diameter is large enough.

In the literature, the contact angles for the electrospun PCL/Gelatin membranes with PCL to Gelatin weight ratios of 9:1, 8:2 and 7:3 were measured as approximately 130°, which is the contact angle for pure electrospun PCL fibers, after 90 days of *in vitro* degradation [108]. Similarly, in this study, for the membranes electrospun from the solutions at the total polymer concentration of 10% and 14% (w/v), the contact angle was also found to be increasing after 10 days of degradation. This confirms that the membranes become more hydrophobic as gelatin dissolves away and PCL weight ratio of the fibers increases. However, for the membrane electrospun from the solution at the total polymer concentration of 6% (w/v), no significant change in the contact angle was observed after 10 days of degradation. The reason might be related to the fibrous structure being lost at the early stage of degradation.

The images of the droplets used to measure the contact angles of the membranes electrospun from the solution at the total polymer concentration of 6%, 10%, and 14% (w/v) at different stages of degradation were shown in Figure 3-16, Figure 3-17, and Figure 3-18,

respectively. The images of the droplets used for all the measurements were shown in Appendix D.

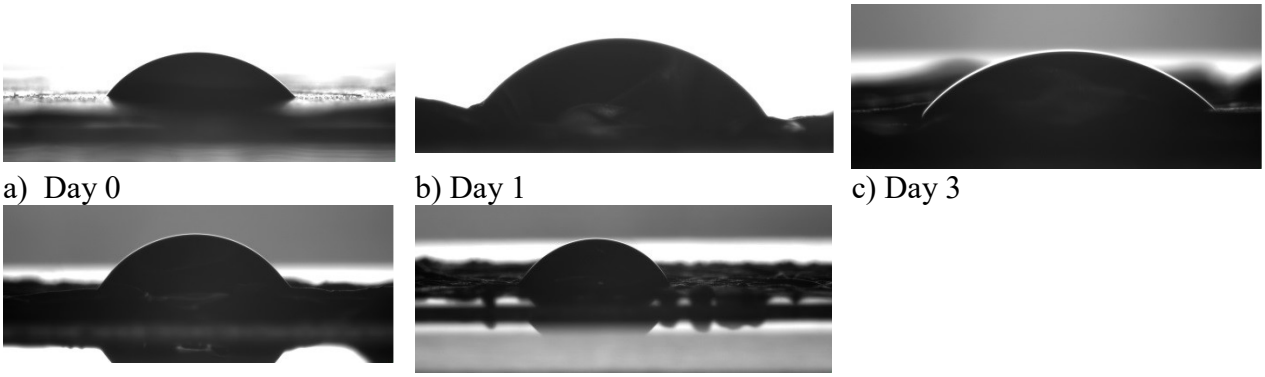

a) Day 0 b) Day 1 c) Day 3

d) Day 6 e) Day 10

Figure 3-16 Contact angles for the membranes electrospun from the solution at the total polymer concentration of 6% (w/v) before degradation and after 1, 3, 6 and 10 days of degradation

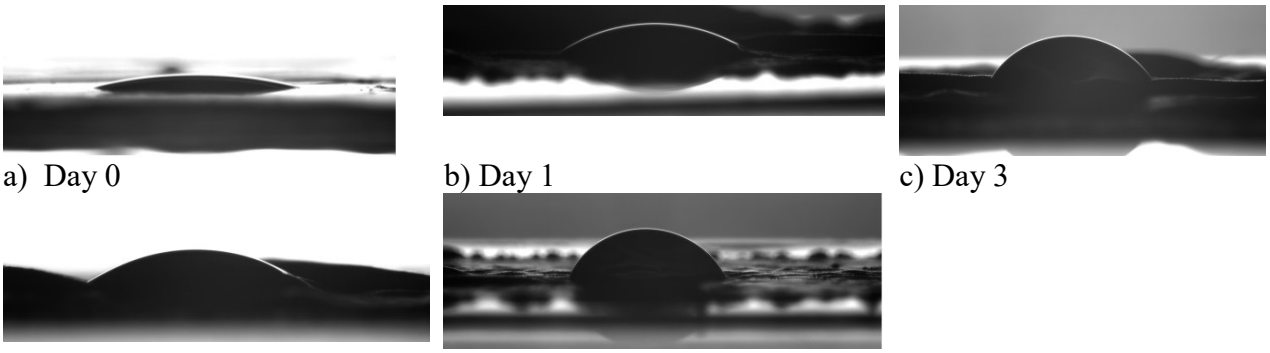

a) Day 0 b) Day 1 c) Day 3

d) Day 6 e) Day 10

Figure 3-17 Contact angles for the membranes electrospun from the solution at the total polymer concentration of 10% (w/v) before degradation and after 1, 3, 6 and 10 days of degradation

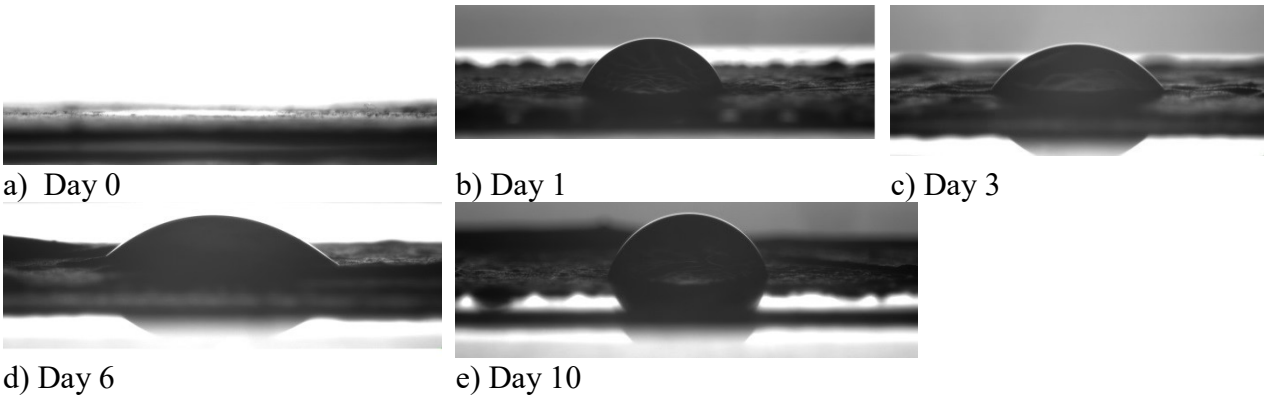

a) Day 0 b) Day 1 c) Day 3

d) Day 6 e) Day 10

Figure 3-18 Contact angles for the membranes electrospun from the solution at the total polymer concentration of 14% (w/v) before degradation and after 1, 3, 6 and 10 days of degradation

4. Conclusion

In this study, the effect of fiber diameter on the degradation profile, elastic modulus, yield strength, and hydrophilicity of the electropsun PCL/Gelatin membranes was investigated. In order to obtain electropsun PCL/Gelatin membranes of three distinct average fiber diameters, the blends of PCL and Gelatin with 1:1 PCL to Gelatin ratio were electrospun at the total polymer concentrations of 6%, 10% and 14% (w/v). The average fiber diameters were calculated as 184 ± 51 nm, 803 ± 349 nm and 2131 ± 701 nm for the membranes electrospun from the solutions at the total polymer concentrations of 6%, 10% and 14% (w/v), respectively. It was seen that the fibrous structure was lost for the membrane electrospun from the solution at the total polymer concentration of 6% (w/v) after the 1st day of hydrolytic degradation. The reason could be that because the fibers were too thin, the number of PCL chains in the individual fibers was not enough to maintain the integrity of the fibers during degradation. On the other hand, fiber diameter did not change significantly for the membranes electrospun from the solutions at the total polymer concentrations of 10% and 14% (w/v) over the course of 10 days of hydrolytic degradation. The reason could be that the fibers electrospun from the solutions at the total polymer concentrations of 10% and 14% (w/v) were large enough that there was sufficient number of PCL chains making up the bulk of the fibers. The degradation period of 10 days was not enough for the hydrolytic degradation to proceed to the extent that low molecular water-soluble species are formed. Since the low molecular species that can dissolve away did not form, the fibers did not lose any PCL mass, and consequently, the diameter of the fibers were preserved during bulk degradation. However, the elastic modulus decreased significantly from 522 ± 63 MPa, 546 ± 56 MPa and 426 ± 77 MPa to 287 ± 128 MPa, 194 ± 27 MPa and 104 ± 20 MPa, after 10 days of degradation for the membranes electrospun at total polymer concentrations

of 6%, 10% and 14% (w/v), respectively probably due to the reduction of molecular weight of PCL chains. Similarly, the yield strength decreased significantly from 15.4 ± 0.4 MPa and 13.8 ± 2.3 MPa to 5.6 ± 0.2 MPa and 4.7 ± 1 MPa after 10 days of degradation for the membranes electrospun at total polymer concentrations of 10% and 14% (w/v), respectively probably due to the decrease in gelatin content of the fibers. The yield strength of the membrane electrospun at the total polymer concentration of 6% (w/v) did not change significantly before and after 10 days of degradation. The reason might be related to the loss of fibrous structure in degraded membranes.

The gravimetric analysis revealed that all the membranes maintained 76%, 61%, 55% and 55% of their initial masses after 1, 3, 6 and 10 days of degradation, which indicates that the changes in surface area of the fibers at nanoscale do not have a significant influence on the degradation profile. It has been anticipated that the decrease in membrane masses is only due to the dissolution of gelatin, since hydrolytic degradation of PCL did not proceed to the extent which the low molecular species that are soluble in water formed.

Finally, the contact angle measurements revealed that hydrophilicity of the membranes decreases as the membranes are degraded, which confirms that gelatin content of the fibers diminished over the course of degradation.

The future work for this research may involve FTIR analysis of the degraded membranes at three different fiber diameters to study the dissolution of gelatin in more detail. In addition, the effect of fiber diameter and hydrolytic degradation on the reduction of molecular weight of the PCL in fibers should be investigated. Moreover, the relation between the loss of fibrous structure and the yield strength and contact angle remaining unchanged after 10 days of degradation for the membrane electrospun at 6% (w/v) concentration should be elucidated. In addition, the effect

of fiber diameter on cell adhesion, proliferation, and migration should be studied for the PCL/Gelatin membranes. The effect of fiber diameter of PCL/Gelatin membranes on the delivery and release profile of growth factors and genes should be studied, as well.

Bibliography

[1] K. Dzobo *et al.*, “Advances in regenerative medicine and tissue engineering: Innovation and transformation of medicine,” *Stem Cells Int.*, vol. 2018, 2018.

[2] F. Akter, *What is Tissue Engineering?* Elsevier Inc., 2016.

[3] F. J. O’Brien, “Biomaterials & scaffolds for tissue engineering,” *Mater. Today*, vol. 14, no. 3, pp. 88–95, 2011.

[4] N. S. Binulal, A. Natarajan, D. Menon, V. K. Bhaskaran, U. Mony, and S. V. Nair, “PCL-gelatin composite nanofibers electrospun using diluted acetic acid-ethyl acetate solvent system for stem cell-based bone tissue engineering,” *J. Biomater. Sci. Polym. Ed.*, vol. 25, no. 4, pp. 325–340, 2014.

[5] P. A. Link and R. L. Heise, “Pulmonary Tissue Engineering 12 . 2 Clinical Need for Pulmonary Tissue Engineering,” pp. 389–411, 2017.

[6] F. Akter, *Principles of Tissue Engineering*. Elsevier Inc., 2016.

[7] W.-J. Li, R. M. Shanti, and R. S. Tuan, *Electrospinning Technology for Nanofibrous Scaffolds in Tissue Engineering*, vol. 9. 2007.

[8] C. M. Murphy, F. J. O’Brien, D. G. Little, and A. Schindeler, “Cell-scaffold interactions in the bone tissue engineering triad,” *Eur. Cells Mater.*, vol. 26, pp. 120–132, 2013.

[9] S. M. Lingala and M. G. M. Mhs. Ghany, “可乐定和右美托嗪啶产生抗伤害协同作用 HHS Public Access,” vol. 25, no. 3, pp. 289–313, 2016.

[10] C. S. Alge, S. M. Hauck, S. G. Priglinger, A. Kampik, and M. Ueffing, “Differential protein profiling of primary versus immortalized human RPE cells identifies expression patterns associated with cytoskeletal remodeling and cell survival,” *J. Proteome Res.*, vol.

5, no. 4, pp. 862–878, 2006.

[11] C. Pan, C. Kumar, S. Bohl, U. Klingmueller, and M. Mann, “Comparative Proteomic Phenotyping of Cell Lines and Primary Cells to Assess Preservation of Cell Type-specific Functions,” *Mol. Cell. Proteomics*, vol. 8, no. 3, pp. 443–450, 2009.

[12] K. Lee, E. A. Silva, and D. J. Mooney, “Growth factor delivery-based tissue engineering: General approaches and a review of recent developments,” *J. R. Soc. Interface*, vol. 8, no. 55, pp. 153–170, 2011.

[13] G. Kerman, A. Rajesh, K. C. Remant, and H. Uludağ, “Gene-based approaches to bone regeneration,” in *Musculoskeletal Research and Basic Science*, 2015.

[14] E. Kijeńska and W. Swieszkowski, “General requirements of electrospun materials for tissue engineering,” *Electrospun Mater. Tissue Eng. Biomed. Appl.*, pp. 43–56, 2017.

[15] L. Ghasemi-Mobarakeh, M. P. Prabhakaran, M. Morshed, M. H. Nasr-Esfahani, and S. Ramakrishna, “Electrospun poly(ε-caprolactone)/gelatin nanofibrous scaffolds for nerve tissue engineering,” *Biomaterials*, vol. 29, no. 34, pp. 4532–4539, 2008.

[16] N. L. Davison, F. Barrère-de Groot, and D. W. Grijpma, *Degradation of Biomaterials*, Second Edi. Elsevier Inc., 2014.

[17] B. P. Biomaterials, “Biodegradable Polymeric Materials,” no. 1987, pp. 1–5, 1999.

[18] R. Mhanna and A. Hasan, “1 . 2 Clinical Need for Tissue Engineering,” pp. 3–34, 2017.

[19] D. Coutinho, P. Costa, and N. Neves, *Tissue Engineering*, vol. 2. 2011.

[20] P. X. Ma, “Scaffolds for tissue fabrication,” *Mater. Today*, vol. 7, no. 5, pp. 30–40, 2004.

[21] R. Vasita and D. S. Katti, “Nanofibers and their applications in tissue engineering,” *Int. J. Nanomedicine*, vol. 1, no. 1, pp. 15–30, 2006.

[22] N. H. A. Ngadiman, M. Y. Noordin, A. Idris, and D. Kurniawan, “A review of evolution

of electrospun tissue engineering scaffold: From two dimensions to three dimensions," *Proc. Inst. Mech. Eng. Part H J. Eng. Med.*, vol. 231, no. 7, pp. 597–616, 2017.

[23] E. J. Carbone, T. Jiang, C. Nelson, N. Henry, and K. W. H. Lo, "Small molecule delivery through nanofibrous scaffolds for musculoskeletal regenerative engineering," *Nanomedicine Nanotechnology, Biol. Med.*, vol. 10, no. 8, pp. 1691–1699, 2014.

[24] J. Bajakova, J. Chaloupek, M. Lacarin, and D. Lukáš, "'Drawing'- the Production of Individual Nanofibers By Experimental Method," *Nanocon*, vol. 9, no. 1, pp. 21–23, 2011.

[25] L. Feng *et al.*, "Super-hydrophobic surface of aligned polyacrylonitrile nanofibers," *Angew. Chemie - Int. Ed.*, vol. 41, no. 7, pp. 1221–1223, 2002.

[26] S. Iijima, "Synthetic nano-scale fibrous matrix," *Nature*, vol. 56, no. June, pp. 354–358, 1991.

[27] S. Ramakrishna and K. Fujihara, *Electrospinning and Nanofibers*. 2005.

[28] D. H. Reneker and A. L. Yarin, "Electrospinning jets and polymer nanofibers," *Polymer (Guildf).*, vol. 49, no. 10, pp. 2387–2425, 2008.

[29] H. Liu, X. Ding, G. Zhou, P. Li, X. Wei, and Y. Fan, "Electrospinning of Nanofibers for Tissue Engineering Applications," *J. Nanomater.*, vol. 2013, pp. 1–11, 2013.

[30] A. Senthamizhan, B. Balusamy, and T. Uyar, *Electrospinning: A versatile processing technology for producing nanofibrous materials for biomedical and tissue-engineering applications*. Elsevier Ltd., 2017.

[31] J. Doshi, and D. H. Reneker, "Electrospinning Process and Applications of Electropsun Fibers" *Journal of Electrostatics*, vol. 35, pp. 151-160, 1995.

[32] Kenry and C. T. Lim, "Nanofiber technology: current status and emerging developments," *Prog. Polym. Sci.*, vol. 70, pp. 1–17, 2017.

[33] S. Lee and S. K. Obendorf, “Use of Electrospun Nanofiber Web for Protective Textile Materials as Barriers to Liquid Penetration,” *Text. Res. J.*, vol. 77, no. 9, pp. 696–702, 2007.

[34] B. Liu, S. Zhang, X. Wang, J. Yu, and B. Ding, “Efficient and reusable polyamide-56 nanofiber/nets membrane with bimodal structures for air filtration,” *J. Colloid Interface Sci.*, vol. 457, pp. 203–211, 2015.

[35] H. Jia, G. Zhu, B. Vugrinovich, W. Kataphinan, D. H. Reneker, and P. Wang, “Enzyme-carrying polymeric nanofibers prepared via electrospinning for use as unique biocatalysts,” *Biotechnol. Prog.*, vol. 18, no. 5, pp. 1027–1032, 2002.

[36] L. Wang *et al.*, “A novel carbon-silicon composite nanofiber prepared via electrospinning as anode material for high energy-density lithium ion batteries,” *J. Power Sources*, vol. 195, no. 15, pp. 5052–5056, 2010.

[37] Z. K. Nagy, K. Nyúl, I. Wagner, K. Molnár, and G. Marosi, “Electrospun water soluble polymer mat for ultrafast release of donepezil HCL,” *Express Polym. Lett.*, vol. 4, no. 12, pp. 763–772, 2010.

[38] M. Khil, D. Cha, H. Kim, I. Kim, and N. Bhattarai, “as Wound Dressing,” *J. Biomed. Mater. Res.*, vol. 67B, no. 2, pp. 675–679, 2003.

[39] M. Tenuta, X. Gao, D. N. Flaten, and B. D. Amiro, “Lower Nitrous Oxide Emissions from Anhydrous Ammonia Application Prior to Soil Freezing in Late Fall Than Spring Pre-Plant Application,” *J. Environ. Qual.*, vol. 45, no. 4, p. 1133, 2016.

[40] A. Formhals, “US Patent 1,975,504,” pp. 1–4, 1934.

[41] H. L. Simons, “Annananz 55,” 1966.

[42] P. K. Baumgarten, “Electrostatic spinning of acrylic microfibers,” *J. Colloid Interface*

Sci., vol. 36, no. 1, pp. 71–79, 1971.

[43] M. Yanilmaz, M. Dirican, and X. Zhang, "Evaluation of electrospun SiO2/nylon 6,6 nanofiber membranes as a thermally-stable separator for lithium-ion batteries," *Electrochim. Acta*, vol. 133, pp. 501–508, 2014.

[44] K. Ohkawa, H. Kim, and K. Lee, "Biodegradation of electrospun poly-(E-caprolactone) non-woven fabrics by pure-cultured soil filamentous fungi," *J. Polym. Environ.*, vol. 12, no. 4, pp. 211–218, 2004.

[45] E. D. Boland, B. D. Coleman, C. P. Barnes, D. G. Simpson, G. E. Wnek, and G. L. Bowlin, "Electrospinning polydioxanone for biomedical applications," *Acta Biomater.*, vol. 1, no. 1, pp. 115–123, 2005.

[46] Y. You, B. M. Min, S. J. Lee, T. S. Lee, and W. H. Park, "In vitro degradation behavior of electrospun polyglycolide, polylactide, and poly(lactide-co-glycolide)," *J. Appl. Polym. Sci.*, vol. 95, no. 2, pp. 193–200, 2005.

[47] B. Ding, M. Yamazaki, and S. Shiratori, "Electrospun fibrous polyacrylic acid membrane-based gas sensors," *Sensors Actuators, B Chem.*, vol. 106, no. 1 SPEC. ISS., pp. 477–483, 2005.

[48] K. H. Lee, H. Y. Kim, Y. M. La, D. R. Lee, and N. H. Sung, "Influence of a mixing solvent with tetrahydrofuran and N,N-dimethylformamide on electrospun poly(vinyl chloride) nonwoven mats," *J. Polym. Sci. Part B Polym. Phys.*, vol. 40, no. 19, pp. 2259–2268, 2002.

[49] K. H. Lee, H. Y. Kim, H. J. Bang, Y. H. Jung, and S. G. Lee, "The change of bead morphology formed on electrospun polystyrene fibers," *Polymer (Guildf).*, vol. 44, no. 14, pp. 4029–4034, 2003.

[50] H. Yoshimoto, Y. M. Shin, H. Terai, and J. P. Vacanti, “A biodegradable nanofiber scaffold by electrospinning and its potential for bone tissue engineering,” *Biomaterials*, vol. 24, no. 12, pp. 2077–2082, 2003.

[51] R. Jaeger, M. M. Bergshoef, C. M. I. Batlle, H. Schönherr, and G. Julius Vancso, “Electrospinning of ultra-thin polymer fibers,” *Macromol. Symp.*, vol. 127, no. 1, pp. 141–150, 1998.

[52] Y. Wang and Y. Lo Hsieh, “Enzyme immobilization to ultra-fine cellulose fibers via amphiphilic polyethylene glycol spacers,” *J. Polym. Sci. Part A Polym. Chem.*, vol. 42, no. 17, pp. 4289–4299, 2004.

[53] M. Li, M. J. Mondrinos, M. R. Gandhi, F. K. Ko, A. S. Weiss, and P. I. Lelkes, “Electrospun protein fibers as matrices for tissue engineering,” *Biomaterials*, vol. 26, no. 30, pp. 5999–6008, 2005.

[54] Y. Zhang, H. Ouyang, C. T. Lim, S. Ramakrishna, and Z. Huang, “Electrospinning of Gelatin Fibers and Gelatin / PCL Composite Fibrous Scaffolds,” pp. 156–165, 2004.

[55] G. Taylor, “Electrically Driven Jets,” *Proc. R. Soc. A Math. Phys. Eng. Sci.*, vol. 313, no. 1515, pp. 453–475, 1969.

[56] D. Reneker and H. Hou, *Electrospinning*. Elsevier Inc., 2015.

[57] A. Haider, S. Haider, and I. K. Kang, “A comprehensive review summarizing the effect of electrospinning parameters and potential applications of nanofibers in biomedical and biotechnology,” *Arab. J. Chem.*, vol. 11, no. 8, pp. 1165–1188, 2018.

[58] K. Garg and G. L. Bowlin, “Electrospinning jets and nanofibrous structures,” *Biomicrofluidics*, vol. 5, no. 1, pp. 1–19, 2011.

[59] N. Ismail, F. J. Maksoud, N. Ghaddar, K. Ghali, and A. Tehrani-Bagha, “Simplified

modeling of the electrospinning process from the stable jet region to the unstable region for predicting the final nanofiber diameter," *J. Appl. Polym. Sci.*, vol. 133, no. 43, pp. 1–11, 2016.

[60] C. J. Angammana, S. Member, and S. H. Jayaram, "Analysis of the Effects of Solution Conductivity on Electrospinning Process and Fiber Morphology," *IEEE Trans. Ind. Appl.*, vol. 47, no. 3, pp. 1109–1117, 2011.

[61] M. Yousefzadeh, *Modeling and simulation of the electrospinning process*. Elsevier Ltd., 2016.

[62] S. Gadkari, "Influence of polymer relaxation time on the electrospinning process: Numerical investigation," *Polymers (Basel).*, vol. 9, no. 10, pp. 1–16, 2017.

[63] N. Bhardwaj and S. C. Kundu, "Electrospinning: A fascinating fiber fabrication technique," *Biotechnol. Adv.*, vol. 28, no. 3, pp. 325–347, 2010.

[64] H. Fong, I. Chun, and D. H. Reneker, "<1-s2.0-S0032386199000683-main.pdf>," *Polymer (Guildf).*, vol. 40, no. 16, pp. 4585–4592, 1999.

[65] N. Kurokawa, F. Endo, T. Maeda, and A. Hotta, *Electrospinning and surface modification methods for functionalized cell scaffolds*. Elsevier Inc., 2017.

[66] R. H. Colby and M. Rubinstein, "Two-Parameter Scaling for Polymers in 9 Solvents," *Macromolecules*, vol. 23, no. 10, pp. 2753–2757, 1990.

[67] P. Gupta, C. Elkins, T. E. Long, and G. L. Wilkes, "Electrospinning of linear homopolymers of poly(methyl methacrylate): Exploring relationships between fiber formation, viscosity, molecular weight and concentration in a good solvent," *Polymer (Guildf).*, vol. 46, no. 13, pp. 4799–4810, 2005.

[68] P. Rai and S. L. Rosen, "An empirical relation between the Mark-Houwink-Sakurada

constants," *J. Polym. Sci. Part B Polym. Phys.*, vol. 35, no. 12, pp. 1985–1987, 1997.

[69] M. G. McKee, G. L. Wilkes, R. H. Colby, and T. E. Long, "Correlations of Solution Rheology with Electrospun Fiber Formation of Linear and Branched Polyesters," *Macromolecules*, vol. 37, no. 5, pp. 1760–1767, 2004.

[70] C. S. Ki, D. H. Baek, K. D. Gang, K. H. Lee, I. C. Um, and Y. H. Park, "Characterization of gelatin nanofiber prepared from gelatin-formic acid solution," *Polymer (Guildf).*, vol. 46, no. 14, pp. 5094–5102, 2005.

[71] Z. Jun, H. Hou, A. Schaper, J. H. Wendorff, and A. Greiner, "Poly-L-lactide nanofibers by electrospinning - Influence of solution viscosity and electrical conductivity on fiber diameter and fiber morphology," *E-Polymers*, vol. 3, no. 1, pp. 1–9, 2003.

[72] J. S. Lee *et al.*, "Role of molecular weight of atactic poly(vinyl alcohol) (PVA) in the structure and properties of PVA nanofabric prepared by electrospinning," *J. Appl. Polym. Sci.*, vol. 93, no. 4, pp. 1638–1646, 2004.

[73] S. Zhao, X. Wu, L. Wang, and Y. Huang, "Electrospinning of ethyl-cyanoethyl cellulose/tetrahydrofuran solutions," *J. Appl. Polym. Sci.*, vol. 91, no. 1, pp. 242–246, 2004.

[74] J. M. Deitzel, J. Kleinmeyer, D. Harris, and N. C. Beck Tan, "The effect of processing variables on the morphology of electrospun," *Polymer (Guildf).*, vol. 42, pp. 261–272, 2001.

[75] C. Wang *et al.*, "Correlation between processing parameters and microstructure of electrospun poly(D,l-lactic acid) nanofibers," *Polymer (Guildf).*, vol. 50, no. 25, pp. 6100–6110, 2009.

[76] H. Hall, "V018a09," *Eur. Cells Mater.*, vol. 21, pp. 286–303, 2011.

[77] Z. Li and C. Wang, “One-Dimensional nanostructures,” pp. 15–28, 2013.

[78] W. Zuo, M. Zhu, W. Yang, H. Yu, Y. Chen, and Y. Zhang, “Experimental study on relationship between jet instability and formation of beaded fibers during electrospinning,” *Polym. Eng. Sci.*, vol. 45, no. 5, pp. 704–709, 2005.

[79] X. Y. Yuan, Y. Y. Zhang, C. Dong, and J. Sheng, “Morphology of ultrafine polysulfone fibers prepared by electrospinning,” *Polym. Int.*, vol. 53, no. 11, pp. 1704–1710, 2004.

[80] T. J. Sill and H. A. von Recum, “Electrospinning: Applications in drug delivery and tissue engineering,” *Biomaterials*, vol. 29, no. 13, pp. 1989–2006, 2008.

[81] T. Wang and S. Kumar, “Electrospinning of polyacrylonitrile nanofibers,” *J. Appl. Polym. Sci.*, vol. 102, no. 2, pp. 1023–1029, 2006.

[82] K. Henriksen and M. A. Karsdal, *Type I Collagen*. Elsevier Inc., 2016.

[83] N. S. Fedarko, *Osteoblast/Osteoclast Development and Function in Osteogenesis Imperfecta*. Elsevier Inc., 2013.

[84] N. Shaw and W. Högler, “Biochemical Markers of Bone Metabolism,” *Pediatr. Bone*, pp. 361–381, 2012.

[85] M. P. Nijsure and V. Kishore, *Collagen-based scaffolds for bone tissue engineering applications*. 2018.

[86] B. Clarke, “Normal bone anatomy and physiology.,” *Clin. J. Am. Soc. Nephrol.*, vol. 3 Suppl 3, pp. 131–139, 2008.

[87] “Gelatin Biopolymer: A Journey from Micro to Nano,” *J. Pharm. Res.*, vol. 8, no. 10, pp. 1387–1397, 2014.

[88] S. Panzavolta, M. Gioffrè, M. L. Focarete, C. Gualandi, L. Foroni, and A. Bigi, “Electrospun gelatin nanofibers: Optimization of genipin cross-linking to preserve fiber

morphology after exposure to water," *Acta Biomater.*, vol. 7, no. 4, pp. 1702–1709, 2011.

[89] R. Selvakumar, S. N. M. Mohaideen, S. Aravindh, C. Sabarinath, and M. Ananthasubramanian, "Effect of Biotin and Galactose Functionalized Gelatin Nanofiber Membrane on HEp-2 Cell Attachment and Cytotoxicity," pp. 35–43, 2014.

[90] K. S. Rho *et al.*, "Electrospinning of collagen nanofibers: Effects on the behavior of normal human keratinocytes and early-stage wound healing," *Biomaterials*, vol. 27, no. 8, pp. 1452–1461, 2006.

[91] K. J. Shields, M. J. Beckman, G. L. Bowlin, and J. S. Wayne, "Mechanical properties and cellular proliferation of electrospun collagen type II.," *Tissue Eng.*, vol. 10, no. 9–10, pp. 1510–7, 2004.

[92] J. A. Matthews, G. E. Wnek, D. G. Simpson, and G. L. Bowlin, "Electrospinning of collagen nanofibers," *Biomacromolecules*, vol. 3, no. 2, pp. 232–238, 2002.

[93] V. Guarino, M. Alvarez-Perez, V. Cirillo, and L. Ambrosio, "HMSC interaction with PCL and PCL/gelatin platforms: A comparative study on films and electrospun membranes," *J. Bioact. Compat. Polym.*, vol. 26, no. 2, pp. 144–160, 2011.

[94] D. I. Zeugolis *et al.*, "Electro-spinning of pure collagen nano-fibres - Just an expensive way to make gelatin?," *Biomaterials*, vol. 29, no. 15, pp. 2293–2305, 2008.

[95] Y. Zhang, Z. M. Huang, X. Xu, C. T. Lim, and S. Ramakrishna, "Preparation of core-shell structured PCL-r-gelatin bi-component nanofibers by coaxial electrospinning," *Chem. Mater.*, vol. 16, no. 18, pp. 3406–3409, 2004.

[96] R. S. Tiğli, N. M. Kazaroğlu, B. Maviş, and M. Gumusderelioglu, "Cellular behavior on epidermal growth factor (EGF)-immobilized PCL/gelatin nanofibrous scaffolds," *J. Biomater. Sci. Polym. Ed.*, vol. 22, no. 1–3, pp. 207–223, 2011.

[97] S. Heydarkhan-Hagvall *et al.*, "Three-dimensional electrospun ECM-based hybrid scaffolds for cardiovascular tissue engineering," *Biomaterials*, vol. 29, no. 19, pp. 2907–2914, 2008.

[98] D. Kai, M. P. Prabhakaran, G. Jin, and S. Ramakrishna, "Guided orientation of cardiomyocytes on electrospun aligned nanofibers for cardiac tissue engineering," *J. Biomed. Mater. Res. - Part B Appl. Biomater.*, vol. 98 B, no. 2, pp. 379–386, 2011.

[99] S. Gautam, A. K. Dinda, and N. C. Mishra, "Fabrication and characterization of PCL/gelatin composite nanofibrous scaffold for tissue engineering applications by electrospinning method," *Mater. Sci. Eng. C*, vol. 33, no. 3, pp. 1228–1235, 2013.

[100] X. He, H. Zhang, and W. Wang, "Electrospun gelatin / PCL and collagen / PLCL scaffolds for vascular tissue engineering," pp. 2335–2344, 2014.

[101] Zhang *et al.*, "Engineering of epidermis skin grafts using electrospun nanofibrous gelatin/polycaprolactone membranes," *Int. J. Nanomedicine*, p. 2077, 2013.

[102] R. Zheng *et al.*, "The influence of Gelatin/PCL ratio and 3-D construct shape of electrospun membranes on cartilage regeneration," *Biomaterials*, vol. 35, no. 1, pp. 152–164, 2014.

[103] P. Kuppan, S. Sethuraman, and U. M. Krishnan, "Interaction of human smooth muscle cells with nanofibrous scaffolds: Effect of fiber orientation on cell adhesion, proliferation, and functional gene expression," *J. Biomed. Mater. Res. - Part A*, vol. 103, no. 7, pp. 2236–2250, 2015.

[104] Z. Guo, J. Xu, S. Ding, H. Li, C. Zhou, and L. Li, "In vitro evaluation of random and aligned polycaprolactone/gelatin fibers via electrospinning for bone tissue engineering," *J. Biomater. Sci. Polym. Ed.*, vol. 26, no. 15, pp. 989–1001, 2015.

[105] L. H. Chong, M. M. Lim, and N. Sultana, “Fabrication and Evaluation of Polycaprolactone/Gelatin-Based Electrospun Nanofibers with Antibacterial Properties,” *J. Nanomater.*, vol. 2015, pp. 1–8, 2015.

[106] R. Yao, J. He, G. Meng, B. Jiang, and F. Wu, “Electrospun PCL/Gelatin composite fibrous scaffolds: Mechanical properties and cellular responses,” *J. Biomater. Sci. Polym. Ed.*, vol. 27, no. 9, pp. 824–838, 2016.

[107] P. Kuppan, S. Sethuraman, and U. M. Krishnan, “Fabrication and investigation of nanofibrous matrices as esophageal tissue scaffolds using human non-keratinized, stratified, squamous epithelial cells,” *RSC Adv.*, vol. 6, no. 31, pp. 26461–26473, 2016.

[108] J. Dulnik, P. Denis, P. Sajkiewicz, D. Kołbuk, and E. Choińska, “Biodegradation of bicomponent PCL/gelatin and PCL/collagen nanofibers electrospun from alternative solvent system,” *Polym. Degrad. Stab.*, vol. 130, pp. 10–21, 2016.

[109] Y. C. Jiang, L. Jiang, A. Huang, X. F. Wang, Q. Li, and L. S. Turng, “Electrospun polycaprolactone/gelatin composites with enhanced cell–matrix interactions as blood vessel endothelial layer scaffolds,” *Mater. Sci. Eng. C*, vol. 71, pp. 901–908, 2017.

[110] B. Feng, H. Duan, W. Fu, Y. Cao, W. J. Zhang, and Y. Zhang, “Effect of inhomogeneity of the electrospun fibrous scaffolds of gelatin/polycaprolactone hybrid on cell proliferation,” *J. Biomed. Mater. Res. - Part A*, vol. 103, no. 2, pp. 431–438, 2015.

[111] B. Feng, H. Tu, H. Yuan, H. Peng, and Y. Zhang, “Acetic-acid-mediated miscibility toward electrospinning homogeneous composite nanofibers of GT/PCL,” *Biomacromolecules*, vol. 13, no. 12, pp. 3917–3925, 2012.

[112] Q. Zhou *et al.*, “Alkali-Mediated Miscibility of Gelatin/Polycaprolactone for Electrospinning Homogeneous Composite Nanofibers for Tissue Scaffolding,” *Macromol.*

Biosci., vol. 17, no. 12, pp. 1–10, 2017.

[113] Q. Zhang, Y. Jiang, Y. Zhang, Z. Ye, W. Tan, and M. Lang, "Effect of porosity on long-term degradation of poly (ε-caprolactone) scaffolds and their cellular response," *Polym. Degrad. Stab.*, vol. 98, no. 1, pp. 209–218, 2013.

[114] J. Širc *et al.*, "Morphological characterization of nanofibers: Methods and application in practice," *J. Nanomater.*, vol. 2012, 2012.

[115] B. Tarus, N. Fadel, A. Al-Oufy, and M. El-Messiry, "Effect of polymer concentration on the morphology and mechanical characteristics of electrospun cellulose acetate and poly (vinyl chloride) nanofiber mats," *Alexandria Eng. J.*, vol. 55, no. 3, pp. 2975–2984, 2016.

[116] S. Sánchez-González, N. Diban, and A. Urtiaga, "Hydrolytic degradation and mechanical stability of poly(ε-Caprolactone)/reduced graphene oxide membranes as scaffolds for in vitro neural tissue regeneration," *Membranes (Basel).*, vol. 8, no. 1, 2018.

Appendix A SEM Micrographs and Fiber Diameter Measurements

Appendix A.1 SEM Micrographs and Fiber Diameter Measurements of the Mats Electrospun out of 6%, 10% and 14% (w/v) Solutions before Degradation

Appendix A.1.1 The SEM Micrographs and Respective Fiber Diameter Measurements for Five Different Regions of the Mat Electrospun out of 6% (w/v) Solution before Degradation

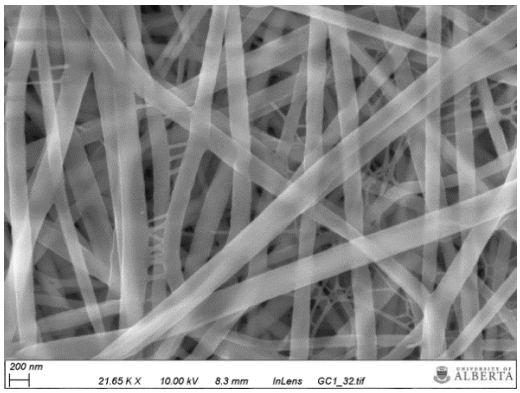

a) 6.1-1 D0

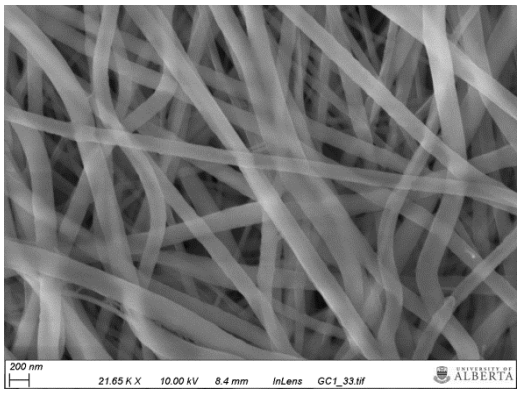

a) 6.1-2 D0

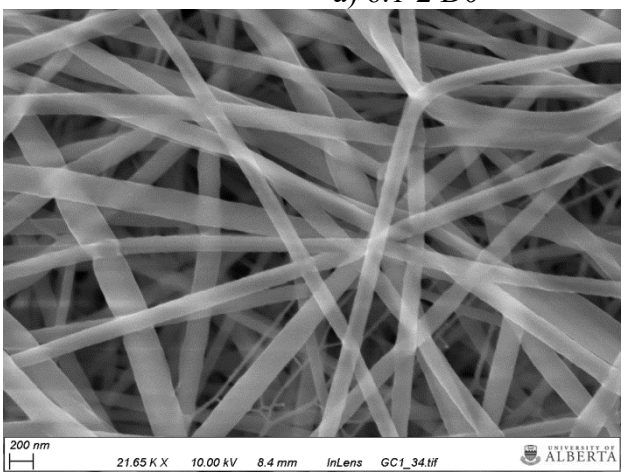

a) 6.1-3 D0

Figure A-1 The SEM micrographs from region 1 of the mat electrospun from the solution at the total polymer concentration of 6% (w/v) before degradation (6.1 D0)

Table A-1 Fiber diameter measurements in nm for 3 different locations at region 1 of the mat electrospun from the solution at the total polymer concentration of 6% (w/v) before degradation

6.1-1 D0	6.1-2 D0	6.1-3 D0
239	233	308
138	254	254
189	153	189
234	211	168
195	166	215
269	163	126
176	224	173
222	237	140
189	193	154
192	181	198
152	221	221
187	186	153
139	161	143
289		
186		

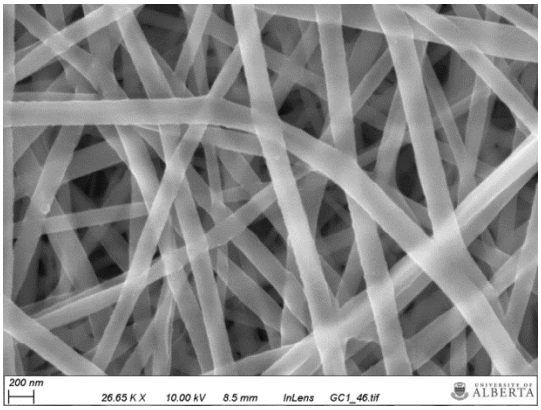

a) 6.2-1 D0

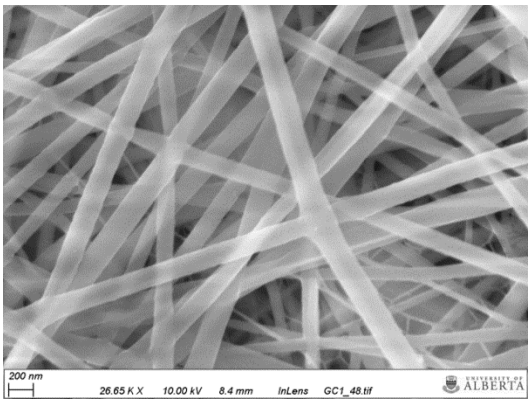

b) 6.2-2 D0

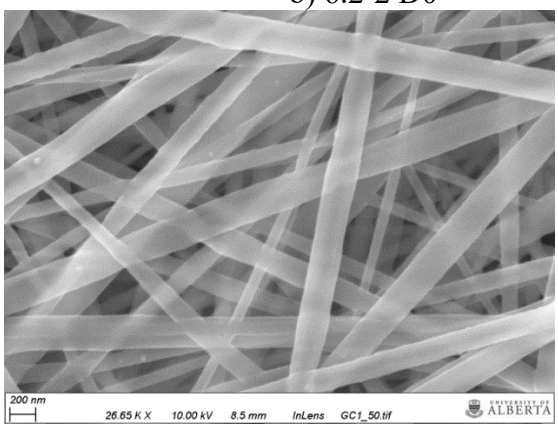

c) 6.2-3 D0

Figure A-2 The SEM micrographs from region 2 of the mat electrospun from the solution at the total polymer concentration of 6% (w/v) before degradation (6.2 D0)

Table A-2 Fiber diameter measurements in nm for 3 different locations at region 2 of the mat electrospun from the solution at the total polymer concentration of 6% (w/v) before degradation

6.2-1 D0	6.2-2 D0	6.2-3 D0
214	188	245
124	214	186
131	171	277
206	141	234
158	149	257
185	112	251
168	146	200
176	165	182
155	152	180
156	207	84
202	146	121
202	224	75
204	171	76
270		77
148		
190		
148		
216		

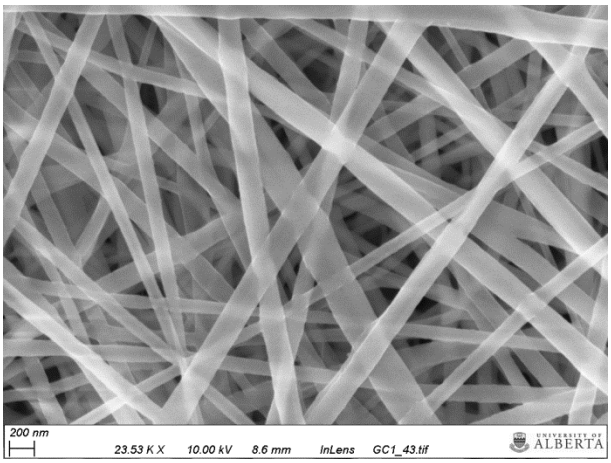

a) 6.3-1 D0

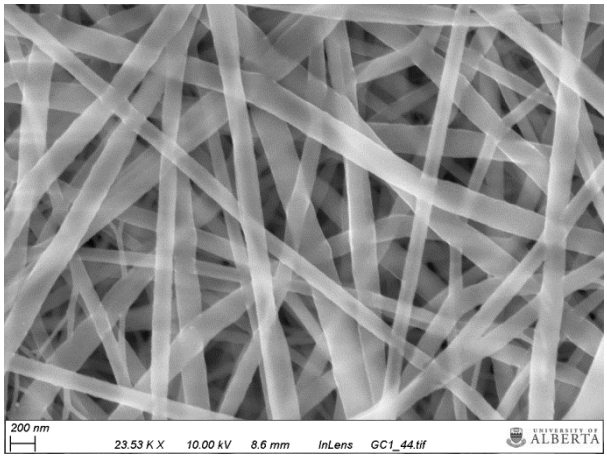

b) 6.3-2 D0

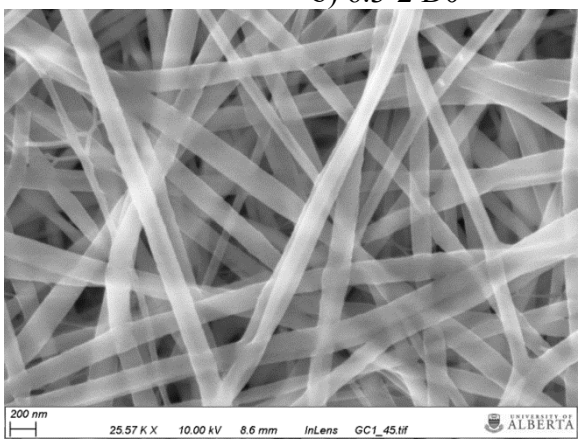

c) 6.3-3 D0

Figure A-3 The SEM micrographs from region 3 of the mat electrospun from the solution at the total polymer concentration of 6% (w/v) before degradation (6.3 D0)

Table A-3 Fiber diameter measurements in nm for 3 different locations at region 3 of the mat electrospun from the solution at the total polymer concentration of 6% (w/v) before degradation

6.3-1 D0	6.3-2 D0	6.3-3 D0
218	209	209
190	138	171
173	205	173
110	219	218
91	161	103
99	248	129
122	235	119
156	200	160
157	124	179
325	206	140
122	98	135
217	151	91
183	136	177
247	238	94
184	123	
117	111	
108	156	
158	242	
144	214	
186	145	
	148	
	230	
	108	
	205	
	205	
	138	
	196	

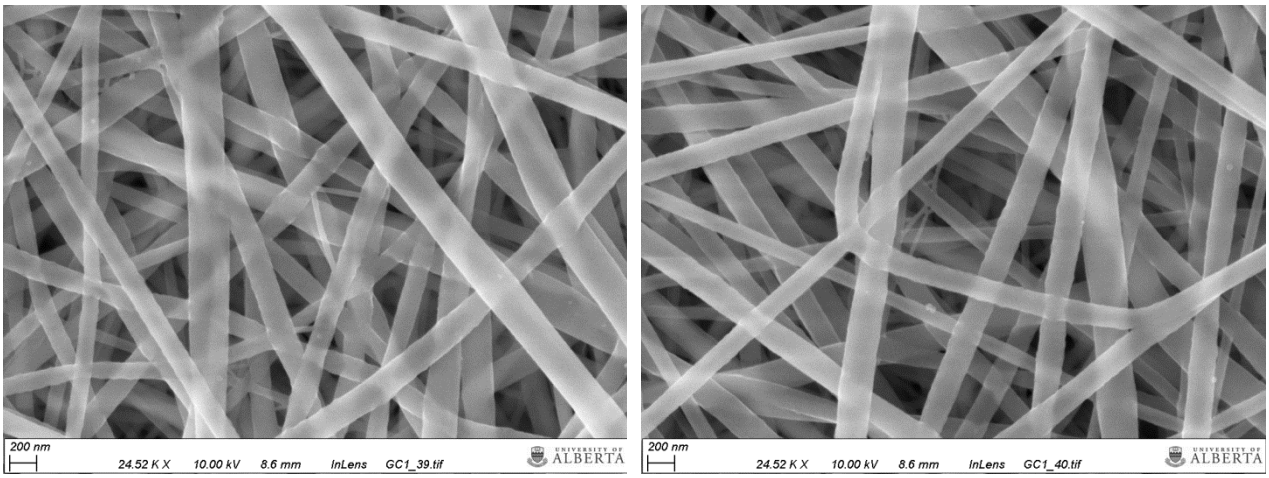

a) 6.4-1 D0 b) 6.4-2 D0

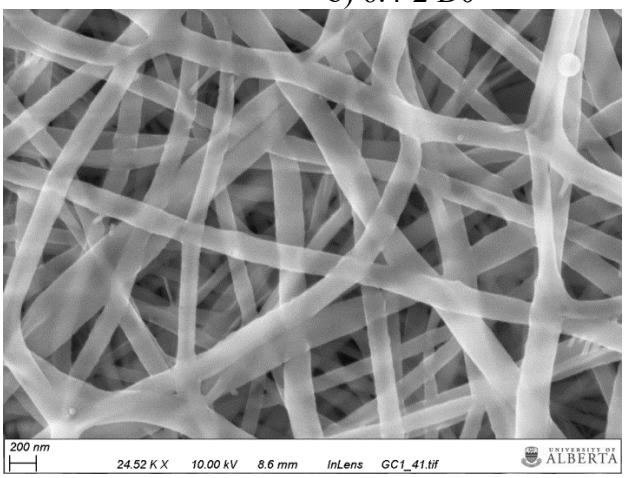

c) 6.4-3 D0

Figure A-4 The SEM micrographs from region 4 of the mat electrospun from the solution at the total polymer concentration of 6% (w/v) before degradation (6.4 D0)

Table A-4 Fiber diameter measurements in nm for 3 different locations at region 4 of the mat electrospun from the solution at the total polymer concentration of 6% (w/v) before degradation

6.4-1 D0	6.4-2 D0	6.4-3 D0
292	248	222
323	217	196
215	162	268
159	215	190
187	172	234
136	308	131
145	187	189
135	199	183
165	190	137
162	166	129
261	121	159
321	130	116
194		136
118		172
178		148
190		242
168		172

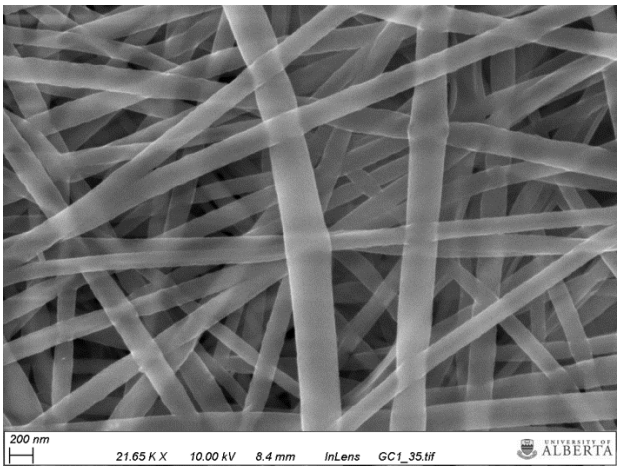

a) 6.5-1 D0

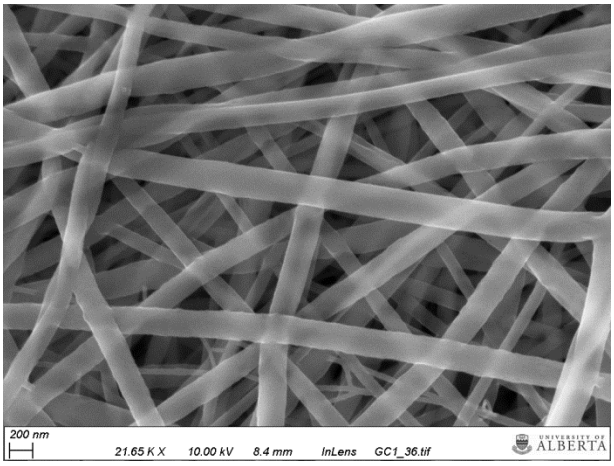

b) 6.5-2 D0

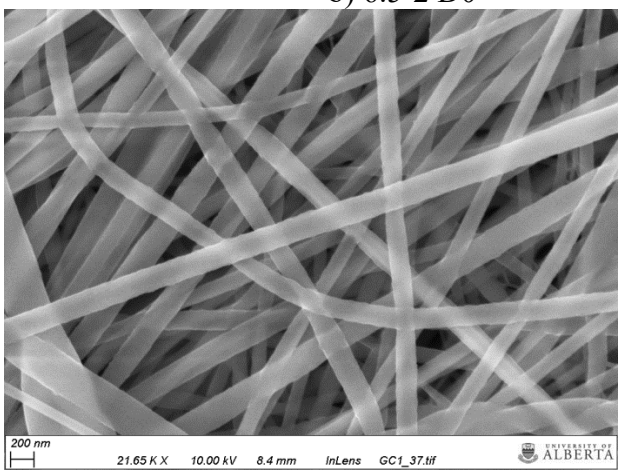

c) 6.5-3 D0

Figure A-5 The SEM micrographs from region 5 of the mat electrospun from the solution at the total polymer concentration of 6% (w/v) before degradation (6.5 D0)

Table A-5 Fiber diameter measurements in nm for 3 different locations at region 5 of the mat electrospun from the solution at the total polymer concentration of 6% (w/v) before degradation

6.5-1 D0	6.5-2 D0	6.5-3 D0
222	224	219
237	248	184
371	225	217
297	242	214
162	228	245
258	286	134
160	231	174
149	181	206
226	142	220
202	100	124
186	196	139
223	292	152
203		175
173		
169		
179		
121		
208		

Appendix A.1.2 The SEM Micrographs and Respective Fiber Diameter Measurements for Five Different Regions of the Mat Electrospun out of 10% (w/v) Solution before Degradation

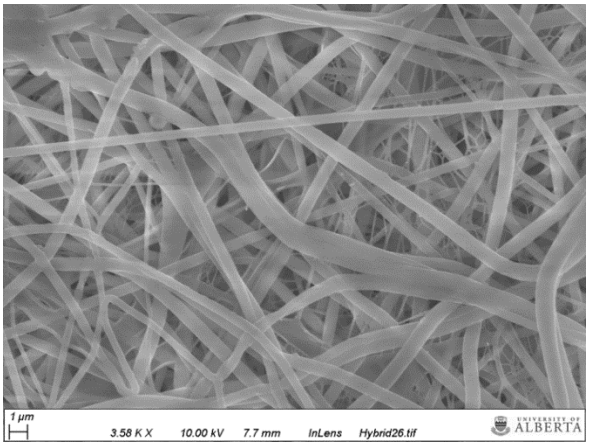

a) 10.1-1 D0

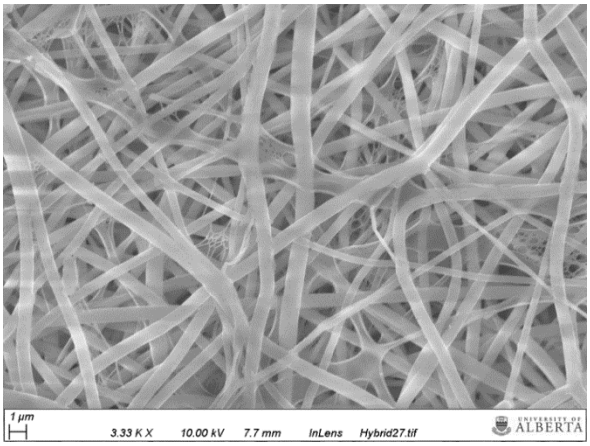

b) 10.1-2 D0

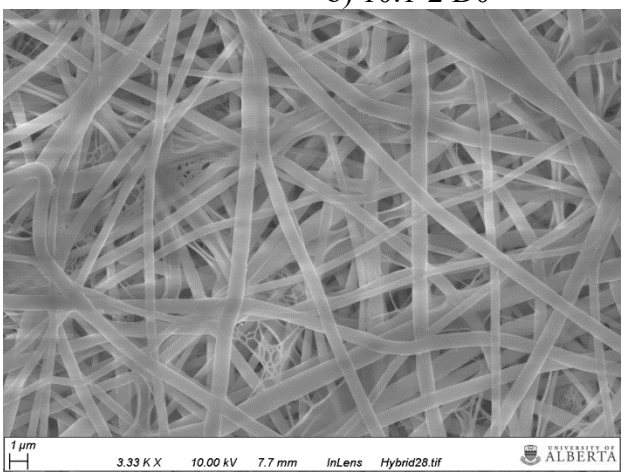

c) 10.1-3 D0

Figure A-6 The SEM micrographs from region 1 of the mat electrospun from the solution at the total polymer concentration of 10% (w/v) before degradation (10.1 D0)

Table A-6 Fiber diameter measurements in nm for 3 different locations at region 1 of the mat electrospun from the solution at the total polymer concentration of 10% (w/v) before degradation

10.1-1 D0	10.1-2 D0	10.1-3 D0
583	749	692
795	892	522
777	811	429
244	676	783
643	885	560
1710	640	967
848	552	605
752	600	511
876	1123	893
540	839	536
491	433	862
901	443	719
740	633	483
553	764	976
438	403	958
457	752	859
503	837	732
665	543	501
645	938	689
868	512	1231
641	788	714
785	879	
690	606	
765	590	
952	528	
542	929	
	804	

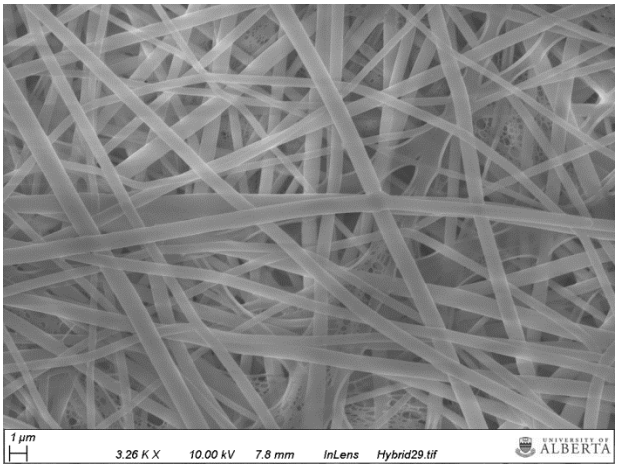

a) 10.2-1 D0

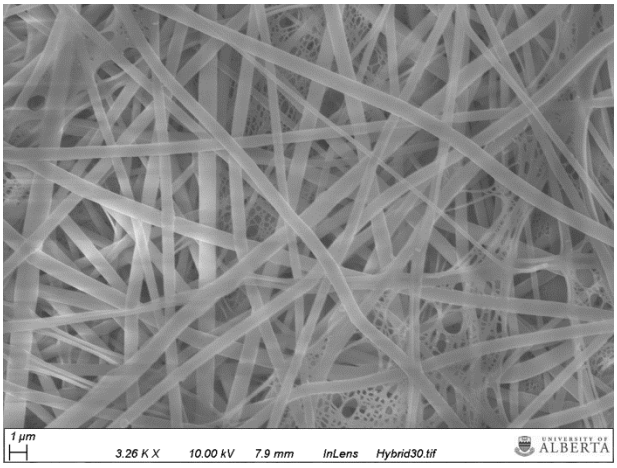

b) 10.2-2 D0

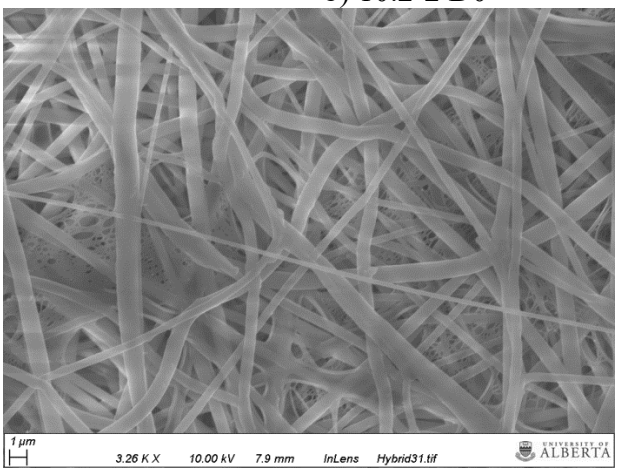

c) 10.2-3 D0

Figure A-7 The SEM micrographs from region 2 of the mat electrospun from the solution at the total polymer concentration of 10% (w/v) before degradation (10.2 D0)

Table A-7 Fiber diameter measurements in nm for 3 different locations at region 2 of the mat electrospun from the solution at the total polymer concentration of 10% (w/v) before degradation

10.2-1 D0	10.2-2 D0	10.2-3 D0
1161	768	999
484	1479	680
1115	653	500
709	847	751
2169	889	506
967	1629	988
522	1139	1090
1939	768	881
775	1218	867
1135	854	332
1274	630	856
514	1349	517
1558	1383	1413
1131	937	743
417	1036	481
2138	459	510
539	1419	741
2416	473	514
511	2398	1145
791	1068	637
2603	480	1055
826	1500	737
	819	436
	833	264
	1604	
	2369	
	581	
	1254	
	791	

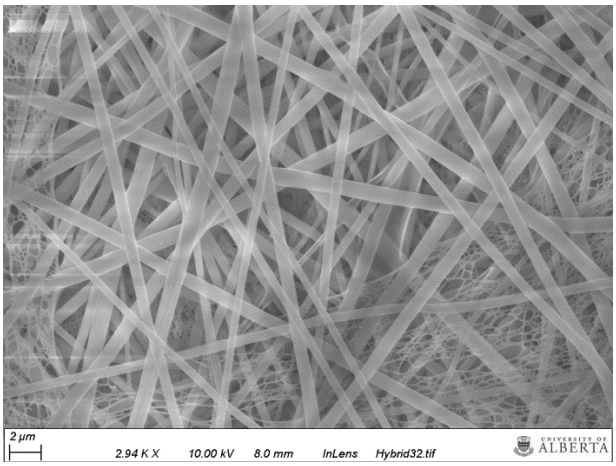

a) 10.3-1 D0

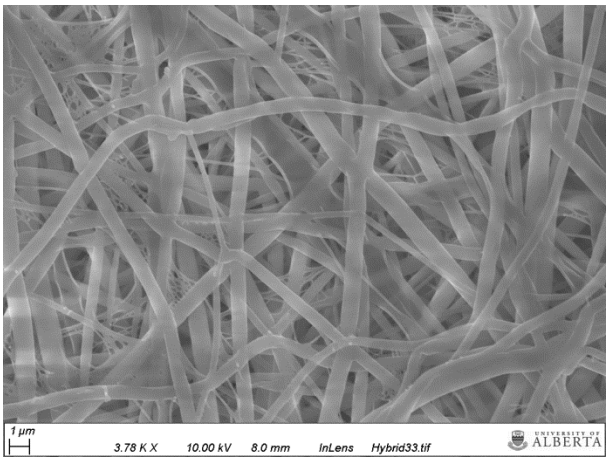

b) 10.3-2 D0

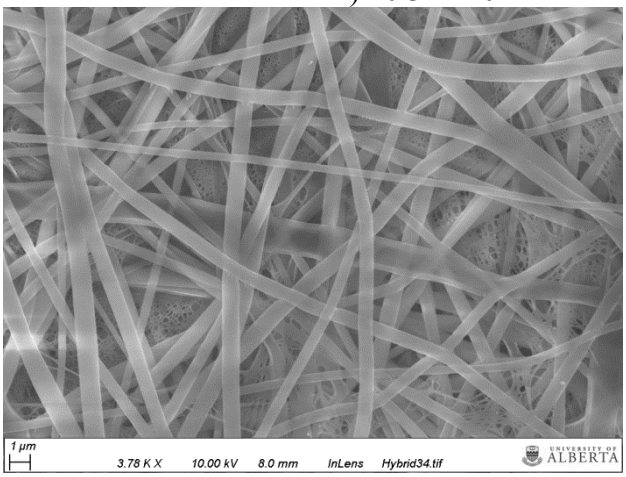

c) 10.3-3 D0

Figure A-8 The SEM micrographs from region 3 of the mat electrospun from the solution at the total polymer concentration of 10% (w/v) before degradation (10.3 D0)

Table A-8 Fiber diameter measurements in nm for 3 different locations at region 3 of the mat electrospun from the solution at the total polymer concentration of 10% (w/v) before degradation

10.3-1 D0	10.3-2 D0	10.3-3 D0
922	574	1043
513	727	769
650	758	456
917	794	567
484	603	1050
610	888	863
1088	1007	797
550	516	572
462	1024	538
573	1017	750
539	724	390
879	709	369
920	496	774
848	604	518
638	668	882
733		1620
1088		547
971		431
927		863
359		771
842		
825		
528		
789		

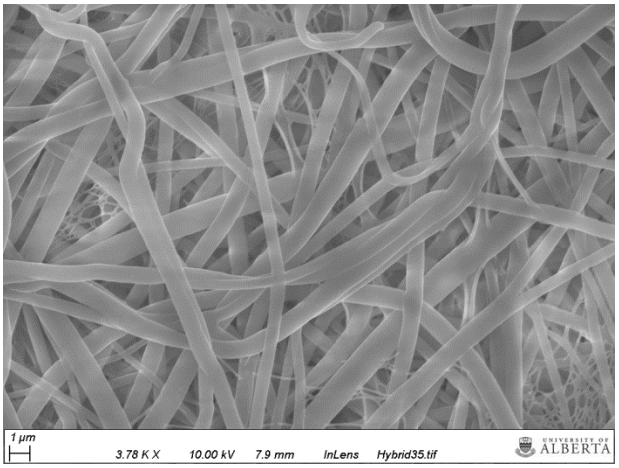

a) 10.4-1 D0

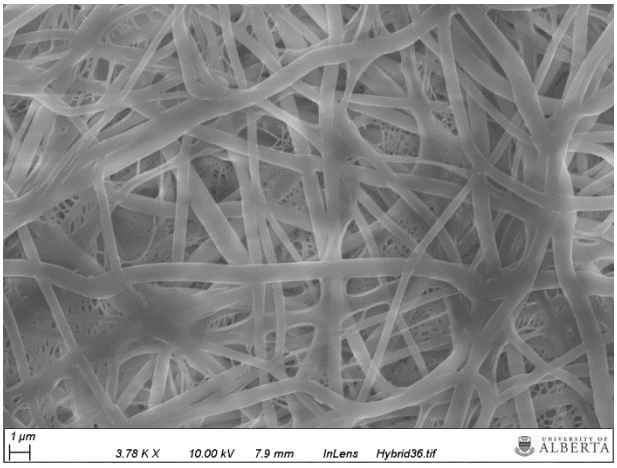

b) 10.4-2 D0

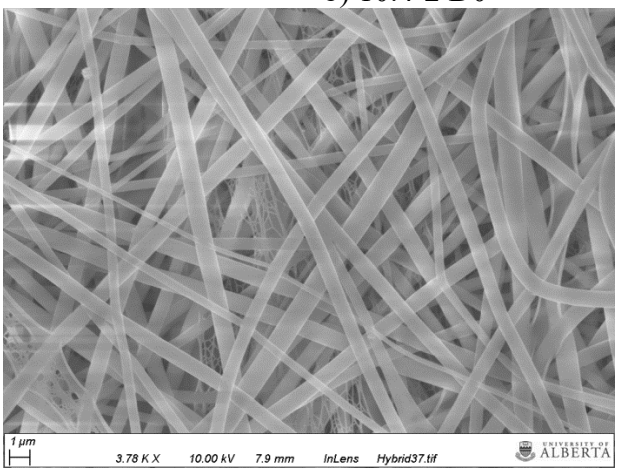

c) 10.4-3 D0

Figure A-9 The SEM micrographs from region 4 of the mat electrospun from the solution at the total polymer concentration of 10% (w/v) before degradation (10.4 D0)

Table A-9 Fiber diameter measurements in nm for 3 different locations at region 4 of the mat electrospun from the solution at the total polymer concentration of 10% (w/v) before degradation

10.4-1 D0	10.4-2 D0	10.4-3 D0
1193	958	765
813	1173	471
1351	750	459
962	488	480
1042	797	885
898	414	913
569	632	753
854	791	1100
1385	1032	867
1277	432	787
706	485	252
480	861	391
813	742	717
472	606	724
521	552	768
		379
		732
		788
		775
		676
		1188
		797
		874
		606
		747
		457
		472

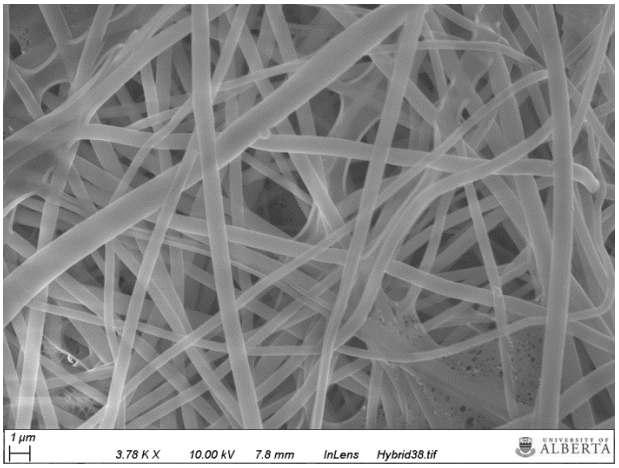

a) 10.5-1 D0

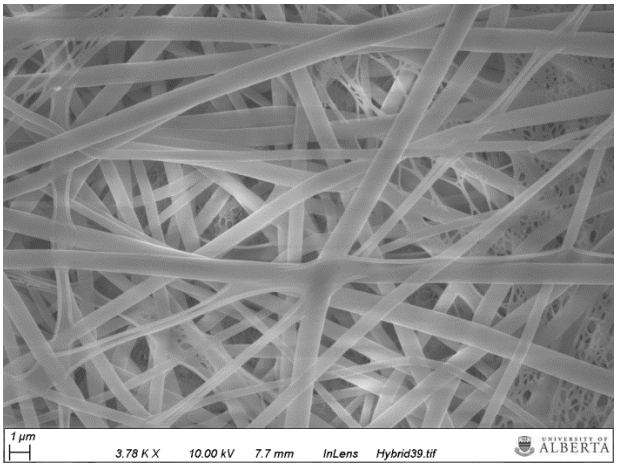

b) 10.5-2 D0

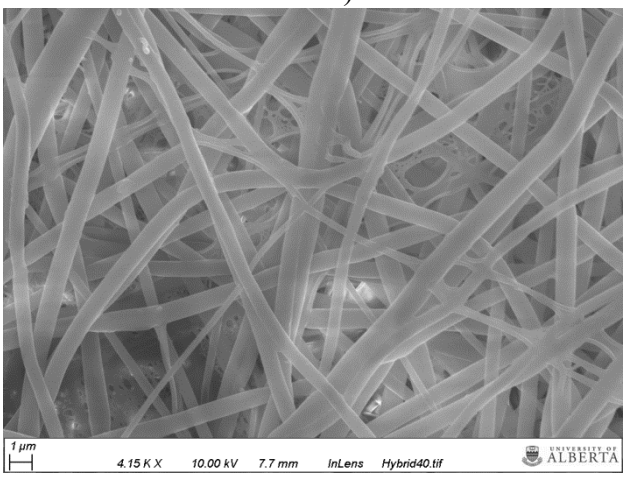

c) 10.5-3 D0

Figure A-10 The SEM micrographs from region 5 of the mat electrospun from the solution at the total polymer concentration of 10% (w/v) before degradation (10.5 D0)

Table A-10 Fiber diameter measurements in nm for 3 different locations at region 5 of the mat electrospun from the solution at the total polymer concentration of 10% (w/v) before degradation

10.5-1 D0	10.5-2 D0	10.5-3 D0
1580	945	663
640	754	936
459	1023	812
415	1156	427
765	983	912
513	1188	272
848	992	786
776	1000	516
887	485	312
754	876	870
585	926	1084
924	1248	824
608	552	753
975	419	934
780	847	573
534	894	737
	804	830
	719	625
	1129	
	365	

Appendix A.1.3 The SEM Micrographs and Respective Fiber Diameter Measurements for Five Different Regions of the Mat Electrospun out of 14% (w/v) Solution before Degradation

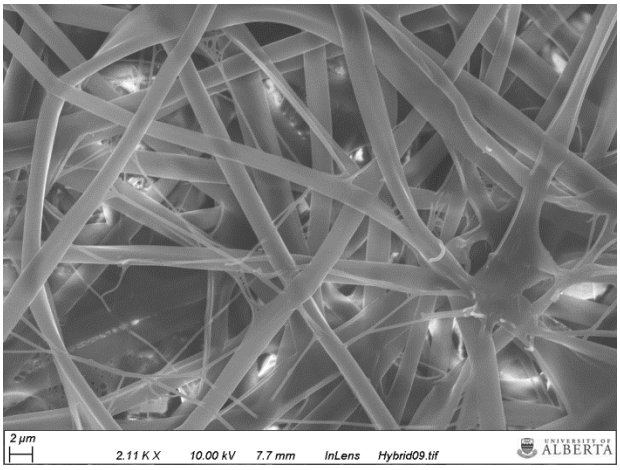

a) 14.1-1 D0

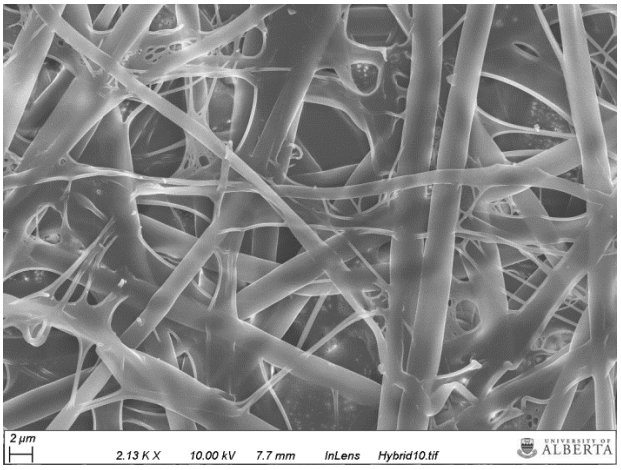

b) 14.1-2 D0

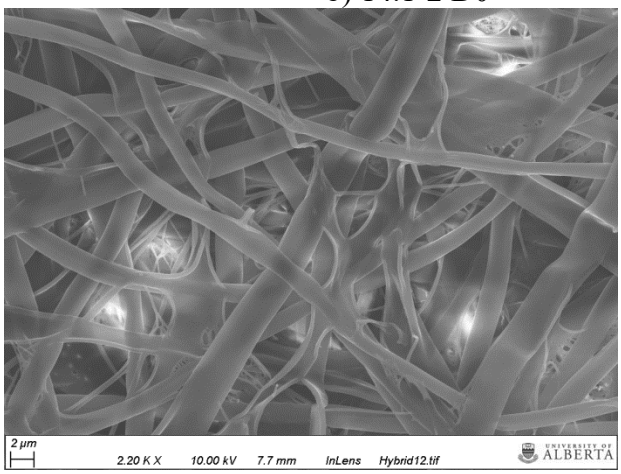

c) 14.1-3 D0

Figure A-11 The SEM micrographs from region 1 of the mat electrospun from the solution at the total polymer concentration of 14% (w/v) before degradation (14.1 D0)

Table A-11 Fiber diameter measurements in nm for 3 different locations at region 1 of the mat electrospun from the solution at the total polymer concentration of 14% (w/v) before degradation

14.1-1 D0	14.1-2 D0	14.1-3 D0
2092	1847	1985
1507	2626	2007
1539	2508	1771
2274	2813	3443
1965	1278	2166
1998	2376	1447
2071	2391	3310
1822	2298	1523
2148	1107	2103
1786	3109	2166
2998		1614
1488		3909
2727		
2924		

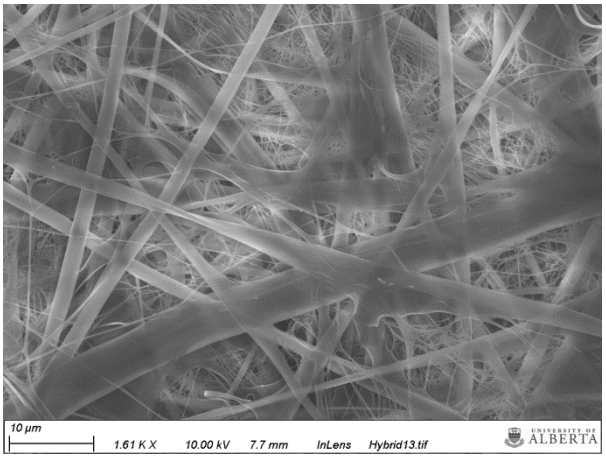

a) 14.2-1 D0

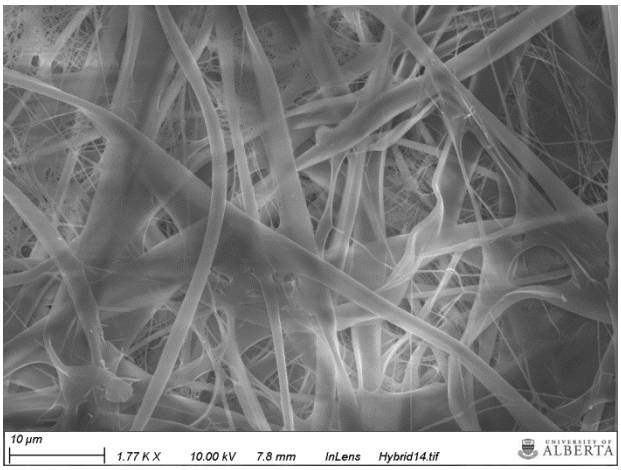

b) 14.2-2 D0

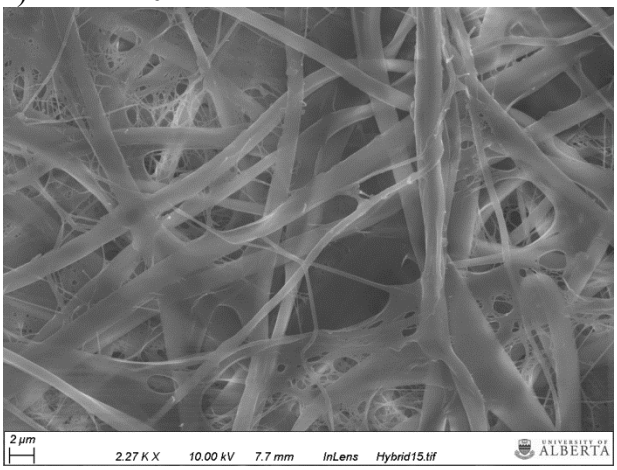

c) 14.2-3 D0

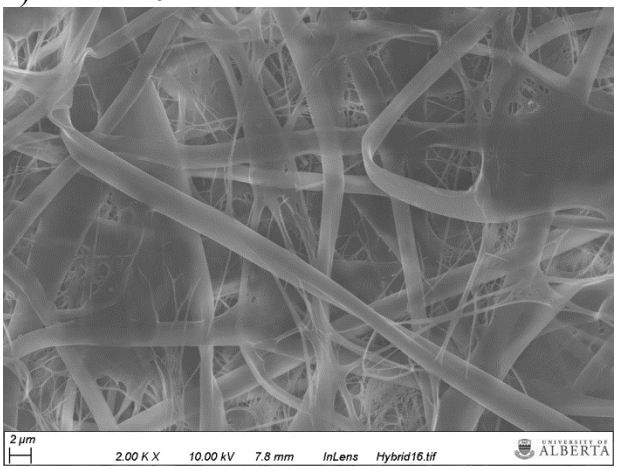

d) 14.2-4 D0

Figure A-12 The SEM micrographs from region 2 of the mat electrospun from the solution at the total polymer concentration of 14% (w/v) before degradation (14.2 D0)

Table A-12 Fiber diameter measurements in nm for 3 different locations at region 2 of the mat electrospun from the solution at the total polymer concentration of 14% (w/v) before degradation

14.2-1 D0	14.2-2 D0	14.2-3 D0	14.2-4 D0
5301	1968	1196	2724
2087	2629	1697	1614
1809	1804	1572	1571
1665	1543	1617	1799
2190	1061		1708
1620			1978
1505			2358
1103			1590

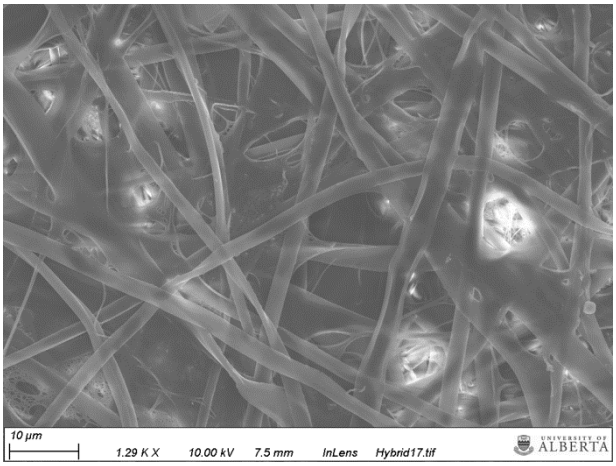

a) 14.3-1 D0

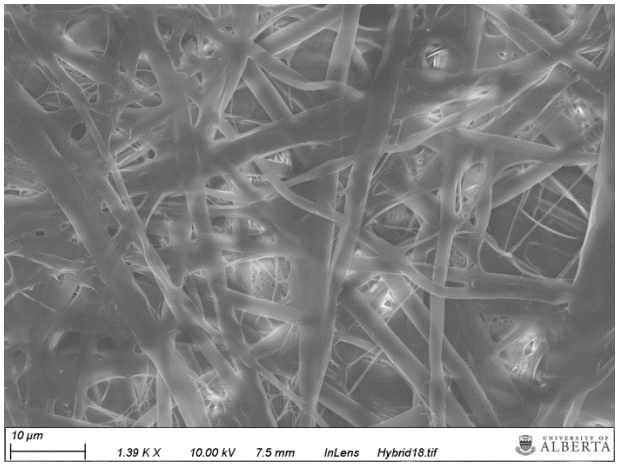

b) 14.3-2 D0

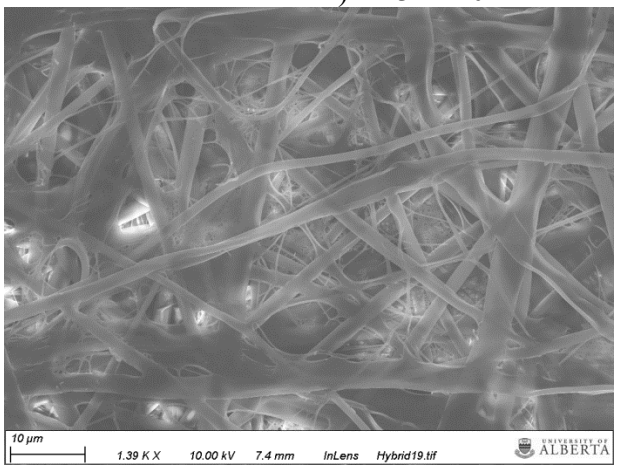

c) 14.3-3 D0

Figure A-13 The SEM micrographs from region 3 of the mat electrospun from the solution at the total polymer concentration of 14% (w/v) before degradation (14.3 D0)

Table A-13 Fiber diameter measurements in nm for 3 different locations at region 3 of the mat electrospun from the solution at the total polymer concentration of 14% (w/v) before degradation

14.3-1 D0	14.3-2 D0	14.3-3 D0
2161	2783	1923
2803	2758	1557
2319	1858	1276
1897	2757	1056
1964	2740	1835
1645	3754	2139
2491	2587	2486
4003	1866	1745
3185	1959	2479
2195	1909	2736
2450	1551	4383
4180	2926	2491
	2198	2309
		3623
		1893
		1291

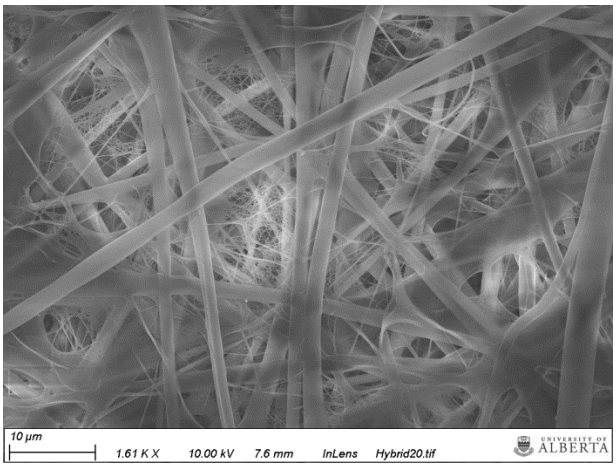

a) 14.4-1 D0

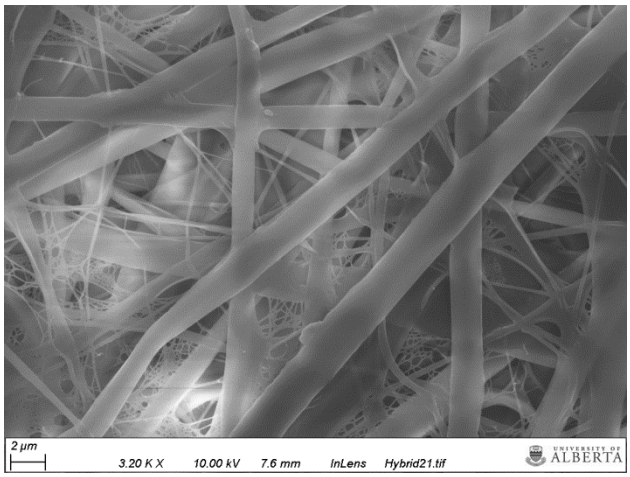

b) 14.4-2 D0

Figure A-14 The SEM micrographs from region 4 of the mat electrospun from the solution at the total polymer concentration of 14% (w/v) before degradation (14.4 D0)

Table A-14 Fiber diameter measurements in nm for 2 different locations at region 4 of the mat electrospun from the solution at the total polymer concentration of 14% (w/v) before degradation

14.4-1 D0	14.4-2 D0
2439	2604
1985	1841
2339	2036
2483	1378
1529	1298
1890	2261
1529	1860
1321	1293
1965	1302
3854	1695
1214	
1243	
1382	
1634	
1609	

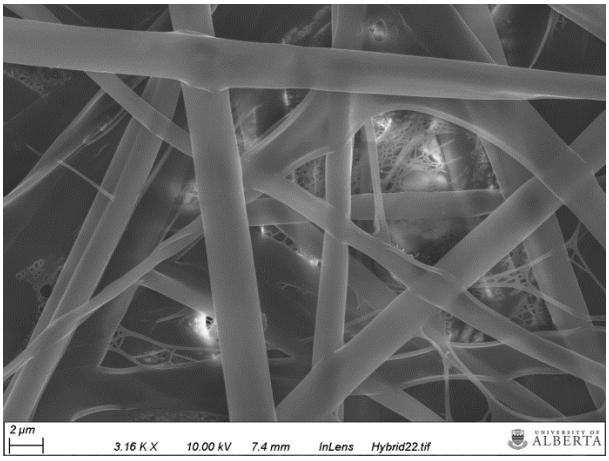

a) 14.5-1 D0

b) 14.5-2 D0

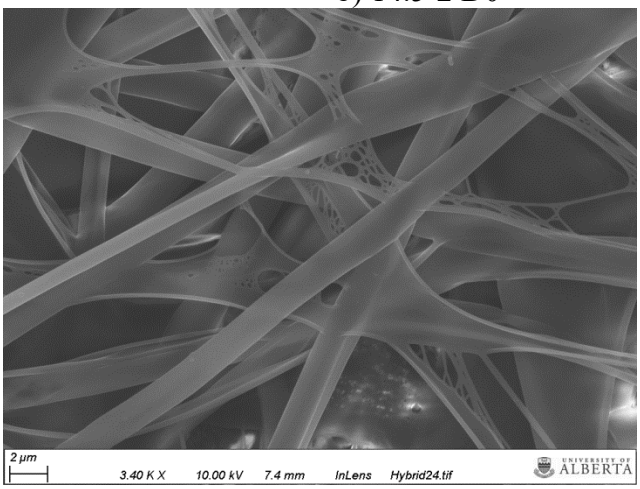

c) 14.5-3 D0

Figure A-15 The SEM micrographs from region 5 of the mat electrospun from the solution at the total polymer concentration of 14% (w/v) before degradation (14.5 D0)

Table A-15 Fiber diameter measurements in nm for 3 different locations at region 5 of the mat electrospun from the solution at the total polymer concentration of 14% (w/v) before degradation

14.5-1 D0	14.5-2 D0	14.5-3 D0
2831	2989	1706
2499	2153	2078
2327	2005	2255
1311	1964	2102
1719	2218	1369
1596	2385	1920
2561	2640	2191
	1464	
	1987	
	2533	

Appendix A.2 SEM Micrographs and Fiber Diameter Measurements of the Mats Electrospun out of 6%, 10% and 14% (w/v) Gelatin/PCL (1:1) in TFE after 1 Day of Degradation

Appendix A.2.1 The SEM Micrograph for the Mat Electrospun out of 6% (w/v) Solution after 1 Day of Degradation

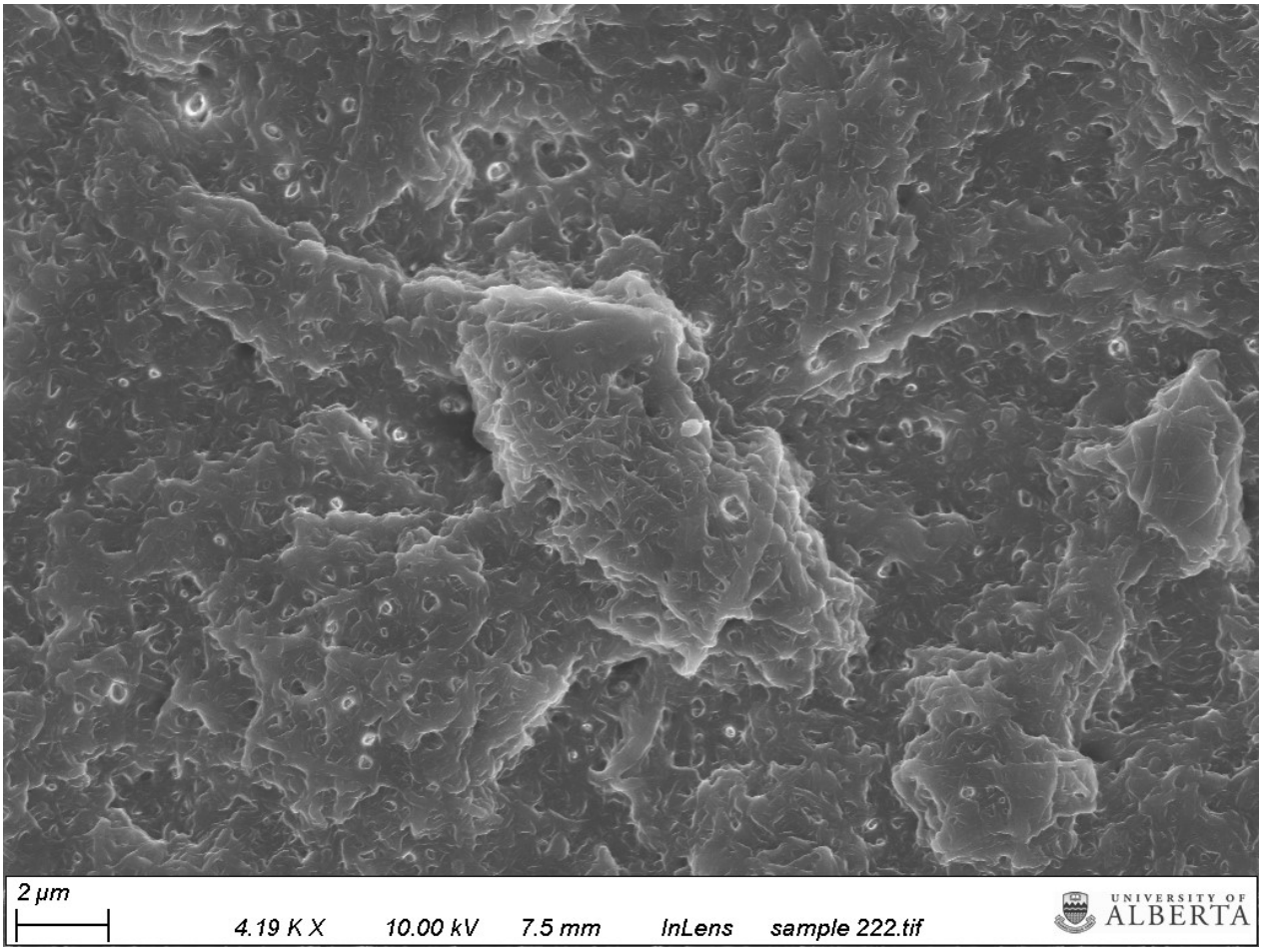

Figure A-16 The SEM micrographs of the mat electrospun from the solution at the total polymer concentration of 6% (w/v) after 1 day of degradation

Appendix A.2.2 The SEM Micrographs and Respective Fiber Diameter Measurements for Five Different Regions of the Mat Electrospun out of 10% (w/v) Solution after 1 Day of Degradation

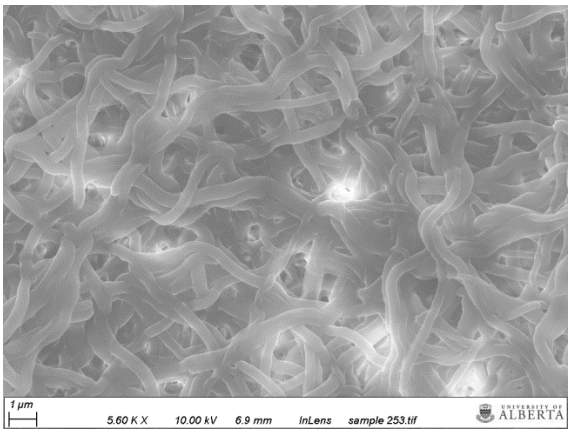

a) 10.1-1 D1

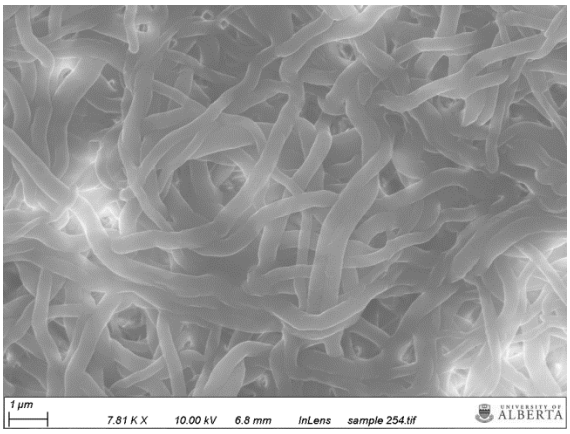

b) 10.1-2 D1

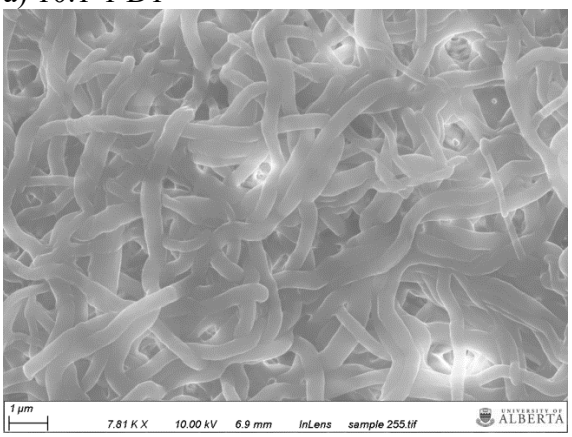

c) 10.1-3 D1

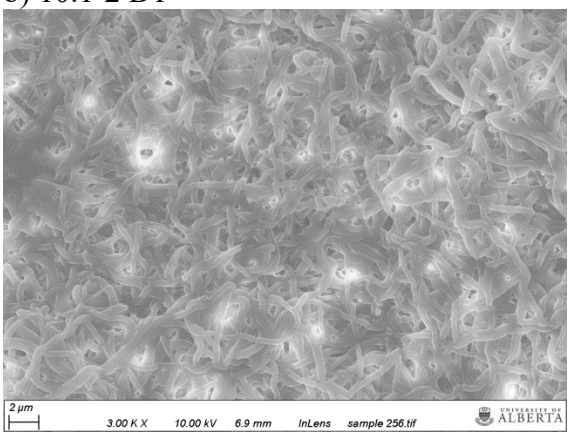

d) 10.1-4 D1

Figure A-17 The SEM micrographs from region 1 of the mat electrospun from the solution at the total polymer concentration of 10% (w/v) after 1 day of degradation (10.1 D1)

Table A-16 Fiber diameter measurements in nm for 4 different locations at region 1 of the mat electrospun from the solution at the total polymer concentration of 10% (w/v) after 1 day of degradation

10.1-1 D1	10.1-2 D1	10.1-3 D1	10.1-4 D1
500	451	442	351
424	499	431	434
403	431	379	504
436	383	385	450
443	340	368	603
			369

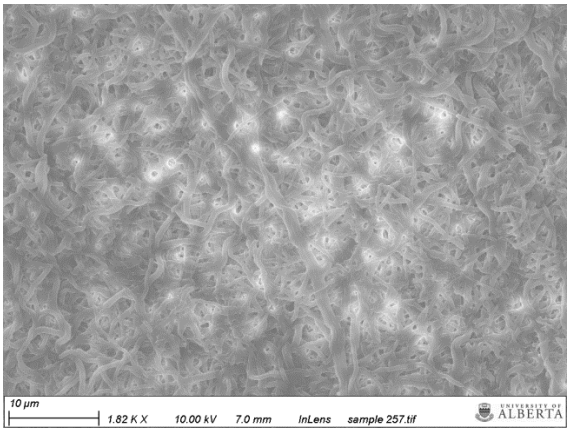

a) 10.2-1 D1

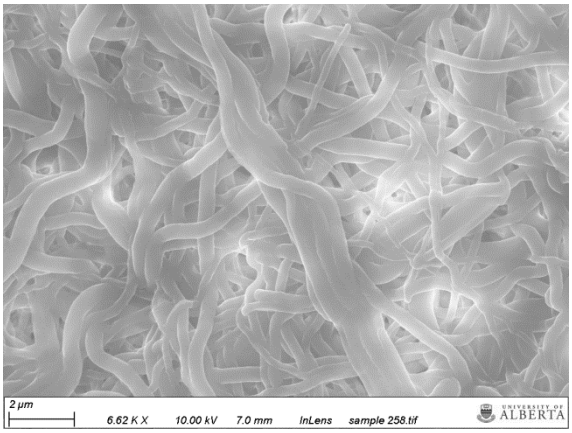

b) 10.2-2 D1

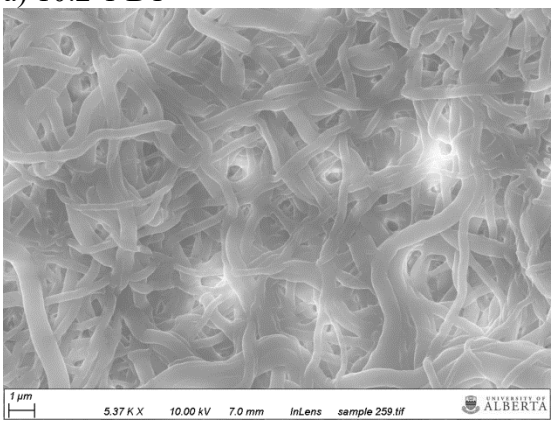

c) 10.2-3 D1

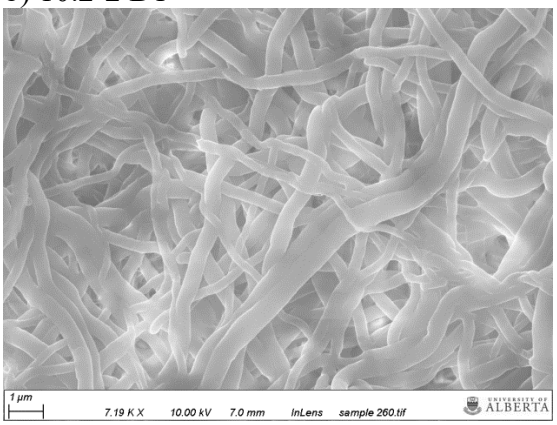

d) 10.2-4 D1

Figure A-18 The SEM micrographs from region 2 of the mat electrospun from the solution at the total polymer concentration of 10% (w/v) after 1 day of degradation (10.2 D1)

Table A-17 Fiber diameter measurements in nm for 4 different locations at region 2 of the mat electrospun from the solution at the total polymer concentration of 10% (w/v) after 1 day of degradation

10.2-1 D1	10.2-2 D1	10.2-3 D1	10.2-4 D1
665	471	364	494
683	577	361	408
508	394	347	309
529	506	419	476
633	449	354	370

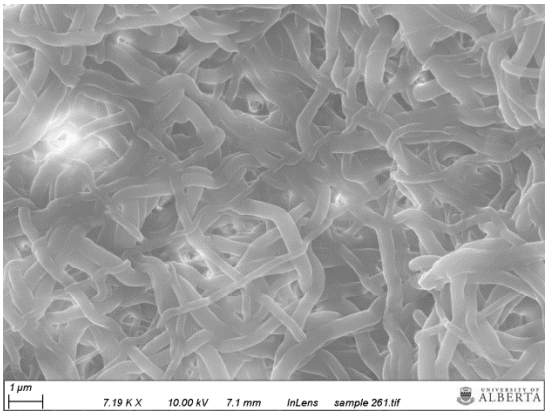

a) 10.3-1 D1

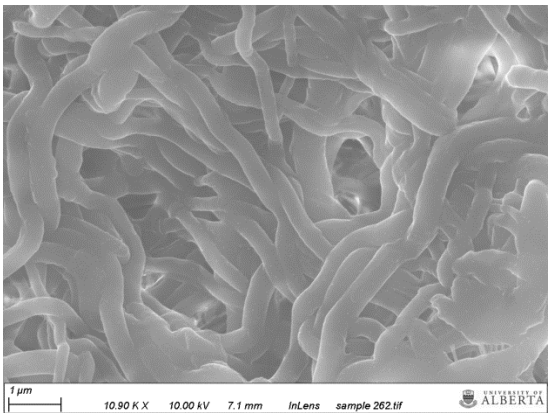

b) 10.3-2 D1

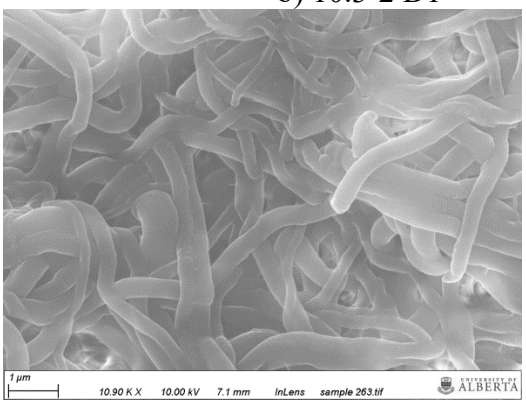

c) 10.3-3 D1

Figure A-19 The SEM micrographs from region 3 of the mat electrospun from the solution at the total polymer concentration of 10% (w/v) after 1 day of degradation (10.3 D1)

Table A-18 Fiber diameter measurements in nm for 3 different locations at region 3 of the mat electrospun from the solution at the total polymer concentration of 10% (w/v) after 1 day of degradation

10.3-1 D1	10.3-2 D1	10.3-3 D1
343	390	404
372	285	345
405	346	475
411	472	333
515	343	342
	473	344
		354
		351

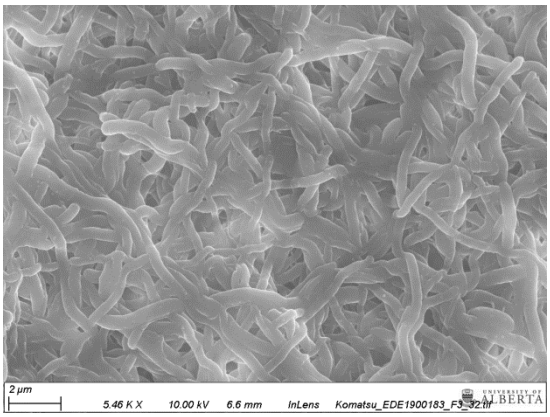

a) 10.4-1 D1

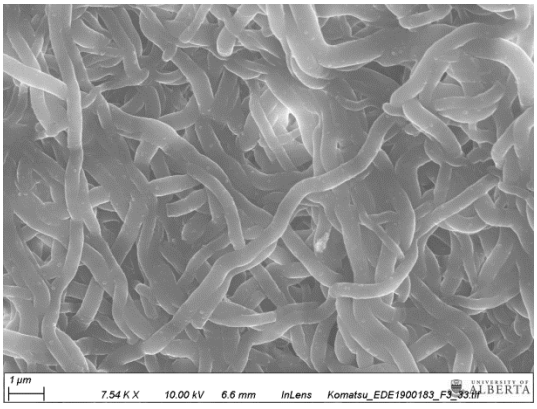

b) 10.4-2 D1

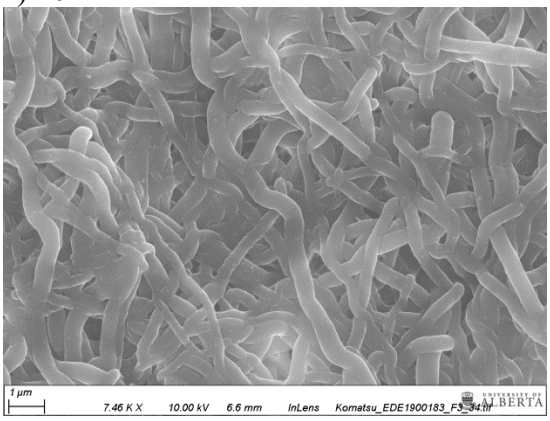

c) 10.4-3 D1

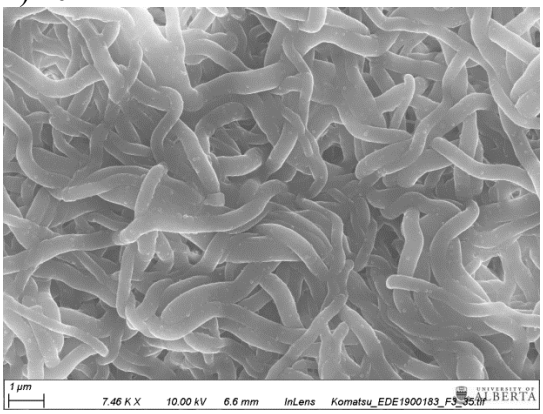

d) 10.4-4 D1

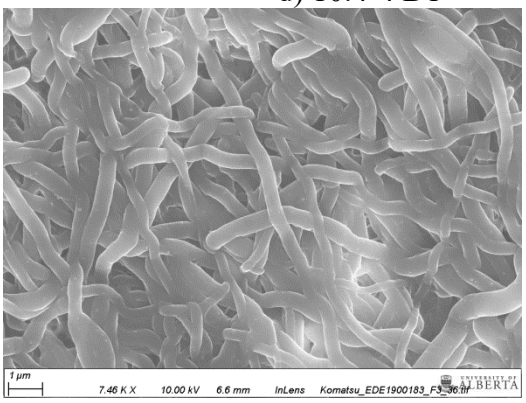

e) 10.4-5 D1

Figure A-20 The SEM micrographs from region 4 of the mat electrospun from the solution at the total polymer concentration of 10% (w/v) after 1 day of degradation (10.4 D1)

Table A-19 Fiber diameter measurements in nm for 5 different locations at region 4 of the mat electrospun from the solution at the total polymer concentration of 10% (w/v) after 1 day of degradation

10.4-1 D1	10.4-2 D1	10.4-3 D1	10.4-4 D1	10.4-5 D1
441	397	466	508	507
361	486	557	652	419
445	463	499	428	450
483	418	415	520	435

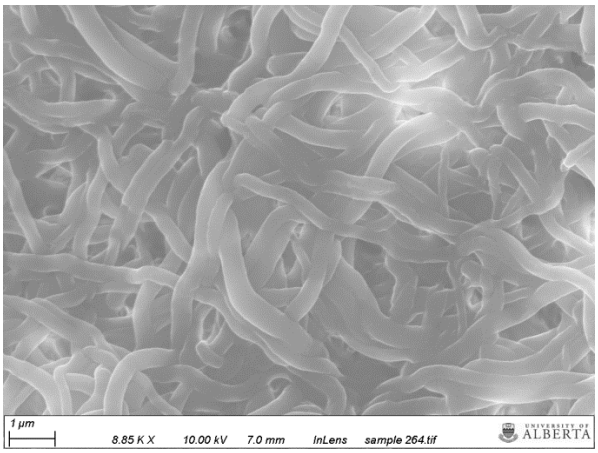

a) 10.5-1 D1

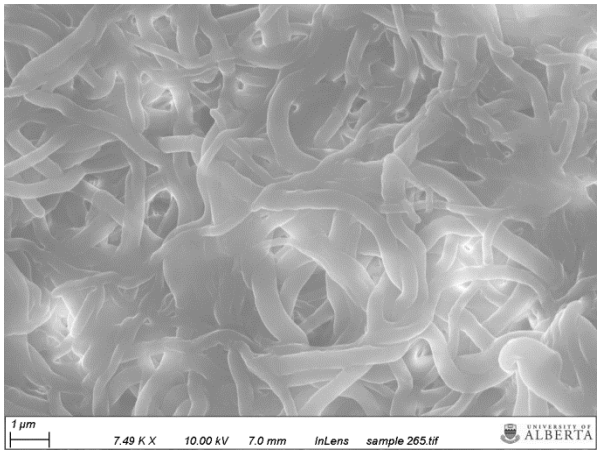

b) 10.5-2 D1

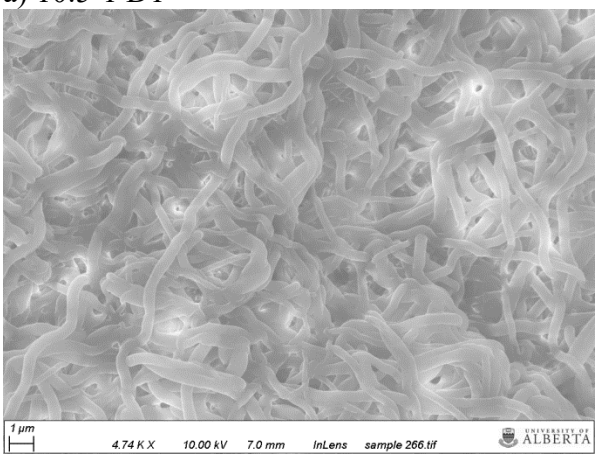

c) 10.5-3 D1

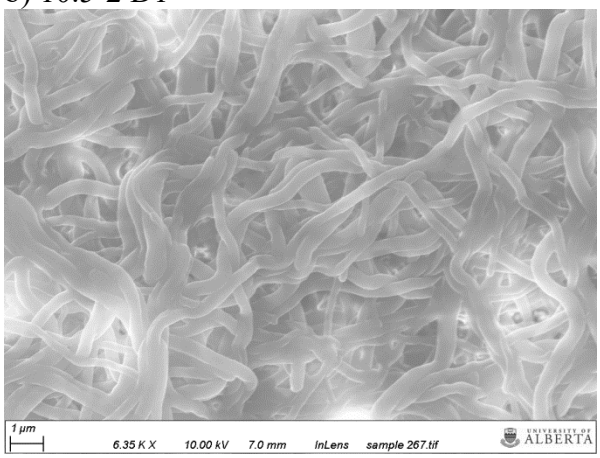

d) 10.5-4 D1

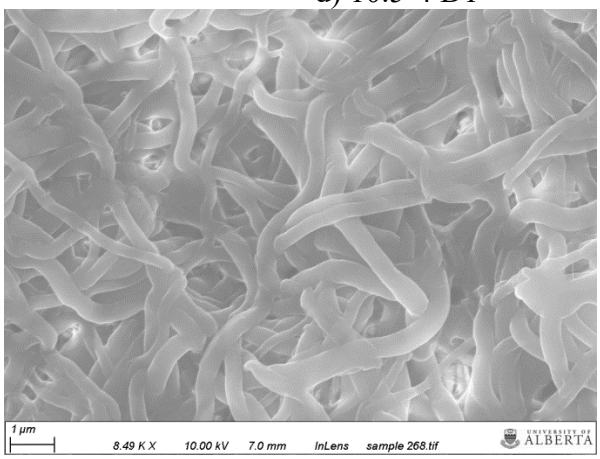

e) 10.5-5 D1

Figure A-21 The SEM micrographs from region 5 of the mat electrospun from the solution at the total polymer concentration of 10% (w/v) after 1 day of degradation (10.5 D1)

Table A-20 Fiber diameter measurements in nm for 5 different locations at region 5 of the mat electrospun from the solution at the total polymer concentration of 10% (w/v) after 1 day of degradation

10.5-1 D1	10.5-2 D1	10.5-3 D1	10.5-4 D1	10.5-5 D1
422	569	531	463	509
323	565	520	544	463
393	405	481	502	523
494	411	419	434	306

Appendix A.2.3 The SEM Micrographs and Respective Fiber Diameter Measurements for Five Different Regions of the Mat Electrospun out of 14% (w/v) Solution after 1 Day of Degradation

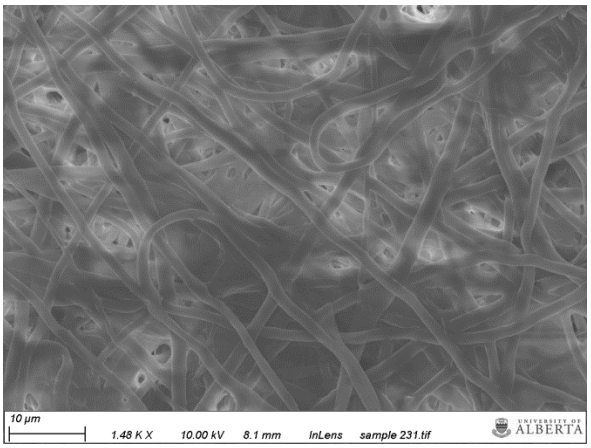

a) 14.1-1 D1

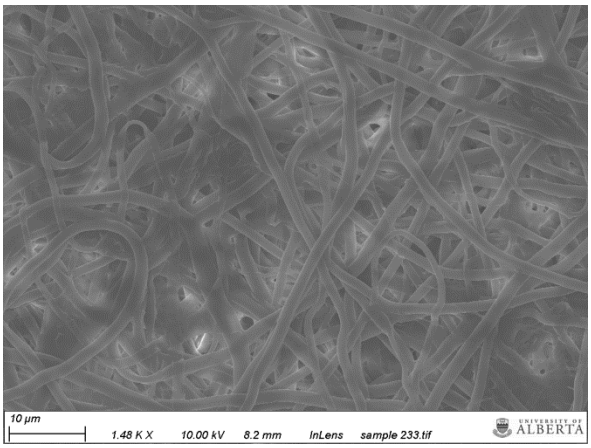

b) 14.1-2 D1

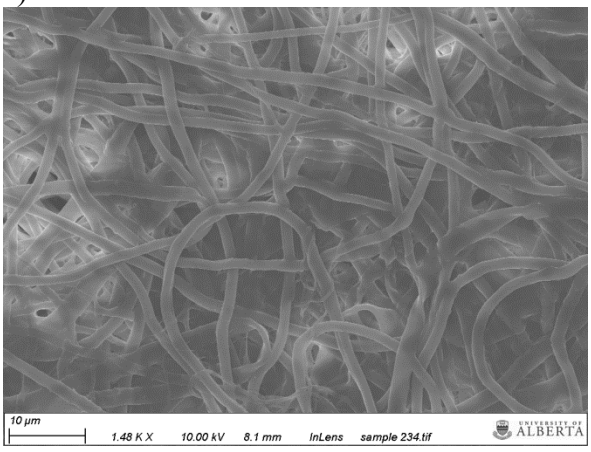

c) 14.1-3 D1

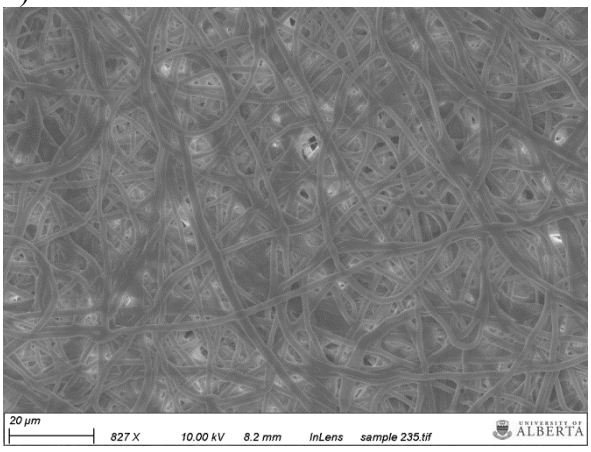

d) 14.1-4 D1

Figure A-22 The SEM micrographs from region 1 of the mat electrospun from the solution at the total polymer concentration of 14% (w/v) after 1 day of degradation (14.1 D1)

Table A-21 Fiber diameter measurements in nm for 4 different locations at region 1 of the mat electrospun from the solution at the total polymer concentration of 14% (w/v) after 1 day of degradation

14.1-1 D1	14.1-2 D1	14.1-3 D1	14.1-4 D1
2203	1566	1369	1610
1656	1547	1608	1854
1642	1763	1494	1424
1751	1296	1346	1704
1276	1608	1385	1575

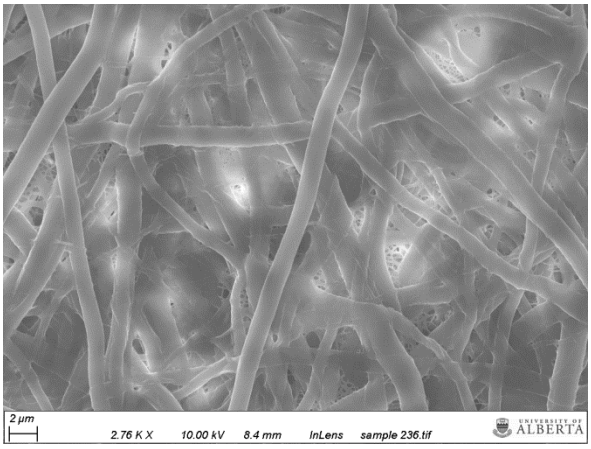

a) 14.2-1 D1

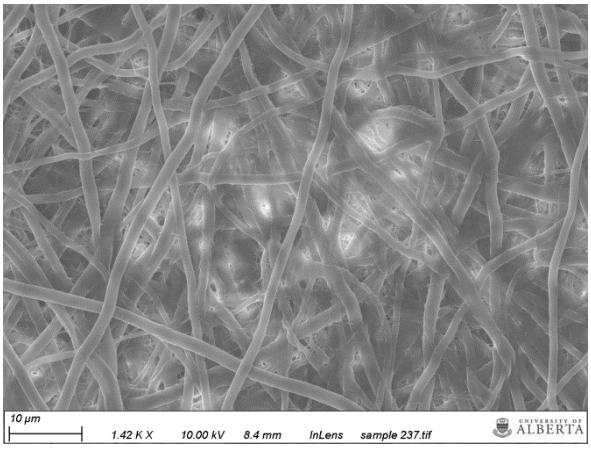

b) 14.2-2 D1

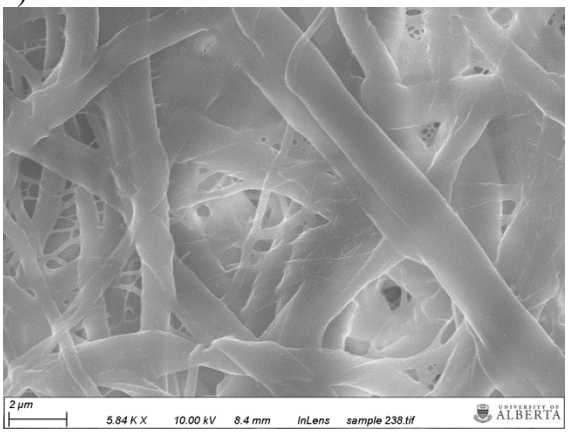

c) 14.2-3 D1

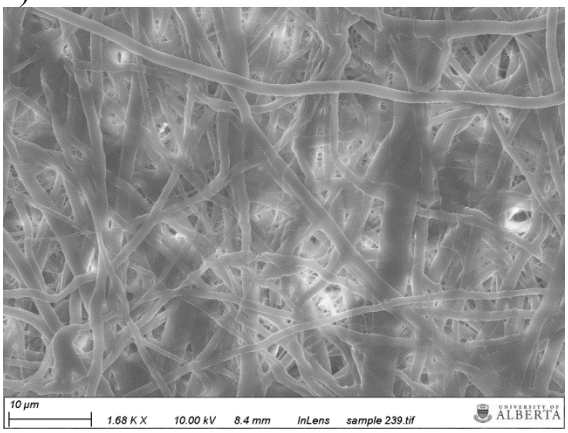

d) 14.2-4 D1

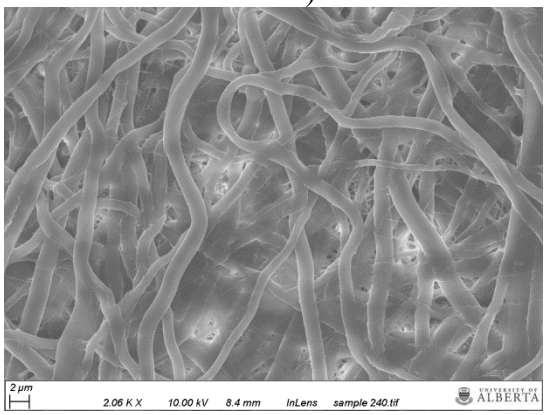

e) 14.2-5 D1

Figure A-23 The SEM micrographs from region 2 of the mat electrospun from the solution at the total polymer concentration of 14% (w/v) after 1 day of degradation (14.2 D1)

Table A-22 Fiber diameter measurements in nm for 5 different locations at region 2 of the mat electrospun from the solution at the total polymer concentration of 14% (w/v) after 1 day of degradation

14.2-1 D1	14.2-2 D1	14.2-3 D1	14.2-4 D1	14.2-5 D1
1227	1792	1558	1414	1618
1319	1647		1625	1667
1463	1235		1165	988
1038	1670		1242	1518
			1605	1544
			1075	1765
				1170

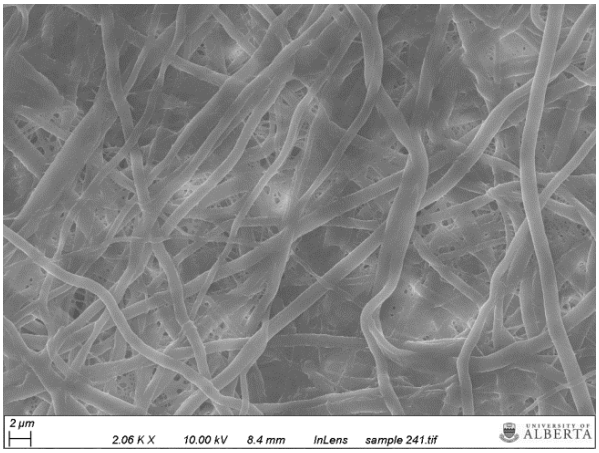

a) 14.3-1 D1

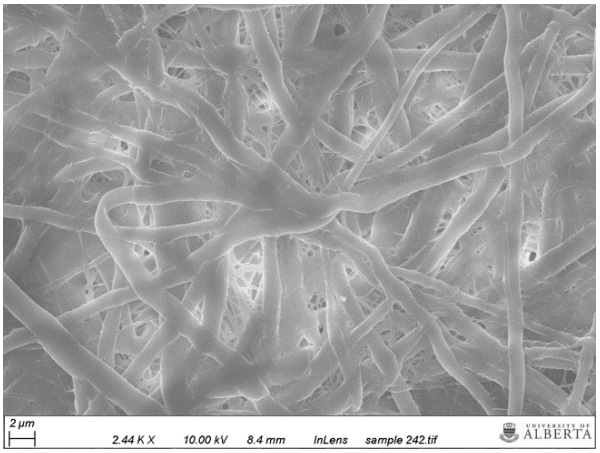

b) 14.3-2 D1

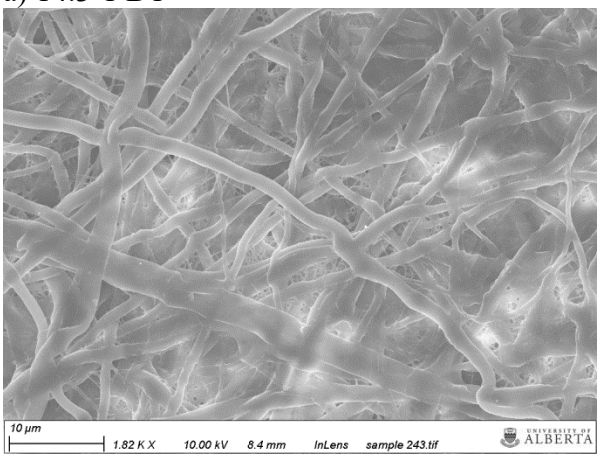

c) 14.3-3 D1

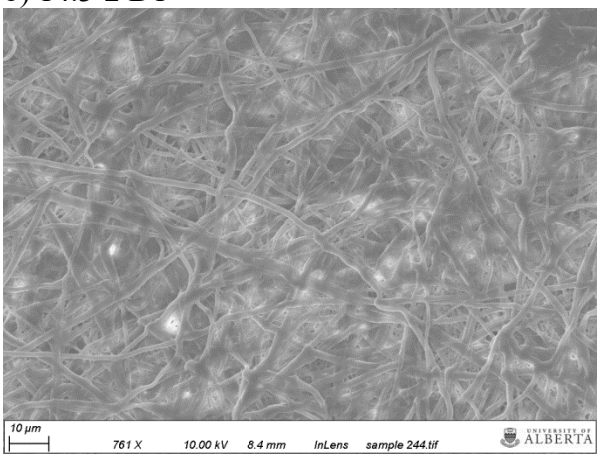

d) 14.3-4 D1

Figure A-24 The SEM micrographs from region 3 of the mat electrospun from the solution at the total polymer concentration of 14% (w/v) after 1 day of degradation (14.3 D1)

Table A-23 Fiber diameter measurements in nm for 4 different locations at region 3 of the mat electrospun from the solution at the total polymer concentration of 14% (w/v) after 1 day of degradation

14.3-1 D1	14.3-2 D1	14.3-3 D1	14.3-4 D1
1093	1771	1888	1835
1016	1194	1513	2159
1172		1337	3161
1457		1302	1642
1391			1522
			1732
			2142
			1922
			1740

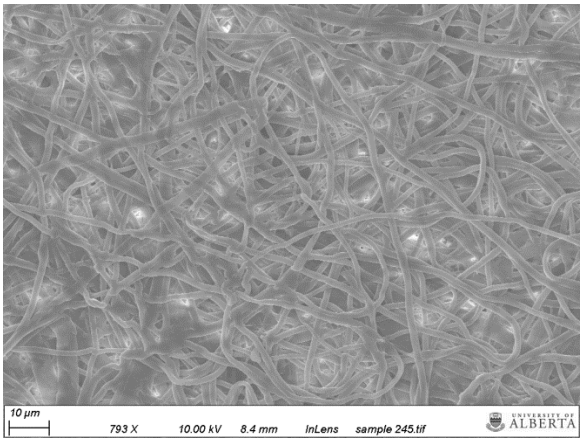

a) 14.4-1 D1

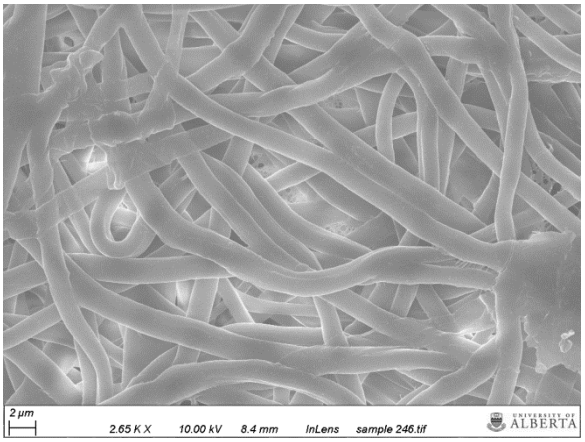

b) 14.4-2 D1

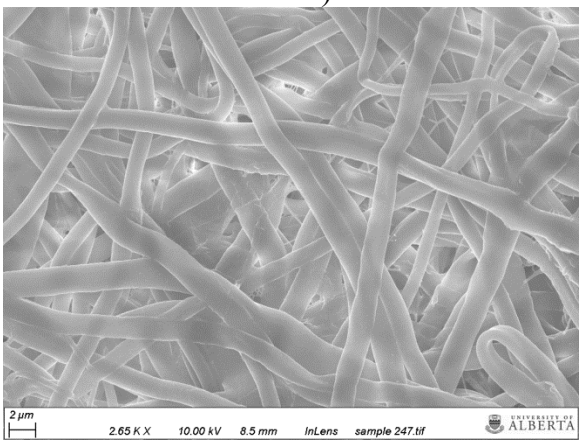

c) 14.4-3 D1

Figure A-25 The SEM micrographs from region 4 of the mat electrospun from the solution at the total polymer concentration of 14% (w/v) after 1 day of degradation (14.4 D1)

Table A-24 Fiber diameter measurements in nm for 3 different locations at region 4 of the mat electrospun from the solution at the total polymer concentration of 14% (w/v) after 1 day of degradation

14.4-1 D1	14.4-2 D1	14.4-3 D1
1652	1991	1327
1991	1689	1685
1627	1871	1664
1902	2137	1438
1768	1540	1662
1893	1494	
1952		
1678		
1520		

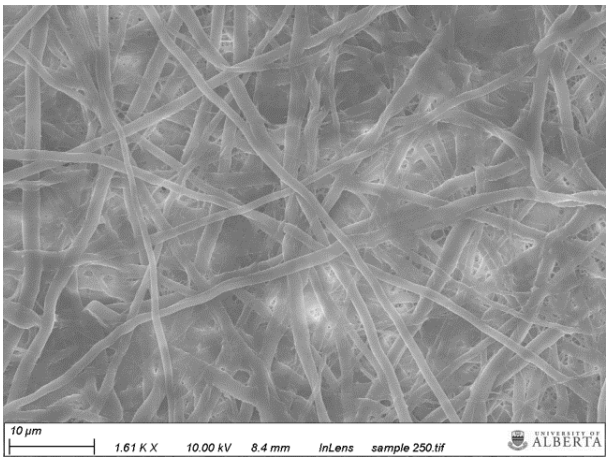

a) 14.5-1 D1

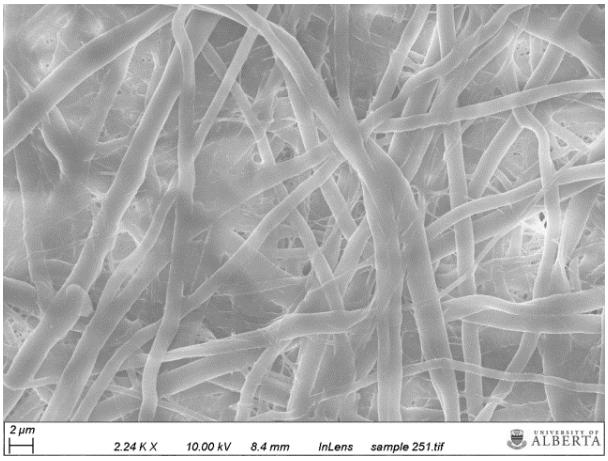

b) 14.5-2 D1

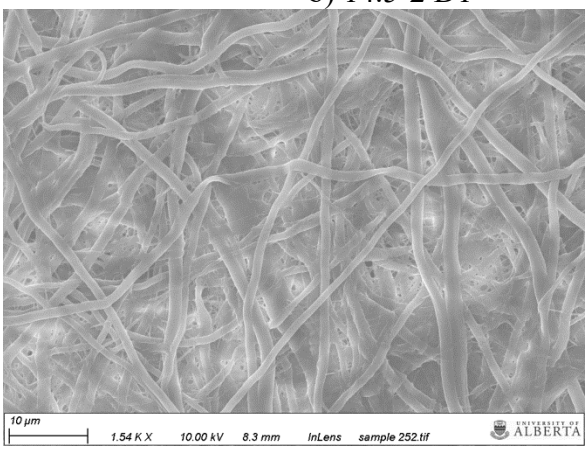

c) 14.5-3 D1

Figure A-26 The SEM micrographs from region 5 of the mat electrospun from the solution at the total polymer concentration of 14% (w/v) after 1 day of degradation (14.5 D1)

Table A-25 Fiber diameter measurements in nm for 3 different locations at region 5 of the mat electrospun from the solution at the total polymer concentration of 14% (w/v) after 1 day of degradation

14.5-1 D1	14.5-2 D1	14.5-3 D1
1006	1597	1768
1070	2004	1824
1370	1973	1702
1706	2437	1013
1636	1639	1298
1675	1434	1294
795		1281

Appendix A.3 The SEM Micrographs and Fiber Diameter Measurements of the Mats Electrospun out of 6%, 10% and 14% (w/v) Gelatin/PCL (1:1) in TFE after 3 Days of Degradation

Appendix A.3.1 The SEM Micrograph for the Mat Electrospun out of 6% (w/v) Solution after 3 Days of Degradation

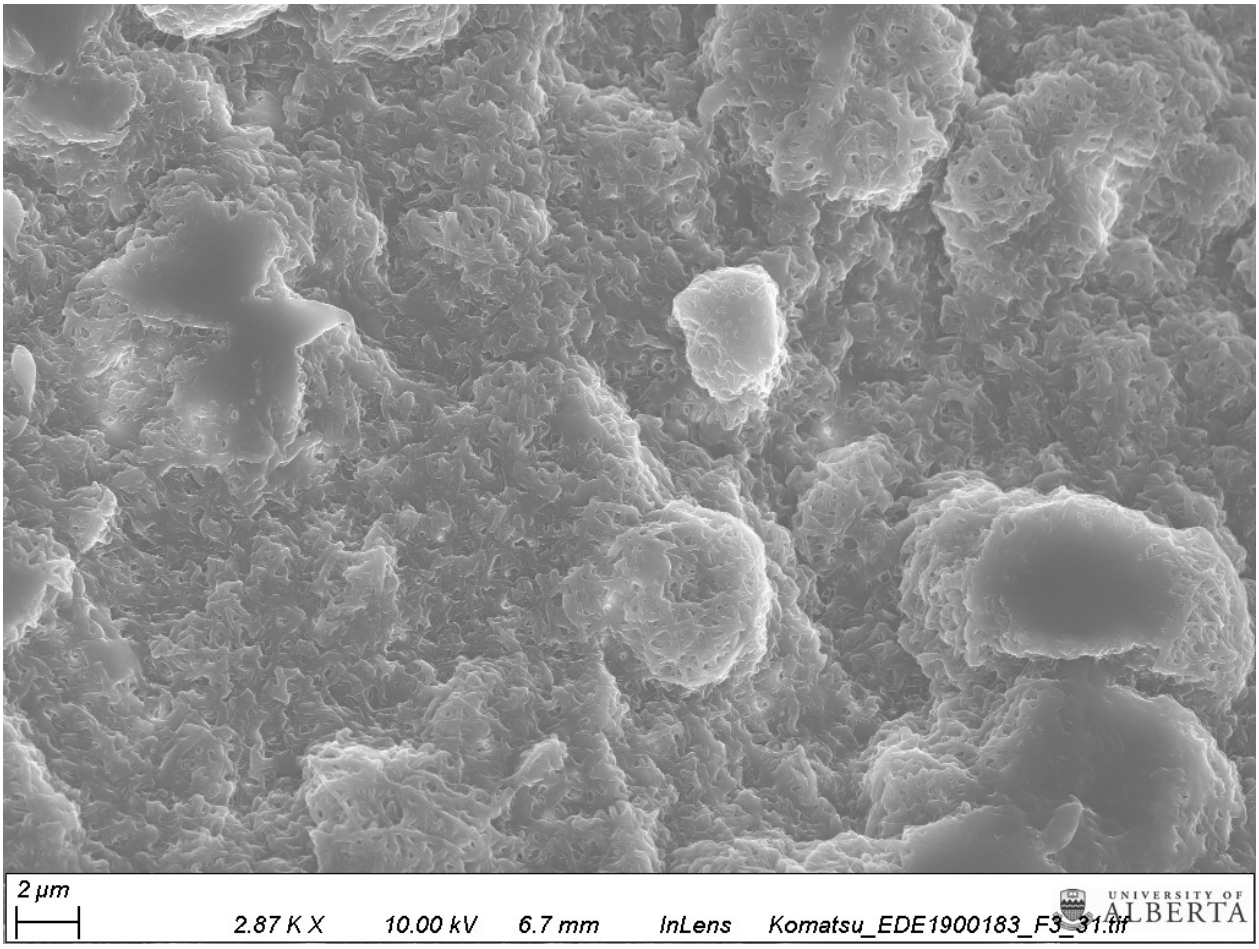

Figure A-27 The SEM micrograph for the mat electrospun from the solution at the total polymer concentration of 6% (w/v) after 3 day of degradation

Appendix A.3.2 The SEM Micrographs and Respective Fiber Diameter Measurements for Five Different Regions of the Mat Electrospun out of 10% (w/v) Solution after 3 Days of Degradation

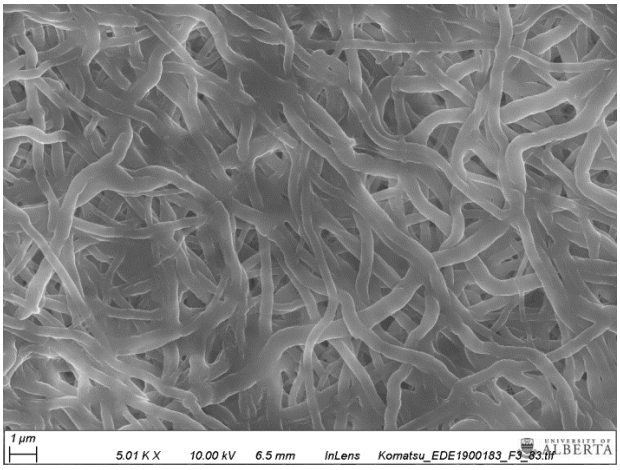

a) 10.1-1 D3

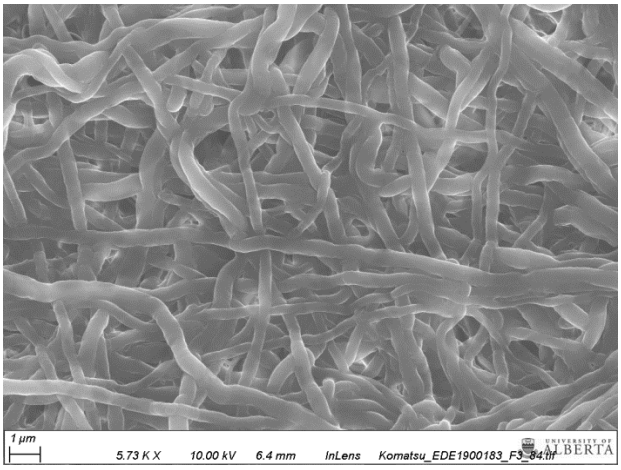

b) 10.1-2 D3

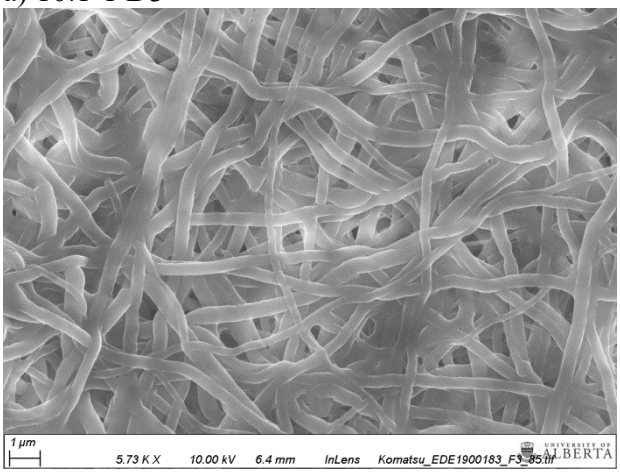

c) 10.1-3 D3

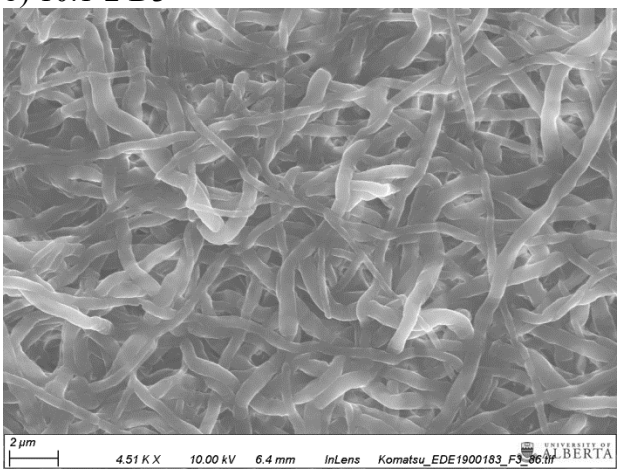

d) 10.1-4 D3

Figure A-28 The SEM micrographs from region 1 of the mat electrospun from the solution at the total polymer concentration of 10% (w/v) after 3 days of degradation (10.1 D3)

Table A-26 Fiber diameter measurements in nm for 4 different locations at region 1 of the mat electrospun from the solution at the total polymer concentration of 10% (w/v) after 3 days of degradation

10.1-1 D3	10.1-2 D3	10.1-3 D3	10.1-4 D3
667	482	523	656
431	497	468	903
520	494	558	661
348	465	507	536
725	576	422	621

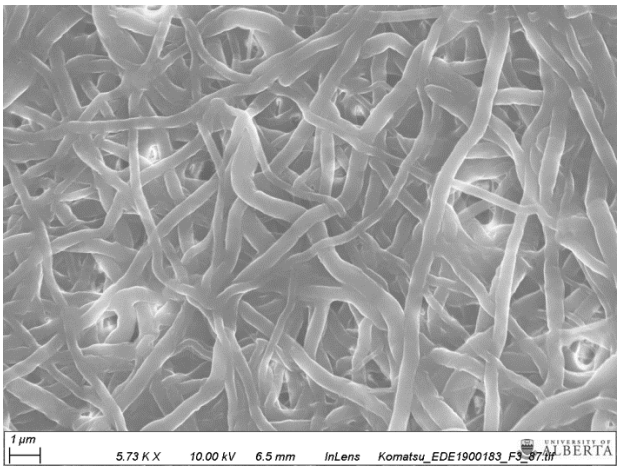

a) 10.2-1 D3

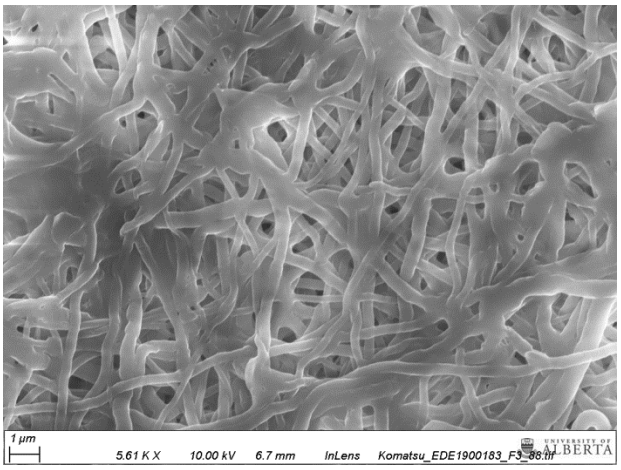

b) 10.2-2 D3

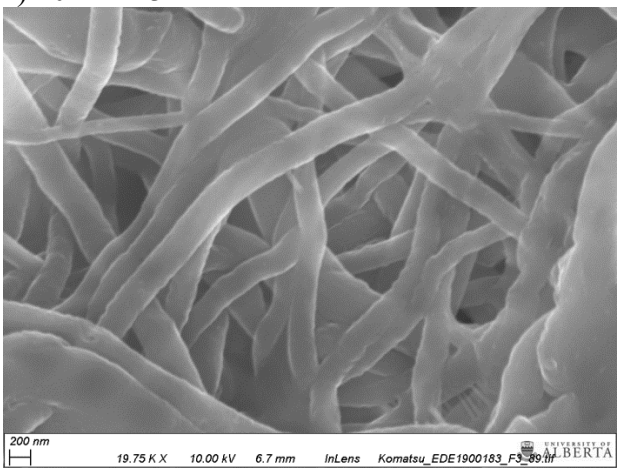

c) 10.2-3 D3

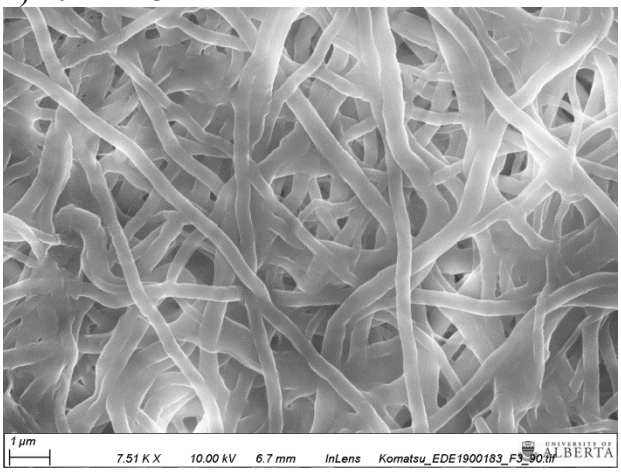

d) 10.2-4 D3

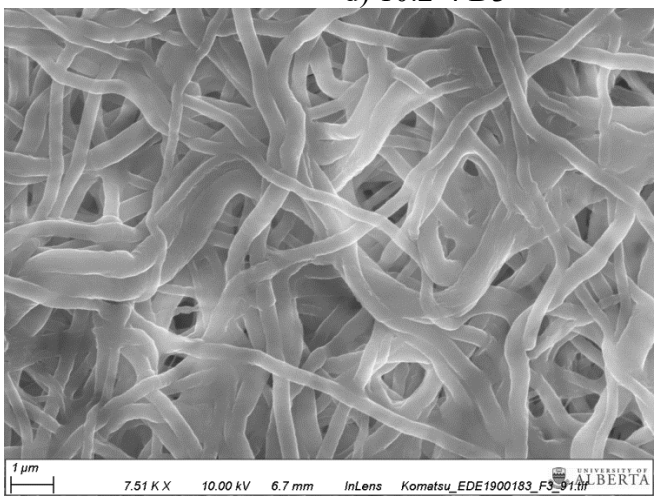

e) 10.2-5 D3

Figure A-29 The SEM micrographs from region 2 of the mat electrospun from the solution at the total polymer concentration of 10% (w/v) after 3 days of degradation (10.2 D3)

Table A-27 Fiber diameter measurements in nm for 5 different locations at region 2 of the mat electrospun from the solution at the total polymer concentration of 10% (w/v) after 3 days of degradation

10.2-1 D3	10.2-2 D3	10.2-3 D3	10.2-4 D3	10.2-5 D3
479	453	318	372	350
458	294	331	487	355
631	307	347	350	395
501	395	255	332	504

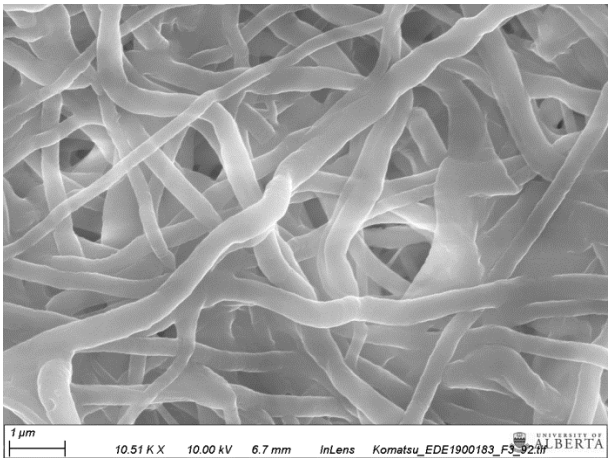

a) 10.3-1 D3

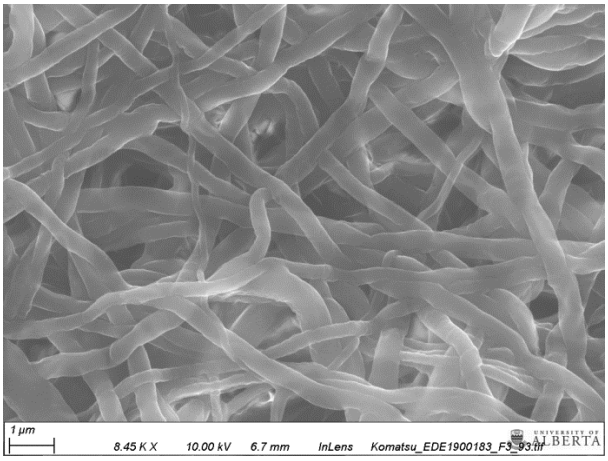

b) 10.3-2 D3

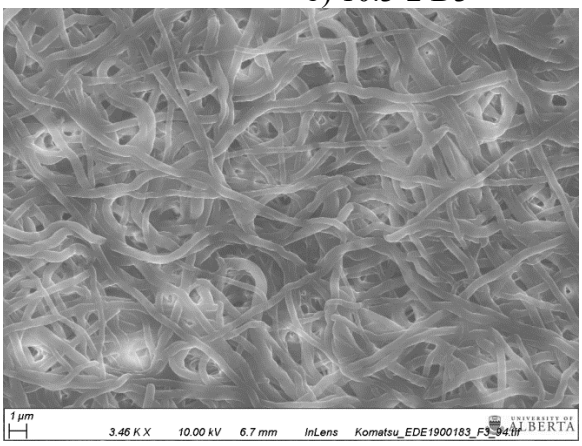

c) 10.3-3 D3

Figure A-30 The SEM micrographs from region 3 of the mat electrospun from the solution at the total polymer concentration of 10% (w/v) after 3 days of degradation (10.3 D3)

Table A-28 Fiber diameter measurements in nm for 3 different locations at region 3 of the mat electrospun from the solution at the total polymer concentration of 10% (w/v) after 3 days of degradation

10.3-1 D3	10.3-2 D3	10.3-3 D3
438	355	539
464	428	621
526	499	454
346	363	557
	409	392
	532	426
	422	342
	505	432

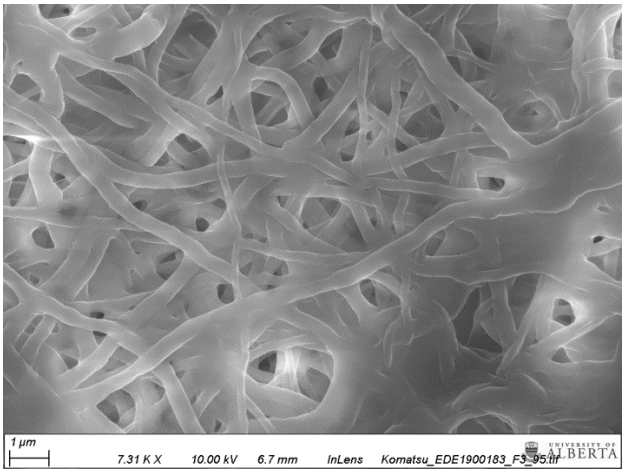

a) 10.4-1 D3

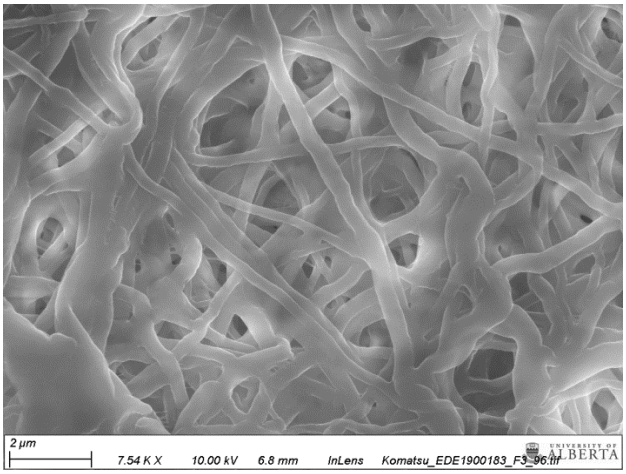

b) 10.4-2 D3

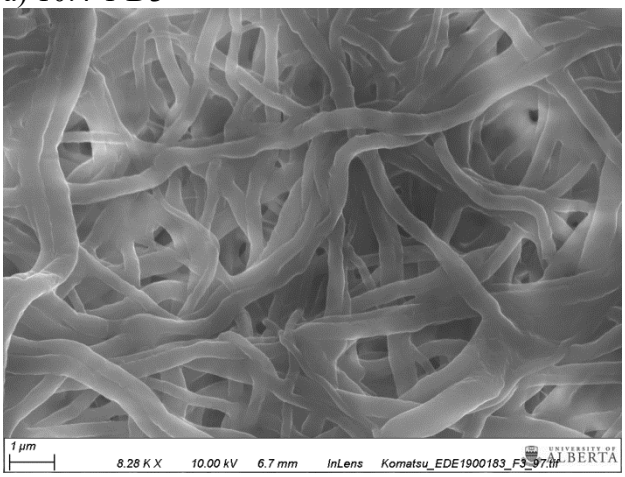

c) 10.4-3 D3

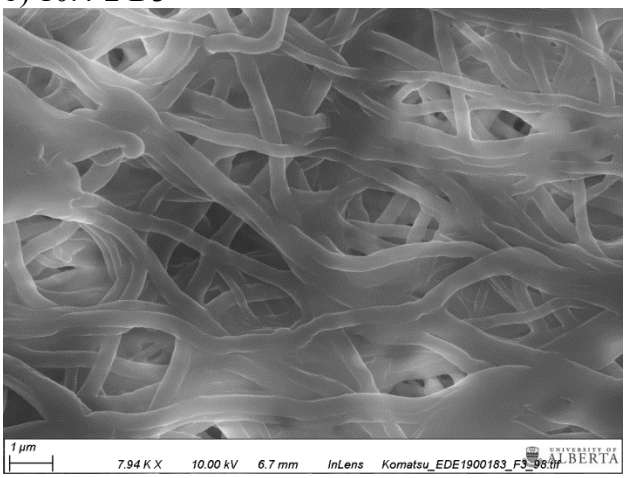

d) 10.4-4 D3

Figure A-31 The SEM micrographs from region 4 of the mat electrospun from the solution at the total polymer concentration of 10% (w/v) after 3 days of degradation (10.4 D3)

Table A-29 Fiber diameter measurements in nm for 4 different locations at region 4 of the mat electrospun from the solution at the total polymer concentration of 10% (w/v) after 3 days of degradation

10.4-1 D3	10.4-2 D3	10.4-3 D3	10.4-4 D3
399	466	463	420
375	318	329	396
437	397	408	353
477	524	425	370
415	253	420	399

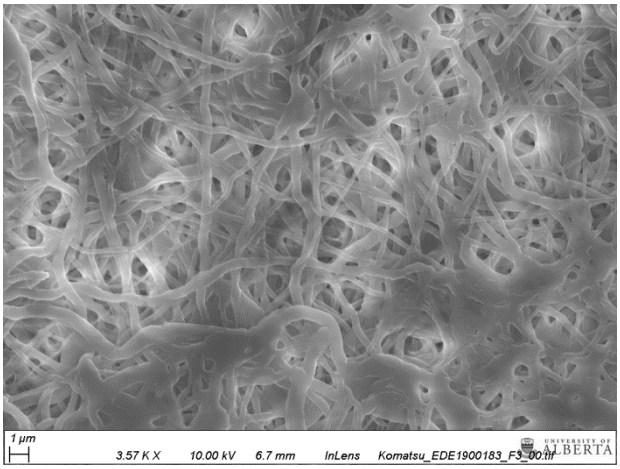

a) 10.5-1 D3

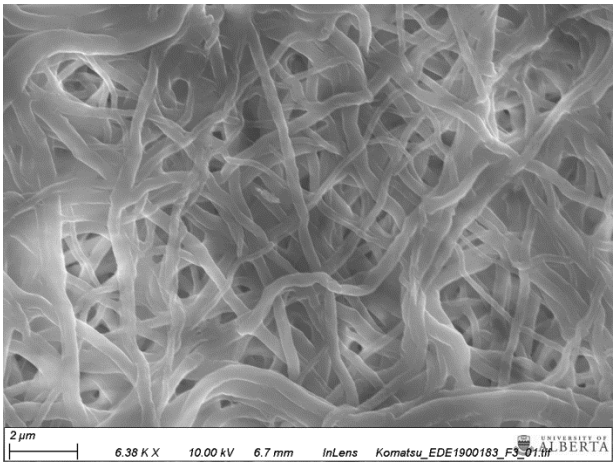

b) 10.5-2 D3

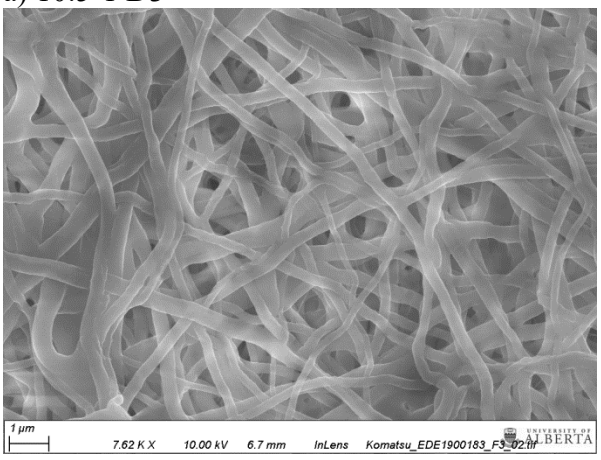

c) 10.5-3 D3

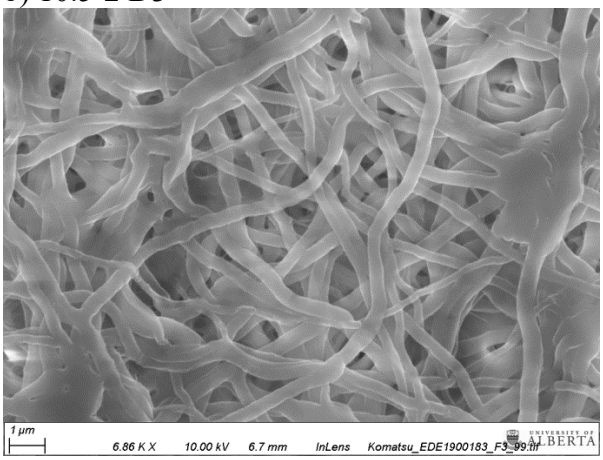

d) 10.5-4 D3

Figure A-32 The SEM micrographs from region 5 of the mat electrospun from the solution at the total polymer concentration of 10% (w/v) after 3 days of degradation (10.5 D3)

Table A-30 Fiber diameter measurements in nm for 4 different locations at region 5 of the mat electrospun from the solution at the total polymer concentration of 10% (w/v) after 3 days of degradation

10.5-1 D3	10.5-2 D3	10.5-3 D3	10.5-4 D3
403	408	456	388
322	343	295	341
618	329	354	414
448	328	294	523
488	298	281	442

Appendix A.3.3 The SEM Micrographs and Respective Fiber Diameter Measurements for Five Different Regions of the Mat Electrospun out of 14% (w/v) Solution after 3 Days of Degradation

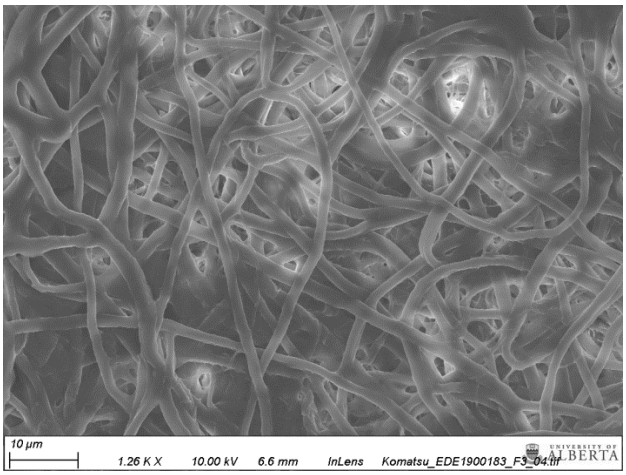

a) 14.1-1 D3

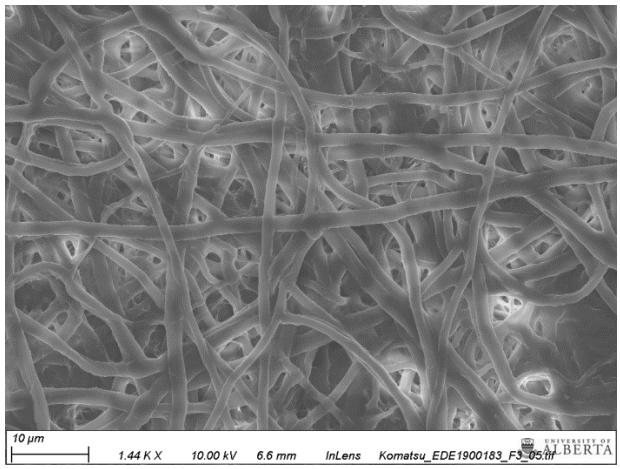

a) 14.1-2 D3

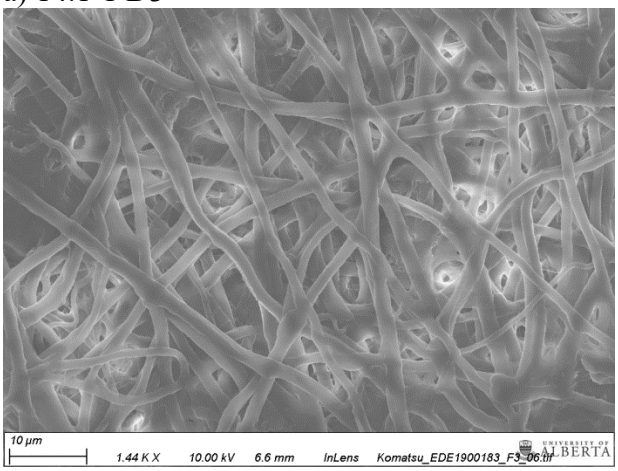

a) 14.1-3 D3

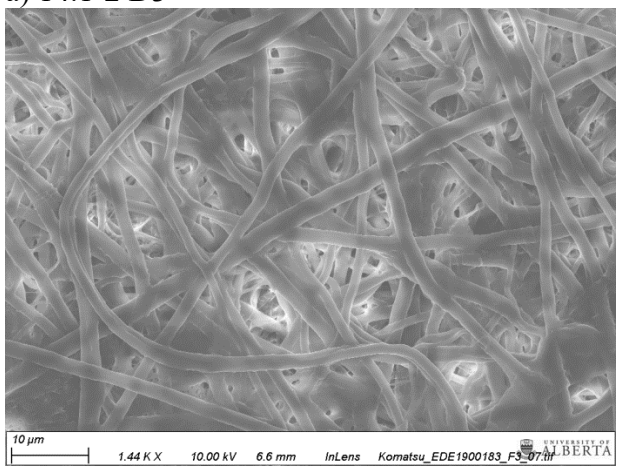

a) 14.1-4 D3

Figure A-33 The SEM micrographs from region 1 of the mat electrospun from the solution at the total polymer concentration of 14% (w/v) after 3 days of degradation (14.1 D3)

Table A-31 Fiber diameter measurements in nm for 4 different locations at region 1 of the mat electrospun from the solution at the total polymer concentration of 14% (w/v) after 3 days of degradation

14.1-1 D3	14.1-2 D3	14.1-3 D3	14.1-4 D3
1536	1765	1843	1672
1532	1210	1448	2452
2025	1275	1391	1723
1568	1591	1457	2086
1997	2014	2138	2328

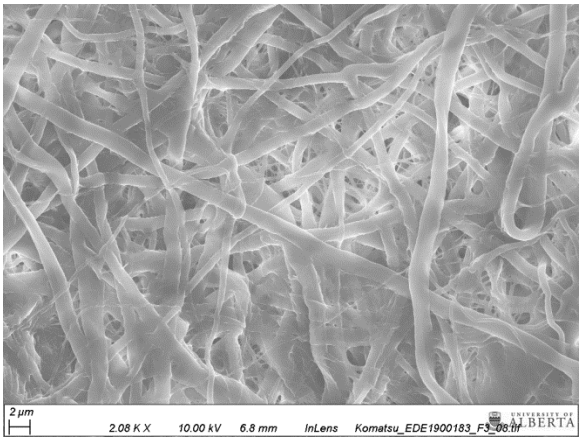

a) 14.2-1 D3

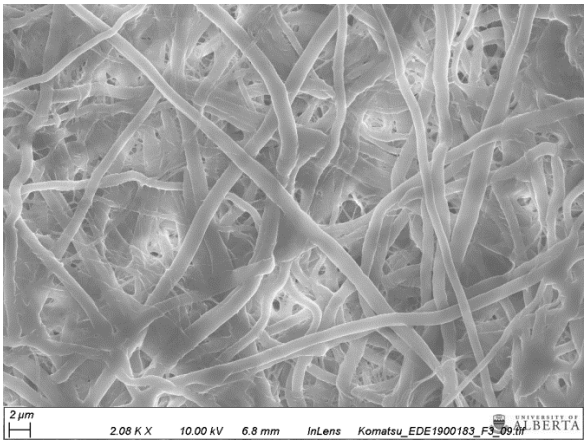

b) 14.2-2 D3

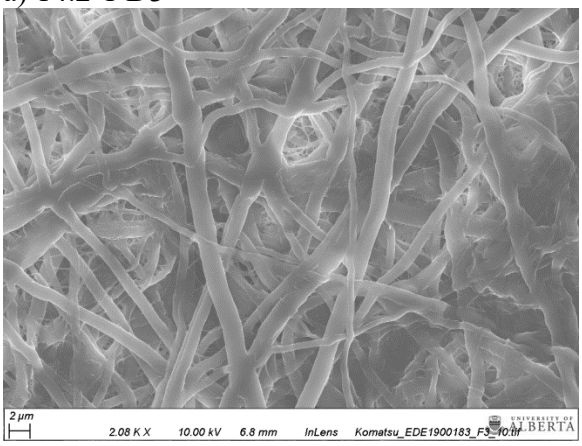

c) 14.2-3 D3

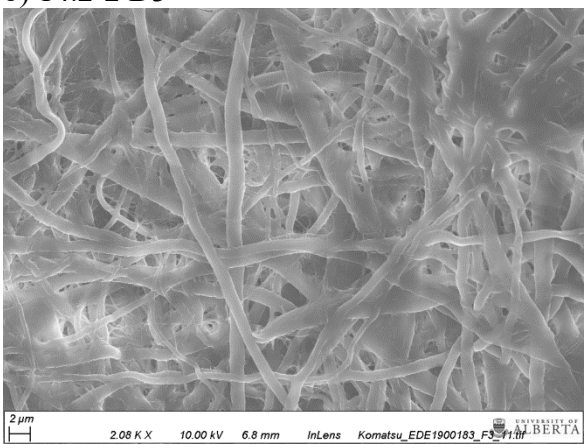

d) 14.2-4 D3

Figure A-34 The SEM micrographs from region 2 of the mat electrospun from the solution at the total polymer concentration of 14% (w/v) after 3 days of degradation (14.2 D3)

Table A-32 Fiber diameter measurements in nm for 4 different locations at region 2 of the mat electrospun from the solution at the total polymer concentration of 14% (w/v) after 3 days of degradation

14.2-1 D3	14.2-2 D3	14.2-3 D3	14.2-4 D3
1519	1504	1930	1597
1094	1708	1822	1146
1326	1898	1728	1368
1222	1544	1712	1410
1089	1189	1208	996

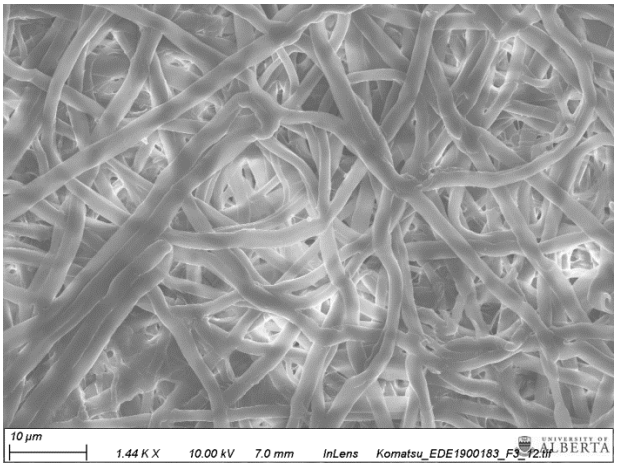

a) 14.3-1 D3

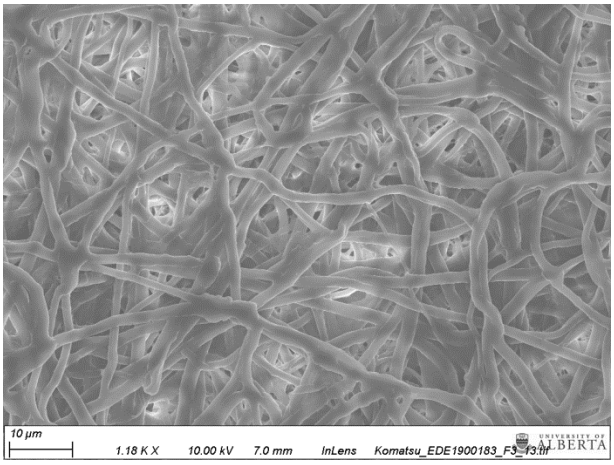

b) 14.3-2 D3

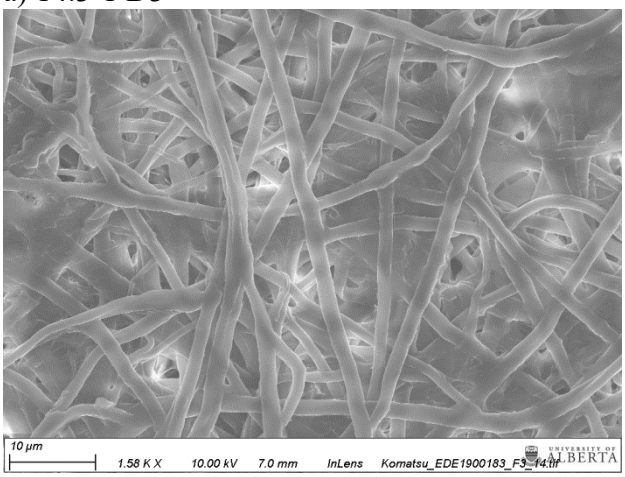

c) 14.3-3 D3

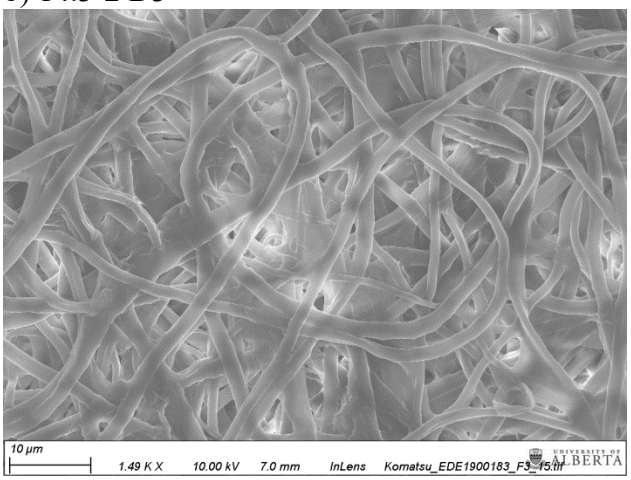

d) 14.3-4 D3

Figure A-35 The SEM micrographs from region 3 of the mat electrospun from the solution at the total polymer concentration of 14% (w/v) after 3 days of degradation (14.3 D3)

Table A-33 Fiber diameter measurements in nm for 4 different locations at region 3 of the mat electrospun from the solution at the total polymer concentration of 14% (w/v) after 3 days of degradation

14.3-1 D3	14.3-2 D3	14.3-3 D3	14.3-4 D3
2385	2157	2087	1975
2127	1911	1792	1905
2121	1556	1533	1993
2183	2010	1758	1976
2339	1965	1884	1873

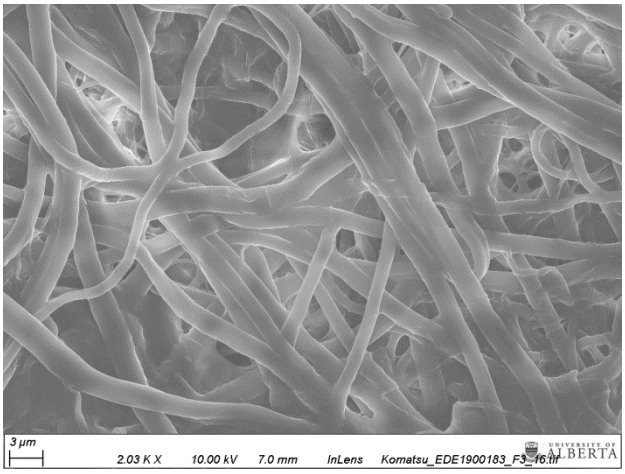

a) 14.4-1 D3

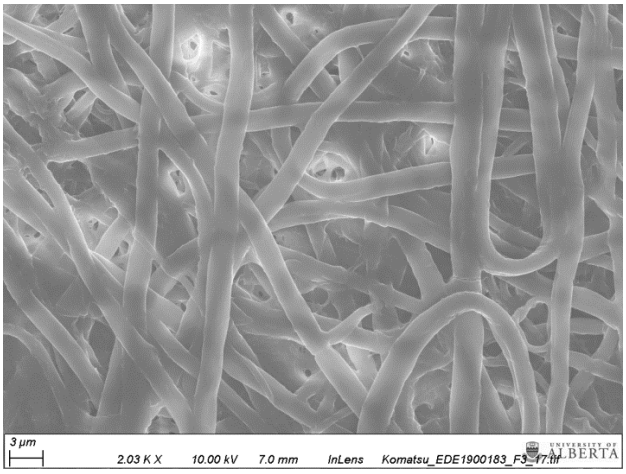

b) 14.4-2 D3

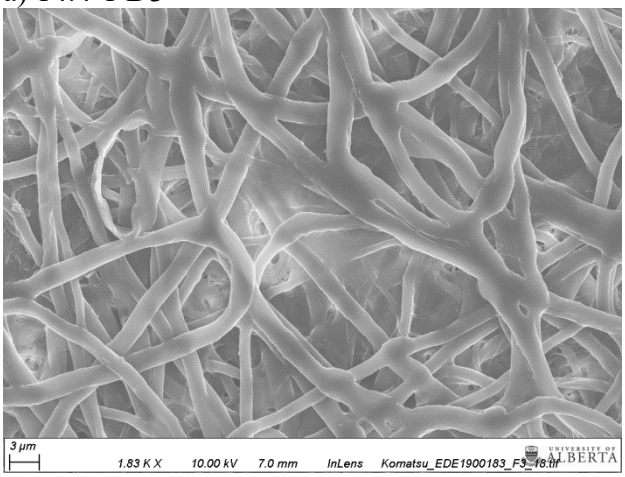

c) 14.4-3 D3

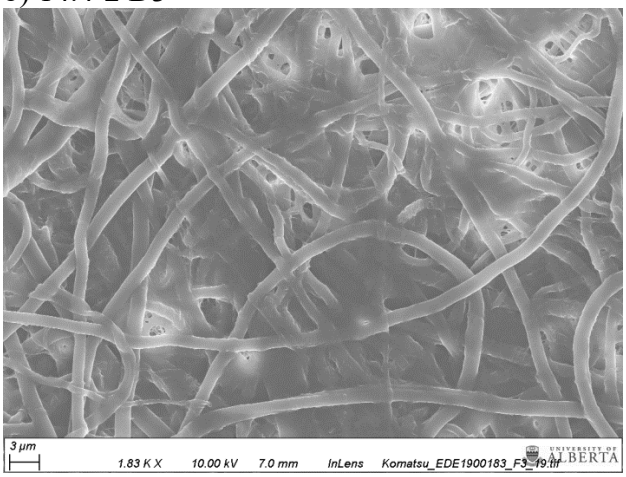

d) 14.4-4 D3

Figure A-36 The SEM micrographs from region 4 of the mat electrospun from the solution at the total polymer concentration of 14% (w/v) after 3 days of degradation (14.4 D3)

Table A-34 Fiber diameter measurements in nm for 4 different locations at region 4 of the mat electrospun from the solution at the total polymer concentration of 14% (w/v) after 3 days of degradation

14.4-1 D3	14.4-2 D3	14.4-3 D3	14.4-4 D3
1857	2353	2046	1545
2181	2134	2159	1455
2224	1943	1823	1299
1784	1914	1677	1305
1746	2121	2090	1590

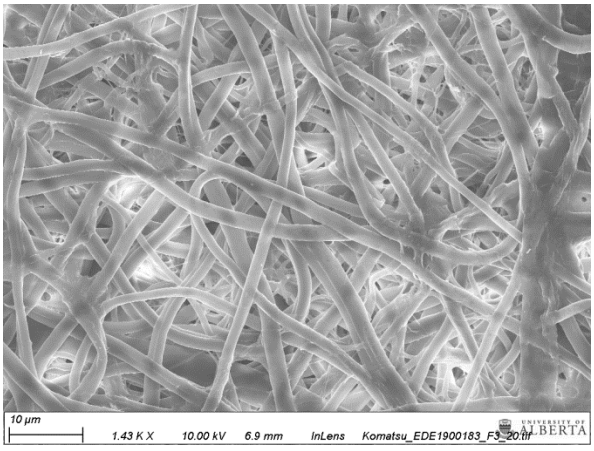

a) 14.5-1 D3

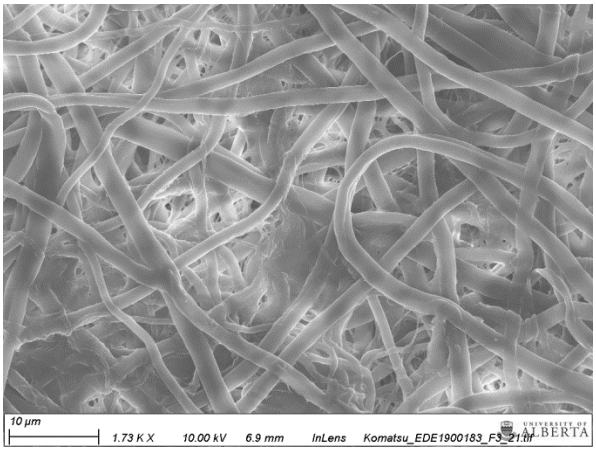

b) 14.5-2 D3

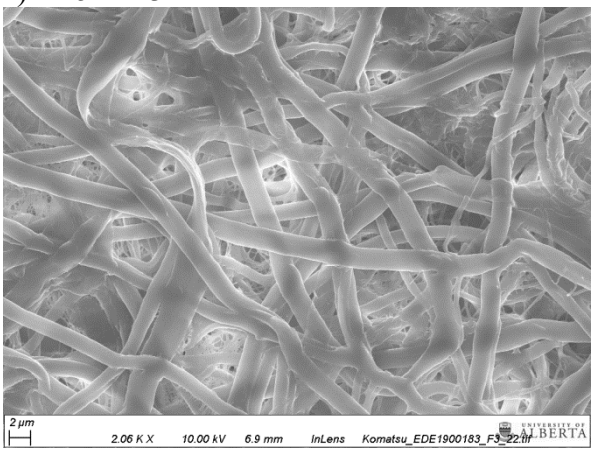

c) 14.5-3 D3

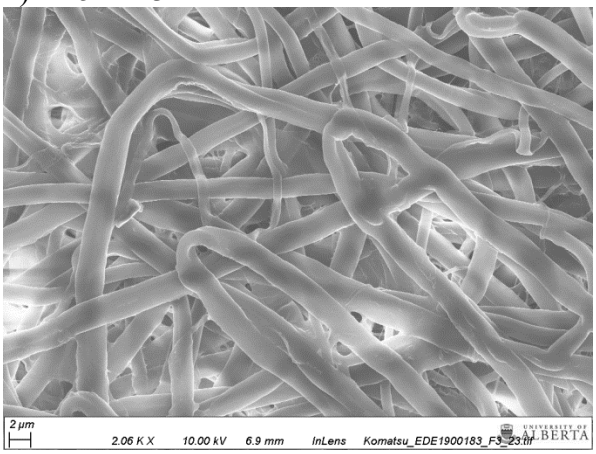

d) 14.5-4 D3

Figure A-37 The SEM micrographs from region 5 of the mat electrospun from the solution at the total polymer concentration of 14% (w/v) after 3 days of degradation (14.5 D3)

Table A-35 Fiber diameter measurements in nm for 4 different locations at region 5 of the mat electrospun from the solution at the total polymer concentration of 14% (w/v) after 3 days of degradation

14.5-1 D3	14.5-2 D3	14.5-3 D3	14.5-4 D3
1992	2316	1490	2533
2036	1862	2134	2137
2319	2280	2083	2704
2316	1985	2146	2015
2061	3017	1973	2357

Appendix A.4 The SEM Micrographs and Fiber Diameter Measurements of the Mats Electrospun out of 6%, 10% and 14% (w/v) Gelatin/PCL (1:1) in TFE after 6 Days of Degradation

Appendix A.4.1 The SEM Micrograph of the Mat Electrospun out of 6% (w/v) Solution after 6 Days of Degradation

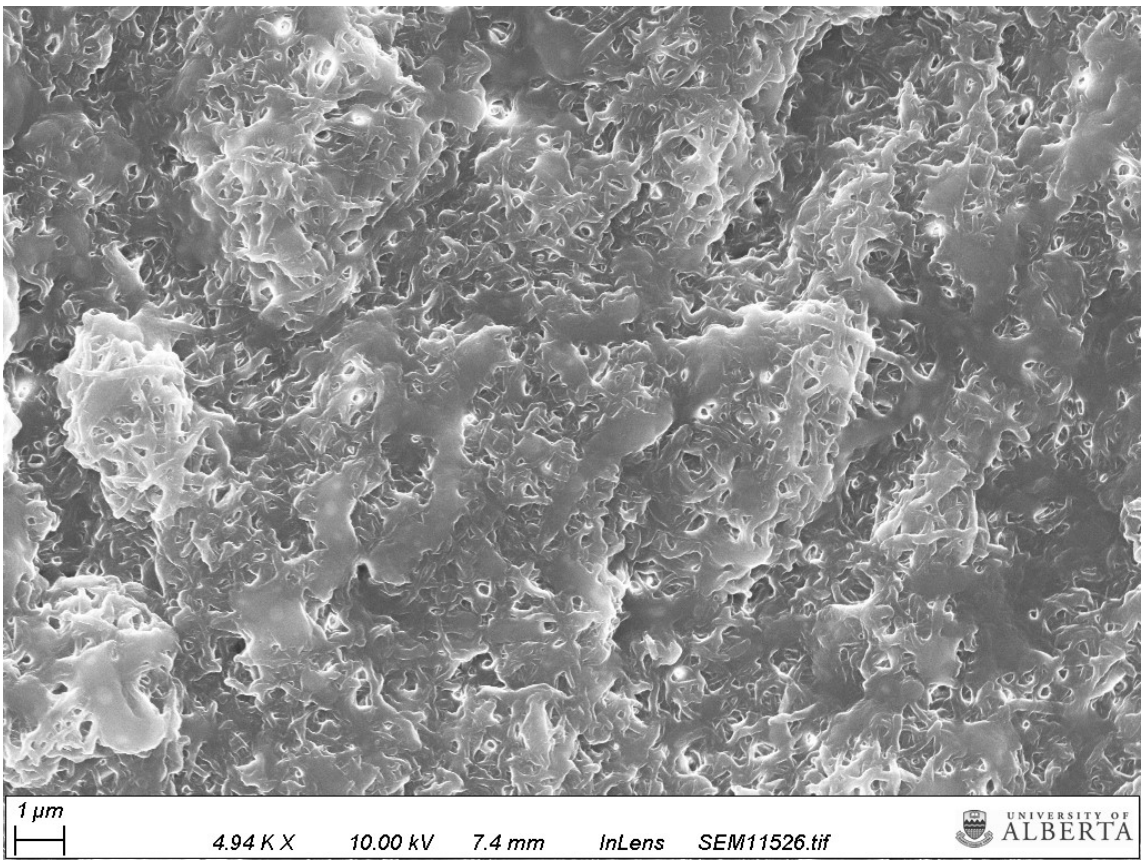

Figure A-38 The SEM micrograph for the mat electrospun from the solution at the total polymer concentration of 6% (w/v) after 6 days of degradation

Appendix A.4.2 The SEM Micrographs and Respective Fiber Diameter Measurements for Five Different Regions of the Mat Electrospun out of 10% (w/v) Solution after 6 Days of Degradation

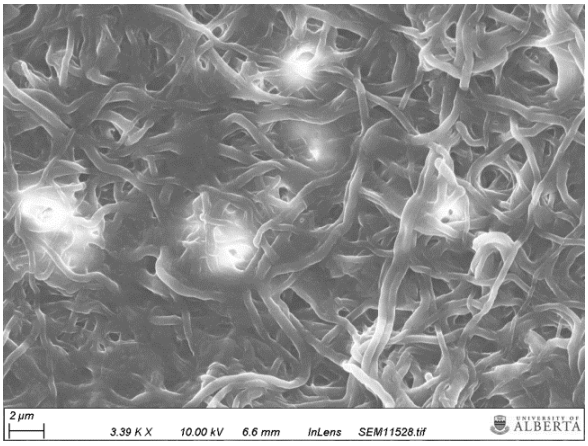

a) 10.1-1 D6

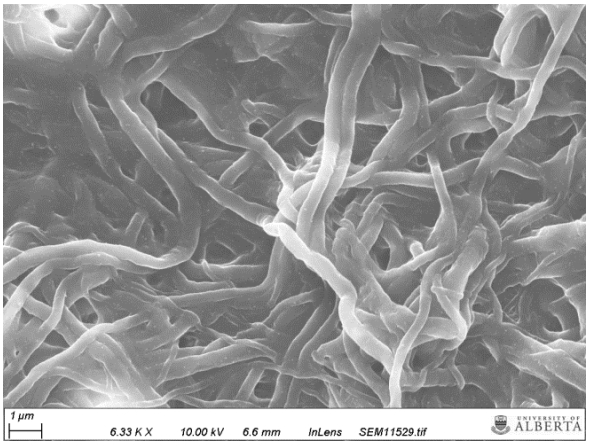

b) 10.1-2 D6

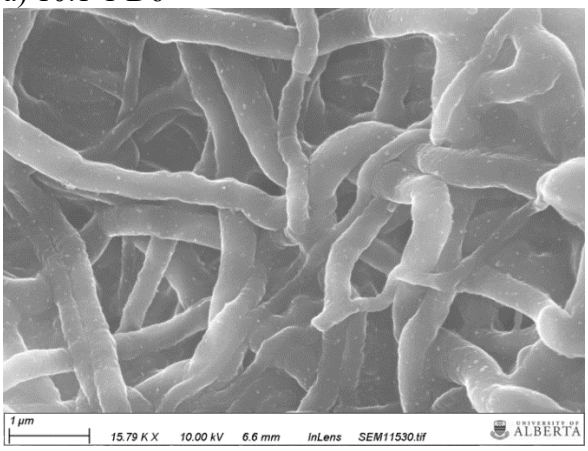

c) 10.1-3 D6

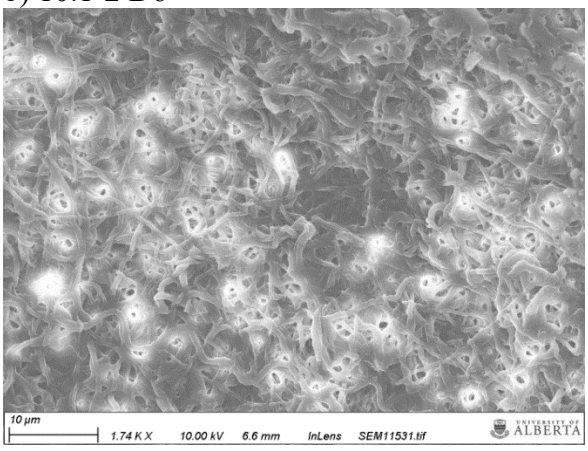

d) 10.1-4 D6

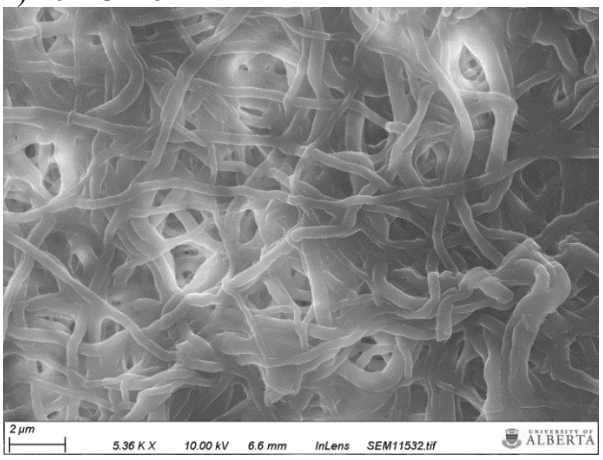

e) 10.1-5 D6

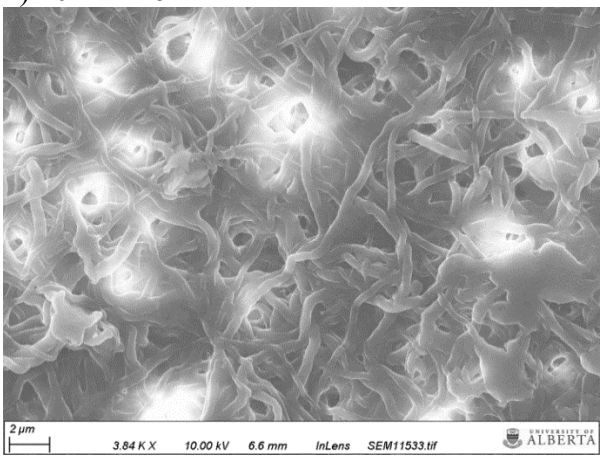

f) 10.1-6 D6

Figure A-39 The SEM micrographs from region 1 of the mat electrospun from the solution at the total polymer concentration of 10% (w/v) after 6 days of degradation(10.1 D6)

Table A-36 Fiber diameter measurements in nm for 6 different locations at region 1 of the mat electrospun from the solution at the total polymer concentration of 10% (w/v) after 6 days of degradation

10.1-1 D6	10.1-2 D6	10.1-3 D6	10.1-4 D6	10.1-5 D6	10.1-6 D6
500	538	439	582	427	443
514	303	347	456	359	503
363	275	437	532	344	
		321		320	

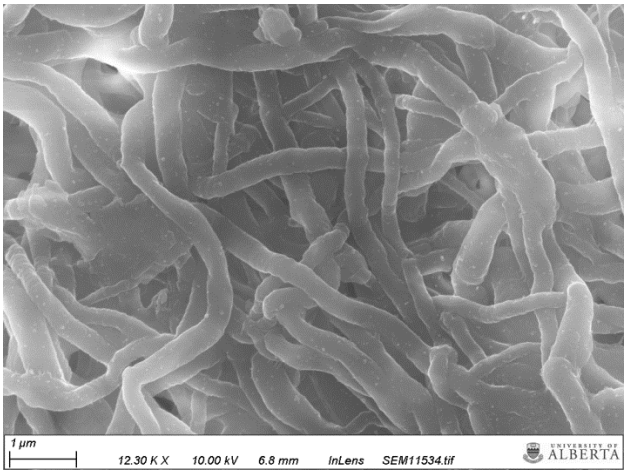

a) 10.2-1 D6

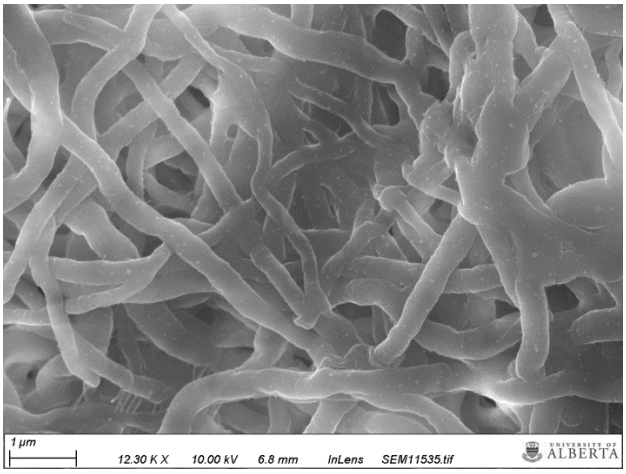

b) 10.2-2 D6

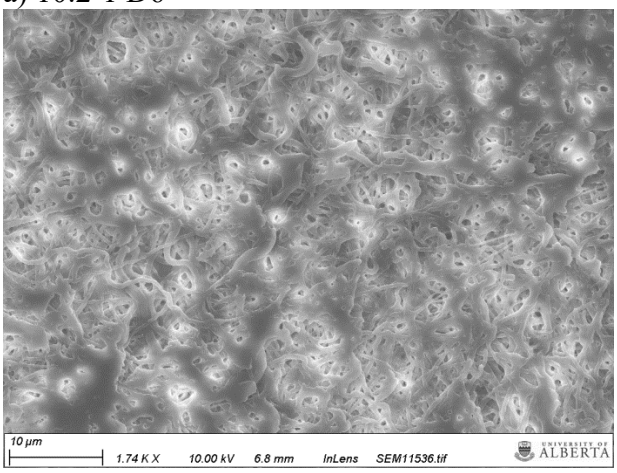

c) 10.2-3 D6

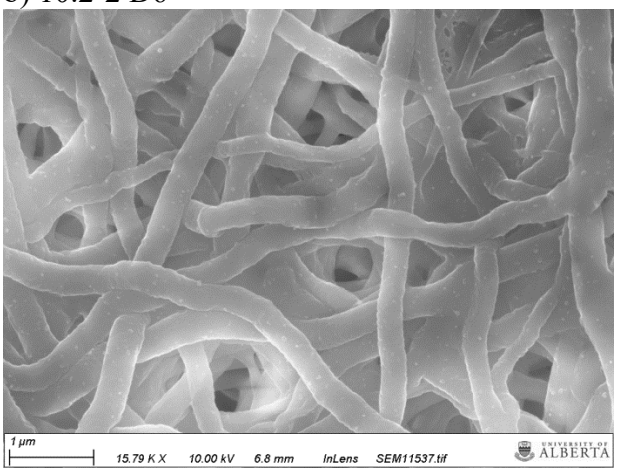

d) 10.2-4 D6

Figure A-40 The SEM micrographs from region 2 of the mat electrospun from the solution at the total polymer concentration of 10% (w/v) after 6 days of degradation (10.2 D6)

Table A-37 Fiber diameter measurements in nm for 4 different locations at region 2 of the mat electrospun from the solution at the total polymer concentration of 10% (w/v) after 6 days of degradation

10.2-1 D6	**10.2-2 D6**	**10.2-3 D6**	**10.2-4 D6**
332	392	358	341
286	379	402	311
	301	293	337
	305		333
	340		380
			292
			282
			341
			319

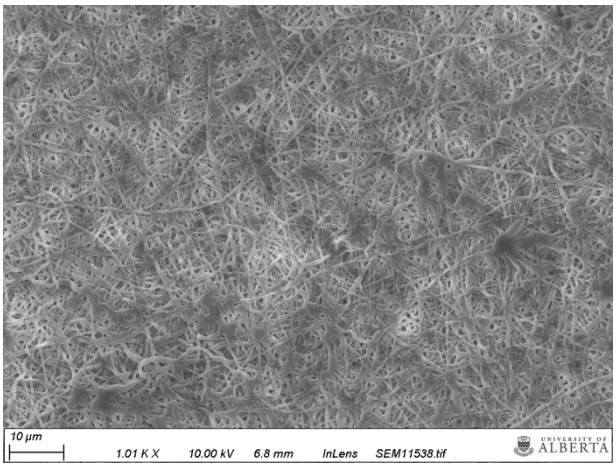

a) 10.3-1 D6

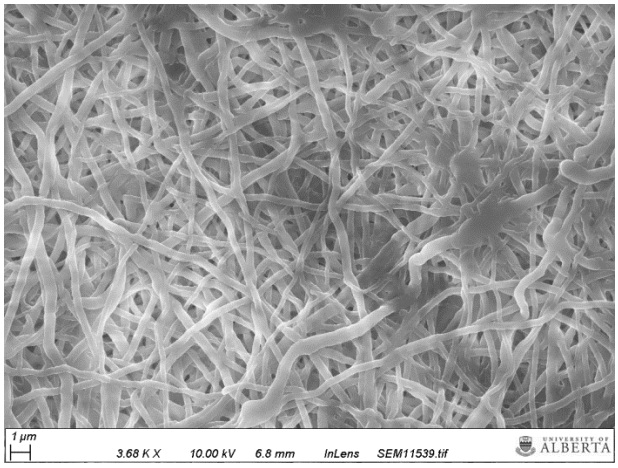

b) 10.3-2 D6

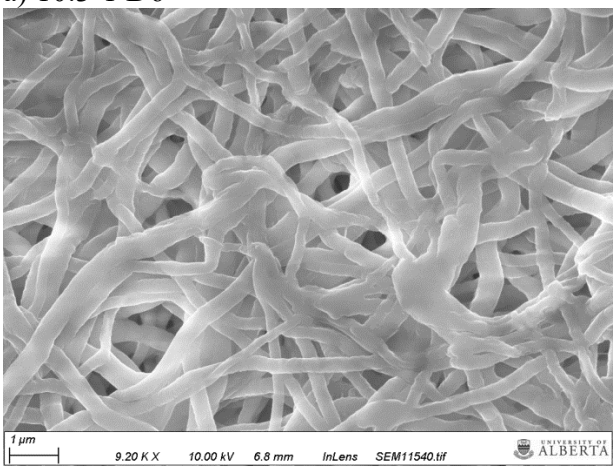

c) 10.3-3 D6

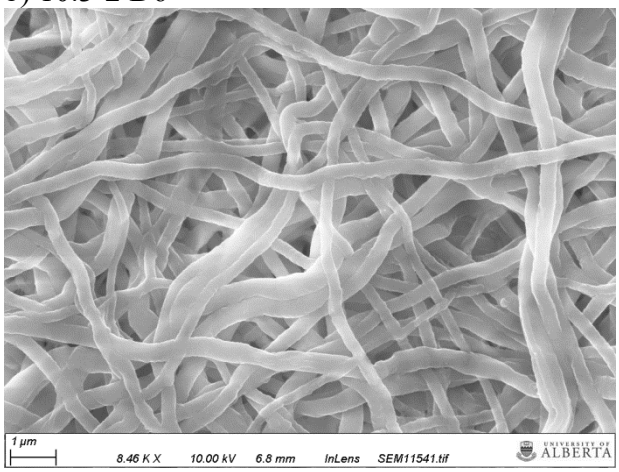

d) 10.3-4 D6

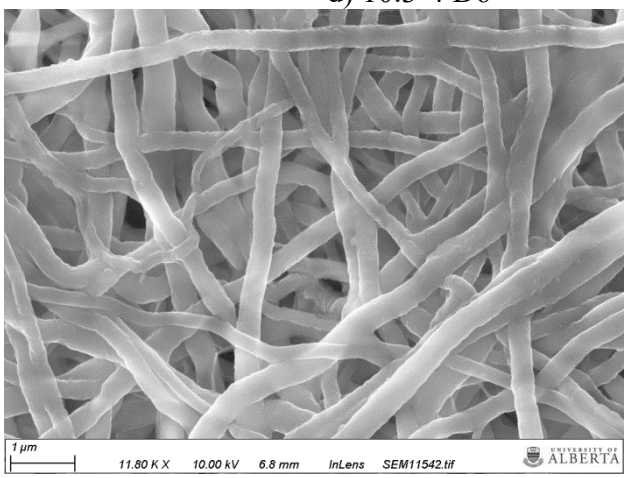

e) 10.3-5 D6

Figure A-41 The SEM micrographs from region 3 of the mat electrospun from the solution at the total polymer concentration of 10% (w/v) after 6 days of degradation (10.3 D6)

Table A-38 Fiber diameter measurements in nm for 5 different locations at region 3 of the mat electrospun from the solution at the total polymer concentration of 10% (w/v) after 6 days of degradation

10.3-1 D6	10.3-2 D6	10.3-3 D6	10.3-4 D6	10.3-5 D6
479	369	315	346	343
519	515	316	345	332
590	540	376	370	302
522		434	407	337

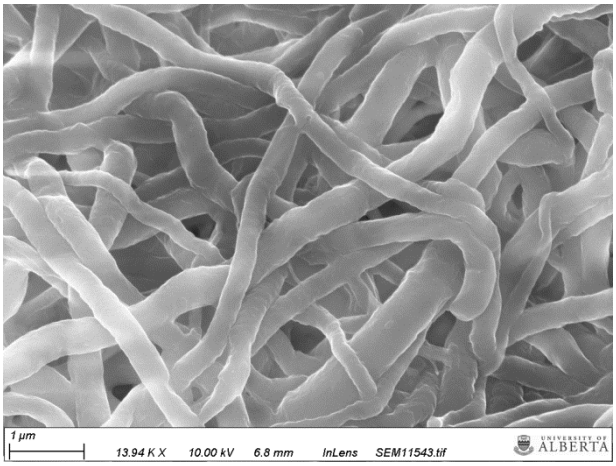

a) 10.4-1 D6

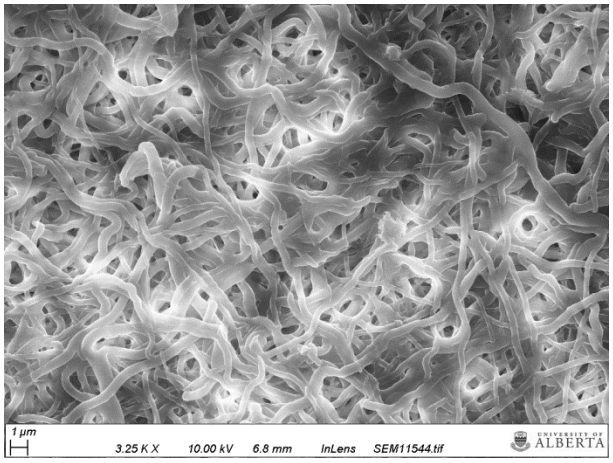

b) 10.4-2 D6

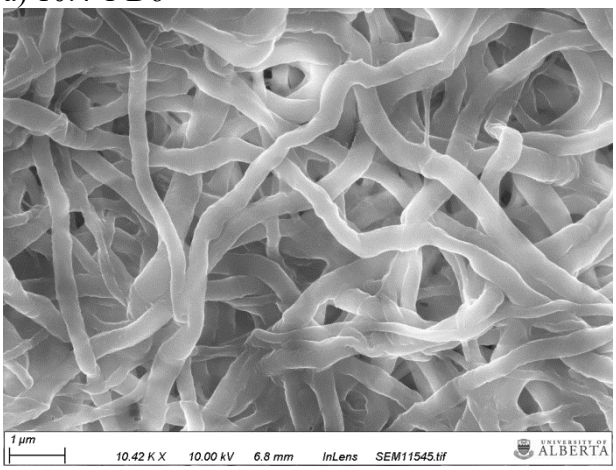

c) 10.4-3 D6

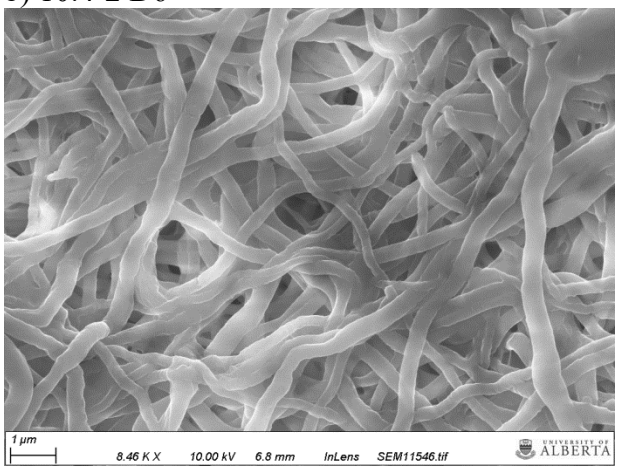

d) 10.4-4 D6

Figure A-42 The SEM micrographs from region 4 of the mat electrospun from the solution at the total polymer concentration of 10% (w/v) after 6 days of degradation (10.4 D6)

Table A-39 Fiber diameter measurements in nm for 4 different locations at region 4 of the mat electrospun from the solution at the total polymer concentration of 10% (w/v) after 6 days of degradation

10.4-1 D6	10.4-2 D6	10.4-3 D6	10.4-4 D6
351	582	322	360
301	557	265	314
490	551	363	334
344	511	498	335
	456	383	331
	387		
	430		
	468		
	343		
	361		

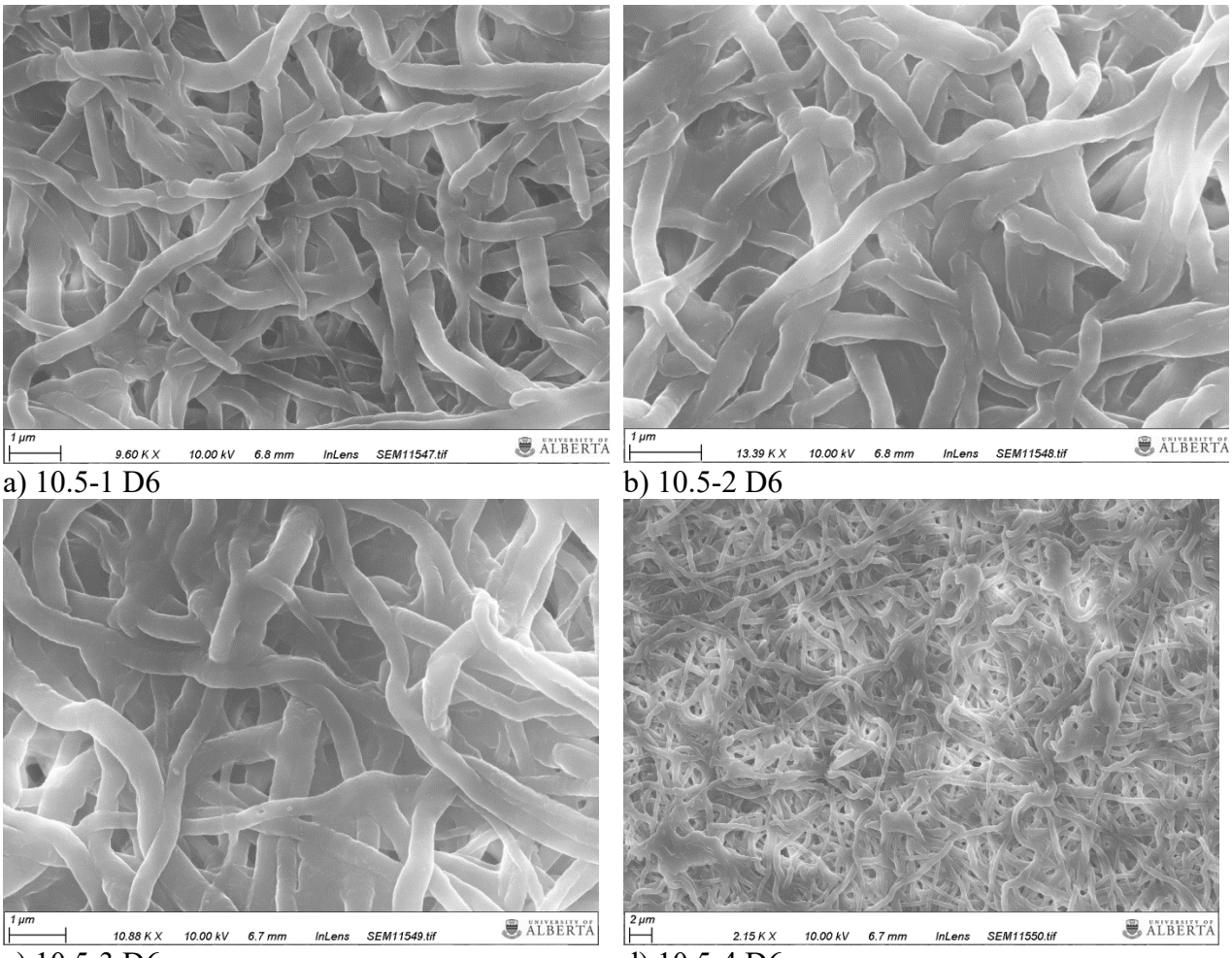

a) 10.5-1 D6 b) 10.5-2 D6

c) 10.5-3 D6 d) 10.5-4 D6

Figure A-43 The SEM micrographs from region 5 of the mat electrospun from the solution at the total polymer concentration of 10% (w/v) after 6 days of degradation (10.5 D6)

Table A-40 Fiber diameter measurements in nm for 4 different locations at region 5 of the mat electrospun from the solution at the total polymer concentration of 10% (w/v) after 6 days of degradation

10.5-1 D6	10.5-2 D6	10.5-3 D6	10.5-4 D6
505	372	412	408
509	302	399	469
570	349	448	465
329	454	585	378
	805	466	438

Appendix A.4.3 The SEM Micrographs and Respective Fiber Diameter Measurements for Five Different Regions of the Mat Electrospun out of 14% (w/v) Solution after 6 Days of Degradation

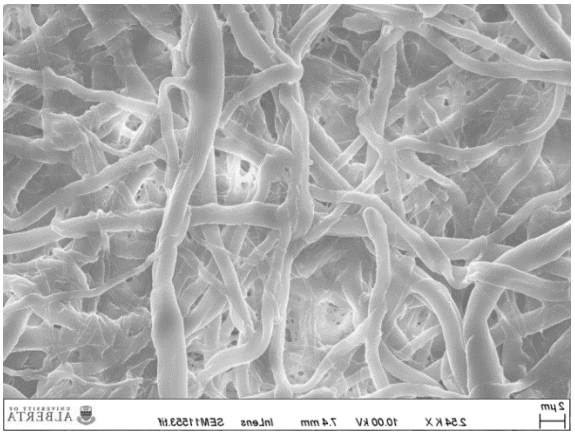

a) 14.1-1 D6

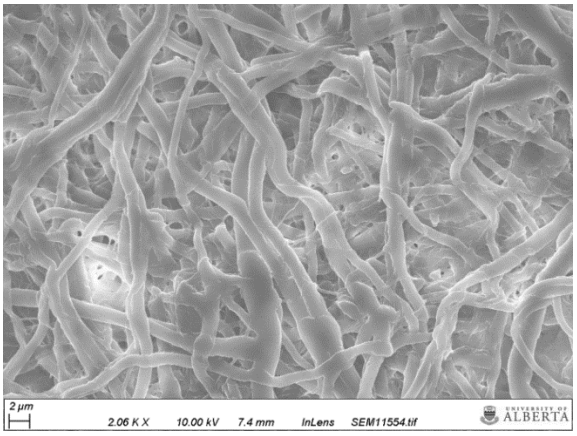

b) 14.1-2 D6

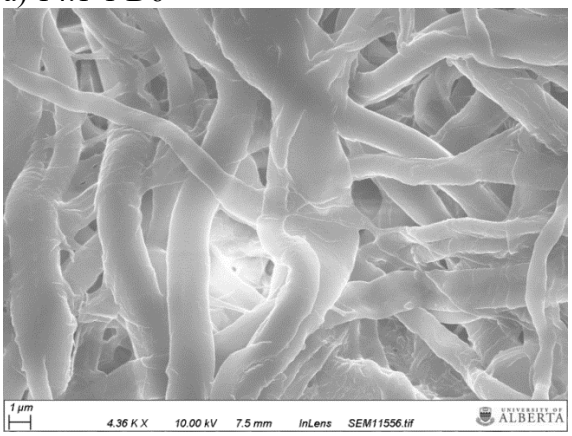

c) 14.1-4 D6

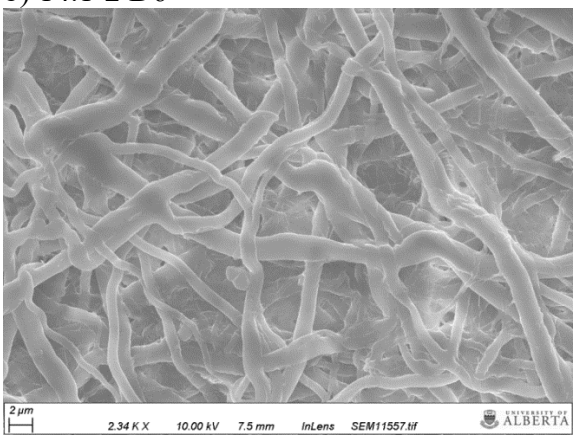

d) 14.1-5 D6

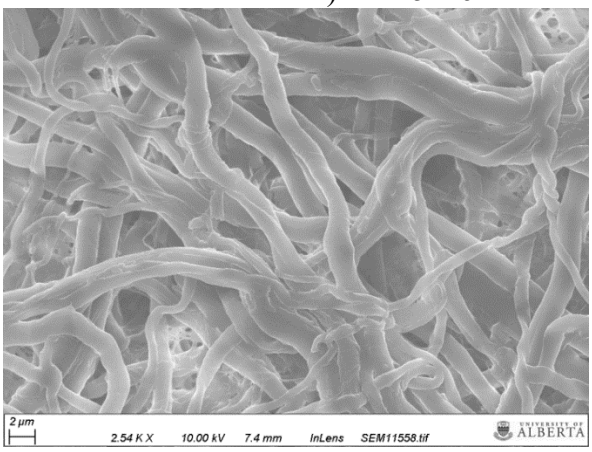

e) 14.1-6 D6

Figure A-44 The SEM micrographs from region 1 of the mat electrospun from the solution at the total polymer concentration of 14% (w/v) after 6 days of degradation (14.1 D6)

Table A-41 Fiber diameter measurements in nm for 6 different locations at region 1 of the mat electrospun from the solution at the total polymer concentration of 14% (w/v) after 6 days of degradation

14.1-1 D6	14.1-2 D6	14.1-4 D6	14.1-5 D6	14.1-6 D6
1133	1064	1152	1317	1830
1210	1529	1000	1983	2105
1309	1342	1901	1757	2039
1448	1013	1523		1947
		2044		

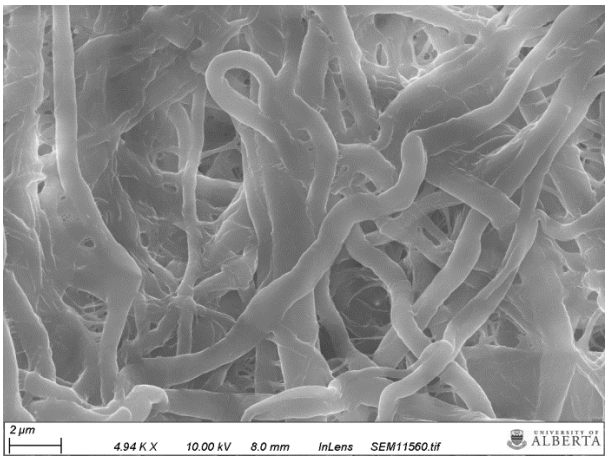

a) 14.2-1 D6

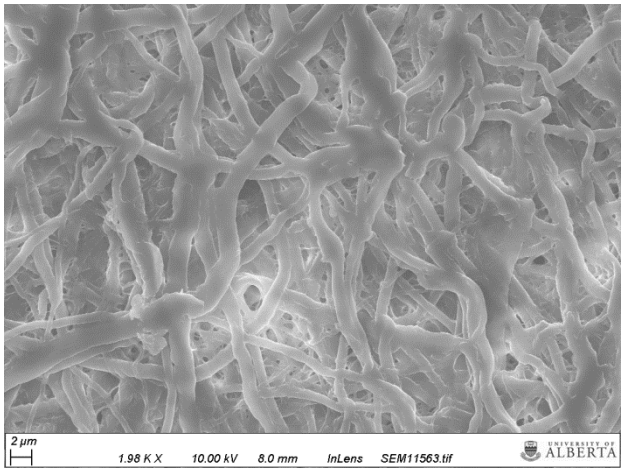

b) 14.2-2 D6

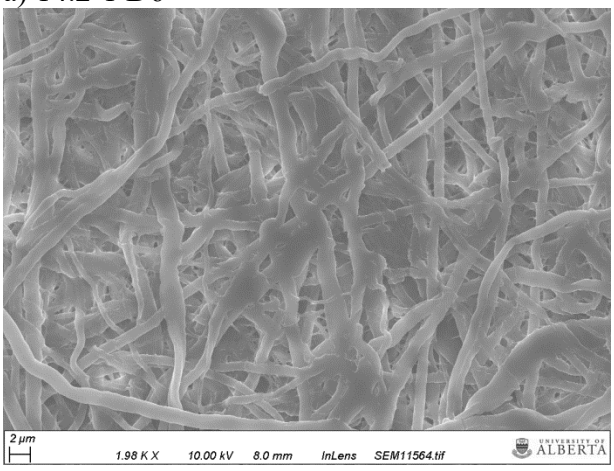

c) 14.2-3 D6

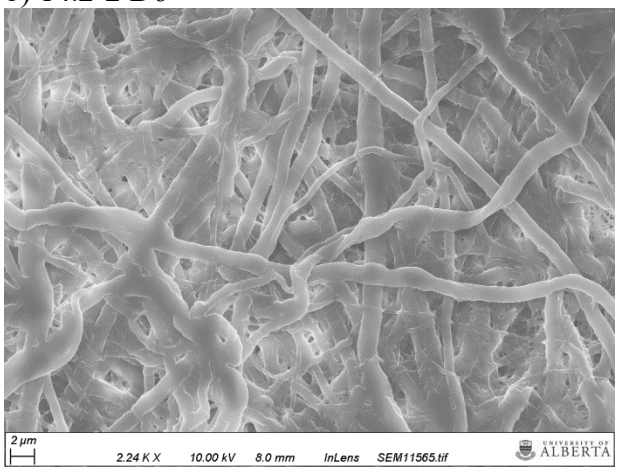

d) 14.2-4 D6

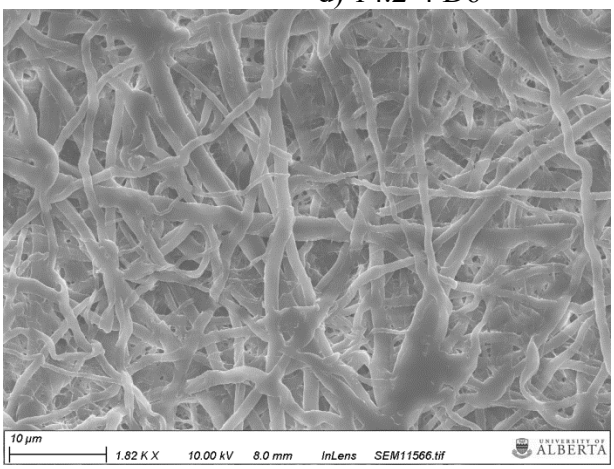

e) 14.2-5 D6

Figure A-45 The SEM micrographs from region 2 of the mat electrospun from the solution at the total polymer concentration of 14% (w/v) after 6 days of degradation (14.2 D6)

Table A-42 Fiber diameter measurements in nm for 5 different locations at region 2 of the mat electrospun from the solution at the total polymer concentration of 14% (w/v) after 6 days of degradation

14.2-1 D6	14.2-2 D6	14.2-3 D6	14.2-4 D6	14.2-5 D6
840	1395	1033	1244	1433
814	1394	1212	1690	1621
	1507	1335	1262	1068
	1087	980	1234	
	1168	1441		
	1697			

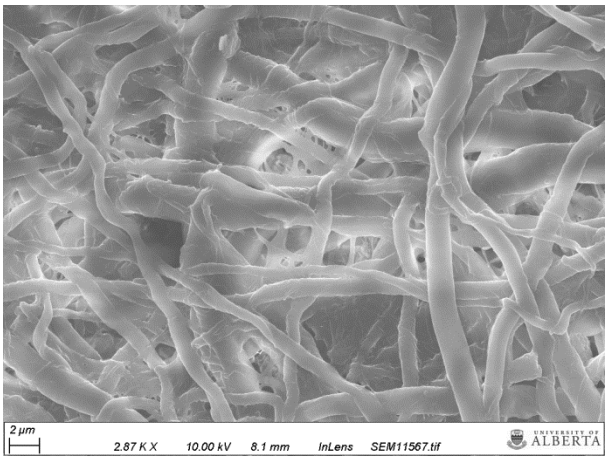

a) 14.3-1 D6

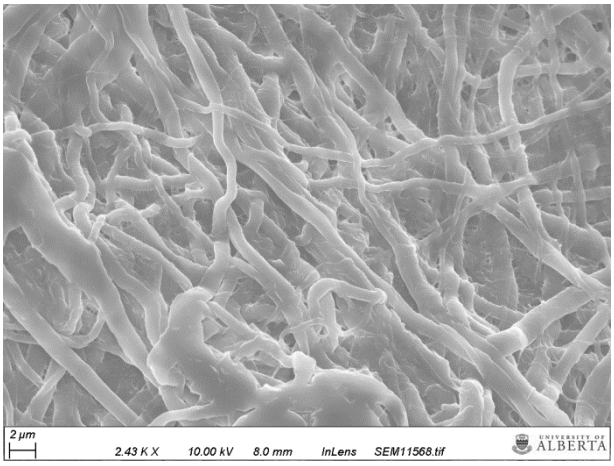

b) 14.3 -2 D6

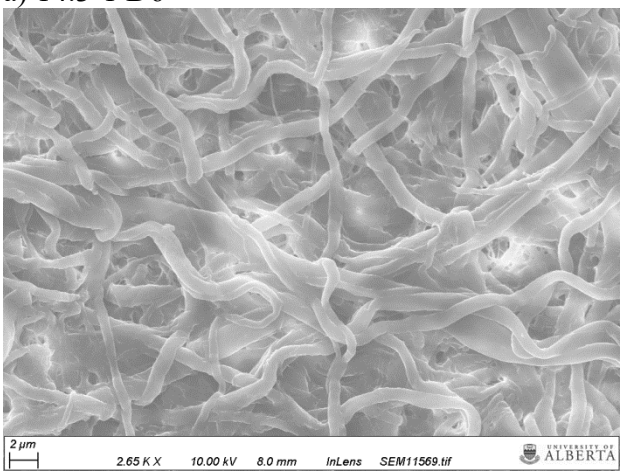

c) 14.3-3 D6

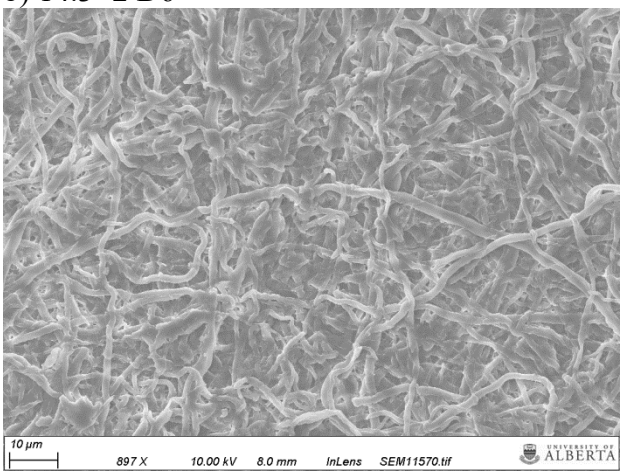

d) 14.3-4 D6

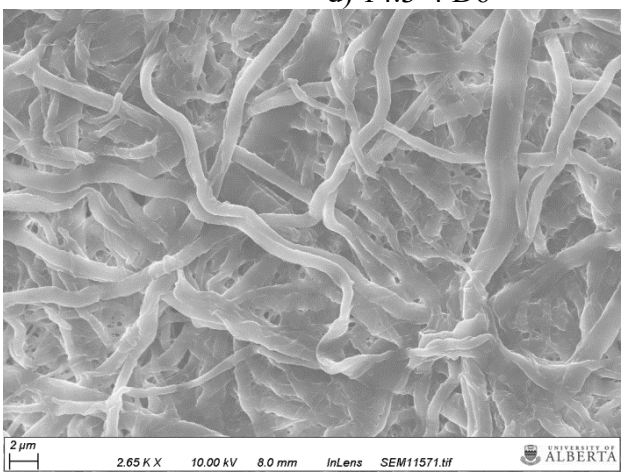

e) 14.3-5 D6

Figure A-46 The SEM micrographs from region 3 of the mat electrospun from the solution at the total polymer concentration of 14% (w/v) after 6 days of degradation (14.3 D6)

Table A-43 Fiber diameter measurements in nm for 5 different locations at region 3 of the mat electrospun from the solution at the total polymer concentration of 14% (w/v) after 6 days of degradation

14.3-1 D6	14.3-2 D6	14.3-3 D6	14.3-4 D6	14.3-5 D6
1728	1200	987	1343	1010
1229	1265	1139	1437	894
1302	1008	950	1210	989
1182	1088	968	1231	1088

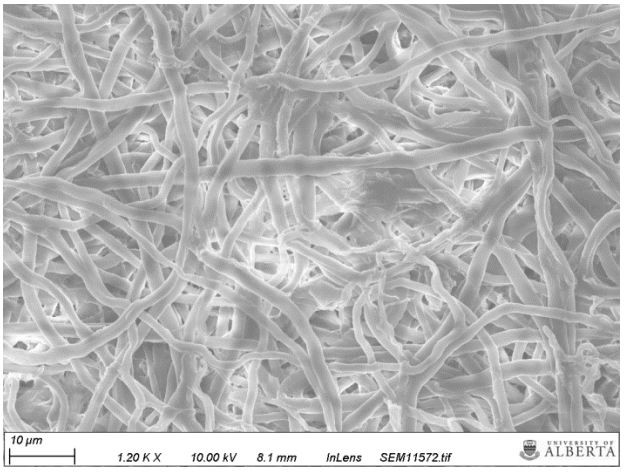

a) 14.4-1 D6

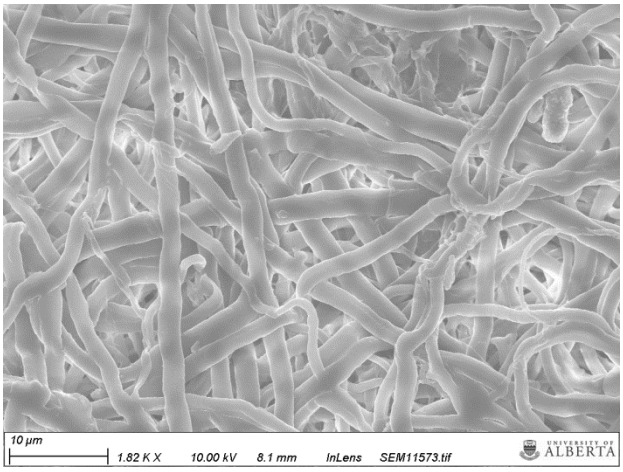

b) 14.4 -2 D6

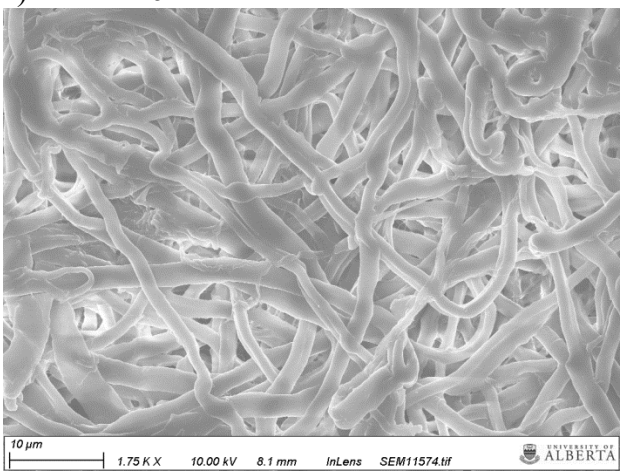

c) 14.4-3 D6

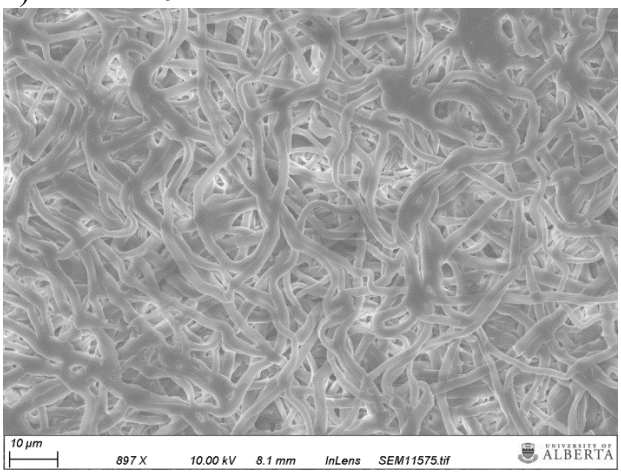

d) 14.4-4 D6

Figure A-47 The SEM micrographs from region 4 of the mat electrospun from the solution at the total polymer concentration of 14% (w/v) after 6 days of degradation (14.4 D6)

Table A-44 Fiber diameter measurements in nm for 4 different locations at region 4 of the mat electrospun from the solution at the total polymer concentration of 14% (w/v) after 6 days of degradation

14.4-1 D6	14.4-2 D6	14.4-3 D6	14.4-4 D6
1990	2558	1380	2911
1717	2246	2327	1943
2336	2132	2154	1847
1674	2085	1812	1950
1525	2606	2580	2806

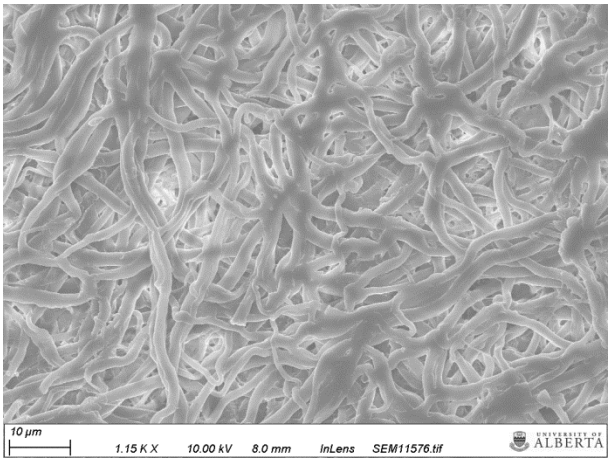

a) 14.5-1 D6

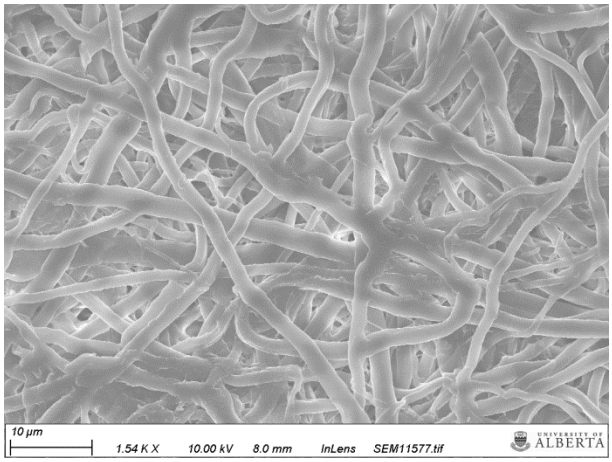

b) 14.5 -2 D6

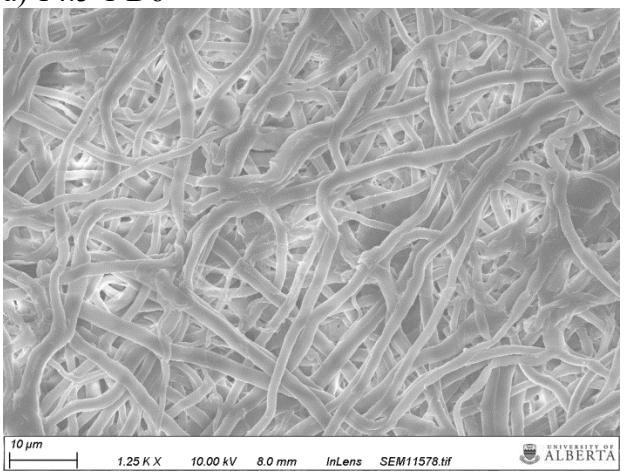

c) 14.5-3 D6

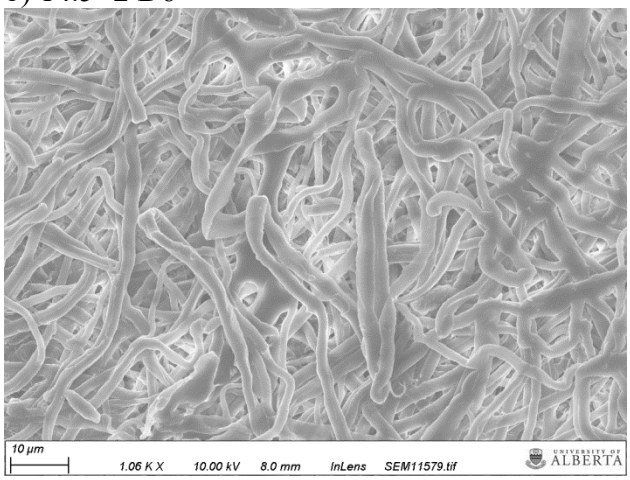

d) 14.5-4 D6

Figure A-48 The SEM micrographs from region 5 of the mat electrospun from the solution at the total polymer concentration of 14% (w/v) after 6 days of degradation (14.5 D6)

Table A-45 Fiber diameter measurements in nm for 4 different locations at region 5 of the mat electrospun from the solution at the total polymer concentration of 14% (w/v) after 6 days of degradation

14.5-1 D6	14.5-2 D6	14.5-3 D6	14.5-4 D6
1629	1980	2451	2308
2271	1580	1914	1867
2153	1967	2069	1900
2111	2202	2204	2253
2012	2502	1501	2245

Appendix A.5 The SEM Micrographs and Fiber Diameter Measurements of the Mats Electrospun out of 6%, 10% and 14% (w/v) Gelatin/PCL (1:1) in TFE after 10 Days of Degradation

Appendix A.5.1 The SEM Micrograph for the Mat Electrospun out of 6% (w/v) Solution after 10 Days of Degradation

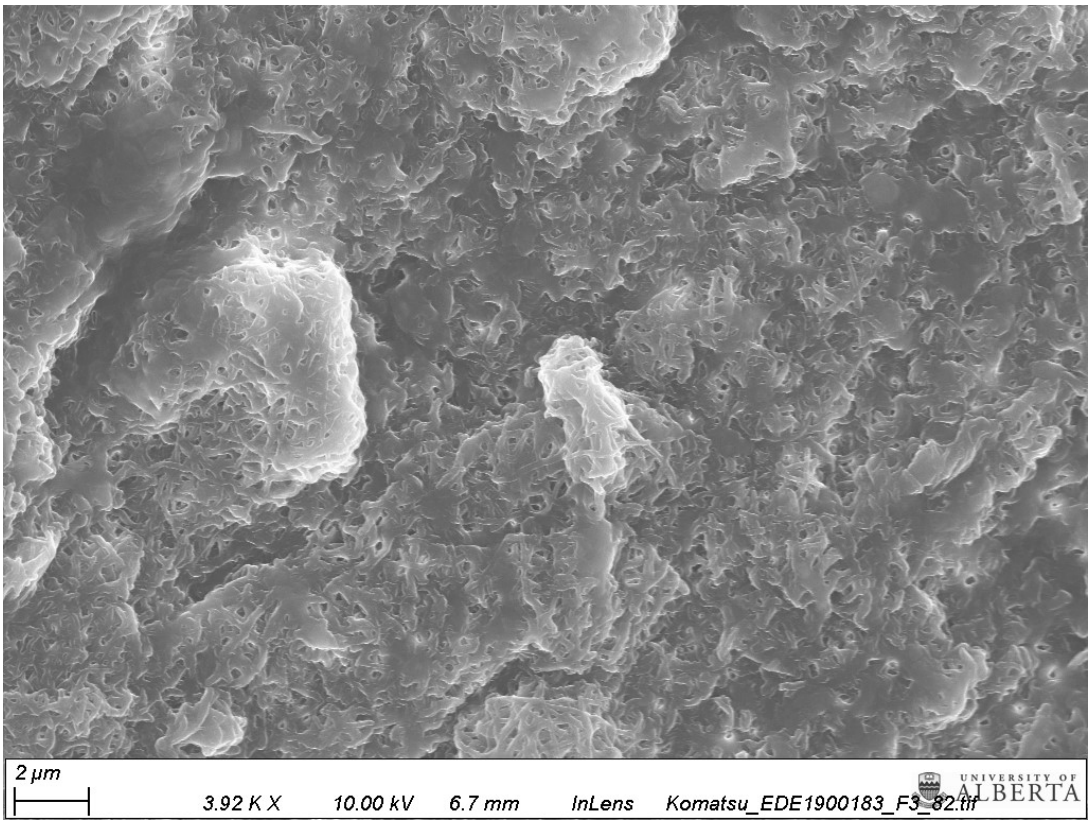

Figure A-49 The SEM Micrograph for the Mat Electrospun from the solution at the total polymer concentration of 6% (w/v) after 10 days of degradation

Appendix A.5.2 The SEM Micrographs and Respective Fiber Diameter Measurement for Five Different Regions of the Mat Electrospun out of 10% (w/v) Solution after 10 Days of Degradation

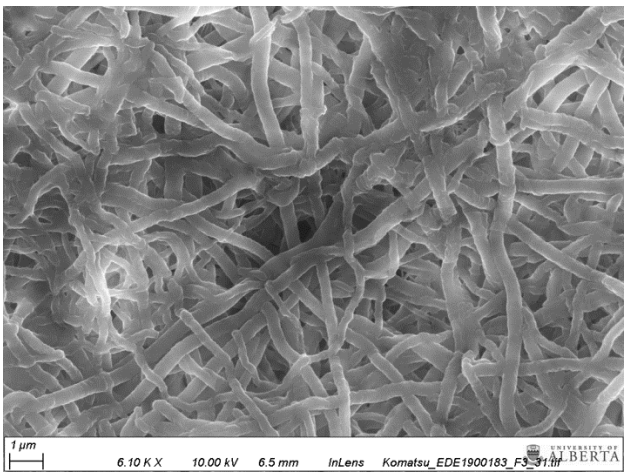

a) 10.1-1 D10

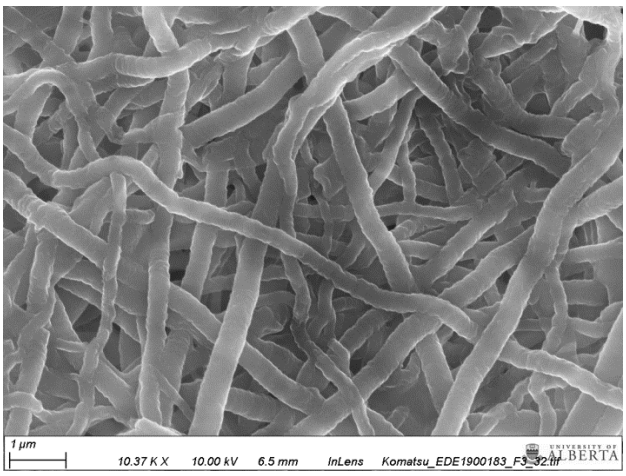

b) 10.1-2 D10

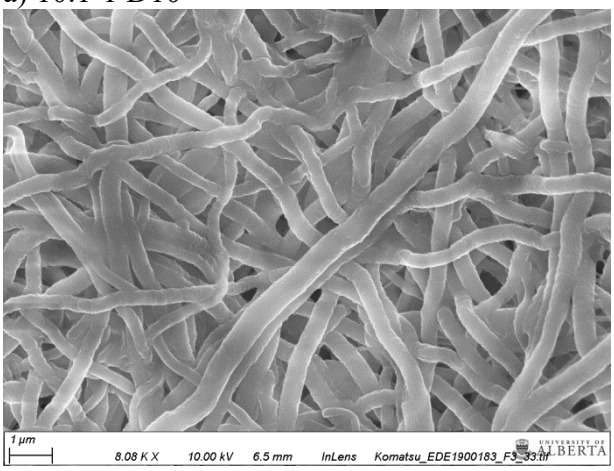

c) 10.1-3 D10

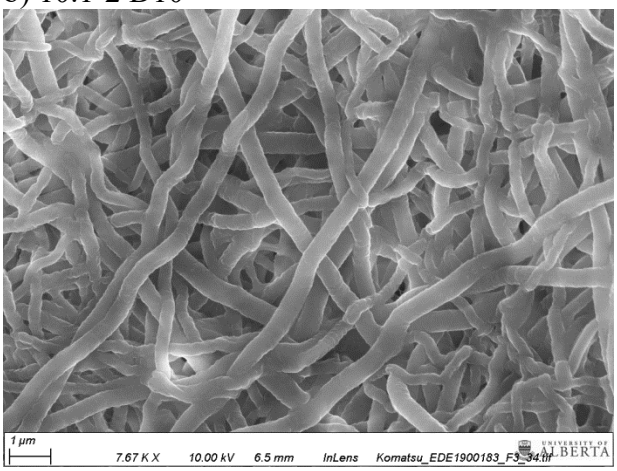

d) 10.1-4 D10

Figure A-50 The SEM micrographs from region 1 of the mat electrospun from the solution at the total polymer concentration of 10% (w/v) after 10 days of degradation (10.1 D10)

Table A-46 Fiber diameter measurements in nm for 4 different locations at region 1 of the mat electrospun from the solution at the total polymer concentration of 10% (w/v) after 10 days of degradation

10.1-1 D10	10.1-2 D10	10.1-3 D10	10.1-4 D10
446	464	427	440
451	450	440	440
352	465	480	482
459	421	445	451
394	429		498
452	398		519

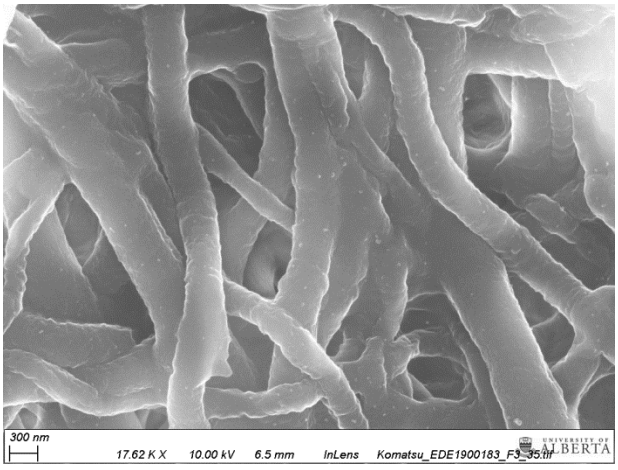

a) 10.2-1 D10

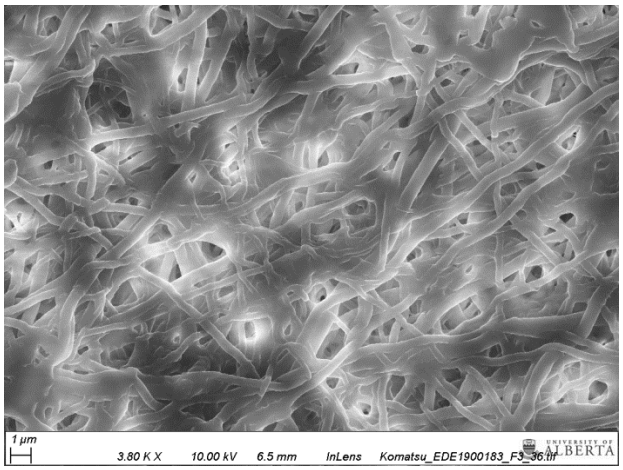

b) 10.2-2 D10

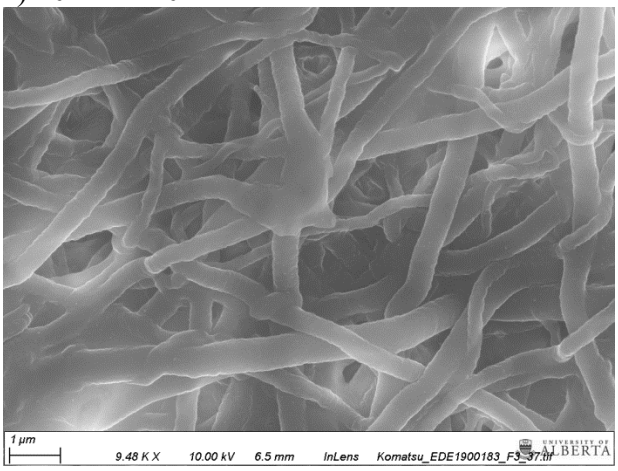

c) 10.2-3 D10

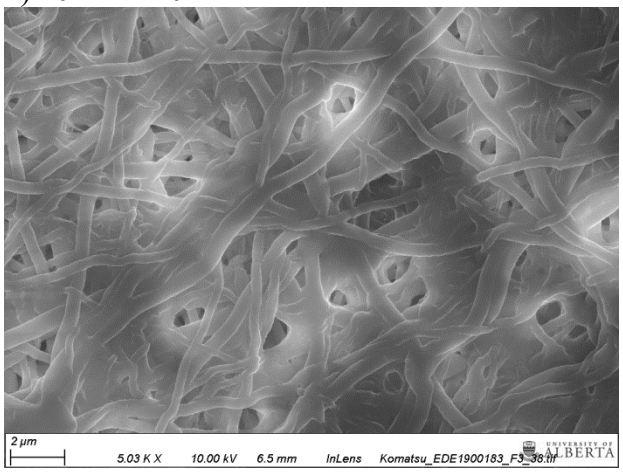

d) 10.2-4 D10

Figure A-51 The SEM micrographs from region 2 of the mat electrospun from the solution at the total polymer concentration of 10% (w/v) after 10 days of degradation (10.2 D10)

Table A-47 Fiber diameter measurements in nm for 4 different locations at region 2 of the mat electrospun from the solution at the total polymer concentration of 10% (w/v) after 10 days of degradation

10.2-1 D10	10.2-2 D10	10.2-3 D10	10.2-4 D10
372	691	506	459
420	485	513	432
	457	505	599
	462	378	504
	473	410	
	537	412	
	509	657	
	546		

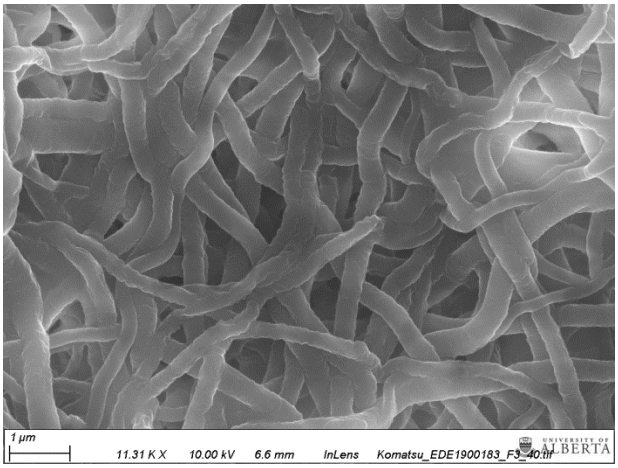

a) 10.3-1 D10

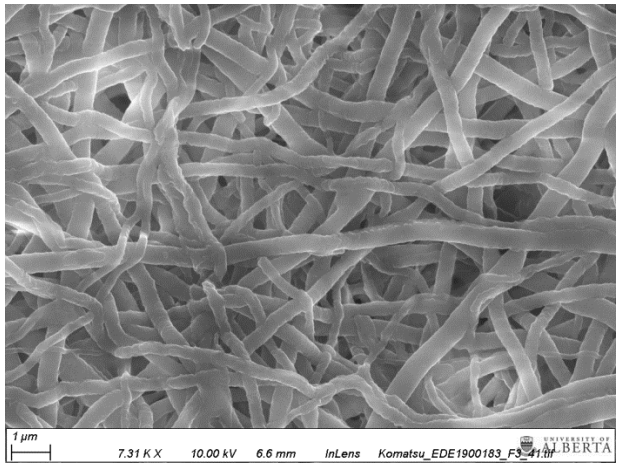

b) 10.3-2 D10

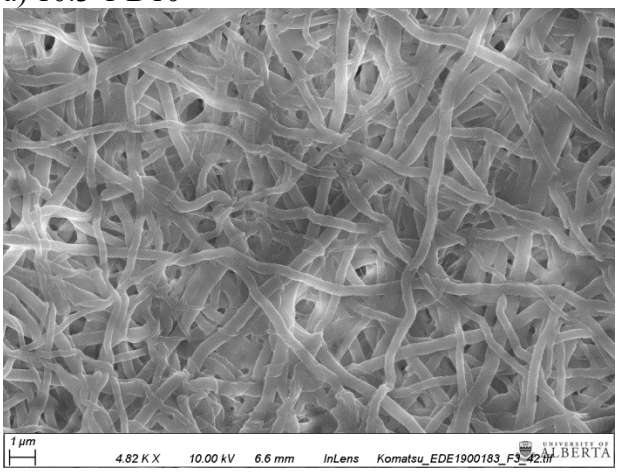

c) 10.3-3 D10

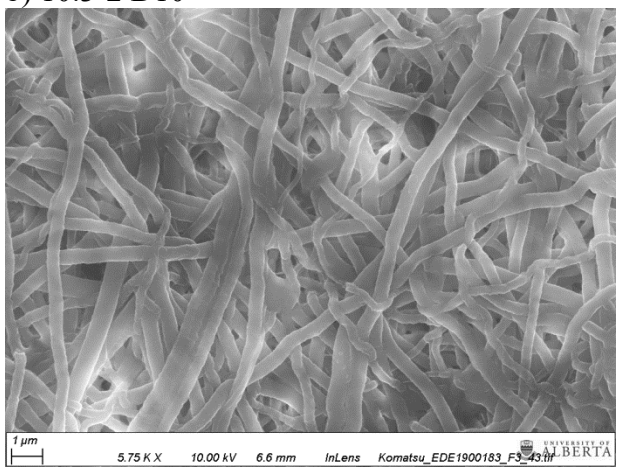

d) 10.3-4 D10

Figure A-52 The SEM micrographs from region 3 of the mat electrospun from the solution at the total polymer concentration of 10% (w/v) after 10 days of degradation (10.3 D10)

Table A-48 Fiber diameter measurements in nm for 4 different locations at region 3 of the mat electrospun from the solution at the total polymer concentration of 10% (w/v) after 10 days of degradation

10.3-1 D10	10.3-2 D10	10.3-3 D10	10.3-4 D10
327	512	468	485
371	515	496	446
414	451	417	382
337	532	460	608
362	456	458	482

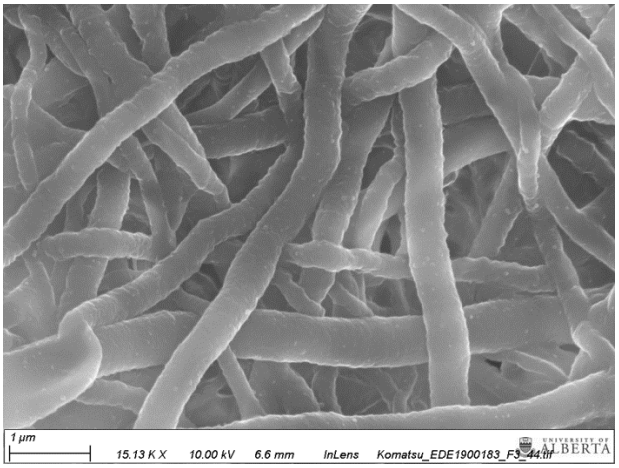

a) 10.4-1 D10

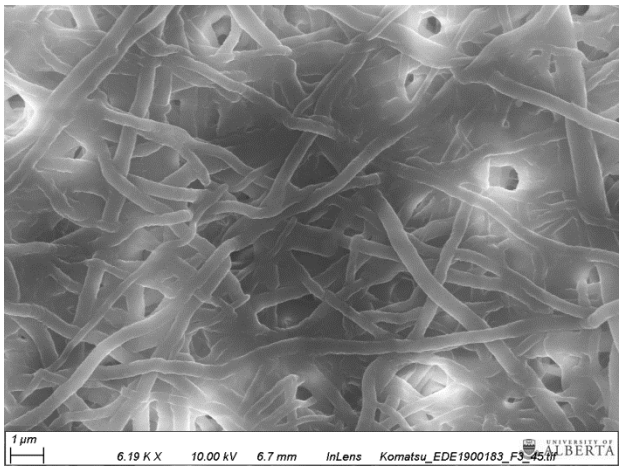

b) 10.4-2 D10

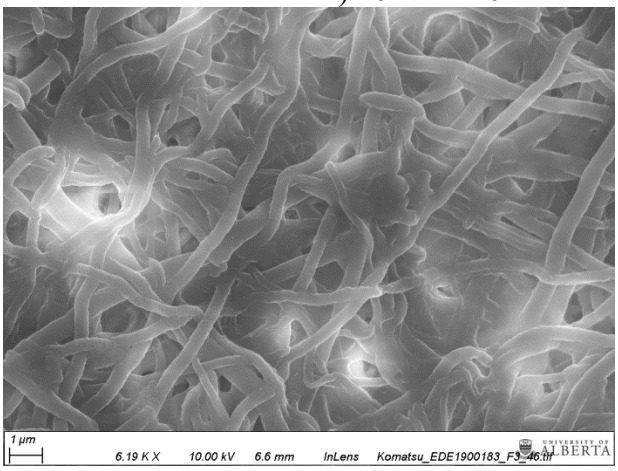

c) 10.4-3 D10

Figure A-53 The SEM micrographs from region 4 of the mat electrospun from the solution at the total polymer concentration of 10% (w/v) after 10 days of degradation (10.4 D10)

Table A-49 Fiber diameter measurements in nm for 3 different locations at region 4 of the mat electrospun from the solution at the total polymer concentration of 10% (w/v) after 10 days of degradation

10.4-1 D10	10.4-2 D10	10.4-3 D10
465	445	473
465	364	429
619	520	447
387	490	474
398	419	411
392	411	450
388	325	
465		
465		
619		
387		

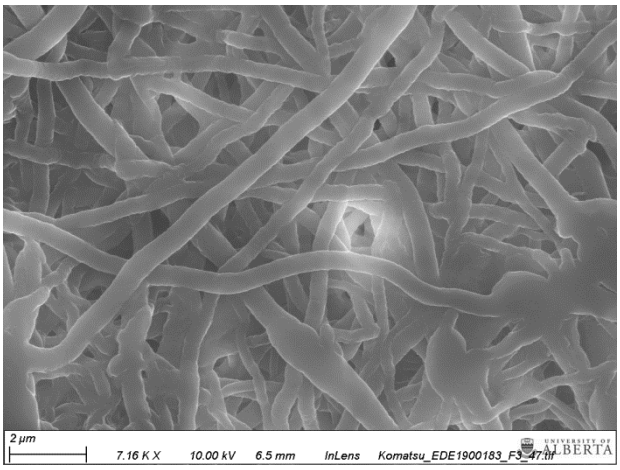

a) 10.5-1 D10

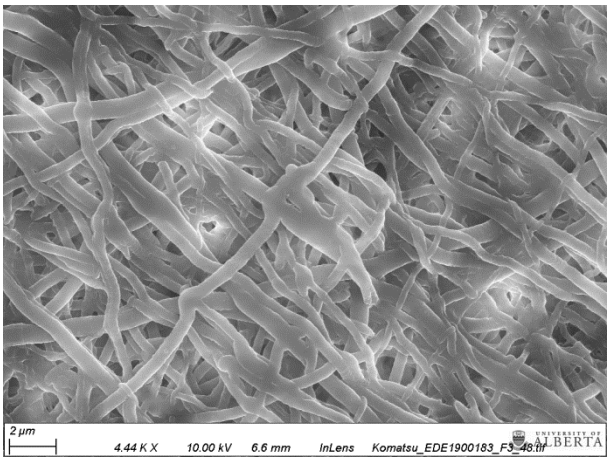

b) 10.5-2 D10

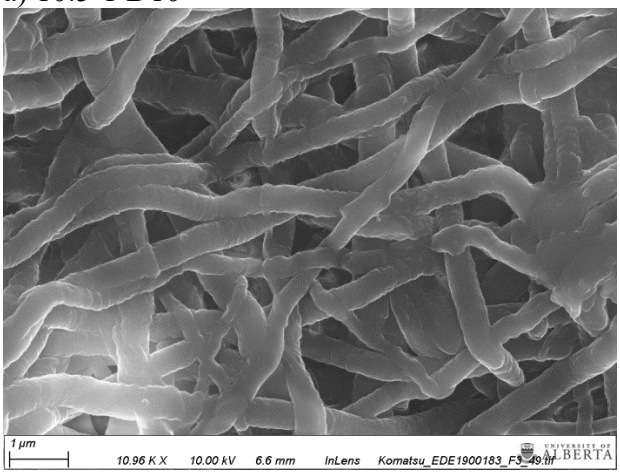

c) 10.5-3 D10

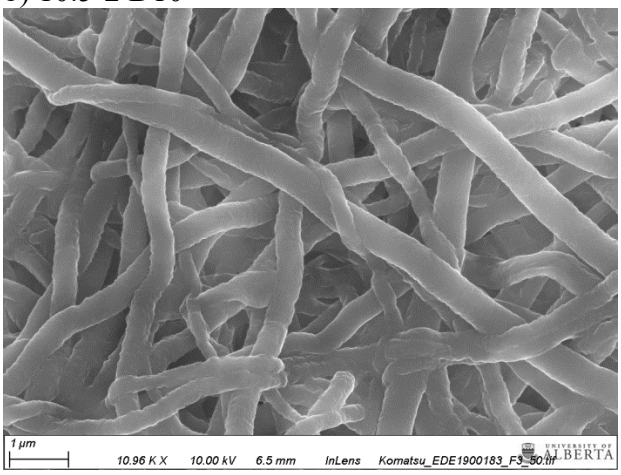

d) 10.5-4 D10

Figure A-54 The SEM micrographs from region 5 of the mat electrospun from the solution at the total polymer concentration of 10% (w/v) after 10 days of degradation (10.5 D10)

Table A-50 Fiber diameter measurements in nm for 4 different locations at region 5 of the mat electrospun from the solution at the total polymer concentration of 10% (w/v) after 10 days of degradation

10.5-1 D10	10.5-2 D10	10.5-3 D10	10.5-4 D10
506	805	485	563
554	569	448	446
631	565	507	575
433	786	501	382
546	518	444	453

Appendix A.5.3 The SEM Micrographs and Respective Fiber Diameter Measurements for Five Different Regions of the Mat Electrospun out of 14% (w/v) Solution after 10 Days of Degradation

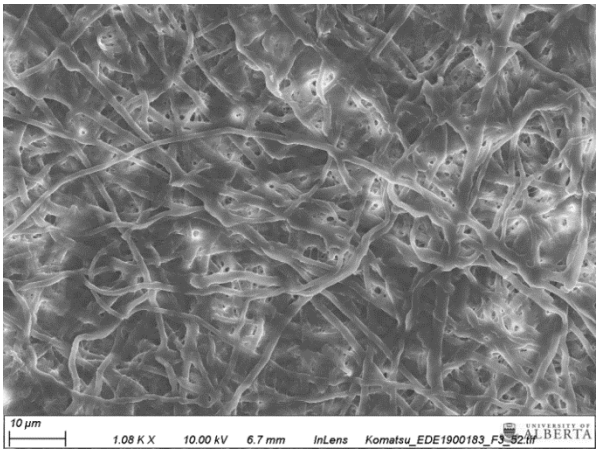

a) 14.1-1 D10

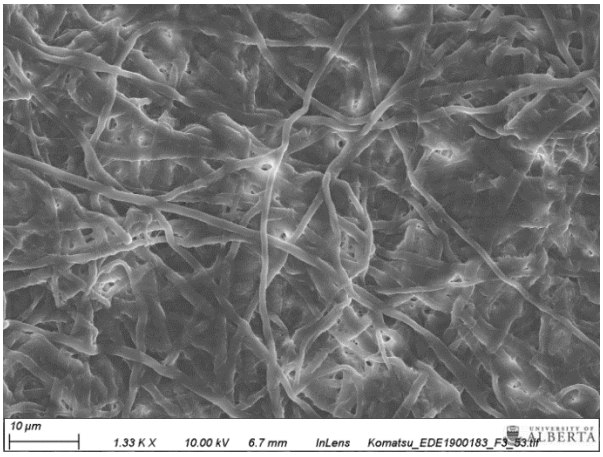

b) 14.1-2 D10

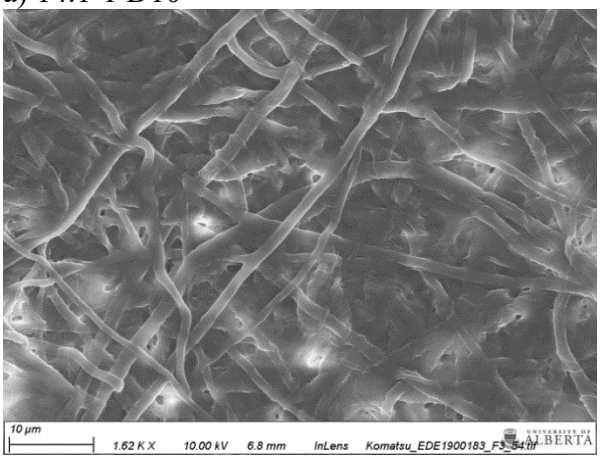

c) 14.1-3 D10

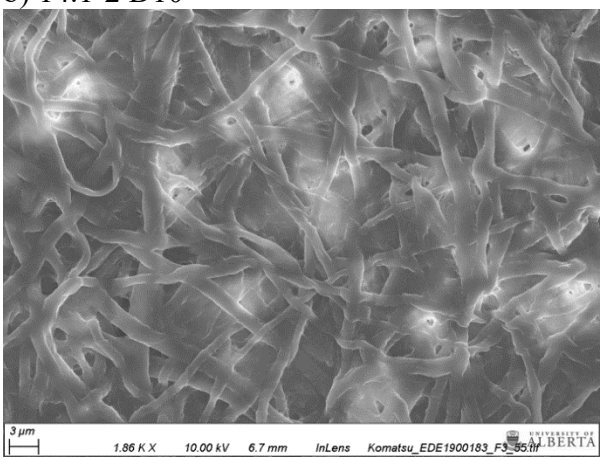

d) 14.1-4 D10

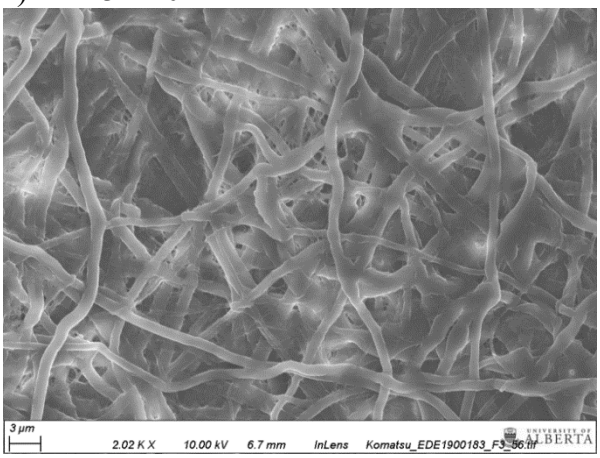

e) 14.1-5 D10

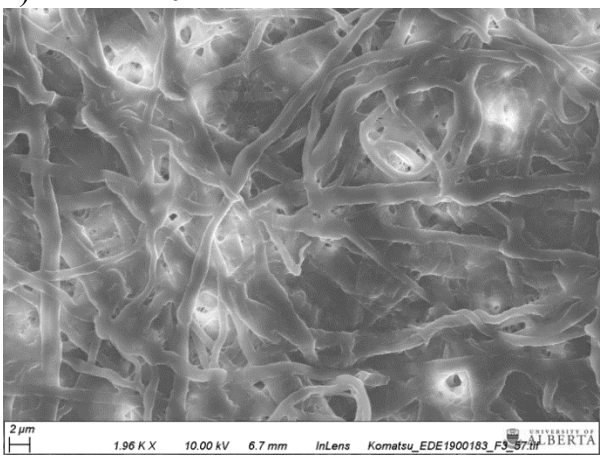

f) 14.1-6 D10

Figure A-55 The SEM micrographs from region 1 of the mat electrospun from the solution at the total polymer concentration of 14% (w/v) after 10 days of degradation (14.1 D10)

Table A-51 Fiber diameter measurements in nm for 6 different locations at region 1 of the mat electrospun from the solution at the total polymer concentration of 14% (w/v) after 10 days of degradation

14.1-1 D10	14.1-2 D10	14.1-3 D10	14.1-4 D10	14.1-5 D10	14.1-6 D10
747	1005	695	1624	937	1924
906	907	1217	1550	1045	1110
869	893	1148	1884	941	
1204	779	1404			

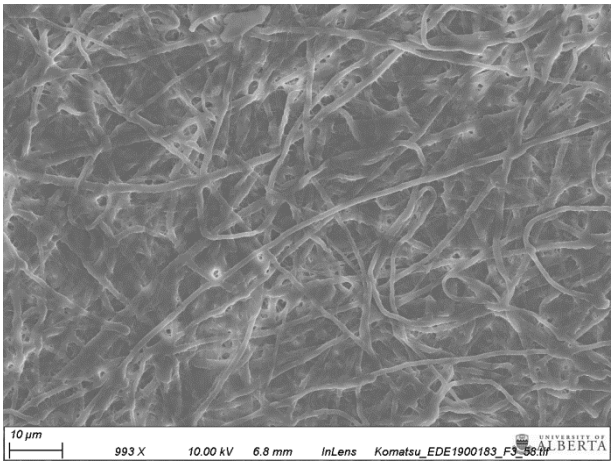

a) 14.2-1 D10

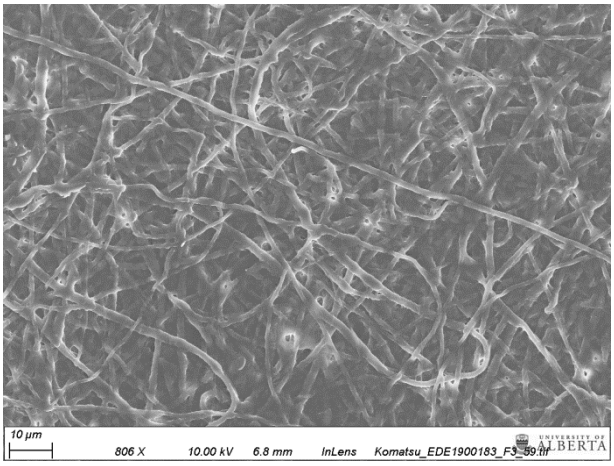

b) 14.2-2 D10

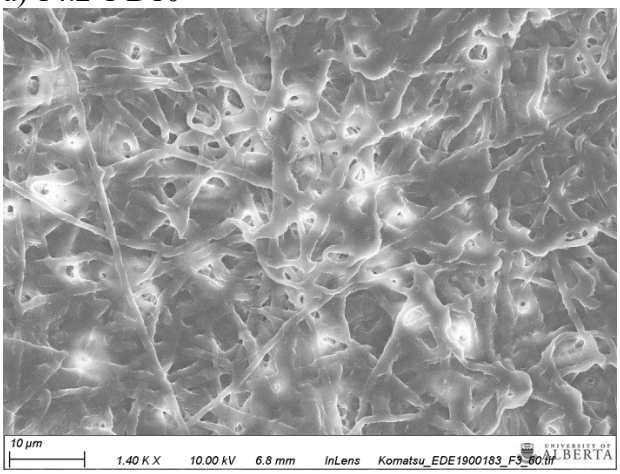

c) 14.2-3 D10

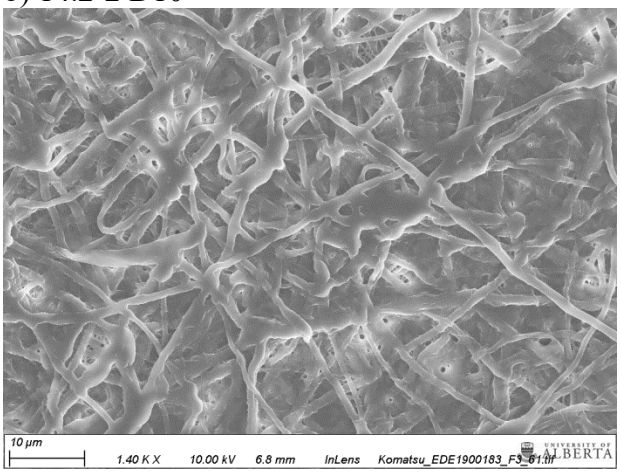

d) 14.2-4 D10

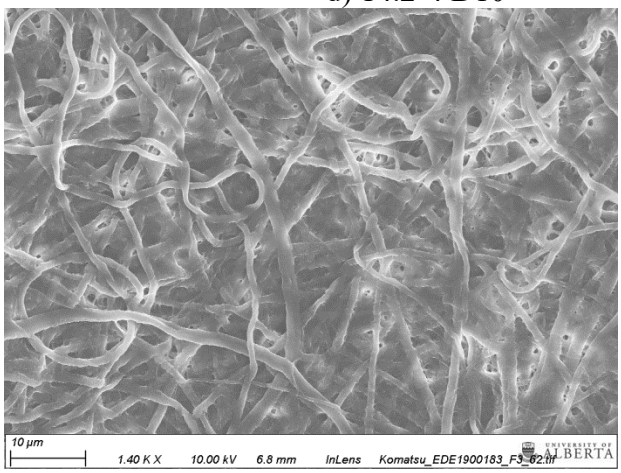

e) 14.2-5 D10

Figure A-56 The SEM micrographs from region 2 of the mat electrospun from the solution at the total polymer concentration of 14% (w/v) after 10 days of degradation (14.2 D10)

Table A-52 Fiber diameter measurements in nm for 5 different locations at region 2 of the mat electrospun from the solution at the total polymer concentration of 14% (w/v) after 10 days of degradation

14.2-1 D10	14.2-2 D10	14.2-3 D10	14.2-4 D10	14.2-5 D10
979	2038	852	930	708
868	1274	721	1412	676
731	1116	789	772	886
1415	1218	942	709	1228

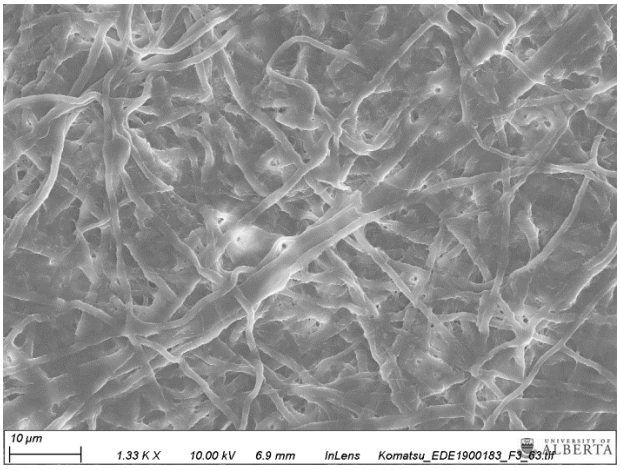

a) 14.3-1 D10

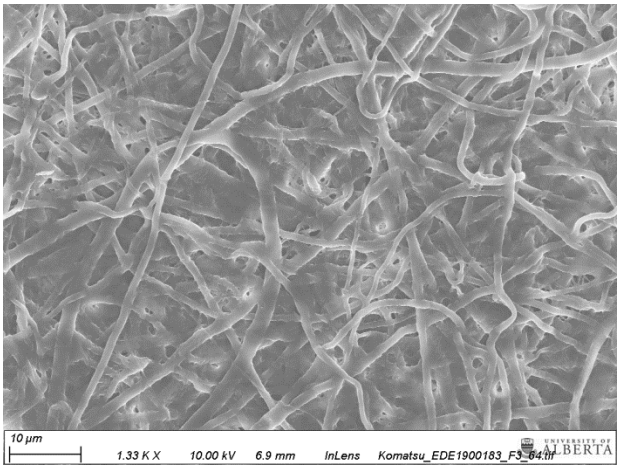

b) 14.3-2 D10

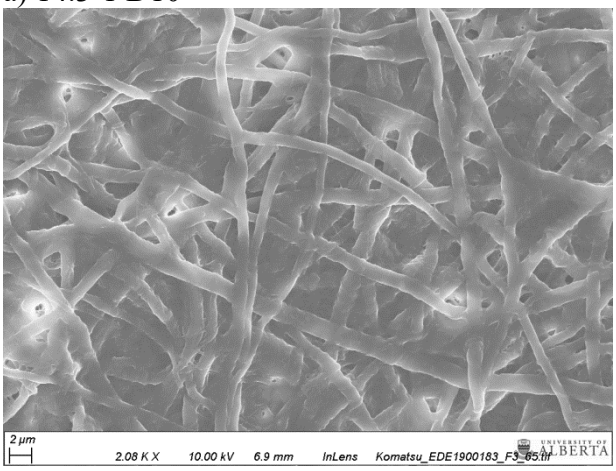

c) 14.3-3 D10

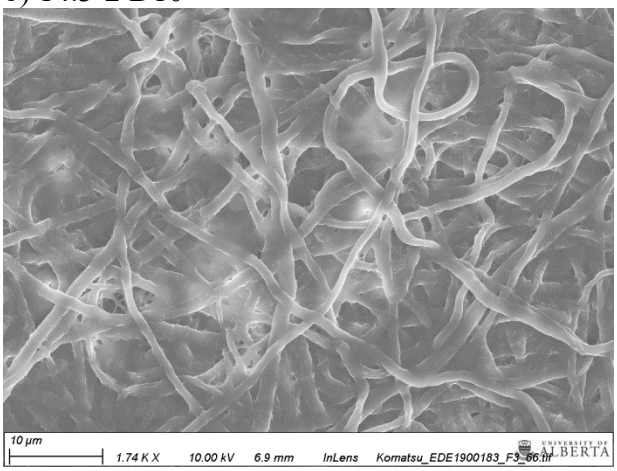

d) 14.3-4 D10

Figure A-57 The SEM micrographs from region 3 of the mat electrospun from the solution at the total polymer concentration of 14% (w/v) after 10 days of degradation (14.3 D10)

Table A-53 Fiber diameter measurements in nm for 4 different locations at region 3 of the mat electrospun from the solution at the total polymer concentration of 14% (w/v) after 10 days of degradation

14.3-1 D10	14.3-2 D10	14.3-3 D10	14.3-4 D10
970	1017	1757	1049
964	1145	896	1525
778	940	765	952
727	1705	906	1471
915	1105	1289	1256

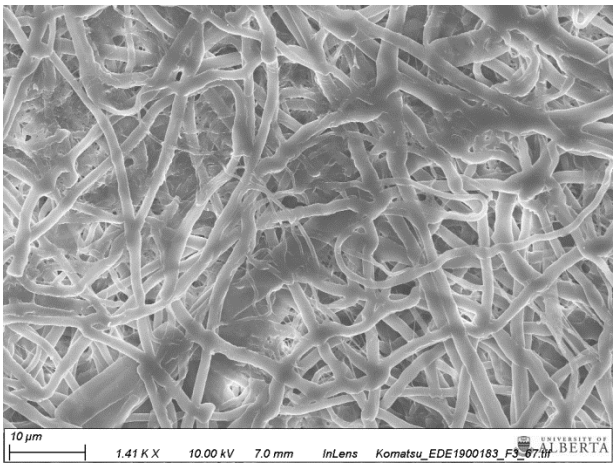

a) 14.4-1 D10

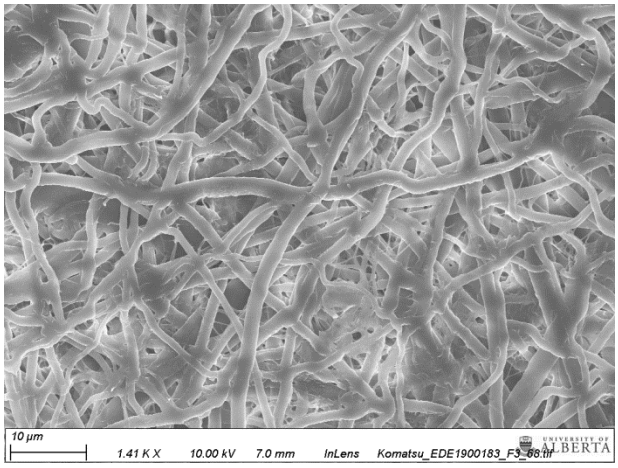

b) 14.4-2 D10

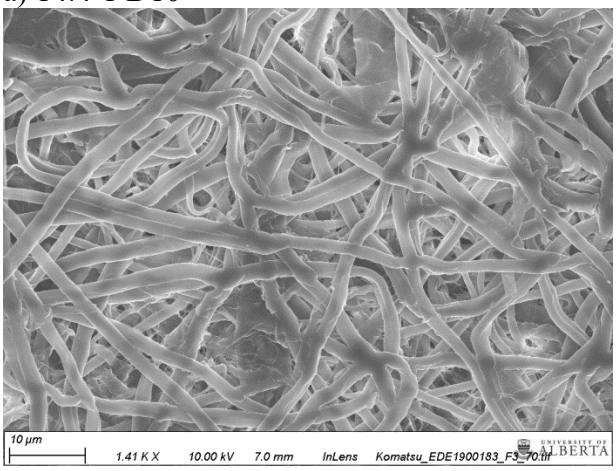

c) 14.4-3 D10

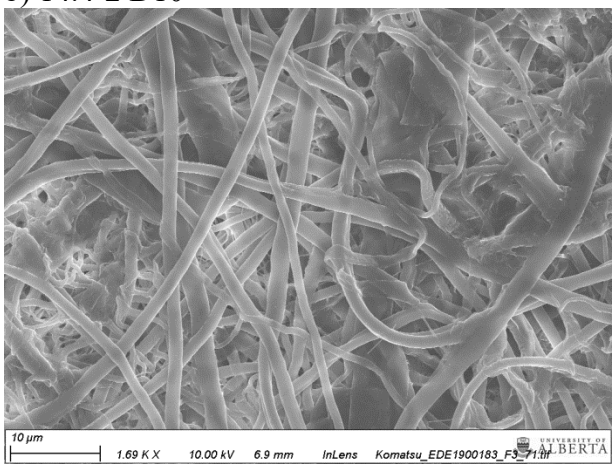

d) 14.4-4 D10

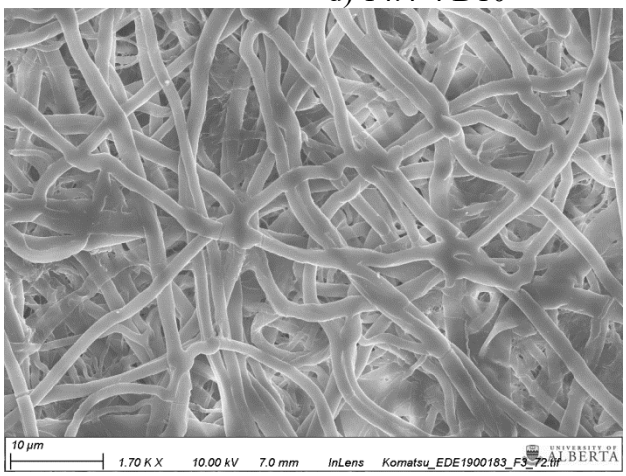

e) 14.4-5 D10

Figure A-58 The SEM micrographs from region 4 of the mat electrospun from the solution at the total polymer concentration of 14% (w/v) after 10 days of degradation (14.4 D10)

Table A-54 Fiber diameter measurements in nm for 5 different locations at region 4 of the mat electrospun from the solution at the total polymer concentration of 14% (w/v) after 10 days of degradation

14.4-1 D10	14.4-2 D10	14.4-3 D10	14.4-4 D10	14.4-5 D10
1268	1578	1767	1388	1220
1205	1188	2267	1482	1608
1929	1513	2126	1517	1364
1475	1997	2297	2241	1388

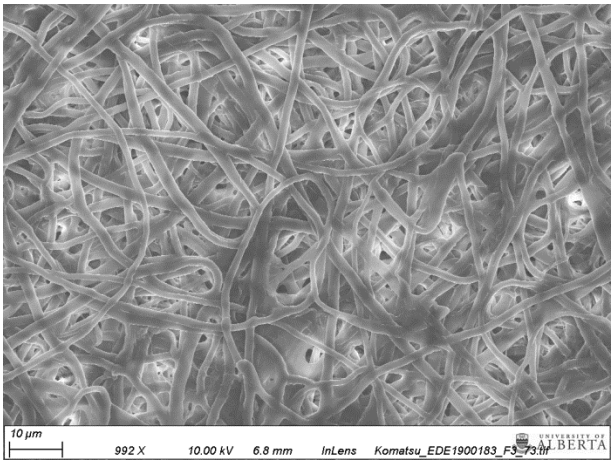

a) 14.5-1 D10

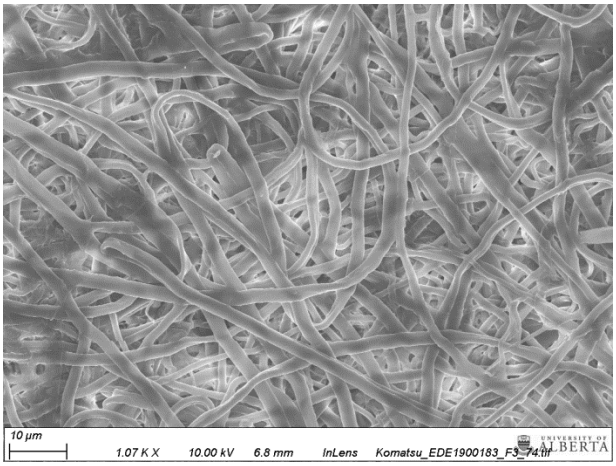

b) 14.5-2 D10

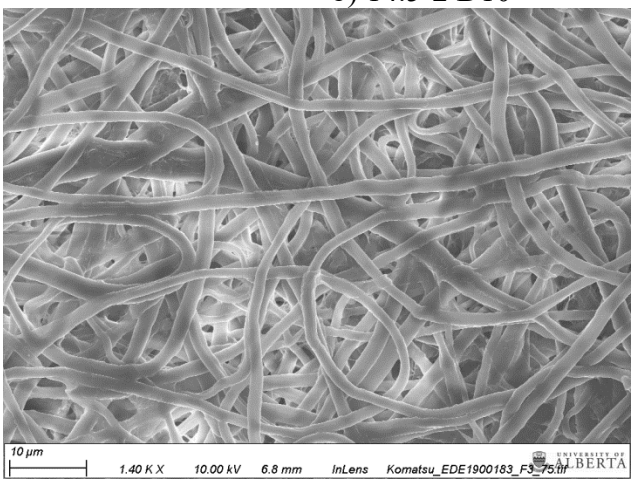

c) 14.5-3 D10

Figure A-59 The SEM micrographs from region 5 of the mat electrospun from the solution at the total polymer concentration of 14% (w/v) after 10 days of degradation (14.5 D10)

Table A-55 Fiber diameter measurements in nm for 3 different locations at region 5 of the mat electrospun from the solution at the total polymer concentration of 14% (w/v) after 10 days of degradation

14.5-1 D10	14.5-2 D10	14.5-3 D10
1972	2641	1984
2131	2146	2271
1999	2640	2490
2301	2533	1867
2198	2579	1448
1428	2634	1935
	2080	2095

Appendix B Gravimetric Analysis

Appendix B.1 Gravimetric Analysis of the Samples Electrospun from the Solution at the Total Polymer Concentration of 6% (w/v) before Degradation and after 1, 3, 6 and 10 Days of Degradation

Table B-1 The weight of the samples electrospun from the solution at the total polymer concentration of 6% (w/v) before and after 1 day of degradation

Sample	Weight before degradation (mg)	Weight after 1 day of degradation (mg)
6.1	9.1	7.3
6.2	10.3	7.8
6.3	8.2	6.6
6.4	9.8	7.9
6.5	11.2	8.6

Table B-2 The weight of the samples electrospun from the solution at the total polymer concentration of 6% (w/v) before and after 3 days of degradation

Sample	Weight before degradation (mg)	Weight after 3 days of degradation (mg)
6.1	11.8	7.4
6.2	11.5	7.6
6.3	9.1	5.3
6.4	8.1	5
6.5	8.2	5.1

Table B-3 The weight of the samples electrospun from the solution at the total polymer concentration of 6% (w/v) before and after 6 days of degradation

Sample	Weight before degradation (mg)	Weight after 6 days of degradation (mg)
6.1	10.3	5.1
6.2	10.5	5.4
6.3	10.6	5.6
6.4	11	6.6
6.5	8.1	4.7

Table B-4 The weight of the samples electrospun from the solution at the total polymer concentration of 6% (w/v) before and after 10 days of degradation

Sample	Weight before degradation (mg)	Weight after 10 days of degradation (mg)
6.1	9.9	4.4
6.2	8.9	3.9
6.3	7.2	3.9
6.4	6.8	3.8
6.5	8.3	5

Appendix B.2 Gravimetric Analysis of the Samples Electrospun from the Solution at the Total Polymer Concentration of 10% (w/v) before Degradation and after 1, 3, 6 and 10 Days of Degradation

Table B-5 The weight of the samples electrospun from the solution at the total polymer concentration of 10% (w/v) before and after 1 day of degradation

Sample	Weight before degradation (mg)	Weight after 1 day of degradation (mg)
10.1	11.6	9.3
10.2	13.5	10.1
10.3	16.9	12.9
10.4	11.8	9
10.5	14.4	10.6

Table B-6 The weight of the samples electrospun from the solution at the total polymer concentration of 10% (w/v) before and after 3 days of degradation

Sample	Weight before degradation (mg)	Weight after 3 days of degradation (mg)
10.1	14	8.5
10.2	12.8	7.9
10.3	16.4	9.8
10.4	14.1	8.5
10.5	17.8	10.7

Table B-7 The weight of the samples electrospun from the solution at the total polymer concentration of 10% (w/v) before and after 6 days of degradation

Sample	Weight before degradation (mg)	Weight after 6 days of degradation (mg)
10.1	18.2	9.2
10.2	11.3	5.8
10.3	17.5	9.7
10.4	15.8	9
10.5	16.4	9.4

Table B-8 The weight of the samples electrospun from the solution at the total polymer concentration of 10% (w/v) before and after 10 days of degradation

Sample	Weight before degradation (mg)	Weight after 10 days of degradation (mg)
10.1	10.9	5.8
10.2	11.8	6.6
10.3	10.3	5.5
10.4	13.2	7.3
10.5	13.1	7.2

Appendix B.3 Gravimetric Analysis for the Samples Electrospun from the Solution at the Total Polymer Concentration of 14% (w/v) before Degradation and after 1, 3, 6 and 10 Days of Degradation

Table B-9 The weight of the samples electrospun from the solution at the total polymer concentration of 14% (w/v) solution before and after 1 day of degradation

Sample	Weight before degradation (mg)	Weight after 1 day of degradation (mg)
14.1	12.3	8.6
14.2	15.3	11.8
14.3	17.2	12.9
14.4	17.5	12.7
14.5	16	11.6

Table B-10 The weight of the samples electrospun from the solution at the total polymer concentration of 14% (w/v) solution before and after 3 days of degradation

Sample	Weight before degradation (mg)	Weight after 3 days of degradation (mg)
14.1	12.5	7.6
14.2	12	7.5
14.3	22	13.2
14.4	18.2	11.7
14.5	15.1	10

Table B-11 The weight of the samples electrospun from the solution at the total polymer concentration of 14% (w/v) solution before and after 6 days of degradation

Sample	Weight before degradation (mg)	Weight after 6 days of degradation (mg)
14.1	17.7	10.3
14.2	22.6	12.4
14.3	11.3	6.2
14.4	23.8	13
14.5	18.6	10.8

Table B-12 The weight of the samples electrospun from the solution at the total polymer concentration of 14% (w/v) solution before and after 10 days of degradation

Sample	Weight before degradation (mg)	Weight after 10 days of degradation (mg)
14.1	16	8.7
14.2	14.5	7.9
14.3	13.8	7.6
14.4	12.7	7
14.5	16.2	8.8

Appendix C Tensile Test

Appendix C.1 Stress-Strain Curves for the Samples Electrospun from the Solution at the Total Polymer Concentration of 6% (w/v) before Degradation and after 1, 3, 6 and 10 Days of Degradation

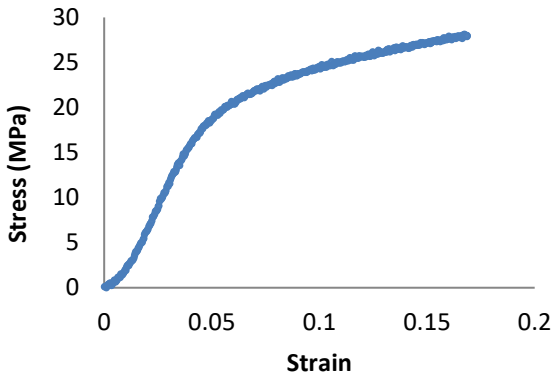

a) 6.1 D0

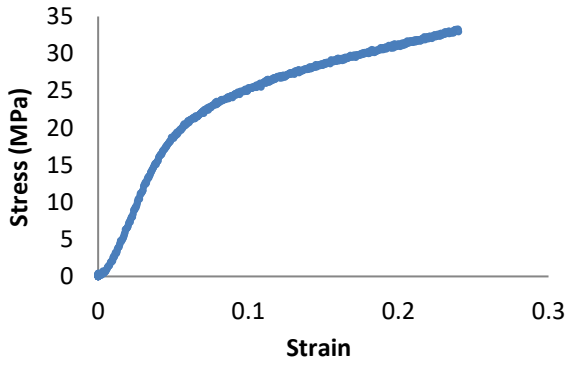

b) 6.2 D0

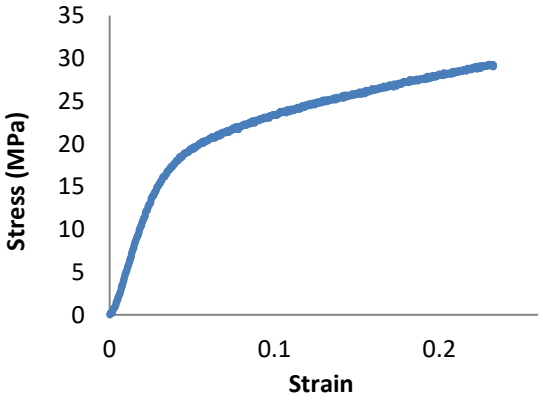

c) 6.3 D0

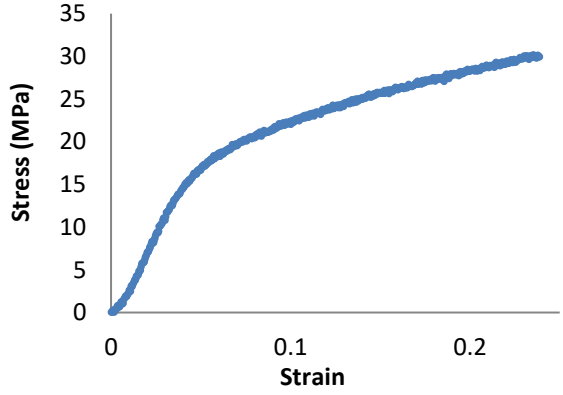

d) 6.4 D0

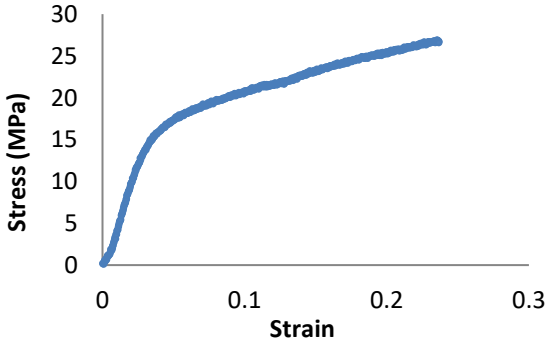

e) 6.5 D0

Figure C-1 Stress-strain curves for the samples electrospun from the solution at the total polymer concentration of 6% (w/v) before degradation

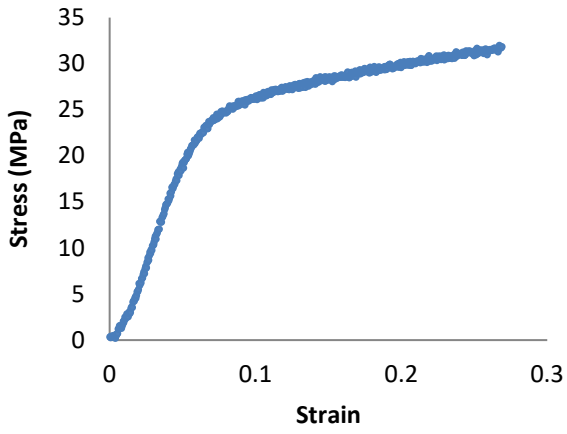

a) 6.1 D1

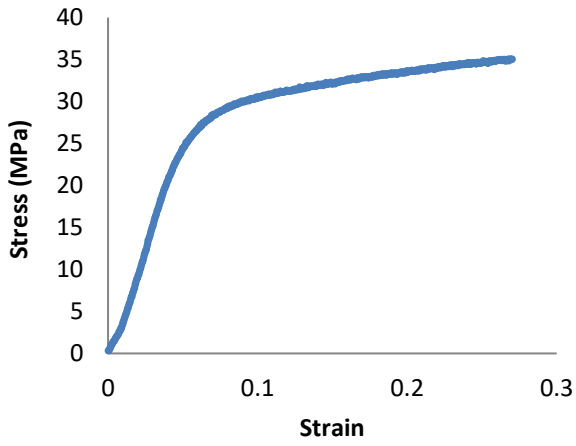

b) 6.2 D1

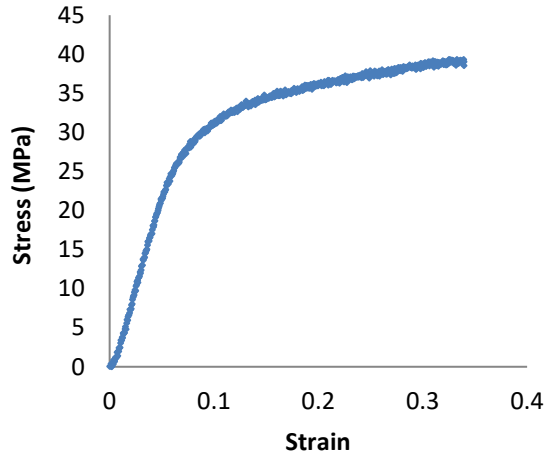

c) 6.3 D1

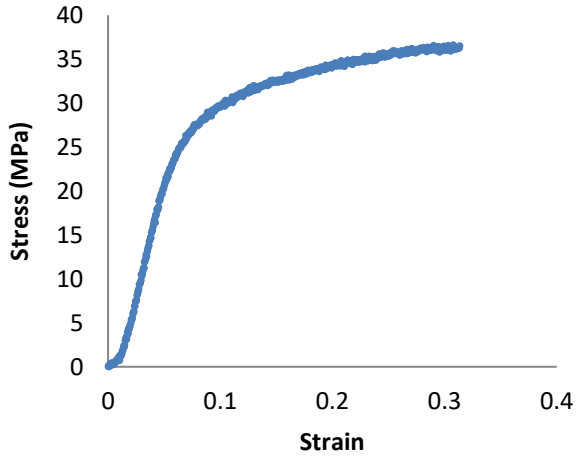

d) 6.4 D1

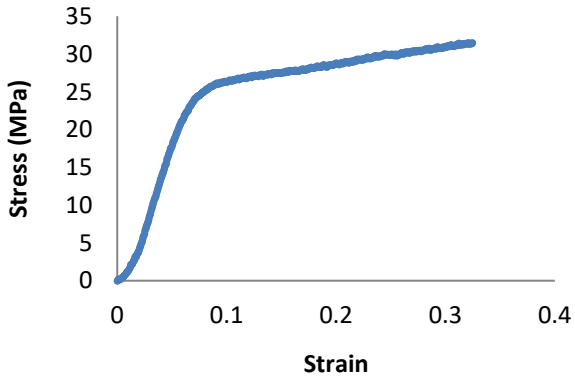

e) 6.5 D1

Figure C-2 Stress-strain curves for the samples electrospun from the solution at the total polymer concentration of 6% (w/v) after 1 day of degradation

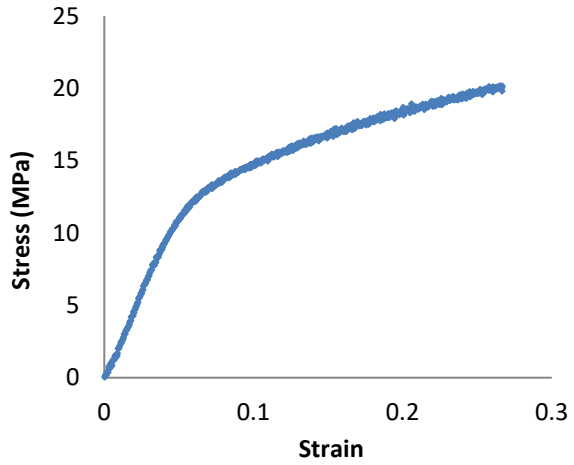

a) 6.1 D3

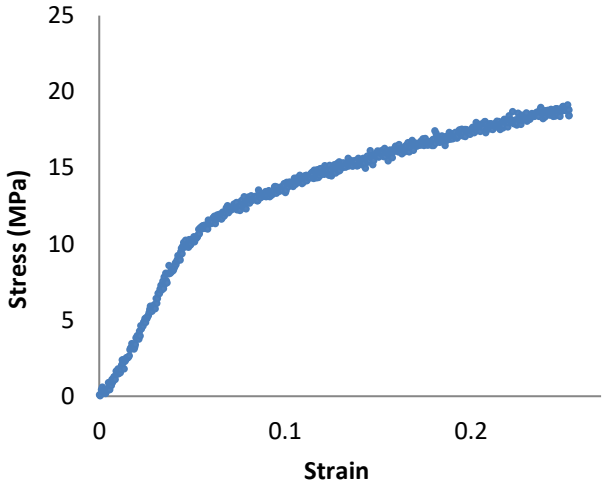

b) 6.2 D3

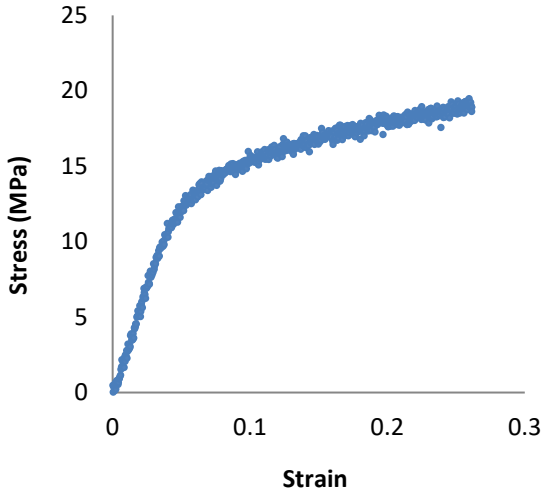

c) 6.3 D3

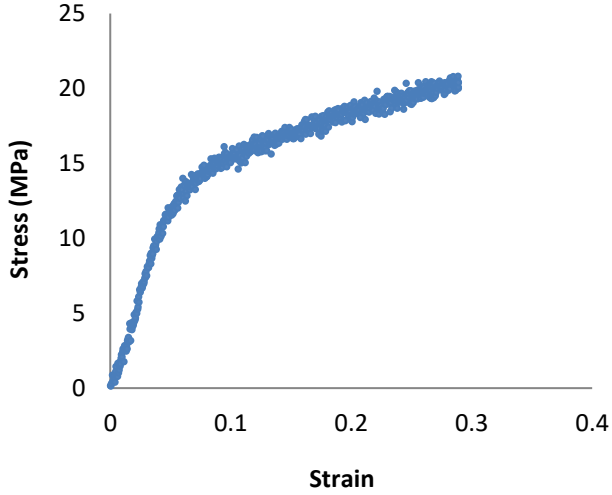

d) 6.4 D3

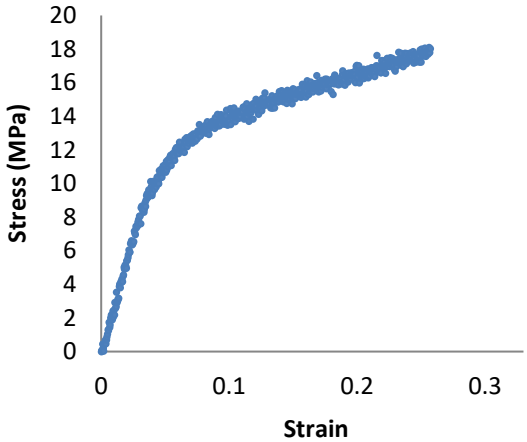

e) 6.5 D3

Figure C-3 Stress-strain curves for the samples electrospun from the solution at the total polymer concentration of 6% (w/v) after 3 days of degradation

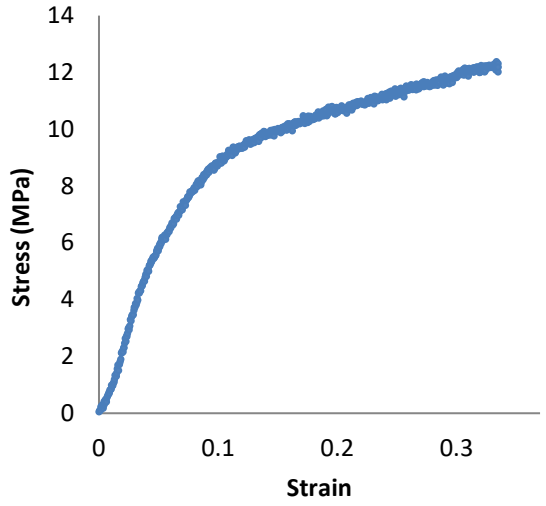

a) 6.1 D6

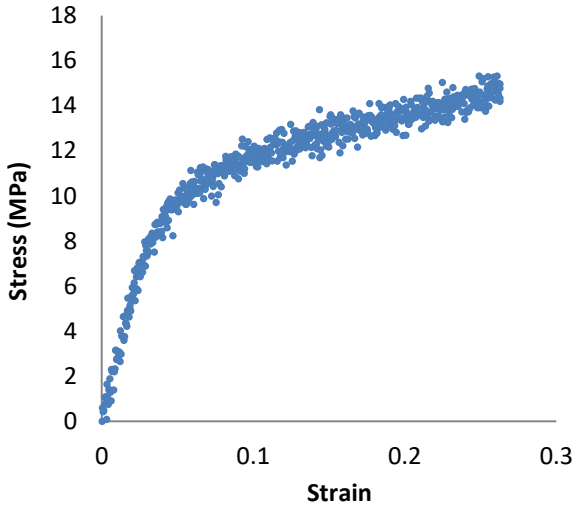

b) 6.2 D6

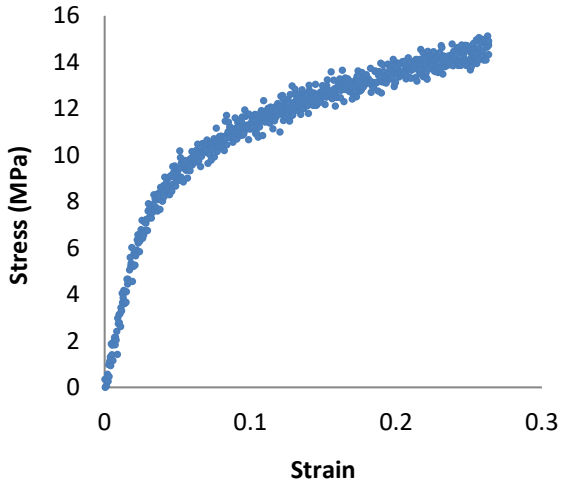

c) 6.3 D6

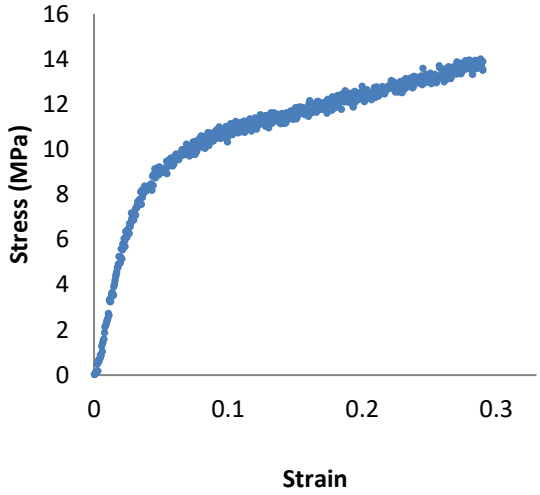

d) 6.4 D6

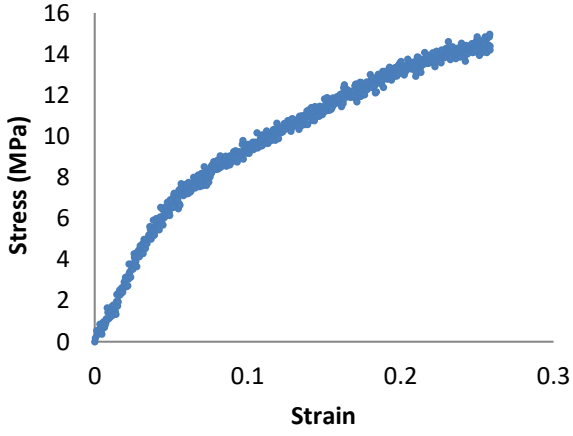

e) 6.5 D6

Figure C-4 Stress-strain curves for the samples electrospun from the solution at the total polymer concentration of 6% (w/v) after 6 days of degradation

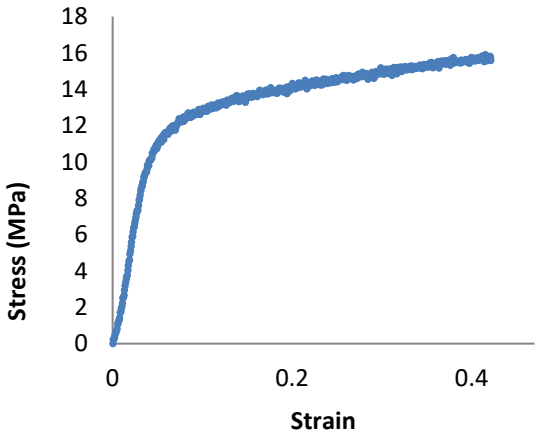

a) 6.1 D10

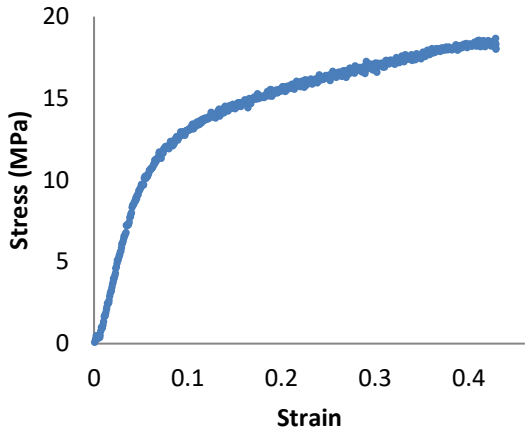

b) 6.2 D10

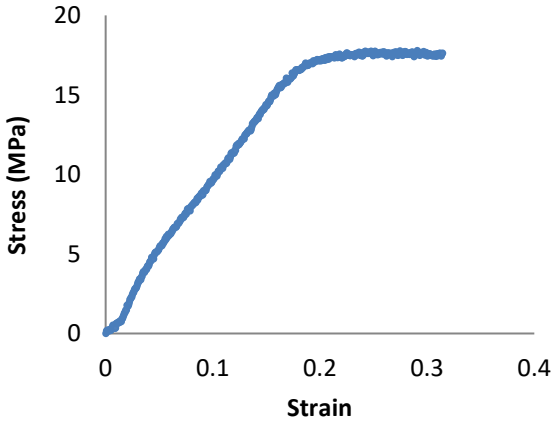

c) 6.3 D10

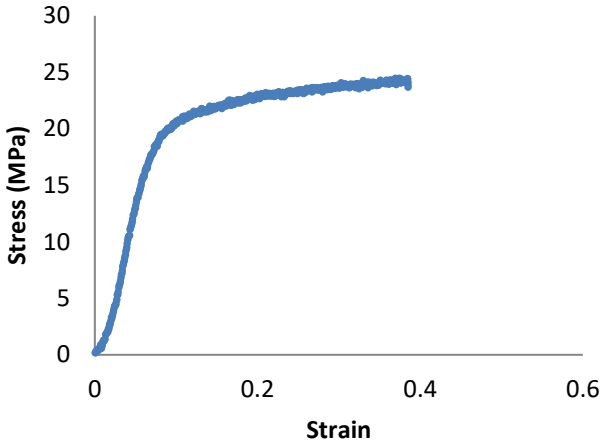

d) 6.4 D10

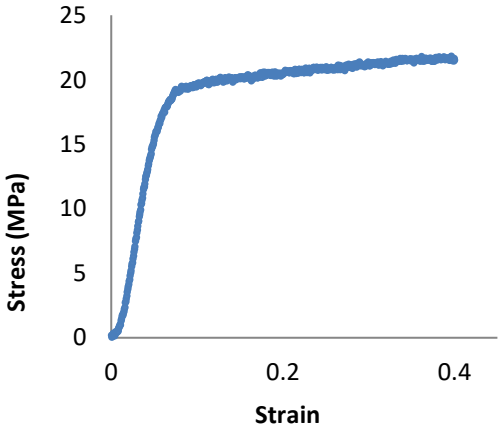

e) 6.5 D10

Figure C-5 Stress-strain curves for the samples electrospun from the solution at the total polymer concentration of 6% (w/v) after 10 days of degradation

Appendix C.2 The Elastic Modulus and Yield Strength for the Samples Electrospun from the Solution at the Total Polymer Concentration of 6% (w/v) before Degradation and after 1, 3, 6 and 10 Days of Degradation

Table C-1 Elastic modulus for the samples electrospun from the solution at total polymer concentration of 6% (w/v) before degradation and after 1, 3, 6 and 10 days of degradation

	Elastic modulus before Degradation (MPa)	Elastic modulus after 1 day of degradation (MPa)	Elastic modulus after 3 days of degradation (MPa)	Elastic modulus after 6 days of degradation (MPa)	Elastic modulus after 10 days of degradation (MPa)
6.1	506	472	254	151	330
6.2	480	603	243	281	242
6.3	599	482	296	296	87.8
6.4	450	555	290	297	357
6.5	574	470	280	157	417

Table C-2 Yield strength for the samples electrospun from the solution at the total polymer concentration of 6% (w/v) before degradation and after 1, 3, 6 and 10 days of degradation

	Yield strength before degradation (MPa)	Yield strength after 1 Day of degradation (MPa)	Yield strength after 3 days of degradation (MPa)	Yield strength after 6 days of degradation (MPa)	Yield strength after 10 days of degradation (MPa)
6.1	17	20.6	10.1	5.2	9.4
6.2	17.2	23.5	10.3	8.2	9.3
6.3	15.3	24.3	11.1	7.2	16.8
6.4	14.7	22.7	11.5	6.9	15.9
6.5	13.8	21.3	9.8	6.6	16.1

Appendix C.3 Stress-Strain Curves for the Samples Electrospun from the Solution at the Total Polymer Concentration of 10% (w/v) before Degradation and after 1, 3, 6 and 10 Days of Degradation

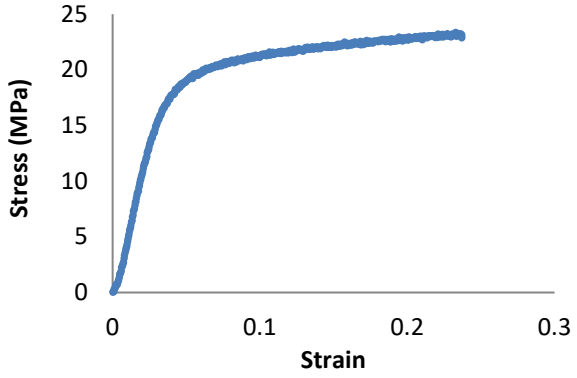

a) 10.1 D0

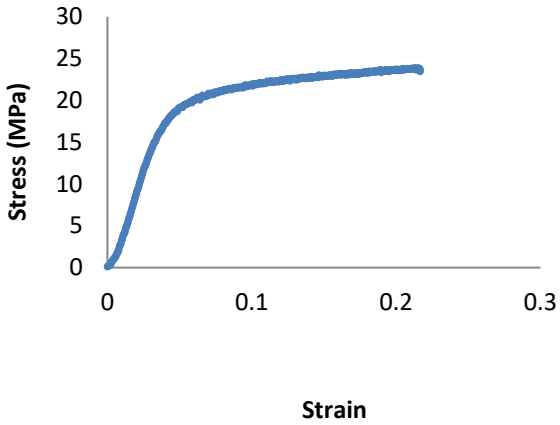

b) 10.2 D0

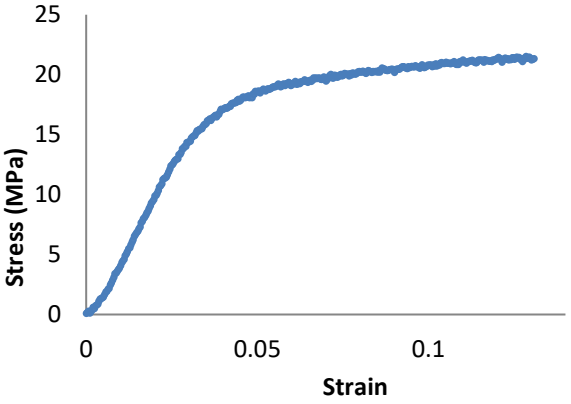

c) 10.3 D0

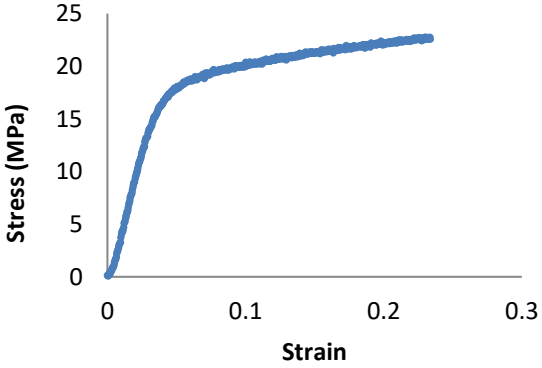

d) 10.4 D0

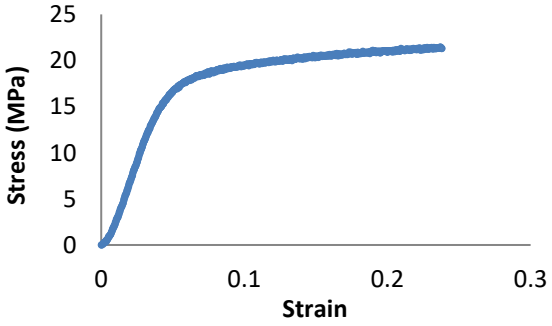

e) 10.5 D0

Figure C-6 Stress-strain curves for the samples electrospun from the solution at the total polymer concentration of 10% (w/v) before degradation

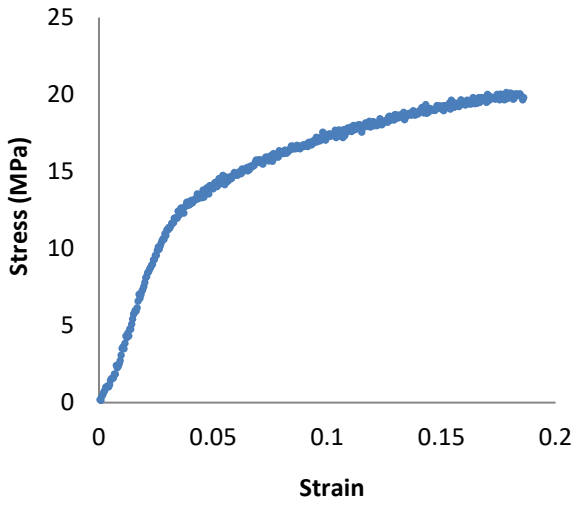

a) 10.1 D1

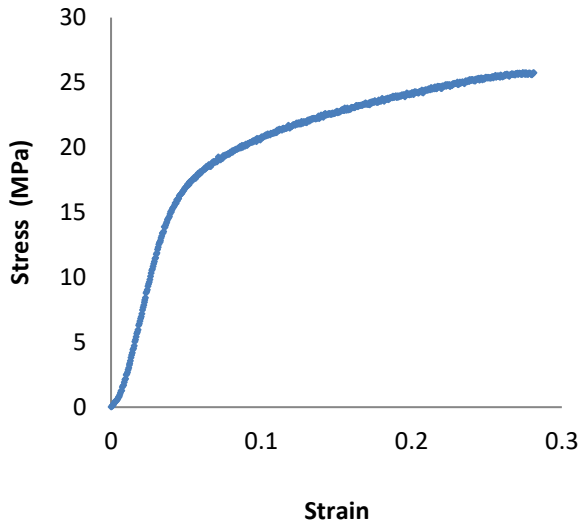

b) 10.2 D1

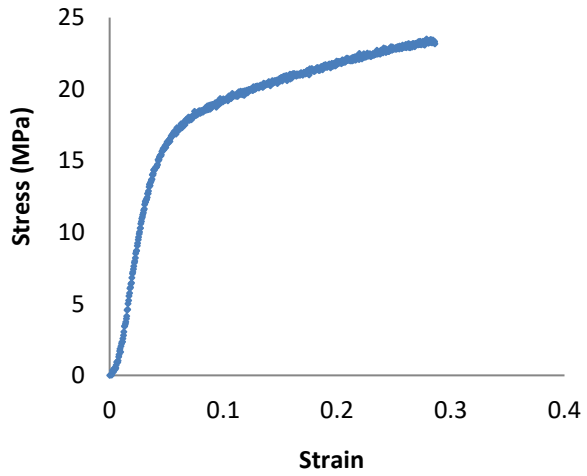

c) 10.3 D1

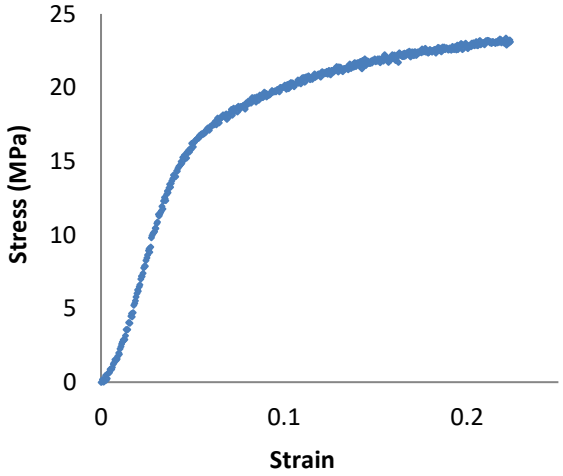

d) 10.4 D1

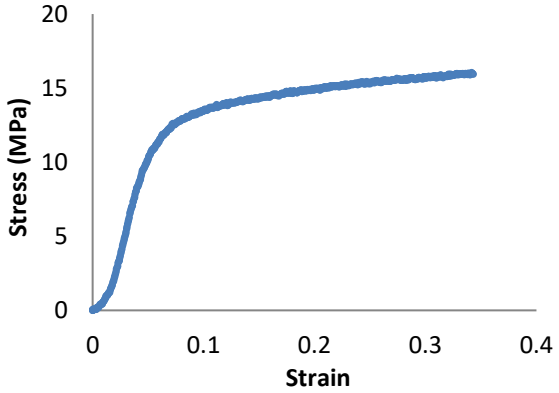

e) 10.5 D1

Figure C-7 Stress-strain curves for the samples electrospun from the solution at the total polymer concentration of 10% (w/v) after 1 day of degradation

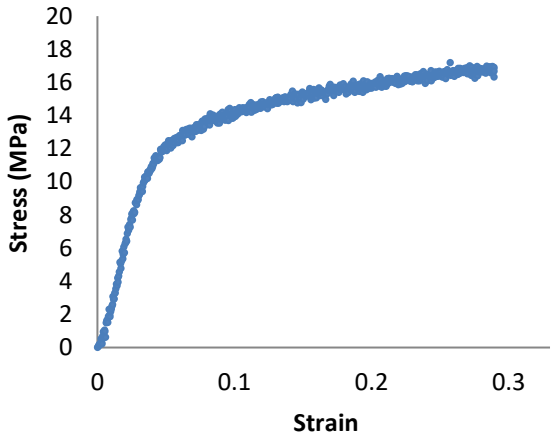

a) 10.1 D3

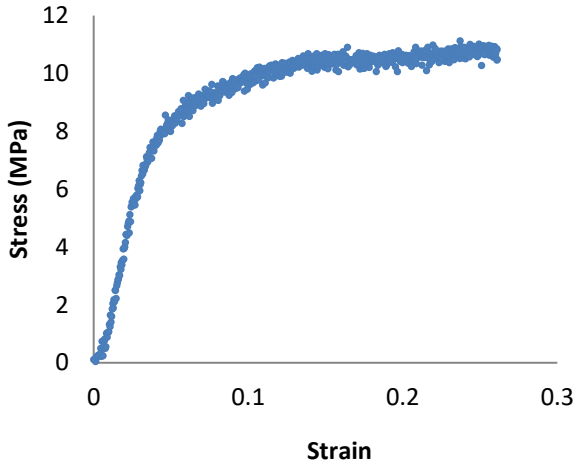

b) 10.2 D3

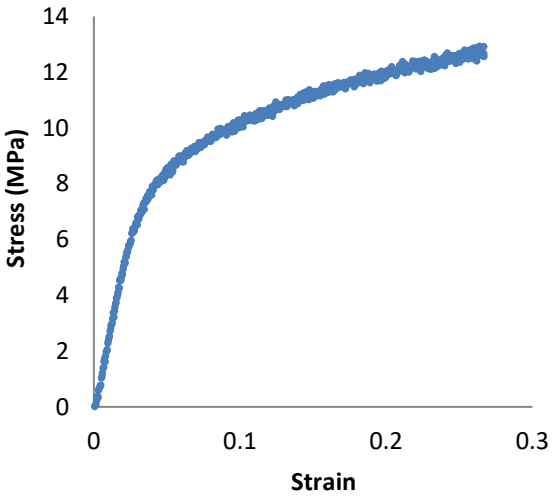

c) 10.3 D3

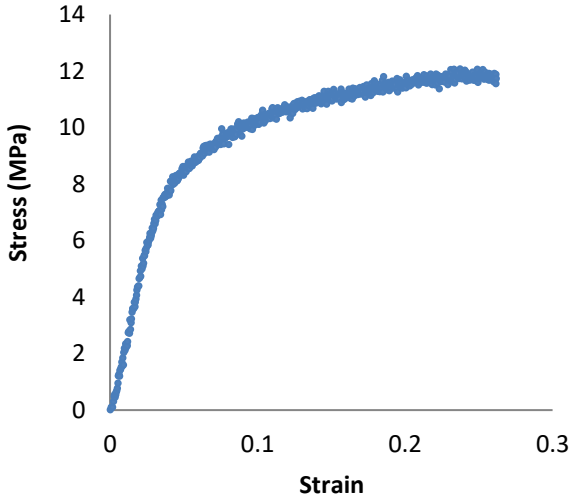

d) 10.4 D3

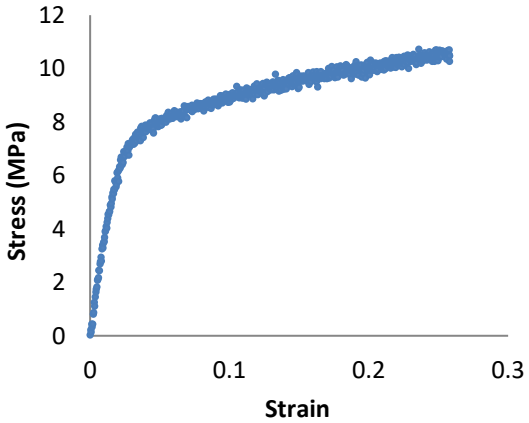

e) 10.5 D3

Figure C-8 Stress-strain curves for the samples electrospun from the solution at the total polymer concentration of 10% (w/v) after 3 days of degradation

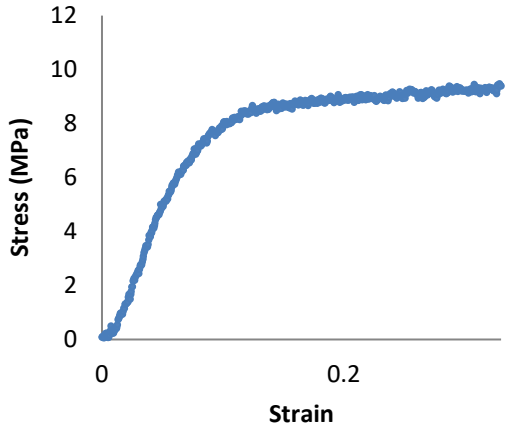

a) 10.1 D6

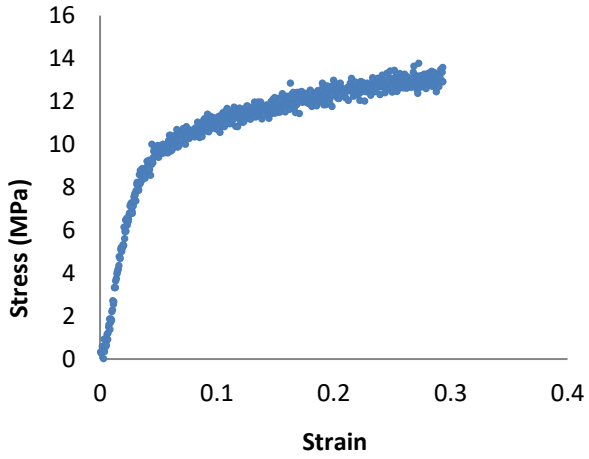

b) 10.2 D6

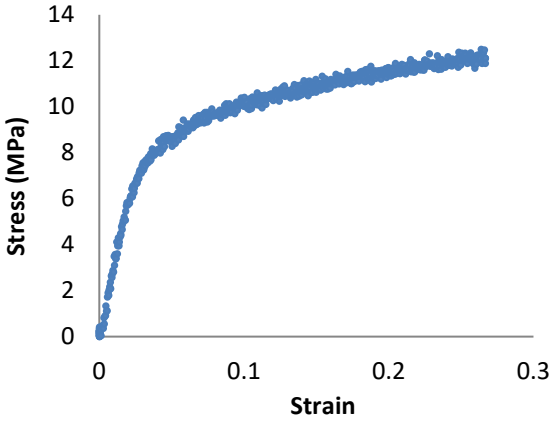

c) 10.3 D6

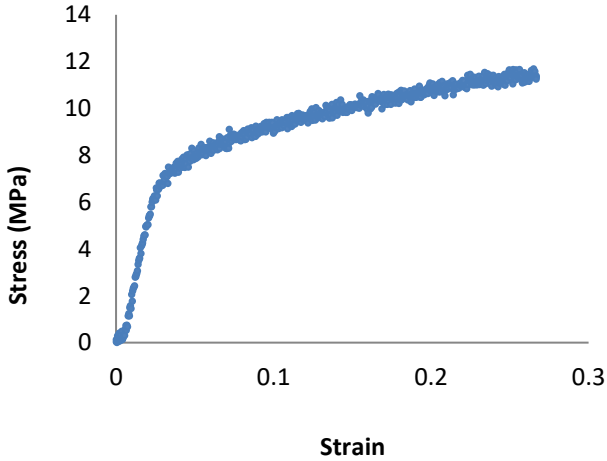

d) 10.4 D6

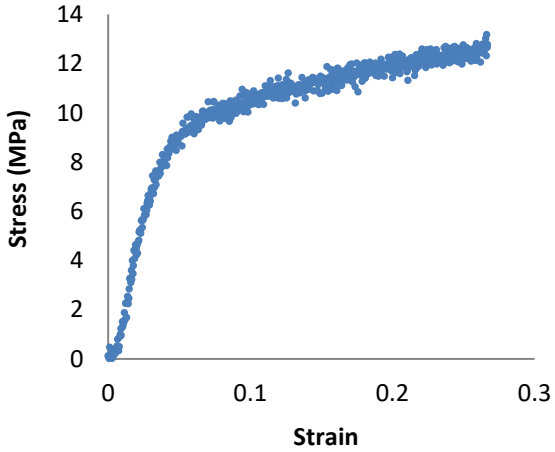

e) 10.5 D6

Figure C-9 Stress-strain curves for the samples electrospun from the solution at the total polymer concentration of 10% (w/v) after 6 days of degradation

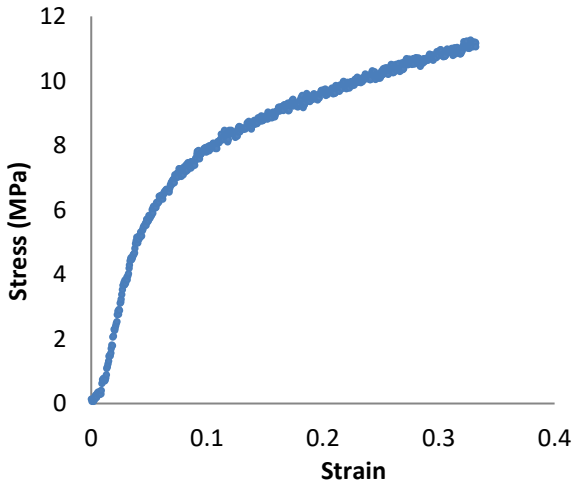

a) 10.1 D10

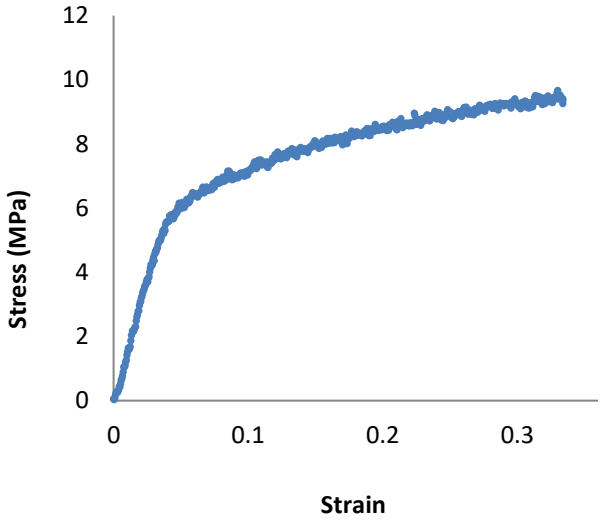

b) 10.2 D10

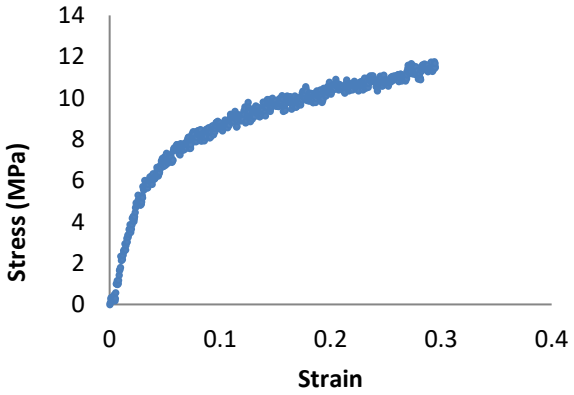

c) 10.3 D10

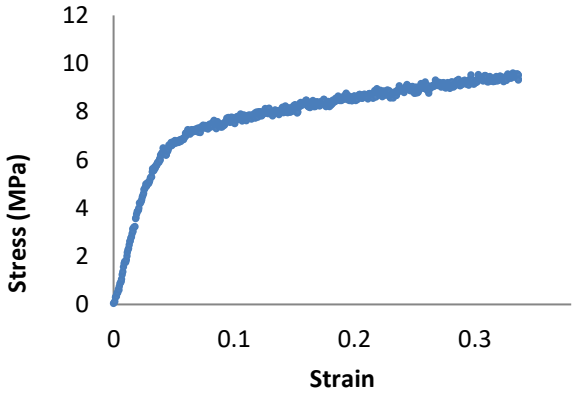

d) 10.4 D10

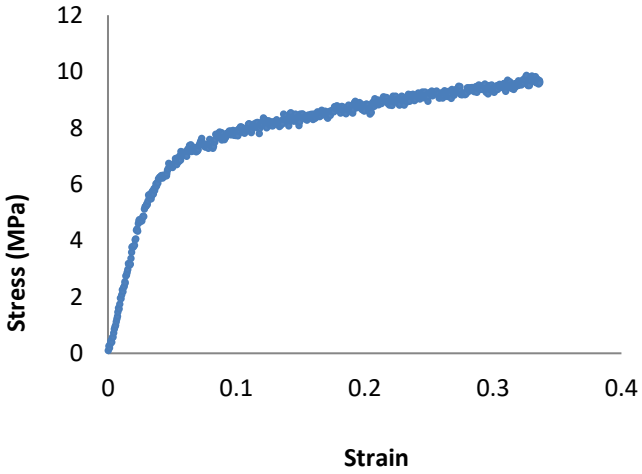

e) 10.5 D10

Figure C-10 Stress-strain curves for the samples electrospun from the solution at the total polymer concentration of 10% (w/v) after 10 days of degradation

Appendix C.4 The Elastic Modulus and Yield Strength for the Samples Electrospun from the Solution at the Total Polymer Concentration of 10% (w/v) before Degradation and after 1, 3, 6 and 10 Days of Degradation

Table C-3 Elastic modulus for the samples electrospun from the solution at total polymer concentration of 10% (w/v) before degradation and after 1, 3, 6 and 10 days of degradation

	Elastic modulus before degradation (MPa)	Elastic modulus after 1 day of degradation (MPa)	Elastic modulus after 3 days of degradation (MPa)	Elastic modulus after 6 days of degradation (MPa)	Elastic modulus after 10 days of degradation (MPa)
10.1	600	456	373	127	179
10.2	567	485	280	329	161
10.3	565	513	270	323	232
10.4	543	457	251	340	202
10.5	453	308	322	312	196

Table C-4 Yield strength for the samples electrospun from the solution at total polymer concentration of 10% (w/v) before degradation and after 1, 3, 6 and 10 days of degradation

	Yield strength before degradation (MPa)	Yield strength after 1 day of degradation (MPa)	Yield strength after 3 days of degradation (MPa)	Yield strength after 6 days of degradation (MPa)	Yield strength after 10 days of degradation (MPa)
10.1	15.5	11.2	9.7	5.9	5.2
10.2	16.1	14.6	6.8	8.2	5.6
10.3	15.3	13.3	6.5	6.5	5.7
10.4	15.2	14	6.9	6.6	5.6
10.5	15	9.8	6.6	7.3	5.8

Appendix C.5 Stress-Strain Curves for the Samples Electrospun from the Solution at the Total Polymer Concentration of 14% (w/v) before Degradation and after 1, 3, 6 and 10 Days of Degradation

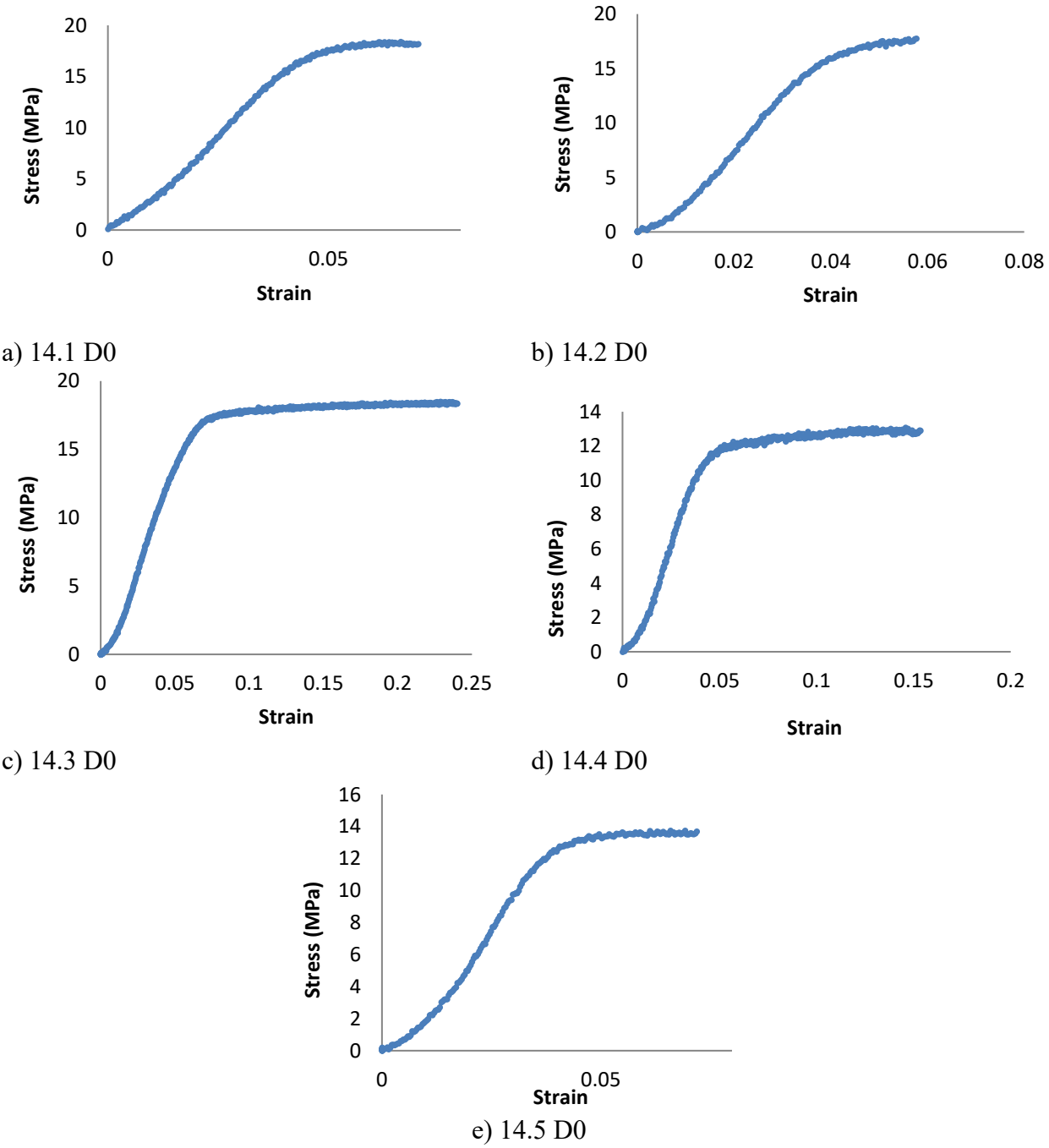

Figure C-11 Stress-strain curves for the samples electrospun from the solution at the total polymer concentration of 14% (w/v) before degradation

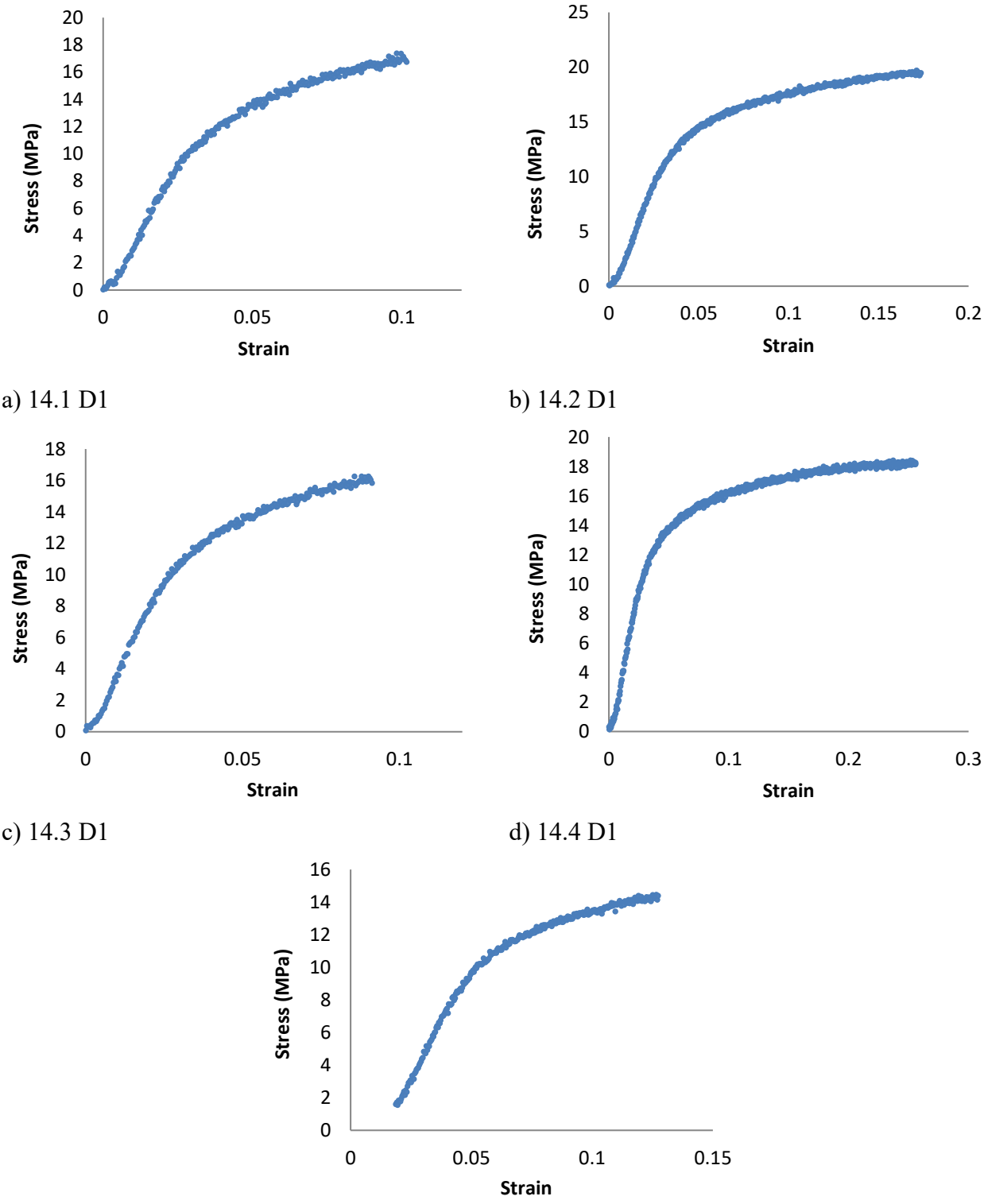

Figure C-12 Stress-strain curves for the samples electrospun from the solution at the total polymer concentration of 14% (w/v) after 1 day of degradation

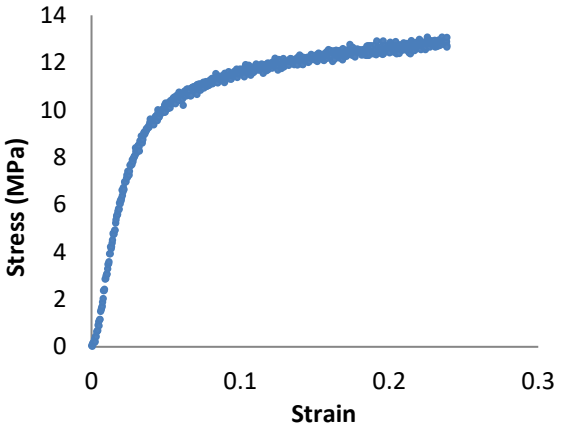

a) 14.1 D3

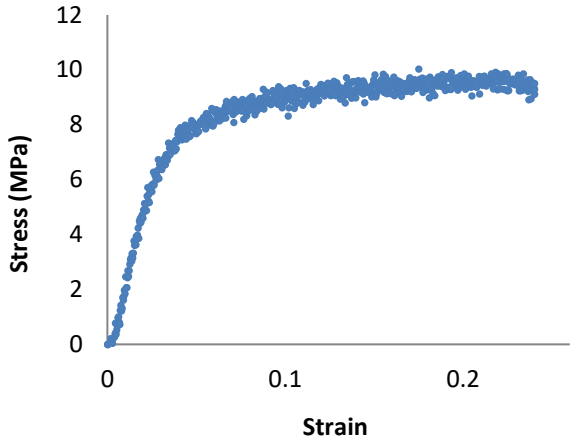

b) 14.2 D3

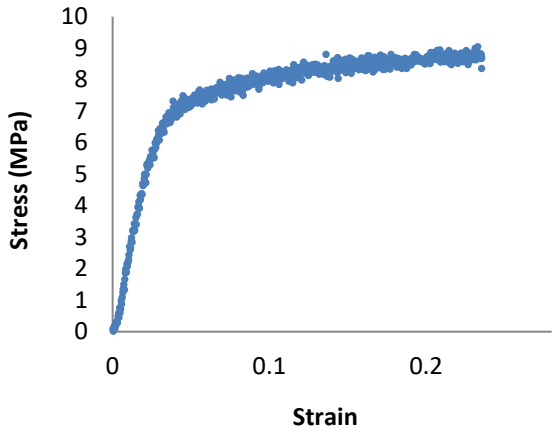

c) 14.3 D3

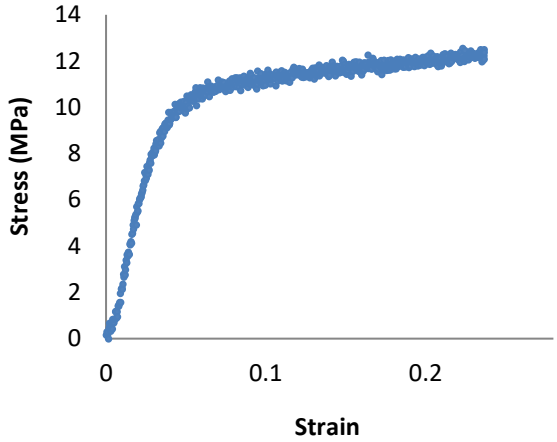

d) 14.4 D3

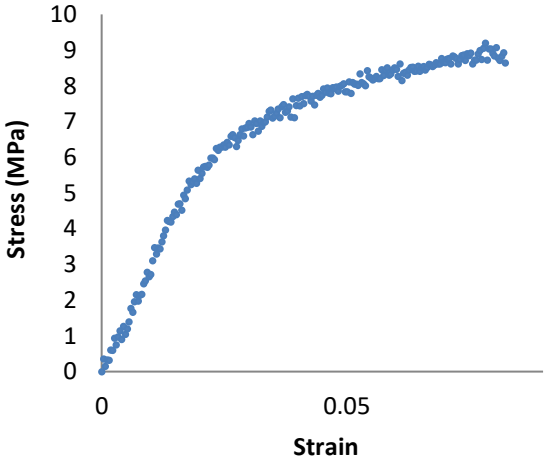

e) 14.5 D3

Figure C-13 Stress-strain curves for the samples electrospun from the solution at the total polymer concentration of 14% (w/v) after 3 days of degradation

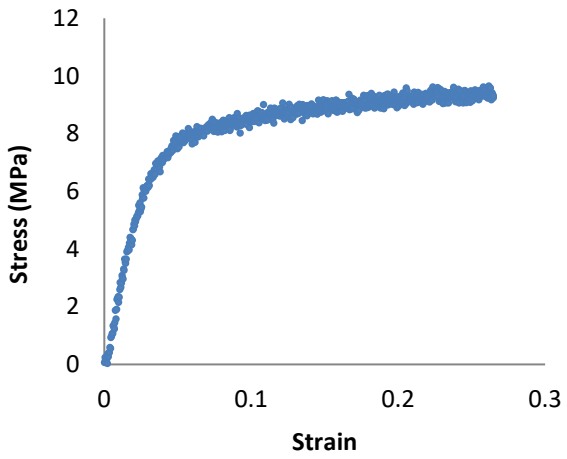

a) 14.1 D6

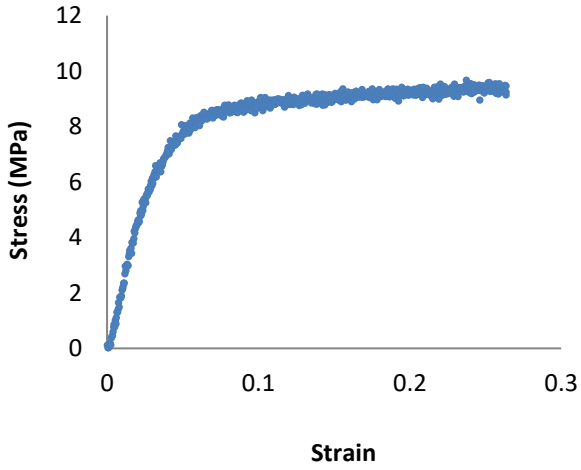

b) 14.2 D6

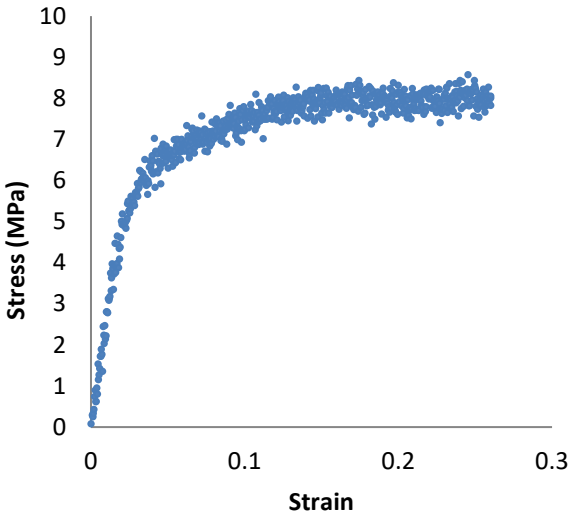

c) 14.3 D6

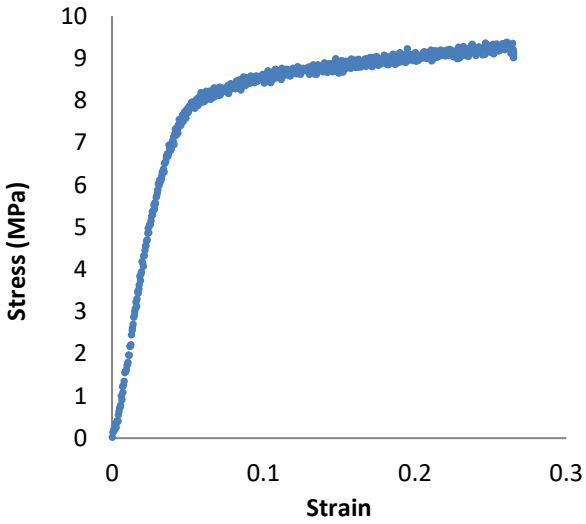

d) 14.4 D6

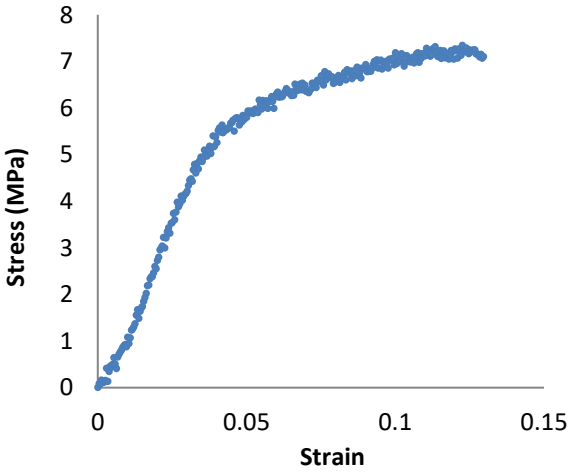

e) 14.5 D6

Figure C-14 Stress-strain curves for the samples electrospun from the solution at the total polymer concentration of 14% (w/v) after 6 days of degradation

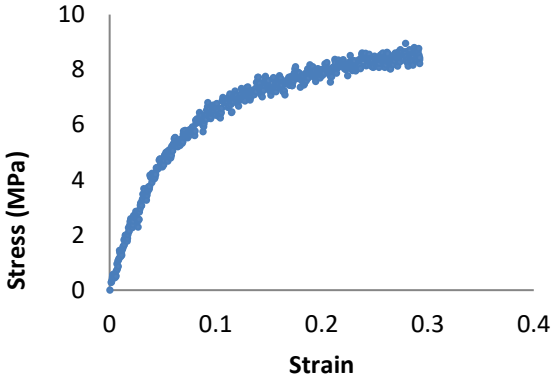

a) 14.1 D10

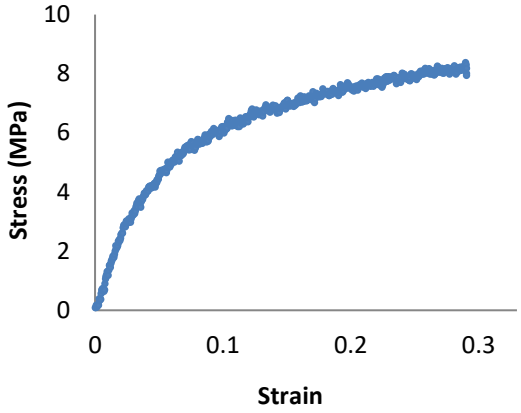

b) 14.2 D10

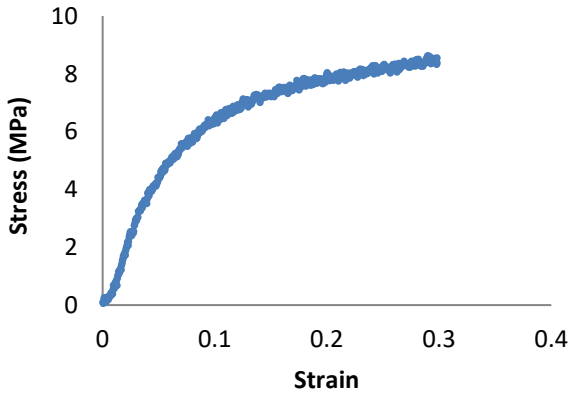

c) 14.3 D10

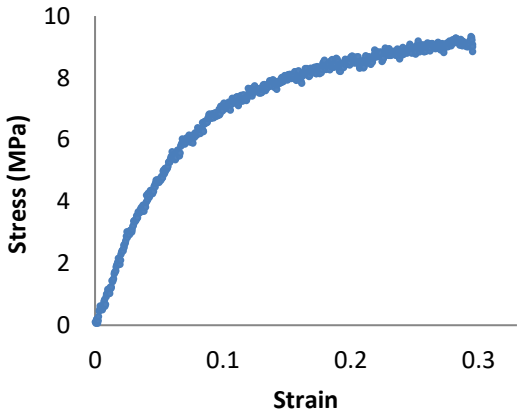

d) 14.4 D10

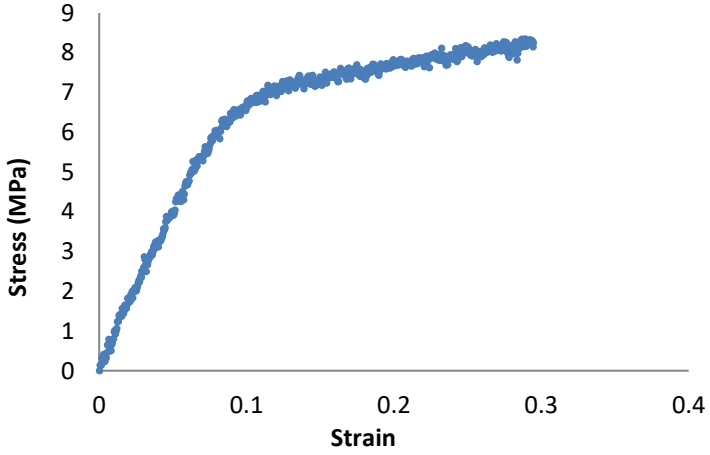

e) 14.5 D10

Figure C-15 Stress-strain curves for the samples electrospun from the solution at the total polymer concentration of 14% (w/v) after 10 days of degradation

Appendix C.6 The Elastic Modulus and Yield Strength for the Samples Electrospun from the Solution at the Total Polymer Concentration of 14% (w/v) before Degradation and after 1, 3, 6 and 10 Days of Degradation

Table C-5 Elastic modulus for the samples electrospun from the solution at total polymer concentration of 14% (w/v) before degradation and after 1, 3, 6 and 10 days of degradation

	Elastic modulus before degradation (MPa)	Elastic modulus after 1 day of degradation (MPa)	Elastic modulus after 3 days of degradation (MPa)	Elastic modulus after 6 days of degradation (MPa)	Elastic modulus after 10 days of degradation (MPa)
14.1	462	448	353	271	90
14.2	523	455	290	245	119
14.3	334	447	269	279	120
14.4	363	451	349	229	114
14.5	449	300	320	182	76

Table C-6 Yield strength for the samples electrospun from the solution at total polymer concentration of 14% (w/v) before degradation and after 1, 3, 6 and 10 days of degradation

	Yield strength before degradation (MPa)	Yield strength after 1day of degradation (MPa)	Yield strength after 3 days of degradation (MPa)	Yield strength after 6 days of degradation (MPa)	Yield strength after 10 days of degradation (MPa)
14.1	16.3	10	7.7	5.9	5.1
14.2	15.5	11.4	6.2	5.5	3.8
14.3	14.3	9.8	5.5	4.9	3.9
14.4	10.8	10.8	7.9	6.1	4.4
14.5	12	9.3	5.8	4.9	6.3

Appendix D Contact Angle

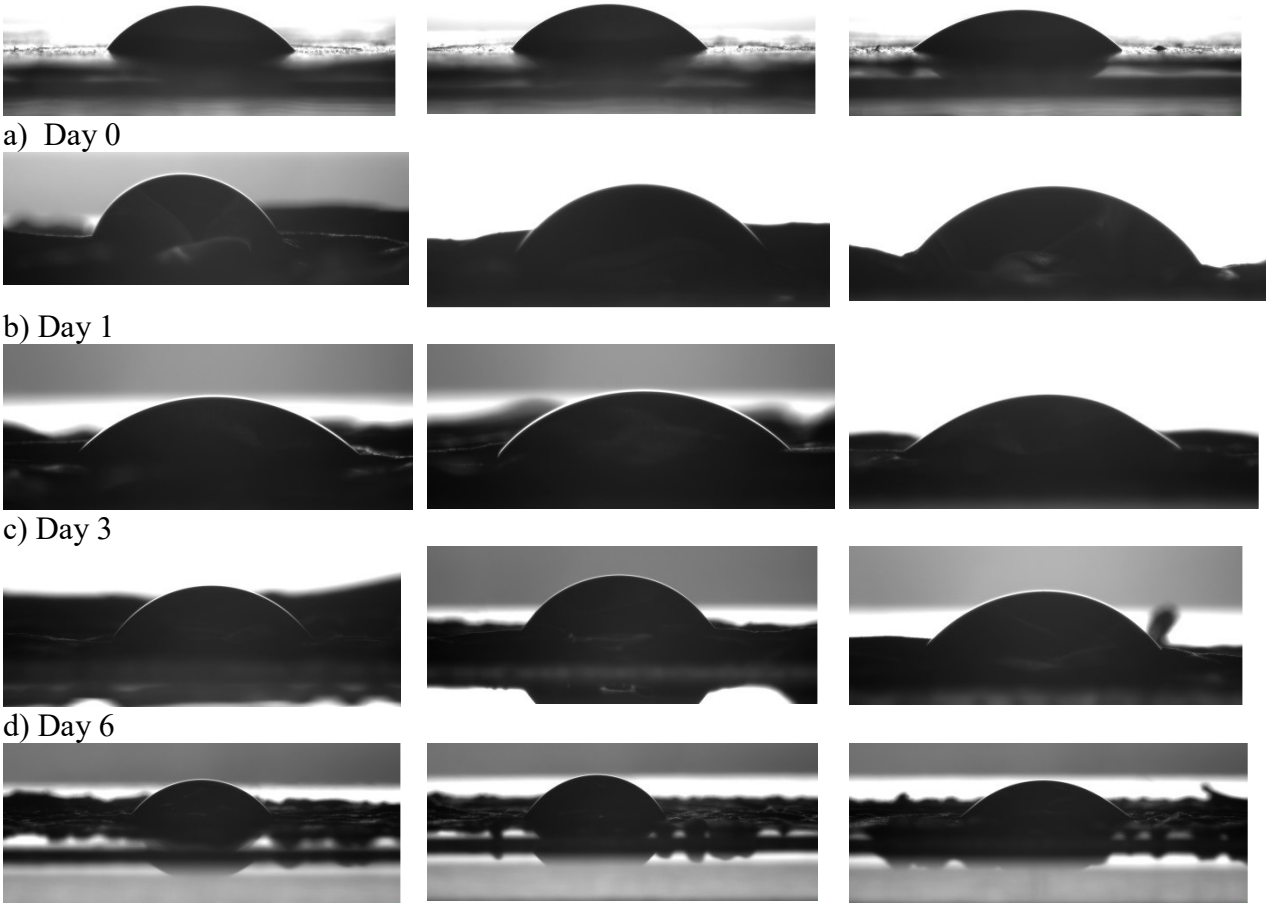

a) Day 0

b) Day 1

c) Day 3

d) Day 6

e) Day 10

Figure D-1 Contact angles for the samples electrospun from the solution at total polymer concentration of 6% (w/v) before degradation and after 1, 3, 6 and 10 days of degradation

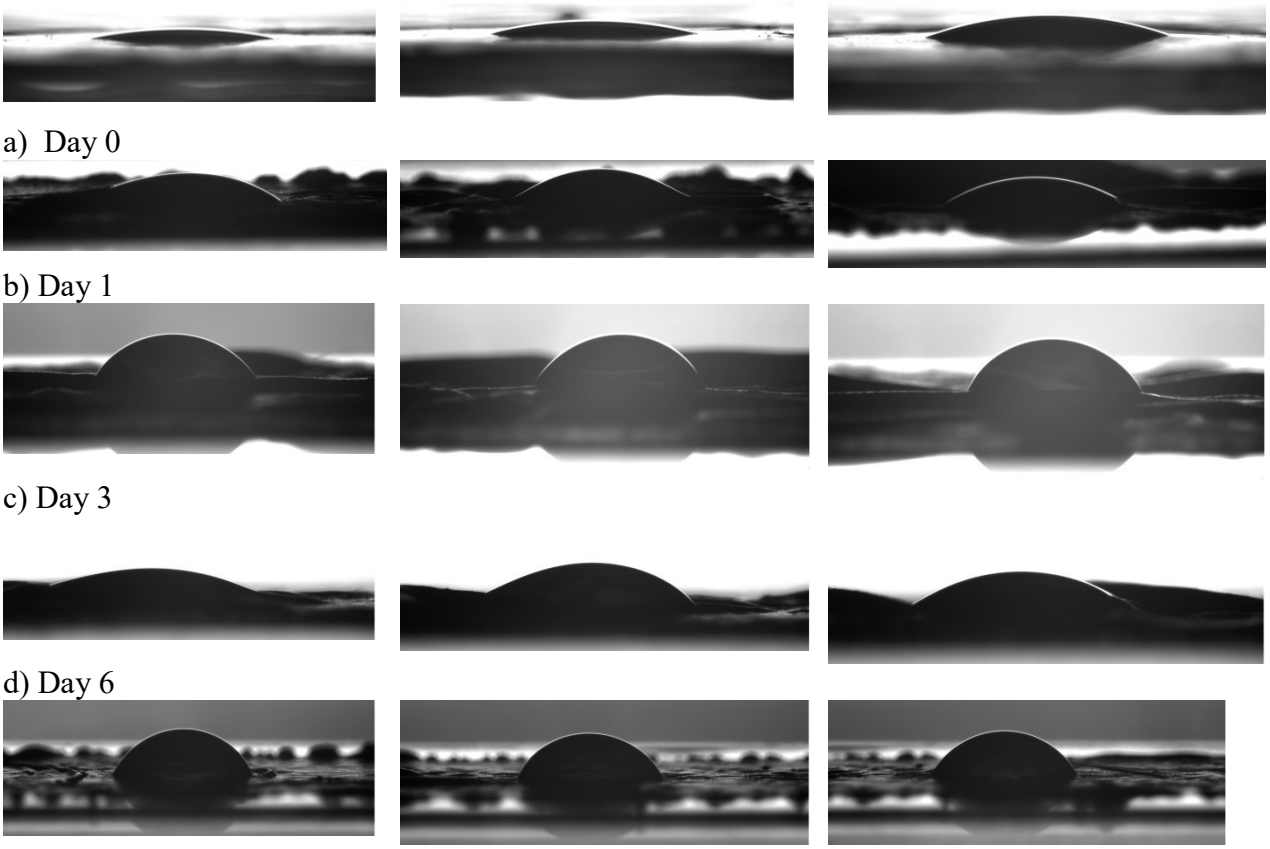

a) Day 0

b) Day 1

c) Day 3

d) Day 6

e) Day 10

Figure D-2 Contact angles for the samples electrospun from the solution at total polymer concentration of 10% (w/v) before degradation and after 1, 3, 6 and 10 days of degradation

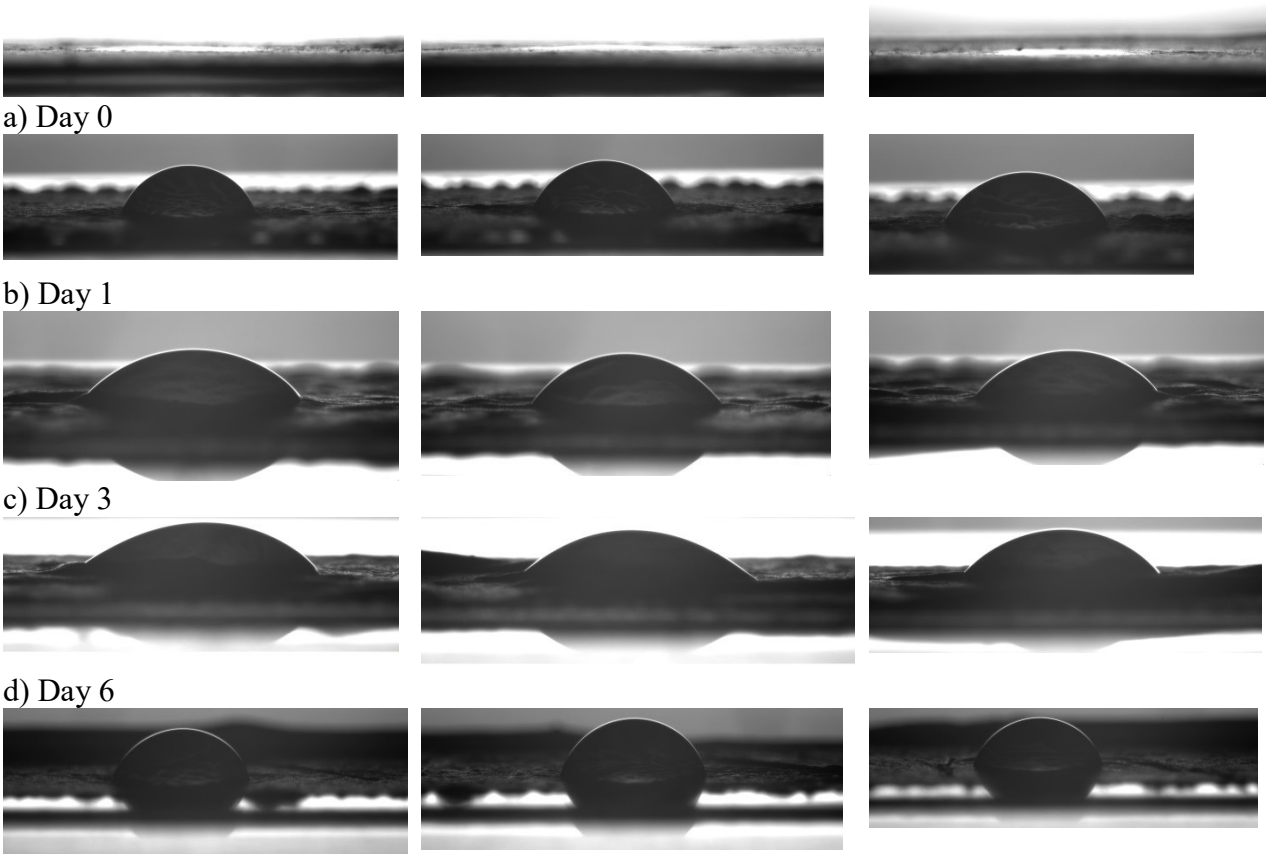

Figure D-3 Contact angles for the samples electrospun from the solution at total polymer concentration of 14% (w/v) before degradation and after 1, 3, 6 and 10 days of degradation